Dissertation

submitted to the
Combined Faculties for the Natural Sciences and for Mathematics
of the Ruprecht-Karls-Universität Heidelberg, Germany
for the degree of
Doctor of Natural Sciences (Dr. rer. nat.)

Presented by
Lda.-Chem. Maria Pilar Arpa Sancet
Born in Zaragoza, Spain
Oral examination: June 4th 2013

Influence of surface properties on adhesion of *Cobetia marina* and accumulation of marine microfoulers in the ocean

Referees:

Prof. Dr. Michael Grunze

Prof. Dr. Joachim P. Spatz

Abstract

Marine biofouling, the colonization of submerged surfaces by unwanted organisms, has an important economic and environmental impact. This PhD thesis focuses on the smaller organisms involved in the biofouling process such as bacteria, diatoms and protozoa also called microfoulers.

As bacteria are usually among the first organisms to settle on submerged surfaces, the characterization of their adhesion to these surfaces is essential for the development of strategies for antifouling, and in particular fouling release coatings. To this end, the adhesion of the bacterium *Cobetia marina* on various model systems for anti-fouling coatings was investigated using a microfluidic shear stress assay which applies shear stresses covering a range of nearly six orders of magnitude from ≈0.01 to 5,500 dyn/cm^2. For this assay, the experimental parameters such as medium, incubation time and increase of the applied volumetric flow were optimized.

In this work various surface properties relevant for bioadhesion were investigated, namely wettability, chemistry, hydration, transition from monolayers to polymeric coatings, and the controlled release properties of metal-organic frameworks as a smart release coating. The surfaces used for this study were self-assembled monolayers (SAMs) with different chemical end-groups and hydration levels, polysaccharide coatings with and without capping of their carboxylic groups, poly[oligo(ethylene glycol)methacrylate] (POEGMA) brushes and copper based metal-organic frameworks (Cu-SURMOF 2). The results showed that in general the hydration of the surface is more important for the resistance against bioadhesion than the wettability. It was demonstrated that the critical shear stress needed for removal of bacteria from a SAM system based on ethylene glycols (EGs) decreased with an increasing number of EG units which is directly related to an increment of hydration. Furthermore, good fouling-release properties of polysaccharide coatings were demonstrated, especially if the free-carboxyl groups of alginic acid (AA) and hyaluronic acid (HA) were capped with a hydrophobic amine. Cu-SURMOFs 2 were investigated as an example of smart release coatings. When bacteria interacted with these surfaces they induced a loss of crystallinity and a harmful effect on themselves. These findings, together with the observed stability of the coatings in artificial seawater (ASW)

and the integrity of the coating in areas without bacteria demonstrated a stimulus response of these surfaces upon presence of bacteria.

In order to compare the performance in the field of the surfaces investigated in the laboratory assays, a set of well characterized samples were immersed into the ocean at the Sebastian test site of the Florida Institute of Technology. The aim of these field tests was to compare the results of the laboratory experiments, which solely investigated a single species under controlled conditions, with field experiments which employed a mixed species marine environment under natural conditions. The results showed that air and water temperature seemed to be an important factor for the abundance of species and composition of the fouling community. Furthermore, the level of hydration of the surfaces was found to be more important for their colonization than their wettability. Some trends that have also been observed in previous laboratory assays such as the good performance of the polysaccharide coatings and the EG SAMs, compared to other SAMs, could be confirmed in the field. Hence, the inert properties of hydrophilic hydrogels could be demonstrated in both laboratory assays and in the natural marine environment.

Kurzfassung

Die als marines Fouling bezeichnete unerwünschte Besiedelung von untergetauchten Oberflächen hat große ökonomische und ökologische Auswirkungen. Diese Dissertation beschäftigt sich mit den kleineren, am Foulingprozess beteiligten Organismen: Bakterien, Diatomeen und Protozoa, gemeinsam auch als Mikrofouler bezeichnet.

Da Bakterien für gewöhnlich zu den ersten Organismen gehören, die untergetauchte Oberflächen besiedeln, ist die Charakterisierung ihrer Anhaftung auf diesen Oberflächen von grundlegender Bedeutung, um Strategien für Beschichtungen mit Antifouling-eigenschaften zu entwickeln. Zu diesem Zweck wurde die Adhäsion des Bakteriums *Cobetia marina* auf verschiedenen Modelloberflächen für Antifoulingbeschichtungen mithilfe eines mikrofluidischen Scherkraft-Assays, welches Scherkräfte im Bereich von ≈0.01 dyn/cm^2 bis 5,500 dyn/cm^2, also beinahe sechs Größenordnungen abzudecken vermag, untersucht. Für diese Versuche wurden die experimentellen Parameter wie z. B. das verwendete Medium, die Inkubationszeit und die Wachstumsrate der applizierten Scherkräfte optimiert.

In Rahmen dieser Arbeit wurden verschiedene, für die Bioadhäsion relevante Oberflächeneigenschaften wie die Benetzbarkeit, chemische Zusammensetzung, Hydratation, der Übergang von Monolagen zu Polymerschichten und die kontrollierte Freisetzung aus metallorganischen Gerüststrukturen als Beispiel für eine Smart-Release-Beschichtung untersucht. SAMs (selbstorganisierende Monoschichten) mit unterschiedlichen chemischen Endgruppen und Hydratationszuständen, Polysaccharid-Beschichtungen mit und ohne Schutz ihrer Carboxyl-Gruppen, POEGMA-Bürsten (Poly(oligoethylenglykol) methacrylat-Bürsten) und kupferbasierte MOFs (metallorganische Gerüststrukturen, *engl.* metal-organic framework) (Cu-SURMOF 2) wurden in dieser Arbeit als wohl-definierte Modelloberflächen genutzt. Die Ergebnisse zeigen, dass die Hydratation der Oberfläche von größerer Bedeutung für die Resistenz gegenüber Bioadhäsion ist als die chemische Zusammensetzung. Es konnte gezeigt werden, dass die kritische Scherkraft, die nötig war, um Bakterien von SAMs aus Ethylenglykol-Gruppen (EG-Gruppen) zu entfernen, mit steigender Anzahl der EG-Gruppen und daraus folgender verstärkter Hydratation abnahm. Desweiteren konnten gute Foul-release-Eigenschaften der Polysaccharid-Beschichtungen gezeigt werden,

insbesondere für Hyaluronsäure und Algininsäure mit geschützten freien Carboxylgruppen. Cu-SURMOFs 2 wurden als Beispiel einer Smart-Release-Beschichtung untersucht. Wenn Bakterien mit dieser Oberfläche interagierten, verursachten einen Abbau der kristallinen Struktur und letztlich eine Schädigung ihrer selbst. Diese Ergebnisse in Kombination mit der festgestellten Stabilität der Beschichtungen in ASW (künstliches Seewasser, *engl.* artificial seawater) belegen eine Reizantwort dieser Oberflächen auf die dort vorhandenen Bakterien.

Um die Leistungsfähigkeit der im Labor untersuchten Oberflächen zu vergleichen, wurden identische Proben im Ozean auf dem Versuchsgelände Sebastian des Florida Institute of Technology getestet. Ziel dieser Versuche war es, die Ergebnisse der auf nur einer Bakterien-Art basierenden Labor-Assays mit Feldversuchen zu vergleichen, welche die komplette Bandbreite der im Ozean vorkommenden Arten unter natürlichen Bedingungen abdecken. Die Auswertung ergab eine starke Abhängigkeit der Anzahl an Spezien und deren Häufigkeit von den vorherrschenden Luft- und Wassertemperaturen. Die Besiedelung der Testoberflächen wurde stärker durch die Hydratation der Oberflächen als durch ihre Benetzbarkeit bestimmt. Manche zuvor in Laborversuchen gemachte Beobachtungen wie beispielsweise die guten Ergebnisse für Polysaccharid-Beschichtungen und EG SAMs, im Vergleich zu anderen SAMs, konnten in den Feldversuchen bestätigt werden. Somit konnten die inerten Eigenschaften hydrophiler Hydrogele sowohl in Labor- als auch in Feldversuchen demonstriert werden.

Sumario

La incrustación biológica marina es la colonización de superficies sumergidas por medio de organismos no deseados. Este fenómeno presenta consecuencias perjudiciales tanto económicas como medioambientales. La presente tesis se centra en las primeras etapas de este proceso está constituido por varias fases: la formación de una película que condiciona la capa superior, la adhesión de bacterias y el establecimiento de micro colonizadores.

Las bacterias suelen ser los primeros organismos en adherirse a las superficies, por lo que un conocimiento de su respuesta respecto a las superficies es esencial para la investigacion de revestimientos. Con este fin se ha investigado la adhesión de la bacteria marina *Cobetia marina* en diversos revestimientos diseñados para combatir la bioincrustación. Los ensayos se llevaron acabo con un aparato que genera microflujos lo cual permite aplicar una tensión cortante sobre la superficie investigada de seis órdenes de magnitud, desde 0.01 dyn/cm^2 hasta 5,500 dyn/cm^2. Con anterioridad a estos ensayos se optimizaron los parámetros experimentales como el medio, el periodo de incubación o la velocidad de incremento de la tensión cortante fueron optimizados.

Durante este trabajo se investigaron las diferentes propiedades de las superficies, concretamente mojabilidad, química, hidratación, transición de monoestratos a polímeros y capacidad de liberación controlada de sustancias. Los modelos de superficies bien definidas que se usaron fueron monoestratos auto-ensamblados (SAMs) con diferentes terminaciones químicas y niveles de hidratación, revestimientos basados en polisacáridos con y sin proteccion de sus grupos carboxilos, microcepillos de poli(metacrilato-etilenglicol) y estructuras metal-orgánicas basadas en cobre (Cu-SURMOFs 2). Los resultados mostraron que la hidratación es una propiedad más importante que la terminación química para aumentar la resistencia contra la bioadhesión del material. Se demostró que la tensión cortante necesaria para desadherir las bacterias en SAMs basados en etilenglicol (EG) disminuyó con el aumento del número de unidades de EG, las cuales facilitan la hidratación. Asimismo se demostraron las buenas propiedades de desadherencia de los revestimientos basados en polisacáridos, especialmente al proteger los grupos carboxilos del ácido hialurónico (HA) y del ácido algínico (AA). Otra superficie investigada fue Cu-SURMOF 2, un revestimiento con la

propiedad de una liberación específica de moléculas. Las interacciones entre las bacterias y dichos revestimientos causaron la pérdida de cristalinidad del material lo que indujo a efectos perjudiciales para las bacterias. De este modo, se verificó un estímulo de estas superficies como respuesta a la presencia de las bacterias.

Una variedad de superficies se sumergió en el mar en una de las instalaciones pertenecientes al Instituto de Tecnología de Florida. El objetivo de este estudio fué la correlación de los ensayos llevados a cabo en el laboratorio, los cuales solo consisten en la investigación de especies individuales, con los experimentos de campo que contienen múltiples especies en su entorno biológico con sus condiciones ambientales naturales. Los resultados demostraron que la temperatura del aire y del agua influyen en la abundancia y composición de los organismos colonizadores. Algunas de las tendencias observadas en los ensayos de laboratorio se pudieron verificar en los experimentos de campo, como por ejemplo el buen rendimiento de los revestimientos basados en polisacáridos y en etilenglicol en comparación con las otras superficies. Por lo tanto, se pudieron demostrar las propiedades inertes de los hidrogeles hidrófilos, tanto en el laboratorio, como en el ambiente natural marino.

Contents

1. Introduction

Marine biofouling, the undesired colonization of submerged surfaces by marine organisms, is caused by the adsorption of a molecular conditioning films onto the surfaces [1] and attachment and growth of sessile organisms [2]. This phenomenon is a major problem for many marine industries with both economic and environmental consequences [3]. As an example of such penalties, it is estimated that 300 million tons of fuel are additionally required each year by the world fleet as a result of hull fouling caused by biofouling [4]. Marine biofouling has been considered to be composed of the formation of conditioning films and the attachment of diverse microfoulers and macrofoulers ranging in size from micrometers such as bacteria, single spores or some diatoms to hundreds of micrometers or even millimeters such as the larvae of invertebrates [5].

Antifouling coatings can be divided into two groups, namely non-fouling and foul-release coatings. Non-fouling coatings inhibit the attachment of organisms, whereas on fouling-release coatings the adhesion strength of the organisms is reduced allowing its release by applying lower shear stresses. Consequently, not only the attachment but also the detachment of organisms has to be investigated. The effectiveness of the coatings depends on their properties, hence they are considered important factors to determine the adhesion of organisms.

The goal of this PhD is to investigate the influence of surface properties on bioadhesion with regard to conditioning film formation and colonization by microfoulers (often referred to as “slime”) which is due to unicellular microorganisms such as bacteria, diatoms and protozoa [5]. For this purpose, the adhesion of the marine bacterium *Cobetia marina* on surfaces with different properties was quantitatively evaluated by a microfluidic shear stress assay. Furthermore, model surfaces used for laboratory assays were submerged into the ocean in order to investigate the adhesion of microfoulers and to connect the results obtained by the laboratory assays to the “real marine world”.

2. Theoretical Background

2.1. Biofouling

Marine biofouling is an unwanted colonization process occurring on both man-made and natural submerged surfaces as the result of the adhesion of undesirable marine organisms. Traditionally, it has been considered to be composed of different stages which appear in a linear succession [6]. Nevertheless, it is misleading to assume this oversimplified model since organisms are capable of settling faster or slower than normally expected or appear in a different succession [5]. Figure 1 shows the different classes of fouling organisms which colonize a surface, their typical order of appearance and the usual time scales at which they settle.

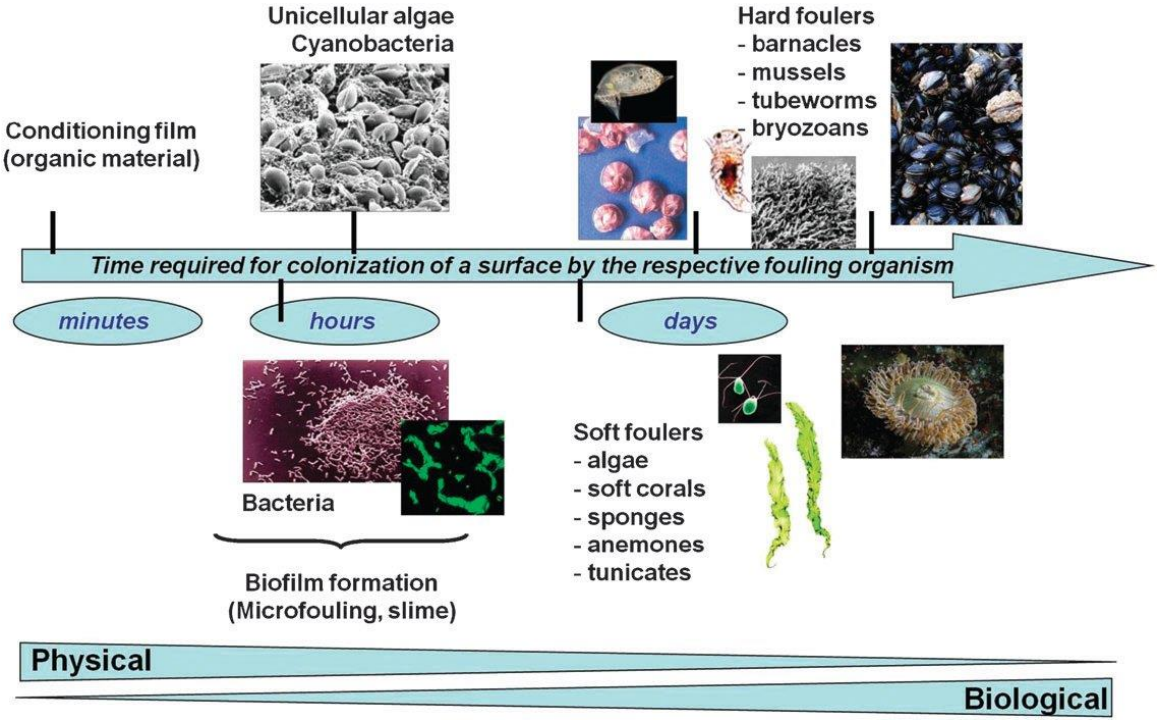

Figure 1. Schema of the biofouling process showing the time required for colonization of a surface by the respective fouling organisms [6]. Single images are from sources mentioned there.

When a "clean" surface is submerged in water, it adsorbs organic material within few minutes, such as proteins or polysaccharides, forming a conditioning layer. This process is principally governed by van der Waals and physical forces [3]. Early attached microorganisms, such as bacteria and unicellular algae, aggregate together and form a biofilm, which is usually referred to as microfouling or slime [1]. This disposition

provides the microorganisms with higher protection from predators, toxins and environmental changes and facilitates the capture of nutrients [3]. Finally, soft and hard fouling organisms, which represent the macrofouling community, overgrow the surface. Soft foulers consist of algae and invertebrates such as sponges, anemones or tunicates, while hard foulers are invertebrates such as barnacles, tubeworms and mussels [1].

Biofouling is a major problem for many marine industries. One of the main adverse effects is the increase of fuel consumption of ships due to a higher frictional resistance of fouled ship hulls and the increase of weight. Some estimations indicate that an additional 300 million tons of fuel are annually required by the international registered fleet as a consequence of the hull fouling [4]. This is related to an increase of frequency of dry-docking operations which causes a loss of time and a waste of resources [7]. Besides the economic consequences, biofouling leads to many environmental problems, such as the introduction of invasive species into foreign environments [8]. Furthermore, ship inventories revealed a double emission of all pollutants, for example global NOx emission [4]. In addition, biofouling harms aquaculture farms as well by blocking the cages and nets, and out competition with the farmed species for space and food [9]. In certain industries such as shipping or water-treatment, bacterial attachment to surfaces may lead to biocorrosion [10], resulting in the damage of metallic surfaces such as pipelines, costing millions of dollars [11]. For all those reasons the prevention of biofouling is desirable. Figure 2 displays a ship hull fouled by the green algae *Ulva* (a) and water pipes with unwanted growth of barnacles (b). These images show examples of surfaces covered by soft and hard foulers respectively.

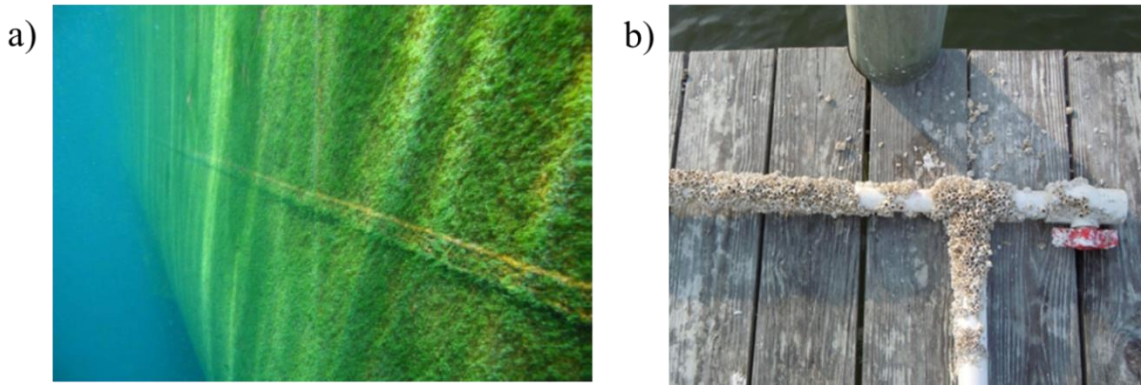

Figure 2. Examples of an advanced state of biofouling. A ship hull covered by the green seaweed *Ulva* [12] (a) and water pipes populated by barnacles (b).

2.2. Bacterial adhesion

2.2.1. Growth phases in bacterial culture

The growth of a bacterial culture basically consists of a succession of phases which are characterized by variations of the growth rate. Figure 3 displays the classical conception of the phases of the bacterial growth.

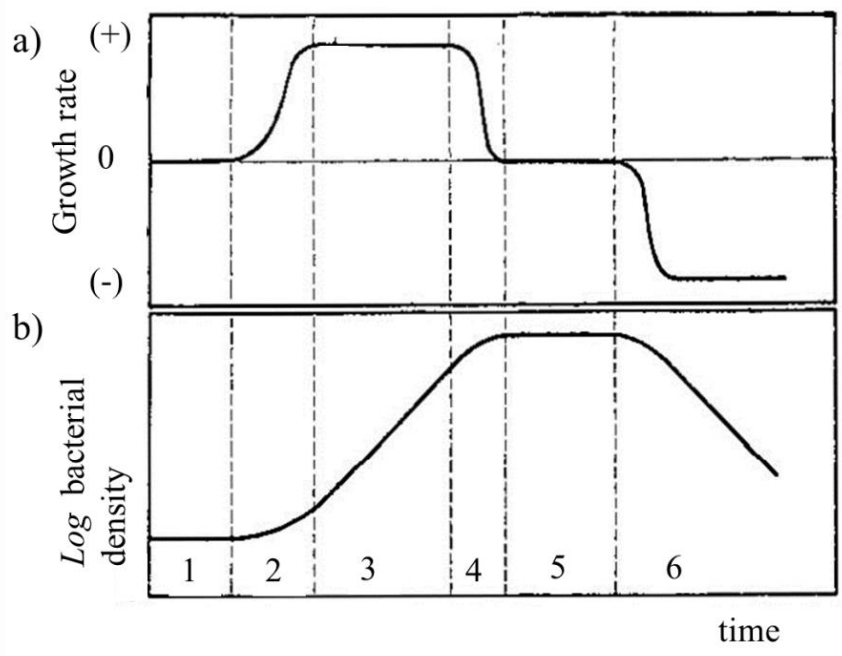

Figure 3. Phases of bacterial growth. Sketch of the growth rate (a) and the logarithm of the bacterial density (b). Vertical dotted lines indicate the limits of the phases [13].

The growth phases are described in Table 1 [13]:

Phase		Description of the growth rate
1	lag	null
2	acceleration	increases
3	exponential	constant
4	retardation	decreases
5	stationary	null
6	decline	negative

Table 1. Bacterial growth phases described according to the growth rates.

Usually, any one or several of these phases may be absent. Frequently, the retardation phase is so short that it is imperceptible [13]. The properties of the bacteria may only be considered constant during the exponential phase [13], thus it can be considered as the most reliable state. That is the reason why most assays prefer to work with bacteria in the exponential phase, also called log phase, for adhesion experiments [14, 15].

2.2.2. Stages of bacterial biofilm development

Aquatic bacteria are more frequently found on solid surfaces than as single, suspended cells [16]. Association in biofilms offers them many advantages, such as promotion of the genetic exchange [11] or increase of protection [17]. Indeed, bacteria in a biofilm are 10-1,000 times more resistant to antibiotics than in their planktonic form [18].

Microbial biofilms can be described as populations of microorganisms which are concentrated at an interface, usually solid-liquid, and typically surrounded by a matrix of extracellular polymeric substances (EPS) [19]. EPS are secreted by microorganisms during growth. Among them various are organic substances such as proteins, polysaccharides, nucleic acids and lipids [20]. It has been reported that EPS play a significant role in the formation and function of microbial aggregates by determining the immediate conditions of life of biofilm cells. Thus, it can be considered as a "house of biofilm cells" [21].

A biofilm is formed when the first cells adhere to a surface making it more attractive for the subsequent bacteria [18]. Bacterial biofilm formation proceeds as a regulated developmental sequence, and five stages are proposed (Figure 4). During the initial stage, loose cells attach to the surface. The second stage is described as the subsequent robust adhesion called irreversible adhesion. Stages three and four involve the maturation: aggregation of cells into microcolonies and subsequent growth [19]. Stage five is the dispersion of the bacteria which is described as their return to transient motility where biofilm cells are sloughed. In this case, the detachment is an active process. A detachment of adherent bacteria can be caused externally either mechanically *e.g.* by applying a fluid shear stress or chemically by adding agents that dissolve the EPS matrix [19].

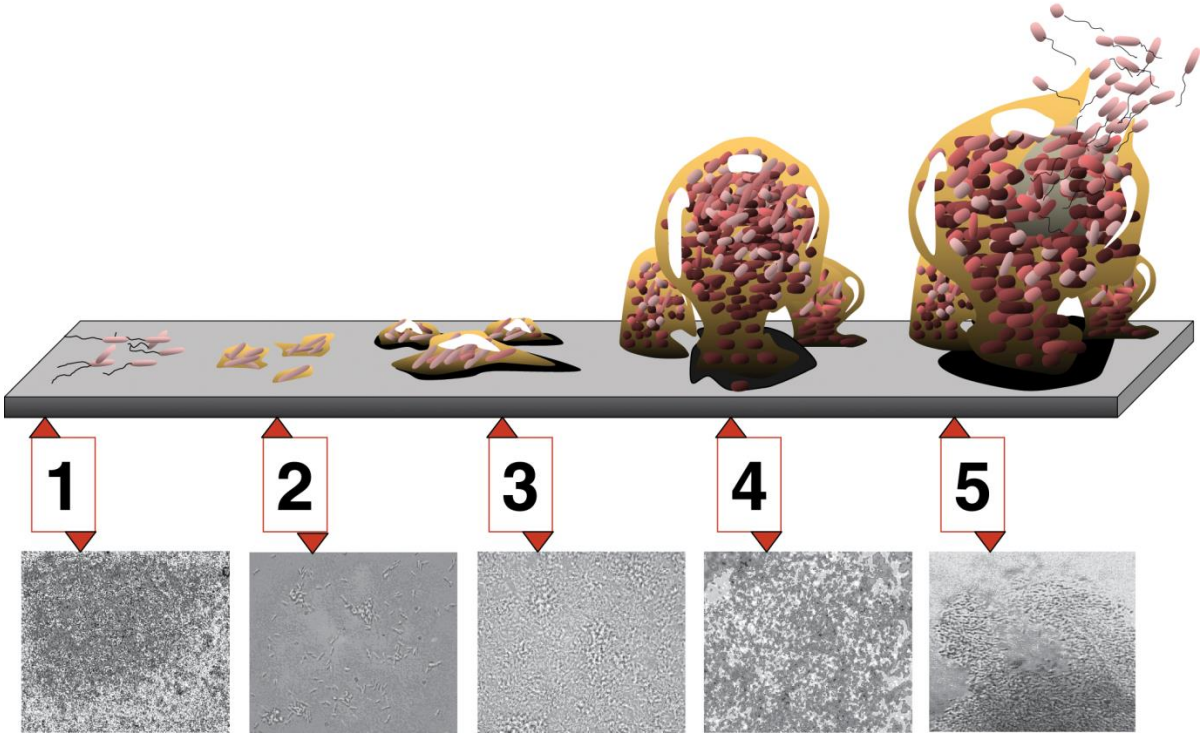

Figure 4. Biofilm formation process which involves five stages: initial attachment (1), irreversible attachment (2), maturation (3 and 4) and dispersion (5) [18]. Images represent the development of the *Pseudomonas aeruginosa* biofilm and are all shown to the same scale. Image was taken from [18].

2.2.3. Adverse effects of bacterial biofilms

The formation of bacterial biofilms leads to several adverse effects with both medical and economic consequences. Several bacteria such as the *Staphylococci*, are associated to infections of medical devices. They opportunistically infect a host, weakened by invasive medical intervention, chemotherapy or a pre-existing disease state [19]. These bacteria also colonize the skin appearing in wounds and implants [22]. Bacteria have many possible points of entry into the body, *e.g.* via catheters, hip replacement, and periodontal disease [19].

Regarding the economic consequences for the marine industries, biofouling poses threats to the safe and efficient operation of vessels and equipment and consequently leads to enormous economic losses for maritime industries [3] (see chapter 2.1). Bacteria have been considered to be involved in the first steps of the biofilm formation. They have been shown to induce settlement in many invertebrate phyla [9], *e.g.* larvae of the tubeworms

Hydroides elegans [23-25] or algae [26, 27]. Hence, the investigation of bacterial adhesion is required in order to facilitate the development of antifouling coatings and aquaculture.

2.2.4. Mechanisms of bacterial adhesion

Microbial biofilms attach to the surfaces by means of their extracellular polymeric substances (EPS) [28] (see chapter 2.2.2). Nonetheless, the mechanisms employed by bacteria to adhere are complicated and diverse. Bacteria are capable of complex assemblage behavior through bacterial quorum sensing (QS) [29] which is a cell-cell communication and gene regulatory mechanisms which allows them to coordinate swarming, biofilm formation, stress resistance, and production of toxins [30].

Furthermore, two physico-chemical approaches describe microbial adhesive interactions. The thermodynamic approach is based on surface free energies of the interacting surfaces and does not include an explicit role for electrostatic interactions. The interacting surfaces are assumed to be in contact with each other under conditions of thermodynamic equilibrium *i.e.* reversible adhesion [31].

Alternatively, the classical DLVO (Derjaguin, Landau, Verwey, Overbeek) theory of colloid stability describes the interaction energies between the interacting surfaces. This approach is based on van der Waals and electrostatic interactions and their decay with increasing distance [32]. Van der Waals forces are generally attractive and result from induced dipole interactions between molecules in the colloidal particle and molecules in the substrate [33]. DLVO interactions determine the characteristic hydrodynamic shear forces to prevent adhesion and to detach adhering micro-organisms. These theoretical calculations have been used to predict the shear forces for bacterial detachment which was experimentally measured using a parallel plate flow chamber [34].

2.3. Cobetia marina

The bacterium nowadays called *Cobetia marina* has been classified and designated differently over time. This is the reason why it is described in the literature under

different names such as *Delaya marina* [35, 36] or *Halomonas marina* [37, 38], even though all refer to the same species, first described by Cobet et al. as *Arthrobacter marinus* [39]. Nonetheless, it was later proposed as *Pseudomonas marina* [40] before being reclassified within the genus *Delaya* [41]. The genera *Delaya*, *Halomonas*, *Halovibrio* and the species *Paracoccus halodenitrificans* were later unified under the generic name *Halomonas* [42]. Analysis of rRNA performed in 2002 suggested that *Halomonas marina* forms a branch clearly separated from *Halomonas* [43]. Later, detailed study based on phenotypic research found evidence to place this species in a new genus, *Cobetia* [44]. The results showed that phylogenetically *H. marina* was too far from other *Halomonas* species to be considered a species of the same genus. Thus, *H. marina* was transferred to a new genus, *Cobetia* gen. nov., as *Cobetia marina* comb. nov. in the family *Halomonadaceae* [44].

The description of *Cobetia marina* is based on several publications. It is a gram-negative marine bacterium which grows in the temperature range from 10°C to 42°C, and between pH 5 and pH 10. This bacterium is used as a model system for marine biofouling [36] because of several features: it is obligatory aerobic, thus allowing an easy handling, and cultures grow rapidly at ambient temperatures. Additionally, *Cobetia marina* is of interest since its biofilms influence secondary colonization by invertebrates and algae [36]. The strain used in this work (DSMZ 4741) is not motile and isolated from a coastal sea sample near Woods Hole (Massachusetts, USA).

2.4. Methods to quantify bacterial adhesion strength

Since fouling-release coatings do not prevent settlement *per se* [45], various methods to evaluate or quantify the adhesion of fouling organisms on these coatings have been developed. The adhesion strength is a highly important value as it quantifies the strength of interaction between cells and surfaces.

Methods to measure cellular adhesion strength have been recently reviewed [46] and can in general be divided into three classes of adhesion assays: centrifugation, micromanipulation and hydrodynamic shear. Hydrodynamic shear assays include spinning disk, radial flow chamber and parallel flow chamber, whereas micromanipulation methods comprehend cytodetachment and micropipette aspiration.

Nonetheless, the most commonly applied techniques for measuring bacterial adhesion strength are assays based on cytodetachment or the parallel plate flow chamber. All techniques have advantages and disadvantages concerning *e.g.* statistics, or applicability in terms of sample handling.

2.4.1. Cytodetachment

Cytodetachment is a technique based on the use of an atomic force microscope (AFM). The cantilever of the AFM is brought into contact with a bacterium attached to the surface. Then, the cell wall is pushed until the elastic restoring cantilever force overcomes the interaction force between the bacterium and the surface under study. Then the cantilever is pulled away from the bacterium yielding an estimate of the attractive force as function of the distance [47]. The force is calculated from the deflection (x) and the stiffness *i.e.* spring constant (k) of the cantilever:

$$F = k \cdot x \tag{1}$$

This method has been used to measure bacterial adhesion regarding infections of medical implants [48], hospital-acquired infections [49] and invasive-tissue [50, 51].

2.4.2. Parallel plate flow chamber

This technique has two main advantages: the flow is well-defined and the chambers can be mounted on the microscope to allow live observation of the organisms during the assays. The chamber usually consists of a sandwich construction of a thin gasket and the investigated substrate between two plates. The bacterial suspension is seeded inside the chamber. Bacteria attached to the bottom of the chamber are subjected to the volumetric flow (Q) by creating a pressure gradient along the channel. As a result, the cells detach from the surface. The principle of this method is shown in Figure 5. The shear stress generated on the walls (τ) can be calculated by Poiseuille´s model [52] as:

$$\tau = \frac{6Q\mu}{h^2 w} \tag{2}$$

This formula can be applied when the height (h) is significantly lower than the width (w) of the chamber [53]. Besides the geometry of the chamber, the shear stress depends on the viscosity of the medium (μ). The results obtained with this simple model are in good agreement with more elaborate calculations which constructed 3-D models that emulate either a flat cell or a dome-shaped cell using a computational fluid dynamic software [54].

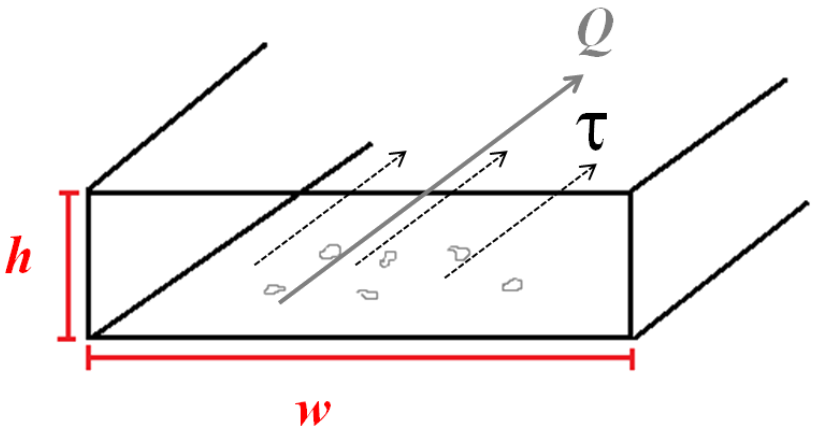

Figure 5 Scheme of the parallel plate flow chamber. The bacteria detach as a result of the shear stress which is uniform within the central area of the bottom of the channel.

Recently, C. Christophis *et al.* developed a parallel plate flow channel setup consisting of four channel systems in parallel [55], hence the investigation of different surfaces under the same conditions is possible. This assay allows to apply shear stresses on the surfaces over a range of nearly six orders of magnitude and has been applied to measure the adhesion of mammalian cells [55-57] on various surfaces such as SAMs or polysaccharide coatings.

2.5. Microfluidic systems

Microfluidics can be described as the science and technology of systems which manipulate or process small amounts of fluids (10^{-9} to 10^{-18} liters). This area of research employs various devices, such as hydrodynamic systems, like the one used in the course of this thesis, or lab-on-a-chip systems, which handle extremely small fluid volumes down to less than picoliters. For that, channels with dimensions of tens to hundreds of micrometres are used [58].

Molecular biology is one of the fields of application of microfluidic systems. Besides measuring the adhesion of organisms [15, 59], as described in the course of this thesis, microfluidic devices are also utilized to characterize the mechanical properties of soft viscoelastic solids such as bacterial biofilms [60].

Another application of these systems is point-of-care diagnostics. The pioneer in the field of microfluidics, G. Whitesides, developed microfluidic paper-based analytical devices. Their fabrication is based on patterning sheets of paper into hydrophilic channels (paper) within hydrophobic barriers [61]. They are inexpensive, easy to use, and designed specifically for use in developing countries, where people cannot afford modestly expensive tests. Even in industrialized nations, typical tests conducted to diagnose disease are expensive. Thus, they are only applied when symptoms appear, nevertheless irreparable damage may have occurred already. For such reasons, there is the need for an economical method to easily diagnose certain diseases, for example by measuring markers of liver function [62].

2.6. Diatoms

Diatoms are unicellular brown algae characterized by their ornate, silicified cells walls also called frustules, which consist of overlapping valves. They can be classified according to their valve symmetry as pinnate (bilateral) or centric (radial). The centric forms are mostly planktonic, whereas the pinnate forms are generally benthic [63]. The latter have been identified as major marine foulers [64]. Diatoms are passively carried to surfaces by the action of water movement and gravitation. With the exception of the motile male gametes, they lack flagella [63]. Consequently, they are not able to select where they attach to. However, after contact with the substratum, a process called gliding is initiated in order to stabilize and reorient the cell [65]. For both motile and sessile adhesion, cells adhere to the surface by secretion of extracellular polymeric substances (EPS) [1].

2.7. The influence of surface properties on bioadhesion

Antifouling coatings can be divided into two groups namely “non-fouling” and “fouling release” coatings. A coating is considered as “non-fouling” if it is able to inhibit the attachment of organisms, whereas “fouling release” refers to those coatings on which the organisms adhere only weakly allowing their release by applying low shear stresses. The effectiveness of antifouling coatings has been found to depend on their properties [12].

Figure 6 displays a collection of such properties which have the potential to affect biofouling. One of the surface properties most frequently investigated is topography, as structured surfaces are a widely used strategy in nature to control environmental interactions. Thus, this fact stimulated the development of bio-inspired surfaces. Two famous examples of biotopography are the lotus and shark skin. The hierarchical structure of the lotus leaf combined with the secreted wax minimizes the contact of water to the surface. This lotus-effect has been imitated by hierarchical synthetic surfaces [66]. Furthermore, in the marine environment the skin of some animals such as the pilot whale, rockfish or crabs has been found to repel biofoulers. Thus those biotopographies were applied successfully in bio-mimetic coatings [2, 67-69].

In the course of this PhD thesis, the surface properties chemistry, wettability, hydration, molecular conformation and porosity were investigated in detail.

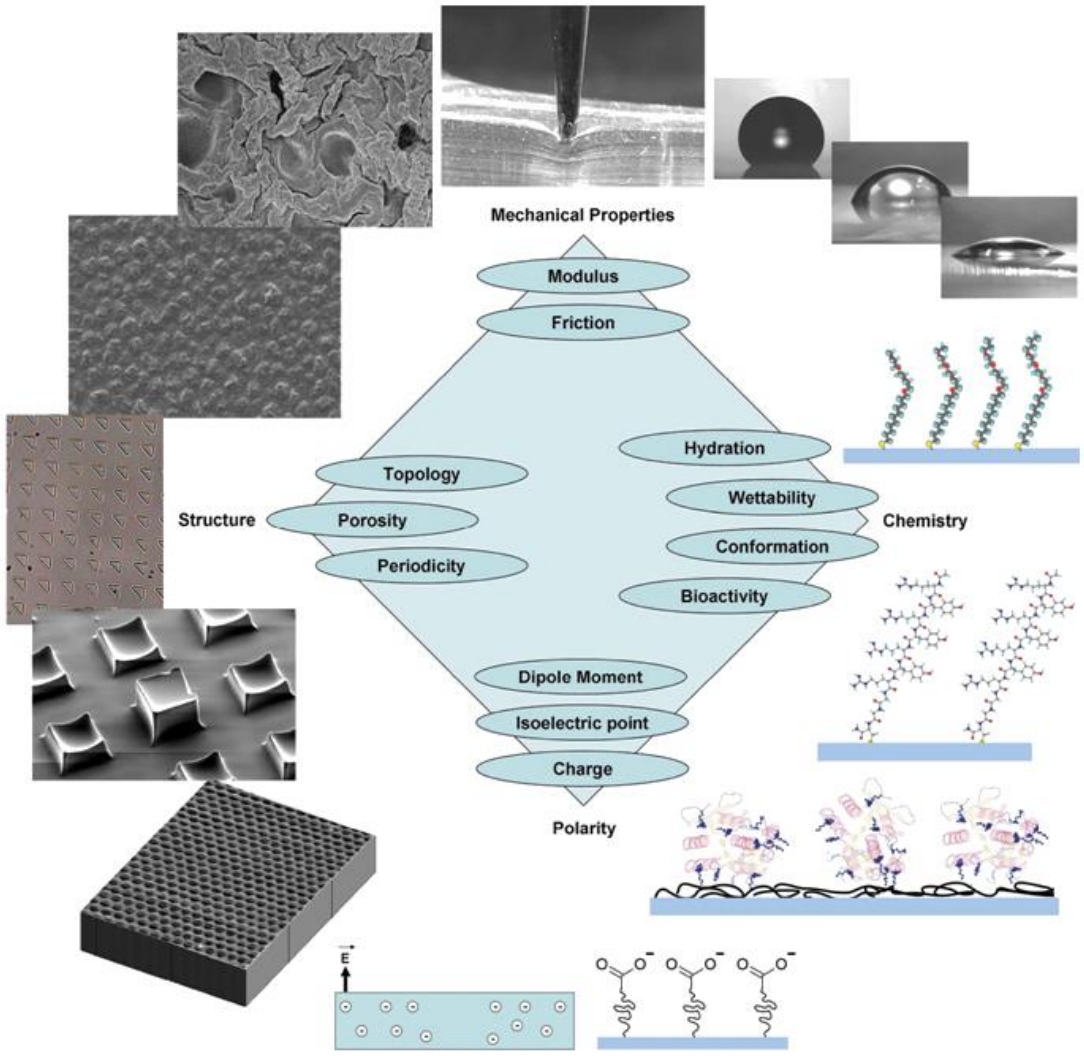

Figure 6. Surface properties relevant for biofouling and development of antifouling coatings [12].

2.7.1. Influence of chemistry

The wettability and surface energy properties are closely related to the chemistry of the surface. To investigate the effect of substratum physicochemistry on bioadhesion, well defined model systems with tunable surface properties are required.

The pioneering work of Nuzzo and Allara demonstrated the stability of self-assembled monolayers (SAM) [70], which led to widespread use of these coatings to investigate the impact of surface chemistry. Hence, SAMs of differently terminated alkanethiolates on gold were chosen as a convenient model system for systematic investigation since they

are highly useful tools to reproducibly prepare coatings with tunable properties in a well-defined manner [71-73]. One major advantage is that the mechanical properties are determined by the substrate while physicochemical properties are determined by the thin organic film. SAMs have been frequently applied to study protein adsorption [74-76], response of mammalian cells [55, 77, 78] and marine biofoulers [15, 35, 79-83] as well as for nanotechnology applications [72, 84].

Numerous studies have shown that the colonization of surfaces by marine organisms depends on their physical and chemical properties, influencing, for example, the biomass accumulated of marine bacteria [35, 82] and algae [83, 85, 86]. In order to disentangle the effect of wetting, hydration, charge, morphology and modulus, model surfaces have increasingly been used in screening tests in recent years [12, 67, 87-91]. A general relationship (albeit with many exceptions [92]) between surface energy and the tendency of a surface to accumulate biomass is known as the Baier curve [93]. Adhesion on surfaces with contact angles below 65°, the Berg limit, is often connected with the balance of water-surface and water self-association [94, 95]. While some studies see clear correlations in adhesion and fouling behavior of selected species with the contact angle [35, 50, 81, 82, 86, 96-99], other studies report only poor or no correlation at all [100, 101] such as the ones which showed that the bacterium *Cobetia marina* and zoospores of the alga *Ulva* adhered equally or even more strongly on some hydrophilic surfaces than to hydrophobic surfaces [15, 80].

2.7.2. Influence of hydration

Previous studies suggested that hydration of the surfaces is an important prerequisite to reduce the adhesion of protein and organisms [6]. One of the most commonly investigated classes of hydrated coatings are ethylene glycol (EG) containing SAMs which are well-known for their protein resistance [102-104], especially polyethylene glycol (PEG) coatings. Nonetheless, recent studies report the gradual degradation of PEG SAMs during long-term experiments [85, 105, 106] impairing their potential as commercial coatings. Liedberg et al. developed a hydrogel prepared by UV-initiated free radical polymerization of the monomers, 2-hydroxyethyl methacrylate (HEMA) and PEG methacrylate that

shows a slow degradation process and additionally inhibits the settlement of a wide range of fouling organisms [107, 108].

Functional groups of the SAMs which contain hydrogen bond acceptor groups but not hydrogen bond donor groups were found to be a prerequisite for surfaces with inert properties [104]. That is likely the reason why EG SAMs with just one EG unit present less resistance against protein and diverse organisms compared to the longer homologues [55, 83] as its hydroxyl oxygen atom acts as a hydrogen bridge donor, and not as an acceptor [6]. Besides, the resistance of EG SAMs to protein adsorption and biofouling can also be explained by the steric repulsion theory [109]. In order to demonstrate that hydration is not the only essential factor which determines the inertness of surfaces, some studies showed that resistance to protein [103] and adhesion of algae cells [86] on EG SAMs with systematically changed wetting properties decreased with increasing wettability.

Another class of hydrated promising anti-fouling coatings are polysaccharides (PS). Their functional variety is extended since the carbohydrate molecular backbone of the monosaccharide has a large number of stereocenters. The PS surfaces which frequently have been investigated are hyaluronic acid (HA), alginic acid (AA), peptic acid (PA) and chondroitin sulfate (CS) which are acidic and highly hydrophilic and build up of a similar carbohydrate backbone but differ in the composition of their functional moieties. HA and CS are natural occurring glycosaminoglycans, composed of repeating di-units of hexauronic acid and a hexosamine [110-113], while PA and AA are more common as constituents within plant cells. AA is also a major component of the extracellular polymeric substances of bacterial biofilms [110] and the cell walls and mucilages of brown seaweeds [114].

The polyssacharides HA, AA and PA were found to be very resistant to protein adsorption and bacteria and cell adhesion [115-117], but they were not able to inhibit adhesion of marine fouling organisms [114]. This observation is due to the presence of bivalent cations in the marine environment as they can be coordinated and bound by the polysaccharides leading to the collapse of their structures and a displacement of water (syneresis). Such coordination is possible due to the deprotonation of the carboxyl group at the neutral pH of seawater. The resulting collapse can be described as the egg-box

model [118] and is based on the induction of calcium cations to the gelation of alginates and pectins [119].

In recent work the free carboxyl-groups of the polysaccharides were modified by capping with the hydrophobic amine trifluoroethylamine (TFEA) in order to prevent this collapse [120]. The hydrophobic capping adds amphiphilic properties to the hydrophilic polymer network [88, 121, 122] and shifts the contact angle to the minimum in the Baier curve [94, 95]. Laboratory assays with a range of test organisms revealed an improvement of the performance of hyaluronic acid coatings [120].

2.7.3. Influence of the conformation of the molecules

Several studies determined the diverse chain conformations which can be adopted by differently hydrated EG SAMs [123-126] showing that the ability of the SAMs to resist protein adsorption depends on the molecular conformation of the EG moieties [102, 127, 128]. The penetration of water molecules into the interior of the SAM leads to a lateral compression of EG monolayers resulting in more highly ordered layers causing an increased protein resistance [103]. Wang *et al.* showed that the SAM surface of helical EG chains provides a template for water nucleation which might consequently prevent a direct contact between protein and surface, whereas water is not stable on a surface with planar EG strands [128].

Further studies investigated the interaction of water molecules with the oligomer chain of the EG terminated SAMs. However, those observations are based on theoretical calculations such as Monte-Carlo simulations [129], density functional calculations [125, 130] or the Hartree-Fock method [128]. The latter demonstrated that water binds more strongly to the helical conformer than to the all-trans conformer, mainly due to the fact that hydrogen bridge bonds can be formed between the hydrogen atoms of water and neighboring oxygen atoms along the chain.

Harder *et al.* used IRRAS to investigate in detail the molecular conformation of hydroxy- and methoxy-terminated EG_3 and EG_6 SAMs and their influence on protein resistance. The study showed that an amorphous or helical conformation decreased protein adsorption while a densely packed all-trans form adsorbed protein [102, 131] suggesting

the importance of interfacial water bound by the EG moieties for resistance to protein adsorption.

Numerous studies focused on the characterization of conformation and properties of EG SAMs containing amide or ester groups which contribute to stabilizing the molecule [124, 126, 132, 133], or a methoxy end-group [102, 103]. Liedberg *et al.* investigated the influence of the lateral hydrogen-bonding groups on the temperature-programmed desorption of EG terminated SAMs with one or four EG moieties containing –COHN- and –COO- linking groups by IRRAS [134]. The study showed that the desorption process of EG_1 occurred by the disordering of the alkyl chains followed by a complex series of decomposition/desorption reactions, whereas the desorption process of the EG_4 occurred by the loss of the oligomer portion and the desorption of the alkylthiolate part of the molecule.

2.7.4. Influence of the transition from monolayers to polymeric coatings

Besides the investigations toward the application of PEG coatings (chapter 2.7.2), a wide range of studies has tested diverse polymer coatings with regard to bioadhesion. A considerable number of such studies were focused on the topographical features of the surfaces. A.B. Brennan *et al.* have been working on mimicking shark skin using polydimethylsiloxane (PDMS) elastomer structures [68, 91, 135, 136]. Further studies investigated the performance of other polymer coatings on poly(methyl methacrilate) (PMMA) [137] with topographical features of different sizes in regard to the adhesion of the fouling green alga *Ulva linza*. Results revealed that the topographical size of the features must be less than the critical size of the organisms.

As another kind of polymer, surface-grafted thermally responsive polymer coatings poly(*N*-isoprophyacrylamide) (PNIPAAM) were synthesized and tested [37, 138] exhibiting bacterial release properties, although various difficulties were encountered with the grafting procedure which led the scientists to explore alternative methods like the formation of SAMs of PNIPAAM-terminated alkane thiolates on gold [139, 140]. Subsequently, uniform PNIPAAM brushes were produced showing a considerable effect on bacterial detachment.

To date, one of the most common scientific approaches to reduce protein adsorption on a surface is based on coatings containing ethylene glycol, especially the polymeric one PEG (see chapter 2.7.2). Even though it is still researched, the mechanisms why which PEG resists protein adsorption is generally attributed to its hydrophilicity and its hydration which is provided through the ethylene glycol (EG) content. Thus, a protein resistance even better than the one of PEG can be expected for those polymers with a higher number of EG units.

Recently, Chilkoti *et al.* developed poly[oligo(ethylene glycol)methacrylate] (POEGMA) brushes [141-143] by surface-initiated atom transfer radical polymerization which present a promising biomedical application. Since the stability of EG based coatings is limited due to the degradation of the polymer [85, 105, 106, 144] we hypothesize that a methacrylate backbone of the POEGMA brushes stabilizes the ethylene glycol hydrogel and thus delays its degradation.

2.7.5. Metal organic frameworks: controlled release of copper

Metal-organic frameworks (MOFs) are highly porous and highly ordered materials which have been used in various applications such as the storage of small molecules, nanotechnology or drug delivery [145-147]. Such frameworks are very well suited for surface modifications, thus their properties can be tailored by using diverse binding units for the framework [148] to optimize the MOFs for specific applications. MOFs feature some similar properties to the zeolites such as the inorganic porous structure. Nonetheless, their variability is substantially larger since they have a considerable number of combinations established by the organic linkers and the connectors which can be inorganic, metallic or metal-oxo.

There are diverse approaches to synthesize MOFs. Lately, the liquid phase epitaxy (LPE) method was introduced to obtain crystalline, highly oriented layers of MOFs on modified gold substrates [149], also referred to as SURMOFs. Recently, a homogeneous coating based on a $(Cu^{2+})_2$ or $(Zn^{2+})_2$ paddle-wheel based 2D structure with benzene-1,4-dicarboxylic acid (bcd) as linker and grown using LPE was synthesized [149]. Such MOF is referred to as Cu- or Zn-SURMOF 2.

The stability of Cu-SURMOF 2 in water, ASW and cell culture medium has recently been investigated [150] and it was shown that these MOFs are stable in both Milli-Q® and ASW for at least one hour. Their compatibility regarding cell culture was demonstrated as the release of Cu^{2+} ions resulting from the dissolution of the Cu-SURMOF 2 in the cell culture medium did not exhibit any inhibitory effects on the adhesion and proliferation of fibroblasts [150].

2.8. Copper based coatings

Copper based coatings being currently the working horse of the coating industry [3, 151] are frequently applied on ship hulls to control biofouling. They are applied either as conventional paint, as ablative coating or embedded into a self-polishing matrix [151, 152]. Current research aims on assessing the performance of these coatings and to reveal if frequent mechanical cleaning yields enhanced protection [153, 154]. However, the damaging effect of the copper released by those coatings on the marine ecosystem has been shown [155-158]. Consequently, the legislation increasingly restricts coatings that constantly release biocides and in some areas of Europe the use of copper based coatings is already restricted *e.g.* for recreational vessels [5, 152, 159]. As an example for the amount of copper release, a copper based coating with a low biocide output of 20 µg/cm^2/day applied to a 65,000 Gross Registered Ton container ship with a length of 260 m releases 950 kg copper per year into the ocean [151].

Thus, the development of a material which avoids the uncontrolled liberation of biocides into the ocean is required. At this point, the question arises whether a new class of smart coatings would be capable of releasing copper only if the target organisms are attached.

2.9. Importance of field tests

Many biological laboratory assays with single species have been established to screen different surface chemistries with respect to their antifouling properties. While such studies are suitable to identify promising formulations, field tests finally reveal whether the respective coatings fulfill the hope raised by the results obtained in the laboratory.

Numerous groups have been performing different types of field tests around the world. In the group of G. E. Swain at the Florida Institute of Technology (FIT), scientists have been performing field tests at Florida's Atlantic coast over weeks and months to test commercial antifouling coatings [45, 154, 160-163]. Some studies collected samples directly from the nature such as mangroves from Bahía Magdalena, Mexico [164], oysters and surrounding water from the Mediterranean coast at Valencia, Spain [165], water of the Indian River Lagoon, USA, [166] or adjacent coastal water along the Suwannee River, USA [167]. Various investigations focused on single specific organisms such as the sponge *Rhopaloeides odorabile* of the Great Barrier Reef, Australia [168] or the tubeworm *Hydroides elegans* of Pearl Harbor, USA [169]. Even if some studies investigated the occurrence of mixed species attached to surfaces, it was only on glass slides [170].

Despite these studies, there is a lack of information about the composition of the initial fouling communities in field experiments on chemically and structurally well-defined model surfaces. Furthermore, since the usual laboratory assays report solely information about single species of organisms, a study regarding the influence of surface properties such as chemistry and hydration on the adhesion of diverse marine organisms in their natural environment is required.

3. Material and Methods

3.1. Bacterial culture

The marine bacterium *Cobetia marina* was used in this work. This aerobic, gram negative bacterium was obtained as dried culture from the DSMZ ("deutsche Sammlung von Mikroorganismen und Zellkulturen", german collection of microorganisms and cell cultures; GmbH, Braunschweig, Germany) (DSM 4741). The bacterial vials were inoculated in 50 ml of marine broth (MB) (2216, Difco, Augsburg, Germany) previously sterilized containing 20 % glycerol. This solution was divided into aliquots of 1 ml and stored at -70°C. MB and artificial sea water (ASW, Instant Ocean, Mentor, Ohio, USA) were prepared according to the manufacturer´s instructions. Marine Agar (MA) was prepared by addition of 2 % Bacto agar (Difco) to MB. Bacteria from frozen stock aliquots were streaked onto MA plate with a previously sterilized inoculating loop following the streak pattern shown in Figure 7. This pattern was used since it allows the formation of individual bacterial colonies. The resulting agar plates were stored at 4°C for a maximum of 4 weeks to avoid possible mutations. The culture method used was a batch culture. For the experiments, a single colony from an agar plate was inoculated into 20 ml sterile MB and grown overnight while shaking on a vibrational table (65 rpm) at room temperature (≈ 21°C).

Figure 7. Streak pattern of an agar plate.

The increase of the optical density at 600 nm wavelength (OD_{600}) with time was measured using a spectrophotometer (Du-70, Beckman Coulter, Krefeld, Germany) in MB in order to determine the different phases of bacterial growth (see chapter 2.2.1). A shown in Figure 8 *C. marina* reached the log phase at an OD_{600} of approximately 0.1 as this value is nearly in the middle of the exponential growth phase. After an overnight culture (≈ 12 h) the bacteria reached the stationary phase with an optical density of $OD_{600} > 1$.

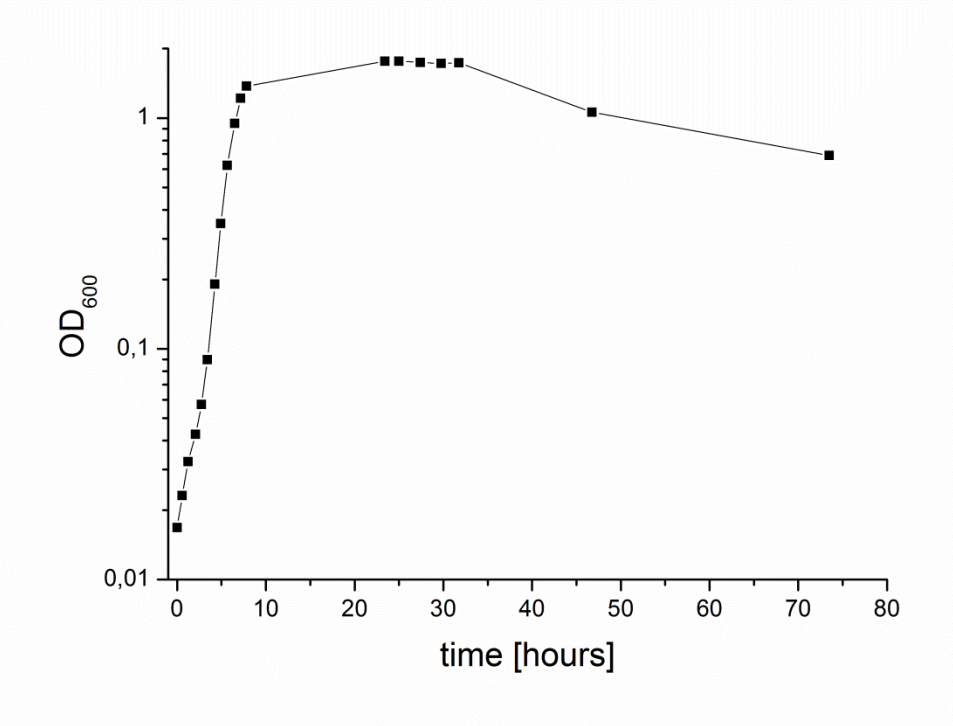

Figure 8: Growth of *Cobetia marina* in MB as measured by OD_{600}.

Most assays described in the literature work with bacteria in the log phase for adhesion experiments [14] as these results are most reliable. Thus, the optical density 0.1 was selected for all bacterial assays performed during this work. To bring the bacteria into the log phase, the overnight culture was diluted 1:100 in MB and held in liquid culture for nearly 3 h. After this, the OD was measured every ≈ 20 min until the desired OD_{600} of 0.1 was reached. This normally took around 4 h. Depending on whether the incubation medium used for the experiments was MB or ASW (see chapter 4.2.1), the bacterial suspension was immediately used for the microfluidic assay or inoculated in ASW prior to the experiments. In order to change the bacterial medium from MB to ASW, the bacterial suspension was harvested by centrifugation (Mikro 22 R, Hettich, Tuttlingen, Germany) for 2 min at 15°C and 10,000 rpm which provided an acceleration force of 9727 g. The resulting pellet was washed and resuspended in sterile (0.45 µm filtered) ASW to remove any residual MB. Prior to use in the detachment experiment, the bacterial suspension was filtered through a 5 µm filter to remove larger bacterial aggregates.

3.2. Microfluidic shear stress device

The microfluidic detachment system used in this work was recently described by C. Christophis in our group [55]. It was developed to quantify cell [55-57] and bacterial adhesion [15]. This microfluidic shear stress device features many advantages as only small surfaces and sample volumes are required, multiple experiments can be run in parallel, sample surfaces can easily be exchanged and shear stresses over a range of nearly six orders of magnitude can be applied (from ≈0.01 dyn/cm^2 to ≈5,500 dyn/cm^2). Furthermore, duration of the experiments is very short (4.5 min). The main advantage of this detachment assay probably lies in the fact that typically roughly 400 bacteria can simultaneously be investigated since their individual detachment over a large range of shear stress is recorded. In contrast to many other approaches, the cell density is accurately known from the beginning of the experiment and, as the field of view remains unchanged, it is possible to work with exactly the same initial seeding density over the entire experiment. In order to minimize the biological variability and duration of the experiments, four sets of surfaces are investigated in parallel with the same batch of bacteria in the same physiological state.

The microfluidic setup basically consisted of four channel systems (see chapter 3.2.1) as shown in Figure 9c which were mounted on a base plate and placed onto the motorized stage of an inverted microscope (TE-2000-U, Nikon, Tokyo, Japan, Figure 9a). Each of the four channel assemblies was connected to the inlet, a liquid reservoir which was pressurized with nitrogen to approximately 700 mbar as shown in Figure 9b. This pressure did not influence the bacteria negatively, since a pressure of 700 mbar is equivalent to the water pressure in 7 m depth where the bacteria can be found in nature [171]. The outlets of the channels were connected to a syringe pump through selection valve (Figure 9a). The applied overpressure assisted the pulling syringe pump at high flow rates. Bacteria were inoculated in the system (Figure 9c). Incubation and detachment process were carried out at room temperature (≈ 21°C).

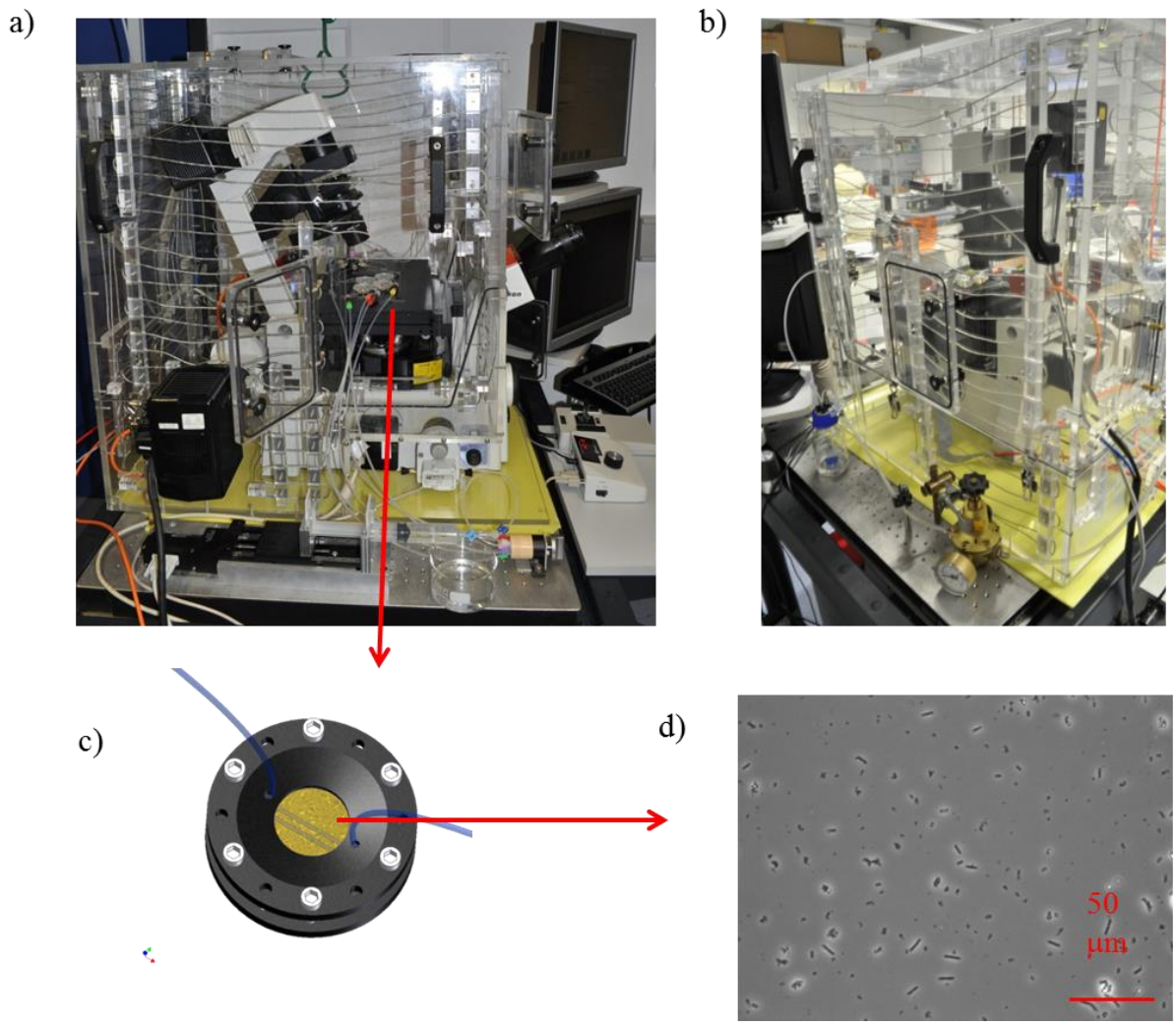

Figure 9. Images of the microfluidic setup: outlet (a) and inlet (b) of the channel system, and one of the channel assemblies (c) showing a typical observed field of view during the experiments (d). Scale bar represents 50 µm.

3.2.1. Channel system

The microfluidic channel assembly consisted of a "sandwich" system with a poly(methyl-methacrylate) disc as top and a aluminum plate as bottom. For the liquid inlet and outlet two holes with a distance of 12 mm were drilled through a 2 mm thick float glass (20 mm x 20 mm) using a diamond tip drill. Top disc and the glass float used as lid were sealed by a 4 mm thick ring which was glued on top of the glass lid. The channels and the rings were made of polydimethoxysiloxane (PDMS, Sylgard 184; Dow Corning, Midland, MI) [172]. Channels which were stored in Milli-Q® (Millipore, Schwalbach, Germany) water and the lids were rinsed with Milli-Q®water and iso-propanol. The channel was positioned onto the upper glass lid and a droplet of ethanol and two cannulae were used to adjust it. After the ethanol

was evaporated, the samples were placed on the platform and the channel systems were mounted one by one. Figure 10 shows the resulting channel assembly.

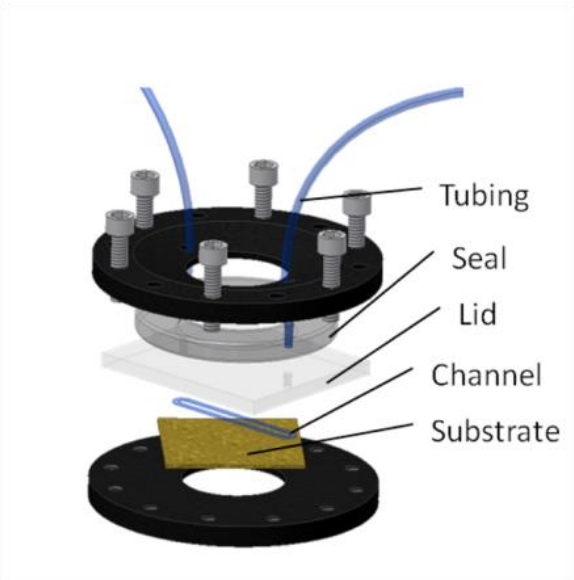

Figure 10. Scheme of the microfluidic channel assembly. Image taken from [59].

All of these elements were tightly interconnected together with polyfluoroalkoxy tubings (VIVI AG, Schenkoon, Switzerland) of 1/16" (1.56 mm) for the inlet and the first centimeters of the outlet and 1/8" (3.2 mm) for the rest of the outlet. Thicker tubings were chosen for the rest of the outlet in order to minimize the pressure drop at high shear forces. The sample of interest which was typically 25 mm x 25 mm in size (approximately the same size as a third of a regular glass slide), was placed onto the "window of the 5 mm thick aluminum plate and the channel system was mounted on it. At least three screws fastened alternately were used for fixation of each channel assembly. The final channel dimensions after assembly were approximately 13 mm x 1 mm x 140 µm. Slight changes of channel dimension were possible and taken into account in the calculation of shear stress (see chapter 4.1).

Prior to each experiment, the complete channel assemblies were mounted. The platform with the four channel assemblies was placed on the stage of the inverted microscope (Figure 11), which was located inside a custom built incubator. Tubings were fixed with adhesive tape to the microscope stage in order to avoid vibrations.

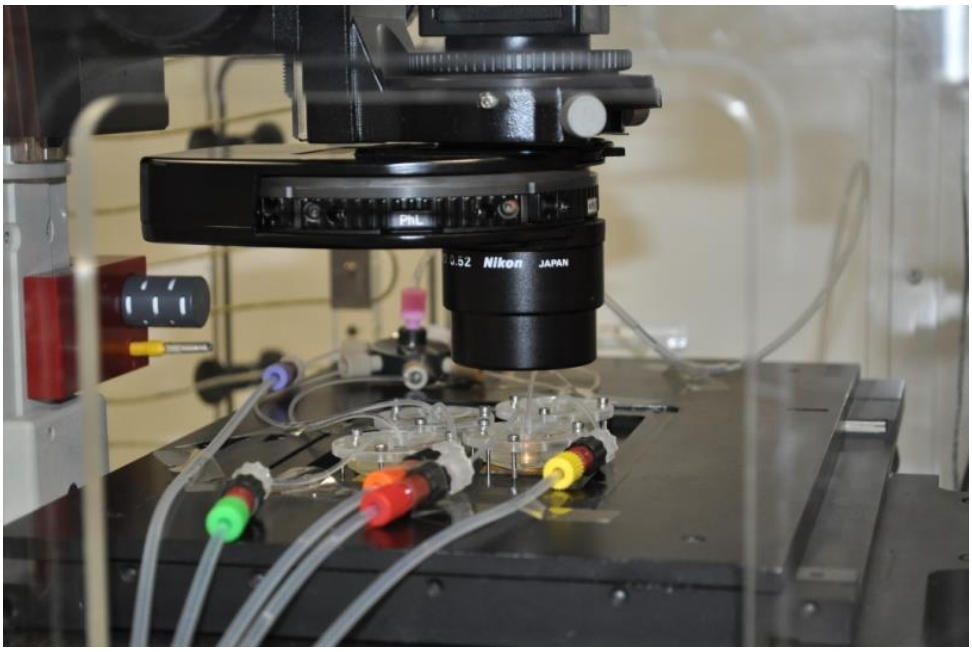

Figure 11. The four assembled channels mounted on the microscope stage.

3.2.2. Applied flow

One of the biggest problems of microfluidic devices is the instability of pressure. To minimize this difficulty and maintain the most reproducible conditions, the whole experiment was done under a nitrogen overpressure of 700 mbar using a precision gas metering valve (Pressluft Götz, Mannheim, Germany). The overpressure served to avoid the formation of bubbles inside the channels and to reach higher maximum flow velocities. Thus, the microfluidic assay was capable of applying high shear stress (up to ≈ 5,500 dyn/cm^2, see chapter 4.1) at the surface of the channel.

Figure 12 shows a scheme of the microfluidic system for one assembled channel. A pressurized reservoir containing the flow medium ASW (Figure 12a) was connected to a manifold connector (Upchurch 7-Port (P-150), IDEX Health Science LLC, Oak Harbor, USA, Figure 12b) which was used as a liquid distributor to the channels' tubing inlets and to inject the bacterial solution with a syringe into the channels (Figure 12c). A selection valve (Valco Cheminert C25-3186, VICI AG, Figure 12e) was positioned between the parallel flow channels (Figure 12d) and the syringe pump (Figure 12f). Each individual flow path to the syringe pump was opened by the valve selector. One tube of the valve selector connected

directly to the manifold was used as “by-pass” which was opened during the incubation time in order to equilibrate the channel system and consequently to avoid microflows.

The syringe pump was custom made and computer controlled using a M.403-4DG translation table purchased from PI (Physics Instruments GmbH & Co.KG, Karlsruhe, Germany). Two plastic wedges were required to firmly secure the syringe to the pump and thus, provided a minimal movement of the syringe caused by stage translation.

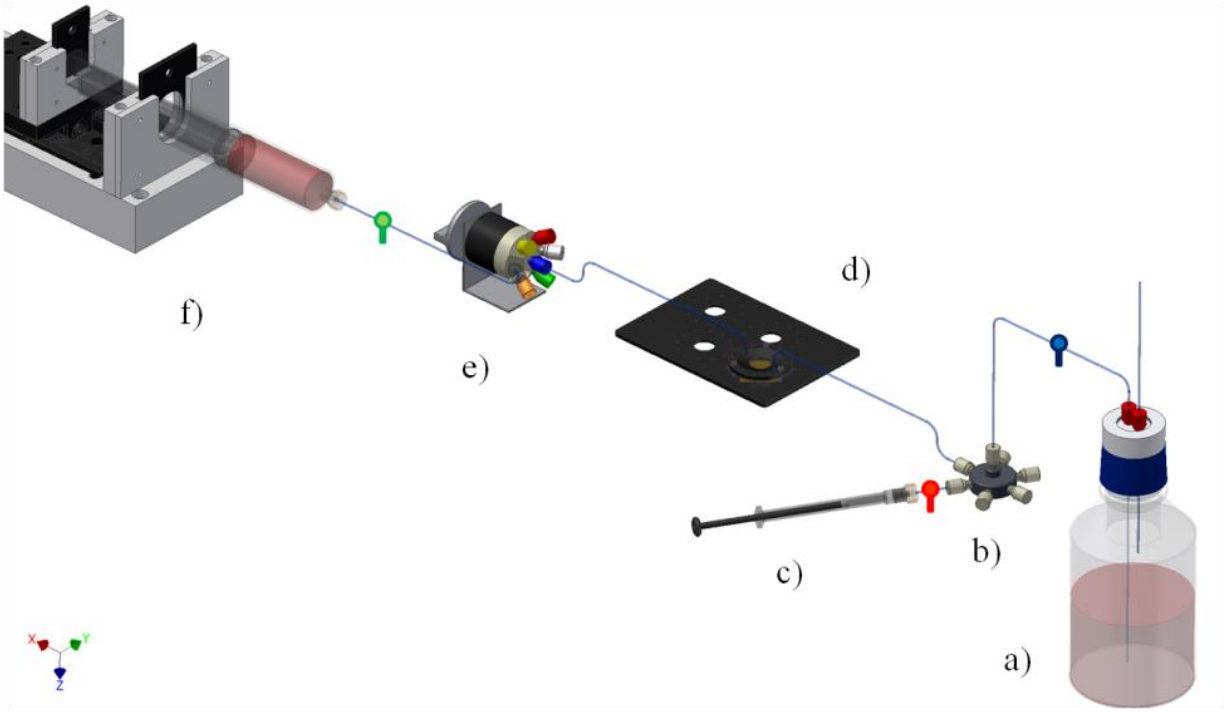

Figure 12. Scheme of the microfluidic flow system. Image taken from [59]. The pressurized reservoir with the flow medium (a) was connected to a manifold connector (b) which distributed the liquid to the channels (d) and through which the bacterial solution was injected by a syringe (c). The selection valve positioned between parallel flow chambers (d) and the syringe pump (f) opened each individual flow path. This valve was connected to the syringe pump (f) which created a flow by pulling the medium through the entire system.

After the incubation time, the pump was started. Its speed was increased stepwise every 5 s by 25.9 %, which resulted in 10 steps for each order of magnitude (Figure 13) and an overall exponential increase of shear stress. The translation stage of the pump was controlled by the software Micromove®. The aspired total volume flow achieved varied in the range of 300 nl/min up to ≈90 ml/min, which corresponds to nearly six orders of magnitude of shear stress.

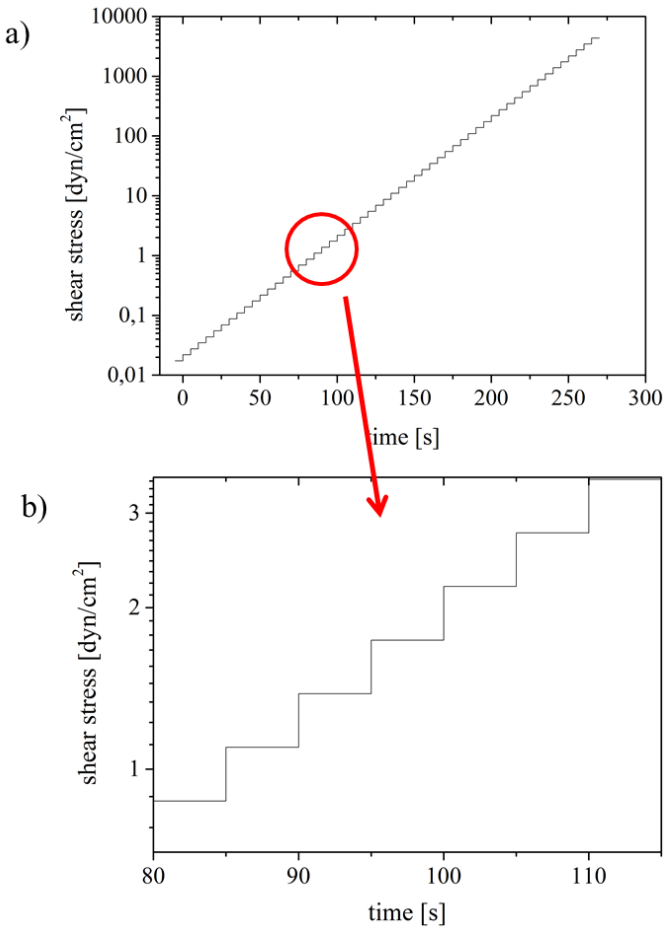

Figure 13. Graphics showing the shear stress applied for a bacterial detachment assay which was time dependent (a) and a magnified part of this graphic (b).

3.2.3. Microfluidic shear stress assay

Prior to the seeding of the bacteria, the microfluidic system was preconditioned with sterile ASW for 5 min. Then the suspension of *Cobetia marina* (OD_{600}=0.1 which corresponds to approximately 10^7 cells/ml) was injected into the channels and bacteria were allowed to adhere for 2 h. After the incubation time, the first channel assembly was positioned over the microscope objective and only in this channel the flow rate was increased stepwise by 26 % every 5 s. The detachment was recorded via video microscopy (TE-2000-U, Nikon, Tokyo, Japan) with a 40x Ph2 objective (field of view of 256 by 192 µm, NA= 0.6) which has a correction ring ELWD. The detachment part of the assay took only 4.5 min. After the detachment experiment in the first channel, the second, third, and fourth channel were positioned in the field of view of the microscope and investigated in the same way.

After the four detachment experiments, the whole fluidic system was purged with nitrogen in order to determine the exact height and width of the channels, which were required for the shear stress calculations (see chapter 4.1). This step was necessary as the motorized focus of the microscope was calibrated to be use in air. Then, the channel systems were dissembled after rinsing with iso-propanol and Milli-Q® water.

3.3. Preparation of self-assembled monolayers

3.3.1. Preparation of gold substrates for self-assembly

Gold substrates were manufactured by Georg Albert (PVD-Beschichtungen, Germany). Extra smooth float glass slides (Nexterion® B, Schott, Mainz, Germany) were used as substrates for deposition of gold films. Thin films of polycrystalline gold were prepared by thermal vapor deposition of 30 nm gold (99.99 % purity) onto glass slides precoated with a 5 nm titanium layer. Evaporation was performed at a pressure of 2×10^{-7} mbar and a deposition rate of 0.5 nm/s, leading to a root-mean-square roughness of approximately 1 nm [173]. Gold substrates were stored under argon until used.

3.3.2. Preparation of self-assembled monolayers

The chemicals used for self-assembly were dodecanethiol (DDT, HS-$(CH_2)_{11}$-CH_3), 11-hydroxy-undecanethiol (HUDT, HS-$(CH_2)_{11}$-OH) and 11-amino-undecanethiol (AUDT, HS-$(CH_2)_{11}$-NH_2), purchased from Sigma-Aldrich (Munich, Germany). 11-tridecafluorooctyloxy-undecanethiol (FUDT), HS-$(CH_2)_{11}$-O-$(CH_2)_2$-$(CF_2)_5$-CF_3) and ethylene glycol (EG) SAMs (hydroxy-n(ethylene glycol)-undecanethiolate, n=mono, tri and hexa (EG_x, HS-$(CH_2)_{11}$-$(OC_2H_4)_x$OH, x=1, 3 and 6) were obtained from ProChimia Surfaces Sp. Z.o.o. (Sopot, Poland). Hydroxy-PEG2000-thiol (PEG, HS-$(CH_2)_2(OCH_2CH_2)_{44}$OH), was purchased from Rapp Polymere GmbH (Tubingen, Germany). Ethanol *p.a.* was also purchased from Sigma-Aldrich. All chemicals were used as received without further purification. The SAMs used for SURMOFs 2 synthesis were 16-mercaptohexadecanoic acid (MHDA) SAMs which were prepared by Zhengbang Wang as described in previous protocols [174]. For this purpose, a MHDA solution was prepared by dissolving MHDA thiol (Aldrich) in a 5 % volume mixture of acetic acid in ethanol to reach the desired concentration of 20 µM.

A clean gold substrate was placed in this solution for 48 h and then rinsed with the pure solvent and dried in a stream of nitrogen.

Figure 14 displays a scheme of the assembly of the SAMs. Prior to the SAMs formation, the gold slides were cleaned in a UV reactor (150 W mercury-vapor lamp, Heraeus Noblelight, model TQ150) for 2 h to remove organic adsorbates from the surface. Subsequently, the substrates were rinsed with ethanol *p.a.* and sonicated in ethanol *p.a.* for 3 min and rinsed again. They were then immersed into the corresponding 1 mM thiol solution in ethanol *p.a.* for 24 h, except for PEG SAMs which required 48 h. After the immersion time, the samples were removed from the thiol solution, rinsed with ethanol *p.a.*, sonicated and rinsed again in order to remove non chemisorbed thiol molecules. Finally the samples were dried in a flow of nitrogen and stored under argon until used for experiments.

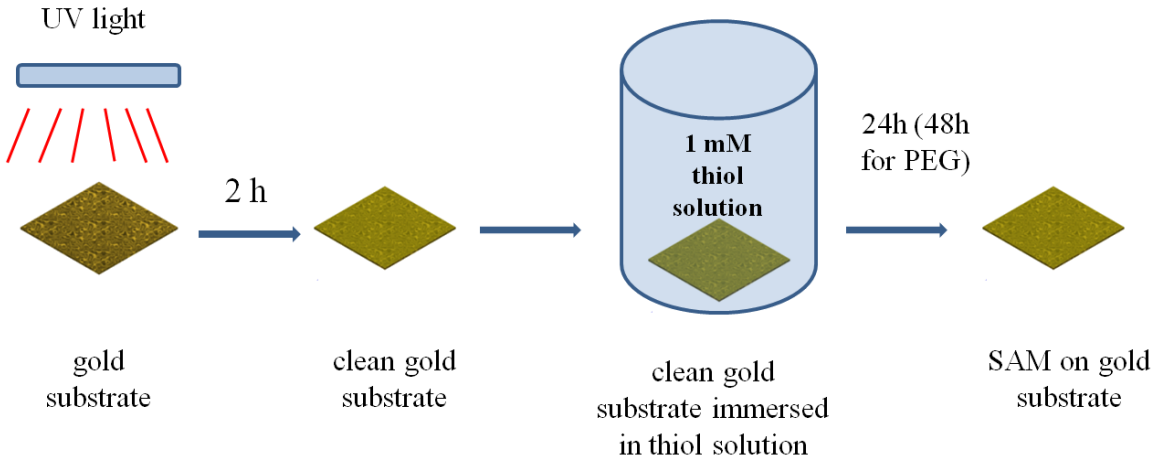

Figure 14. Scheme of the preparation of SAMs. Gold substrate was cleaned by UV light for 2 h, rinsed and sonicated with ethanol and placed into the thiol solution.

3.4. Preparation of Polysaccharides

In this work three different polysaccharides were investigated (Figure 15): hyaluronic acid (HA), chondroitin sulfate (CS) and alginic acid (AA) with and without trifluoroethylamine (TFEA) modification. These surfaces were prepared in our group by Stella Bauer following published protocols [120, 175] as shown in Figure 16.

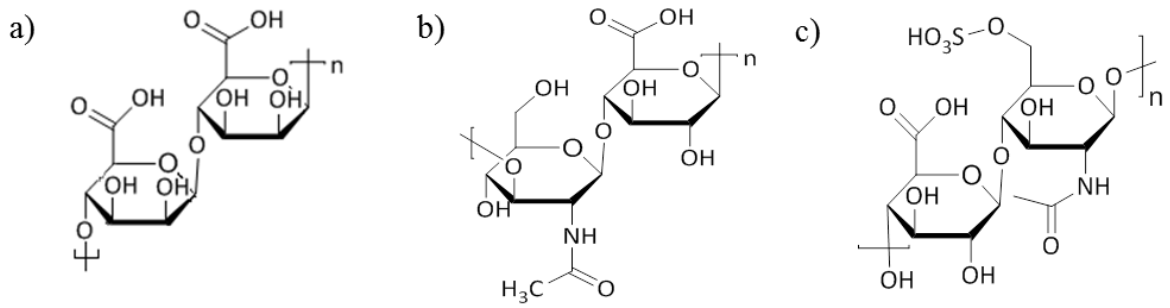

Figure 15. Polysaccharides used in this work: alginic acid (AA) (a), hyaluronic acid (HA) (b) and chondroitin sulfate (CS) (c).

All the chemicals used for the polysaccharide synthesis were purchased from Sigma-Aldrich (Munich, Germany). Nexterion B® glass slides were used as substrates. Glass slides were cleaned by successive sonication for 30 s in solvents of increasing polarity (toluene, ethyl acetate, ethanol *p.a.* and Milli-Q® water). After drying in a flow of nitrogen, the samples were functionalized with hydroxyl groups by an O_2-plasma (O_2 pressure 0.4 mbar, 3 min, 150 W, 100-E, TePla, Wettenberg, Germany). These activated surfaces were then immersed in a 5 % 3-aminopropyltrimethoxy silane (APTMS) solution in dry acetone for 30 min under sonication. The polysaccharides were dissolved in 4-(2-hydroxyethyl)-piperazine-1-ethane sulfonic acid (HEPES) buffer solution (10 mM, pH 6-7, polysaccharide concentration 1 mg/ml). When the solution turned clear, N-hydroxysuccinimide (NHS, 0.01 M) and N-(3-dimethyl amino propyl)-3-ethyl carbodiimide hydrochloride (EDC, 0.05 M) were added. After 15 min, the APTMS coated surfaces were immersed in the activated polysaccharide solution. After 18 h the reaction solution was replaced by Milli-Q® water. The samples were leached for three days on a vibrational table in Milli-Q® water in order to remove any uncoupled molecules. The substrates were then removed and rinsed with Milli-Q® water and blown dried in a stream of nitrogen.

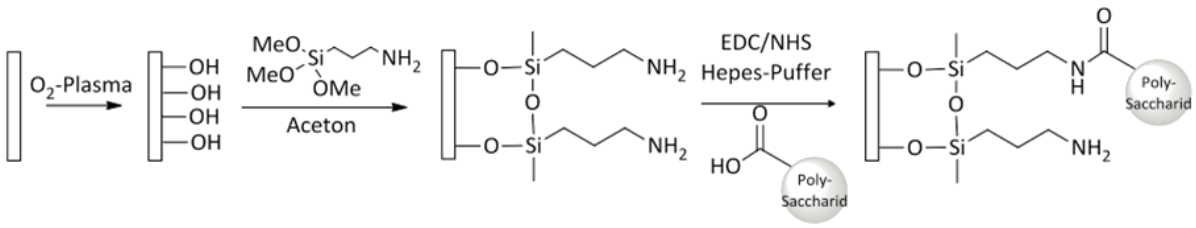

Figure 16. Scheme of polysaccharide preparation. Image was adapted from [175].

To modify the polysaccharides with TFEA, they were immersed for 15 min in a solution of NHS (5 mM) and EDC (25 mM) in HEPES to reactivate free-remaining carboxyl groups. Subsequently, a 40 mM solution of TFEA in HEPES was added. After 18 h, the samples were

removed and rinsed with Milli-Q® water. Figure 17 shows a scheme of this modification process.

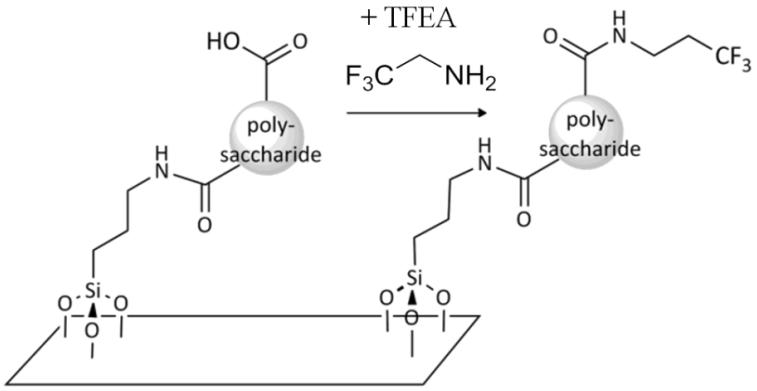

Figure 17. Scheme of polysaccharide modification with TFEA. Image by courtesy of Stella Bauer.

3.5. Preparation of Metal Organic Framework

SURMOFs 2 were prepared by employing the spray method [149] a technique which has been successfully used in other layer-by-layer fabrication schemes for coating substrates *e.g.* polyelectrolyte multilayers [89]. The samples were prepared by Zhengbang Wang in collaboration with the group of Prof. C. Wöll (Insitute of Functional Interfaces (IFG), Karlsruhe Institute of Technology). Figure 18 shows the scheme of the spray setup used in this work [149]. SURMOFs 2 layers were grown on MHDA SAMs. These substrates were placed on a sample holder (Figure 18h) inside of the spray chamber (Figure 18g) and subsequently sprayed with a 1 mM ethanol solution of $M_2(CH_3COO)_4 \cdot H_2O$, M= Cu or Zn) for 10 s and then with a 0.2 mM 1,4-benzendicarboxylic acid (CBD) solution for 20 s at room temperature. Between each step, the substrates were rinsed with ethanol. These three solutions were stored in containers (Figure 18.d, c and f). Such reservoirs were connected to a gas supply (Figure 18a) by nozzles (Figure 18.g) in order to produce an aerosol from the reactants and solutions. These aerosols were deposited on the substrate in a similar manner occurring during the liquid phase epitaxy (LPE) process. The nozzles, the sample and its holder were situated inside the spray chamber. The gas flow was properly applied with help of the gas flow controller (Figure 18b) and three-way valve gas distributor (Figure 18c). Critical parameters of the spray procedure were: carrier gas pressure (1.5 bar), liquid pressure (0.2 bar), flow rate (0.25 ml/s), and distance between the nozzle and the target (0.1 m).

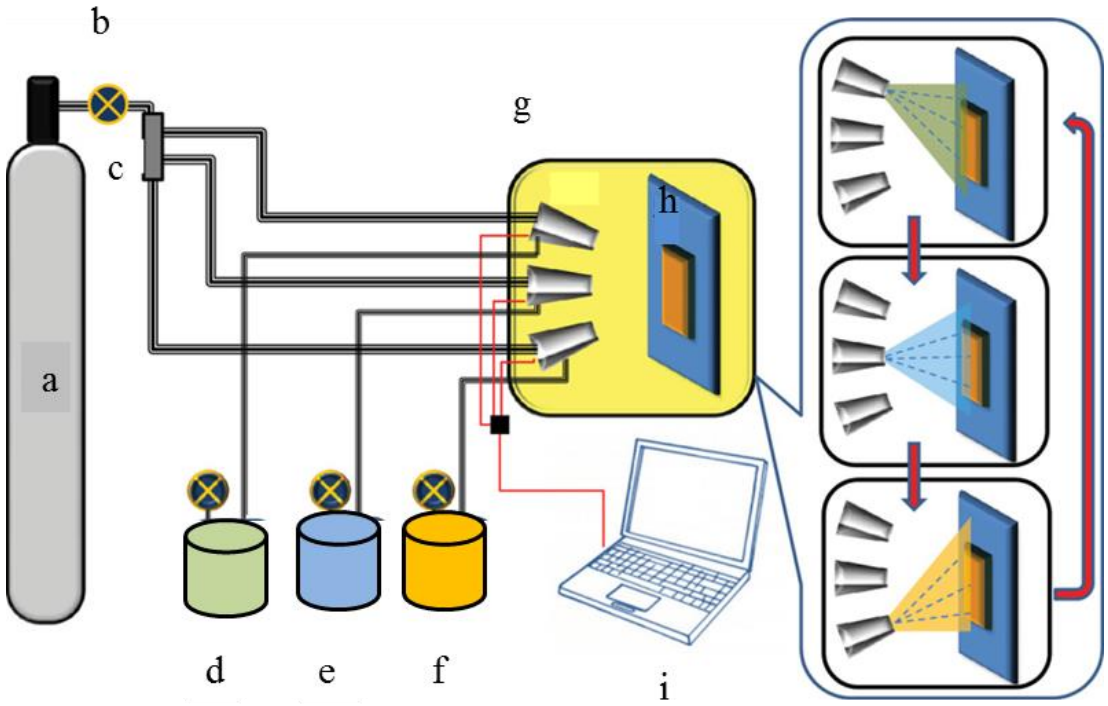

Figure 18. Setup employed for the fabrication of SURMOFs 2 with the spray method [149].

All of these spray steps which were controlled through a computer (Figure 18i) forms one layer of the MOFs. The number of deposited layer varied depending on the desired thickness of the SURMOFs 2. For the synthesis of the SURMOFs 2 with 80, 120 or 160 nm thickness, 10, 15 or 20 layers were required respectively.

3.6. Preparation of polymer brushes

Poly[oligo(ethylene glycol) methyl methacrylate] (POEGMA) surfaces were prepared according to published protocols [143, 176]. The samples were kindly provided by collaboration with the lab of Prof. A. Chilkoti (Duke University, USA). For this study, two different oligo(ethylene glycol) methacrylate monomers were used: hydroxyl (–OH) terminated with an average side chain M_n 360, and methoxy (–OCH_3) terminated with an average side chain M_n 475. All reagents were purchased from Sigma-Aldrich. Coatings were synthesized as follows: Schott Nexterion® B glass slides were cleaned in a solution of H_2SO_4:H_2O_2 (3:1) for 30 min. After rinsing with deionized water and drying, the cleaned slides were immersed in aminopropyltriethoxysilane (10 %) solution in ethanol for 30 min and were then rinsed with ethanol and dried at 120°C for 3 h. Subsequently, slides were placed in a solution of bromoisobutyryl bromide (1 %) and triethylamine (1 %) in

dichloromethane for 30 min, rinsed with dichloromethane and ethanol, and blown dry with nitrogen. Slides were then immersed at room temperature in a degassed polymerization solution of Cu(I)Br (5 mg/ml), bipyridine (12 mg/ml) and oligo(ethylene glycol) methacrylate (300 mg/ml) under argon. Finally, slides were removed from the polymerization solution after 12 h, rinsed with deionized water and dried with nitrogen.

3.7. Live/dead bacterial assay

The live/dead® BacLight™ bacterial viability kit (Invitrogen, Carlsbad, CA, USA) was used to determine the viability of the bacteria after 2 h incubation on Cu-SURMOF 2 (120 nm) and MHDA SAM used as a reference. This assay was often used in previous studies [177, 178]. Mixtures of Syto® 9 green-fluorescent nucleic acid stain and the red-fluorescent nucleic acid stain propidium iodide were used. Such stains differed both in their ability to penetrate healthy bacteria and in their spectral properties. The green-fluorescent nucleic acid stain labeled all bacteria. Whereas the red one was only able to penetrate dead bacteria since living cells had intact membranes which made them impermeable to this dye. This assay, which was well suited for a bacterial analysis using fluorescence microscopy, was performed following the manufacturer´s experimental protocol. The surfaces were incubated in the bacterial solution for 2 h. A 1:1 mixture of both stains was mixed thoroughly by centrifugation. After incubation of the samples, 3 µL of the dye mixture was added for each ml of bacterial solution. The samples were then incubated at room temperature in the dark. After 15 min, the samples were removed from the solution and rinsed with Milli-Q®. The surfaces were air dried in the dark prior to analysis by fluorescence microscopy.

Samples were analyzed with an upright microscope (90-i, Nikon, Tokyo, Japan) with suitable optical filters (BV-2A and Texas red HYQ, Nikon, Tokyo, Japan) using an objective with 40x magnification. The ratio between bacteria with damaged membranes and all bacteria present on the surfaces was calculated from fluorescence microscopy images. Image processing was performed using ImageJ software version 1.44p (Rasband, W.S., ImageJ, U. S. National Institute of Health, Bethesda, Maryland, USA, http://rsb.info.nih.gov/ij). This analysis software was successfully used in previous studies [179, 180].

3.8. Critical point drying of bacteria for SEM imaging

Critical point drying is an established method to remove liquid present in biological samples in a precise and controlled way by dehydrating them prior to SEM examination. During evaporation of water within a biological sample, surface tension in the liquid body pulls against the solid structure, which the liquid is in contact with, causing damaging effects on the biological specimen. In order to avoid that, the critical point drying method is utilized. This technique is based on the principle of continuity of state for which there is no apparent difference between the liquid and gas state of a medium to avoid crossing the liquid-vapour boundary. Thus, the surface tension within this interphase is reduced to zero avoiding the damaging effects of the surface tension on the biological samples. This may occur via two possible paths from the liquid phase to the gas phase without crossing their interphase. One possibility to achieve that is by using the freeze-drying method (see chapter 3.9) which means going around to the left from the liquid-vapour boundary (see Figure 19) by decreasing temperature and pressure simultaneously. In critical point drying, this occurs by increasing the temperature and pressure up to the critical values, where the liquid and the vapour have the same density and hence they cannot be distinguished.

Since the critical point of water (T_{crit}= 374°C and p_{crit}= 221 bar [181]) is inconvenient due to the possibility to cause heat damage to the specimen, an alternative transitional medium is required. Carbon dioxide (CO_2) is the most common and convenient transitional medium for critical point drying (T_{crit}= 31°C and p_{crit}= 73 bar [181]). As water is not miscible with CO_2, a third medium is required as intermediate fluid, in this case ethanol.

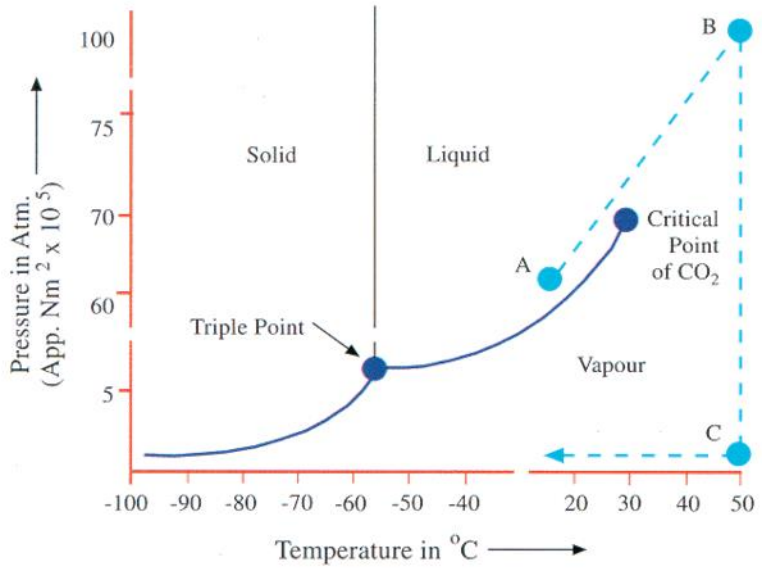

Figure 19. Phase diagram of CO_2 [181].

For SEM imaging, bacterial solution (OD_{600}=0.1) was incubated on DDT SAM and glass slides for 15 min, 1 h and 4 h. Afterwards bacteria were fixed in a 2,5 % glutaraldehyde/ASW solution for 1 h at room temperature. Subsequently, containers containing the samples were flooded with ASW. The salt concentration was slowly decreased by increasing the dilution with distilled water for 10 min at: 100 % ASW, 50 % ASW, 50 % fresh water and 100 % fresh water. After this treatment the samples were dehydrated by ethanol exchange using ethanol *p.a.*/water mixtures with 30 %, 50 %, 70 %, 90 % and twice 100 % ethanol content. Each step lasted 10 min. The samples were then transferred in the chamber of the critical point dryer (CPD 030 critical point dryer, Bal-Tec, Pfäffikon, Switzerland) which was previously filled with 100 % ethanol. Once a temperature of 10°C and a pressure of 50 bar was reached, the ethanol was gradually exchanged with CO_2, consequently the chamber was emptied of liquid and filled with CO_2 keeping the sample covered until all ethanol was removed. This procedure was repeated approximately 10 times. After every step, the CO_2 content was increased and thus, the pressure was higher. Subsequently, the chamber was filled to the top with liquid CO_2 and heated to a temperature above the critical temperature, thereby reaching a temperature of 40°C and a pressure of 90 bar.

Immediately after removing the samples from the chamber, they were sputtered with a 5 nm carbon layer in a BAL-TEC MED020 coating system sputter for SEM imaging.

3.9. Freeze-drying

Helium ion microscopy imaging (as described in chapter 3.11.9) was used to obtain images of adherent bacteria. As this method requires ultra-high vacuum (UHV) conditions in the sample chamber, samples of the bacteria had to be dried prior to imaging. In order to minimize morphological changes during the process of drying, freeze-drying of the plunge-frozen samples was chosen. First, small droplets of bacterial suspension were placed on TEM grids coated with a holey carbon film (Quantifoil® R 2/4, Quantifoil Micro Tools GmbH, Jena, Germany). After a few minutes, during which a number of bacteria adhered to the surface, the TEM grid was mounted in a plunge freezer (Max Planck Institute of Biochemistry, Martinsried, Germany). After blotting with stripes of filter paper (Whatman® qualitative filter paper, Grade 1, Whatman plc, Kent, UK) to remove excess liquid, the coated TEM grid with adherent, fully hydrated bacteria was plunge-frozen using a liquid ethane-propane-mixture (37 % ethane, 63 % propane, Linde AG, Pullach, Germany) as a cryogen and kept in a

reservoir filled with liquid nitrogen. The heat capacity of the liquid alkane mixture well below its boiling point and the good heat transfer between the liquid and the sample ensured very high cooling rates in the sample and thus a glass transition of the liquid water. This process called vitrification prevents the formation of ice crystals, which would certainly damage the morphology of the sample. Now the plunge-frozen samples were stored under liquid nitrogen and transferred into a vacuum chamber equipped with a cryogenic sample holder. In this chamber the samples were kept under high vacuum (HV) conditions ($p < 10^{-6}$ mbar) while the temperature was increased steadily from -180°C to room temperature over the course of approx. 2 days, allowing the amorphous ice to sublimate.

3.10. Field tests

3.10.1. Static immersion field test

Prior to describe the performance of the field tests, it is necessary to emphasize that a major effort was underwent to guarantee the integrity of the samples, including on-site preparation of the surfaces at FIT. Nonetheless, it still only reflects a single time point for a given set of environmental constrains including season, weather, test site, and many more. In standard immersion tests, the samples are usually submerged during several months or years.

In November and December 2010, several sets of coatings were immersed into the ocean for up to 48 h. The test site of the FIT in the Indian River Lagoon is located at the east coast of Florida near Sebastian (27° 53´ 59´´N, 80° 28´28´´W) as shown in Figure 20a. The Sebastian site is about 5 km north of the Sebastian inlet. Most samples were immersed for 2 h, 6 h, 12 h and 48 h because of their expected fast degradation. The only exceptions were the ethylene glycol SAMs, for which the 48 h time point was left out. The polysaccharide coatings were submerged for 24 h and the POEGMA brushes were submerged for 24 h and 48 h. In order to ensure the same environmental conditions and consequently, comparability within experiments, all samples were immersed in sets and all sets were immersed at exactly the same starting time. Ultrasmooth Nexterion® B glass slides were used as control surfaces and included in every set of samples. An additional glass slide was positioned in front of the outermost sample to provide identical conditions within the whole set of samples.

The test samples were placed into polypropylene holders for microscope slides (Figure 20b) and submerged into the tanks of the Sebastian site, with the top approximately 0.4 m below

the water surface. Water was constantly pumped from the lagoon into the tanks to provide the same conditions as in the ocean.

a) b)

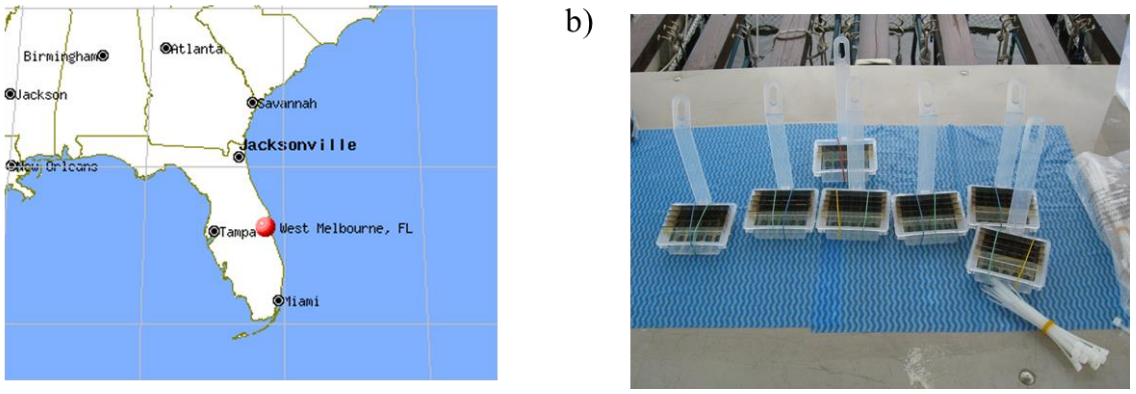

Figure 20. Map of the test site location(a) and image of the submerged sets of samples (b).

The experiments were carried out twice, starting on different days (experiment N1 and N2). Table 2 summarizes the different experimental time periods and the immersed samples. Experiment N1 included 35 and N2 44 samples. After the desired immersion time, a large poly(propylene) box was filled with ocean water and the slides were transferred into the box under water without taking the slides through the air water interphase. This procedure was used in order to avoid detachment of adherent material from the surfaces while bringing them through the air-water interphase. All samples were fixed according to the protocol given below.

Experiment N1: date of immersion: November 30th 2010.	
Immersion time [h]	Submerged samples
0	Every sample
2	DDT, AUDT, FUDT, HUDT, PEG and EGn (n=1, 3 and 6) SAMs and glass slide
6	
12	
48	DDT, AUDT, FUDT, HUDT and PEG SAMs, glass slide and –OH and $–OCH_3$ POEGMAs

Experiment N2: date of immersion: November 30th 2010.	
Immersion time [h]	Submerged samples
0	Every sample
2	DDT, AUDT, FUDT, HUDT, PEG and EGn (n=1, 3 and 6) SAMs and glass slide
6	
12	
24	AA, AA+TFEA, HA, HA+TFEA, CS and CS+TFEA polysaccharides, glass slide and –OH and $–OCH_3$ POEGMAs
48	DDT, AUDT, FUDT, HUDT and PEG SAMs, glass slide and –OH and $–OCH_3$ POEGMAs

Table 2. Summary of immersion times and immersed surfaces used for the experiments.

It is necessary to emphasize that a major effort was underwent to guarantee the integrity of the samples, including on-site preparation of the surfaces at FIT. However, it still only reflects a single time point for a given set of environmental constrains including season, weather, test site, and many more. In standard immersion tests, the samples are usually submerged during several months or years.

3.10.2. Sample fixation

After removing the samples, they were fixed with formaldehyde for 1 h. For that, formaldehyde (37 %) was added to the 200 ml volume in the plastic container to reach the

desired concentration of 2.5 % formaldehyde. Subsequently, containers were flooded with Artificial Sea Water (ASW, Instant Ocean®). The salt concentration was slowly decreased by increasing the dilution with distilled water for 10 min at: 100 % ASW, 50 % ASW, 50 % fresh water and 100 % fresh water. After this treatment the samples were dehydrated by ethanol exchange using ethanol/water mixtures with 30 %, 50 %, 70 %, 90 % and twice 100 % ethanol content, for 10 min each. Subsequently, ethanol was exchanged with 100 % Hexamethyldisilazane (HMDS, Sigma-Aldrich) for 3 min. After this treatment, the samples were air dried and transferred to a desiccator to avoid subsequent water condensation or accumulation of dust. HDMS drying was used as a field compatible alternative to Critical Point Drying (CPD) [182] as no critical point dryer was available.

3.10.3. Sample analysis

The samples were analyzed by phase contrast microscopy (TE-2000-U, Nikon, Tokyo, Japan) using a 15x Ph1 objective with a field of view (FOV) of 672 µm by 504 µm at the University of Heidelberg. For each sample, 20 FOVs distributed across the surface were recorded, resulting in a total recorded and analyzed surface area of 6.8 mm^2. The most frequently found organisms larger than 10 µm were identified and counted. The diatoms were classified into the genuses taxa and the protozoa to a subclass taxon according to literature [154, 183-187] in collaboration with Kelly Zargiel from the group of G. Swain (department of marine and environmental systems, Florida Institute of Technology).

3.11. Analytical techniques

3.11.1. Contact angle goniometry

The water contact angle θ (CA) is a parameter which indicates the wettability of a surface [188]. In the case of liquid droplet on a flat surface, this parameter is defined as the angle between the tangent to the solid-liquid interface and the tangent to the liquid-vapor interface. Figure 21 shows images of water contact angles on both, hydrophobic (DDT SAM) and hydrophilic (glass slides) surfaces. It can be noticed that hydrophobic surfaces have a larger

water contact angle whereas the contact angle decreases with increasing wettability of the surface due to a stronger interaction of the liquid with the solid.

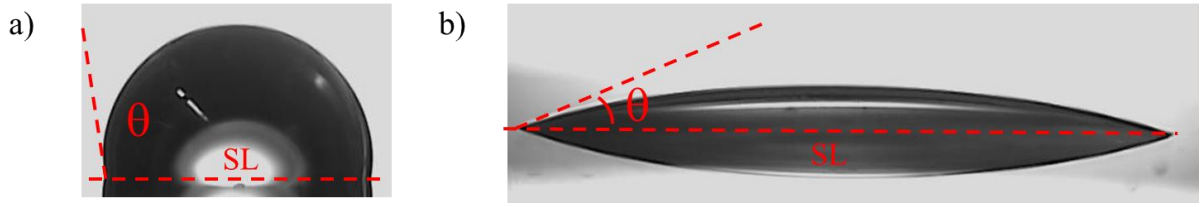

Figure 21. Contact angles of water on hydrophobic (DDT SAM, a) and hydrophilic (glass slide) substrates (b).

There are different models to describe the contact angle. The contact angle on an ideal surface can be determined by the Young equation [189]:

$$\cos\theta_Y = \frac{\gamma_{SL} - \gamma_{SV}}{\gamma_{LV}} \tag{3}$$

This equation is only applicable to ideal surfaces which are defined as smooth, rigid, chemically homogeneous, insoluble and non-reactive [190]. γ_{SL}, γ_{SV}, γ_{LV} are the solid-liquid, solid-vapor and liquid-vapor interfacial tensions. θ_Y indicates the Young contact angle. This equation is only valid for the ideal case, but in reality, both topography and chemistry of the surface influence the contact angle.

Roughness of the surfaces influences their wettability in two different forms [190]. The liquid may penetrate into grooves, which is referred to as "homogeneous wetting". Wenzel developed an equation [191] for the CA of homogeneous wetting on rough surfaces (θ_W):

$$\cos\theta_W = z \cdot \cos\theta_Y \tag{4}$$

In this equation, z indicates the roughness ratio which is defined as the ratio between the actual and the projected solid surface area, θ_Y is the CA calculated by the Young equation. However, air bubbles may be trapped in grooves underneath the liquid which is defined as "heterogeneous wetting". That is for example the case for the lotus effect (see chapter 2.7). The wetting in this case can be described by the Cassie-Baxter equation [192]. The Cassie contact angle θ_{CB} is dependent on the surface contact fraction of the liquid droplet (φ). This model considers air to be the second chemistry and applied in the following form:

$$\cos\theta_{CB} = \varphi \cdot (\cos\theta_Y + 1) - 1 \quad (5)$$

In this work, surfaces were characterized by their sessile water contact angle which was measured using a custom build goniometer under ambient conditions. A camera records an image of the water droplet on the surface. The shape of the droplet is modeled by the Young-Laplace equation and the contact angle at the interface is calculated using the program CAM 3.02.01 (Kölsch, P.; Motschmann, H.; Orendi, H.). To get better statistic results, the contact angle was measured at three different spots on each surface from which the mean value was calculated.

3.11.2. Spectral ellipsometry

Spectral ellipsometry is an optical technique to determine the thickness of thin films on solid substrates using polarized light. Its working principle is shown in Figure 22. Unpolarized polychromatic light from a light source is linearly polarized to two polarization states (s- and p- polarized whether the electric field of the polarization state is parallel or perpendicular to the plane of incidence) by a polarizer. When incident polarized light is reflected from a surface with a thin film, the polarization and intensity of the light change according to the properties of the film. The knowledge of how the s- and p- components of the light change upon reflection or transmission in relation to each other is essential for ellipsometry. Due to the interaction with the substrate, the light is adsorbed, and the reflected light which has an undergone amplitude is not linear but elliptically polarized instead [193].

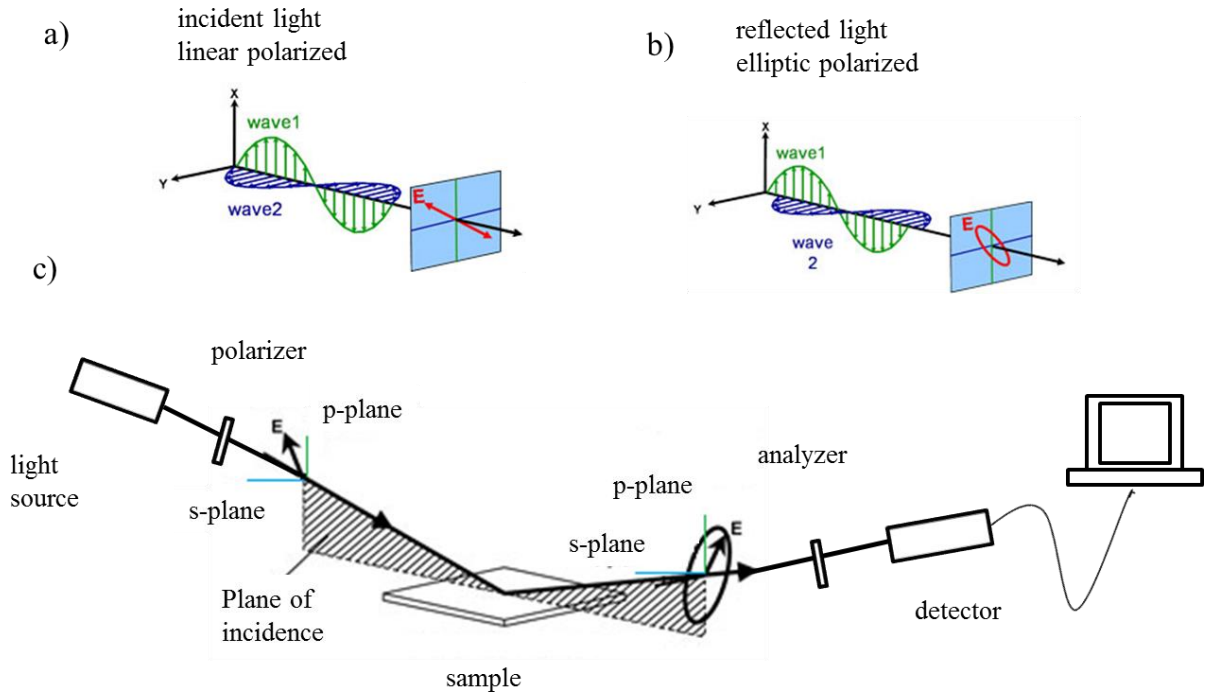

Figure 22. Working principle of spectral ellipsometry. A linearly polarized incident light (a) which was provide from the light source and polarized by polarizer, is reflected by the sample becoming an elliptically polarized light (b). This light was analyzed and detected to determine optical constants and film thickness by computer calculations. Figure 22c represents a sketch of an ellipsometry setup. Image adapted from [194].

The reflected light passes through a rotating analyzer. The detector measures intensity and phase shift between s- and p-polarized light. This is the ellipsometry measurement of Ψ and Δ [195]:

$$\rho = \tan(\Psi)\exp(i\Delta) \tag{6}$$

$$r_s = \left(\frac{E_{r0}}{E_{i0}}\right)_s = \frac{n_i\cos(\Phi_i) - n_t\cos(\Phi_t)}{n_i\cos(\Phi_i) - n_t\cos(\Phi_t)}, \qquad r_p = \left(\frac{E_{r0}}{E_{i0}}\right)_p = \frac{n_t\cos(\Phi_i) - n_t\cos(\Phi_t)}{n_i\cos(\Phi_i) - n_t\cos(\Phi_t)} \tag{7}$$

As the ellipsometry parameters Δ and Ψ cannot be converted directly into optical constants, a modeling analysis using an iterative procedure (least-squares minimization) is required. The unknown optical constants and/or thickness based on the applied model are varied and both ellipsometry parameters are calculated by the Fresnel equation. Those experimental data which match best with the model provide the desired parameters. In the case of multilayer samples the model considers the optical constants and thickness parameters of all individual layers, thus each layer has to be modeled individually. Although ellipsometry is suited for calculations of thin surfaces in ranges from sub-nanometers to a few microns, there are some

surfaces that are difficult to measure like films deposited on glass substrates, since the reflection from the backside of the glass strongly interferes with the reflection from the surface.

In this work, film thicknesses were measured using a M-44 multiple wavelength ellipsometer from J. A. Woollam Co., Inc. (Lincoln, NE, USA) which was aligned at a fixed incident angle of ≈75° to the surface. An arc lamp, a high pressure Xe discharge point source lamp operating in a wavelength range between 200 and 1,000 nm was used as a light source. The data analysis was done with the modeling software WVASE^{TM} from J. A. Woollam Co. The SAMs and conditioning layer were modeled as a single Cauchy layer model with an estimated refractive index of 1.45.

3.11.3. X-ray diffraction

The use of X-rays for structure determination presents many advantages which stem from the nature of their interactions with matter, as the wavelengths of the radiation in this electromagnetic spectrum region are similar to the sizes of atoms and interatomic distances [196]. In addition, diffraction from single crystals is one of the most accurate techniques to provide detailed information about the deposition of atoms in a solid. For these reasons, X-ray diffraction (XRD) is a well-suited technique to obtain information of the crystallographic structure of solid samples.

In this work, XRD measurements of Cu-SURMOF 2 coatings were conducted using a Bruker D8-Advance diffractometer with θ-2θ geometry. As X-Ray source Cu K_α radiation (λ= 1.54 Å) focused by a Göbel mirror was used. For the Cu $K_{\alpha 1}$ line of the beam spectrum the lattice spacing and the material combinations were optimized. Measurements were recorded by a PSD detector (MBraun, Garching, Germany) by a Cu K_α radiation at 40 kV/30 mA, with a step size of 0.007 degrees and scan time of 3 s in the range of 2θ = 5°-30°.

3.11.4. X-ray photoelectron spectroscopy

X-ray photoelectron spectroscopy (XPS) is one of the most important techniques to analyze the chemical composition of surfaces based on the photoelectric effect. A surface is irradiated by X-rays which cause electrons to emit from the substrate with a kinetic energy E_{kin}. This process is described by the Einstein equation [197]:

$$E_{kin} = h\nu - E_B - \Phi \quad (8)$$

whereby E_B is the electron binding energy, $h\nu$ is the photon energy of the incident X-rays and Φ is the work function of the analyzer. Φ is an instrumental parameter, which is adjusted by setting the Fermi edge emission of a clean metallic sample to zero binding energy as an energy calibration [198].

The layer thickness (d) can be determined by the attenuation of a suitable signal (Au4f for SAMs on gold and Si2p for glass) according to Lambert-Beer´s law:

$$d = \lambda \cdot cos\ \theta \cdot \ln \frac{I_0}{I(d)} \quad (9)$$

where I represents the intensity of the signal before (I_0) and after transmission $I(d)$ through the material. $Cos\theta$ is the cosine of the take-off angle and λ the attenuation length of photoelectrons (see Table 3).

The stoichiometric ratio (N_A/N_B) of two elements (A and B) can be determined by applying the statistical model, which assumes a homogeneous distribution of two elements in the substrate:

$$\frac{N_A}{N_B} = \frac{I_A}{I_B} \cdot \frac{\sigma_B}{\sigma_A} \cdot \frac{\lambda_B}{\lambda_A} \quad (10)$$

In this equation, $\sigma_{A,B}$ is the element-specific cross section for the emission of a photoelectron and $I_{A,\ B}$ the signal intensity. Numerical values of the utilized attenuation lengths and cross sections of the elements are shown in Table 3.

Orbital	Au4f	C1s	N1s	O1s	S2p	Si2p
λ [Å]	26.1	21.4	18.7	15.9	24.2	26.7
σ	9.79	1.0	1.77	2.84	0.59	0.29

Table 3. Parameters used for XPS measurements: attenuation length of photoelectrons (λ) and cross section of the elements (σ) [199] for Mg Kα as determined by Nikolaus Meyerbröker [200]. The values of the cross sections are normalized to the C1s cross section of 22,200 b (1 b = 10^{-28} m^2).

In this work, the XPS measurements of film purity, composition and thickness were realized using a Leybold-Heraeus MAX 200 X-ray photoelectron spectrometer equipped with a magnesium anode without monochromator as the X-ray source (K_α, 1253.6 eV). The raw spectra were divided by the transmission function and analyzed by a standard fitting

procedure by adapting the peaks to a symmetrical Gaussian-Lorentzial product function with 80 % Gaussian portion.

All the XPS measurements were acquired by first taking a survey scan spectrum. Subsequently, detail spectra were recorded for quantitative analysis of each atomic species of interest. All the important measurement parameters are shown in Table 4. The dwell time and the number of scans were chosen according to the investigated signal. The step size determines the energy difference between two measuring points.

Orbitals	Start (eV)	End (eV)	Step (eV)	Dwell (s)	Pass Energy (eV)	Scans
Survey	1000	-4.8	0.4	0.01	96	10
Au4f	95	75	0.2	0.04	48	10
C1s	295	275	0.2	0.1	48	12
N1s	410	385	0.2	0.25	48	32
O1s	540	520	0.2	0.12	48	12
S2p	170	145	0.2	0.25	48	32
Si2p	114	95	0.2	0.1	48	15

Table 4. Parameters for recorded XPS spectra.

3.11.5. Infrared Reflection-Absorption Spectroscopy (IRRAS)

Infrared (IR) spectroscopy is a well-established technique for the characterization of surfaces and adsorbate films, which provides specific information about the chemical composition and structure of thin surface layers and adsorbed molecules [193]. One of the most powerful attributes of this diverse and versatile analytical technique is its qualitative aspects. The frequencies of vibrational motion in molecules fall into the IR spectral range ($\lambda \approx$ 760 nm-100 µm). IR radiation illuminates the sample surface which leads to vibrations of adsorbed molecules.

IR radiation striking a surface can be absorbed or reflected. The spectrum of reflected light displays a dip at the vibrational transition frequency whose depth is proportional to the surface density of adsorbed species. Infrared reflection-absorption spectroscopy (IRRAS) is based on this principle. The presence or absence of particular vibrational bands in an IRRAS spectrum can be used for the characterization of an adsorbed overlayer.

The absorption of radiation at the frequency ω for electric dipole transition from an initial state | *I* > to a final state | *f* > is given by equation:

$$I(\omega) \sim \left|\overrightarrow{\mu_{fi}} \cdot \vec{E}\right|^2 g(\omega) \tag{11}$$

In this equation, the function g (ω) describes the absorption lineshape, $\overrightarrow{\mu_{fi}}$ is the transition dipole moment and $\overrightarrow{E}$ is the electric field vector at the surface. For a perfect conductor, the component of the molecular dipole parallel to the surface is compensated by its image and screened by a metal substrate. The combination of these two screening effects leads to the so-called *pseudo-selection rules* at a metal surface which means that spectral lines corresponding to vibrational modes accompanied by atomic displacements parallel to the surface are strongly suppressed. Thus, only spectral lines originated from vibrations perpendicular to the surface are observed [193]. In this case, instead of equation 13, the following one may be applied:

$$I(\omega) \sim \left|(\mu_z)_{fi} E_z\right|^2 g(\omega) \tag{12}$$

The IRRAS data of this work were recorded under ambient conditions with a Bruker VERTEX 80 Fourier transform IR spectrometer (Brucker, optics GmbH, Ettlingen, Germany) equipped with a grazing angle (80°) reflection spectroscopy accessory. The measurement chamber was continuously purged with dry air. The reported spectra are described as $-\log(R/R_0)$, where R is the reflectance of the sample, whereas R_0 is the reflectance of the reference, a perdeuterated 1-hexadecanethiol SAM on gold.

The resulting spectra were smoothed and corrected by baseline correction using the Brucker OPUS® software.

3.11.6. Scanning electron microscopy

Scanning electron microscopy (SEM) is one of the most widespread techniques to analyse surface topography and morphology of microorganisms. The principle of this technique is based on focusing a high energy electron beam onto the sample and detecting the interaction of the incident electrons with the surface in order to obtain images. The resulting electrons and electromagnetic radiation can be detected by different kinds of detectors. To produce an image a secondary electron detector is the most commonly used equipment. The electron source consists of an electron gun or rather a cathode that emits electrons which are

accelerated towards the anode. SEM measurements are generally conducted within a high vacuum chamber to reduce interactions between emitted electrons and gas molecules.

Detection limitations, *i.e.* spatial resolution *d*, are closely related to the wavelength λ of the incident beam:

$$d = \frac{\lambda}{2 \cdot \mathrm{NA}} \tag{13}$$

In SEM, electrons are used instead of photons which take the advantages of the *de Broglie relation*, which describes the relation between mass, energy and wavelength of a particle.

$$\lambda = \frac{h}{p} = \frac{h}{\sqrt{2 m_e E}} \tag{14}$$

h, *p*, *E* and m_e represent the Planck constant, momentum, electron energy and electron mass respectively. The combination of both relations (13) and (14) shows that the resolution can considerably be improved by using electrons, which have a significantly higher mass than photons and therefore a smaller wavelength at the same energy.

Environmental scanning electron microscopy (ESEM) is a kind of SEM that allows a preparation of sensitive samples like organic and hydrated matter without complex drying procedures which would be necessary for high vacuum microscopy. Furthermore, due to the design of the gaseous secondary electron detector (GSE, Everhart Thornley detector) in the ESEM the sample preparation can be done without coating with carbon or gold, while under normal high vacuum SEM the sample would have been coated in order to avoid charging.

To evaluate the morphology changes of the bacteria after incubation on Cu-SURMOFs 2 surfaces, images were obtained on a FEI Philips XL 30 field emission gun environmental scanning electron microscopy (FEG-ESEM) operated at an acceleration voltage of 15 kV under a chamber pressure of 100 Pa and under high vacuum (10^{-5} Pa). For that, the samples were sputtered in a Baltec MED 020 sputter coater with a 5 nm thick conductive layer of Au/Pd (80%/20%).

In this work, a LEO 1530 from Zeiss (Oberkochen, Germany) SEM was also used to observe the morphology of the bacteria *C. marina*. To render the surface electrically conductive before imaging, samples were sputtered with a very thin layer of graphite (MED020 coating system, Bal-Tec AG, Pfäffikon, Switerland).

3.11.7. Atomic force microscopy

Atomic force microscopy (AFM) is an imaging technique applied as a non-optical way to map the 3D-surface of a sample down to atomic resolution. This technique is used for several bacteria related applications such as the study of bacterial morphology [201, 202] and its morphological changes [203] or the evaluation of the interaction forces between bacteria [49].

Figure 23 shows a scheme of an atomic force microscope as described previously. The most important part of an AFM is the force-sensing cantilever [204] which is placed parallel to the surface. The cantilever has a sharp tip at its end which is scanned over the investigated surface. AFM measures the interaction force between the tip and the surface. This force depends on the nature of the sample, the used tip, and the distance between them.

The substrate is placed on top of a scanner which is made from piezoelectric material and responsible to move the sample in XYZ direction. A laser measures the deflection of the cantilever. The signal can be plotted in the computer and displayed as a height image. The tip may be dragged across the surface (contact mode), or it may vibrate as it moves (alternating current mode). This mode has the advantage that as there is no lateral friction forces applied to the surface and there is no destruction or damage on the material.

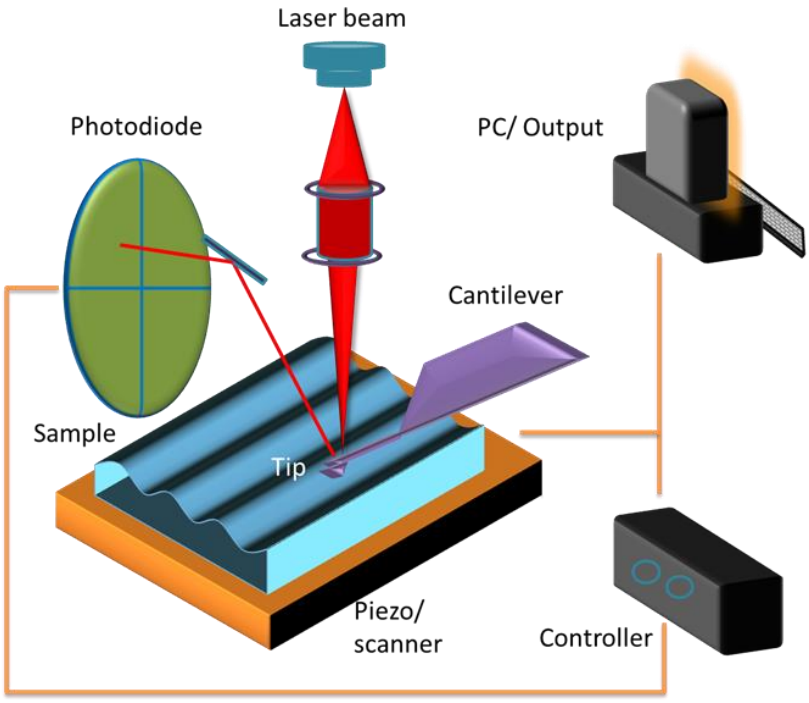

Figure 23. Scheme of an atomic force microscope. Image courtesy of Carlos Azucena.

Samples were characterized by using an Asylum Research Atomic Force Microscope, MFP-3D BIO. The AFM was operated at 25°C in an isolated chamber in alternating current mode (AC mode). AFM cantilevers were purchased from Ultrasharp^{tm} MikorMasch. Three types of AFM-cantilevers were used, a NSC-35 (resonance frequency 315 kHz; spring constant: 14 N/m), a NSC-36 (resonance frequency: 105 KHz; spring constant: 0.95 N/m) and a NSC-18 (resonance frequency: 75 kHz; spring constant: 3.5 N/m).

3.11.8. Light microscopy

Light microscopy is probably the most widespread technique for visual analysis in the field of biology. This technique basically consists of an objective lens which forms a magnified real image of the sample at a specific distance from the objective known as intermediate image plane which is located at the front focal plane of the ocular, another magnifying lens. The image can be detected by a camera which must be located at the intermediate image plane or a projection of the intermediate image [205].

An important parameter of objectives is the numerical aperture (*NA*) which determines the achievable resolution. In this equation, *n* is the index of refraction and α represent the aperture angle:

$$NA = n \cdot \sin\alpha \tag{15}$$

Since the resolution limit is reached when the contrast between two points becomes too small to be distinguished as two separate points, phase contrast optics were applied to reach higher contrast.

The microscope used in this work was an inverted fluorescent microscope (TE-2000-U Nikon, Tokyo, Japan) which was placed into a custom built incubator (see chapter 3.2) which was made of transparent poly(methyl methacrylate) (PMMA). This semi-automatic microscope had a programmable stage and a shutter as well, which allow long term observation of biological specimens. The camera utilized for imaging was a cooled 2 megapixels black/white camera. For bacteria observation a 40x Ph2 air objective (Nikon, Tokyo, Japan) with a correction ring and a *NA* = 0.6 was used.

3.11.9. Helium ion microscopy

Helium ion microscopy (HeIM) is an imaging technique based on a helium ion beam. The concept relies upon a cryogenically cooled, sharp tip in an UHV vacuum system, to which small amounts of gas can be admitted. The ion source is based on field ion emission from the apex of a sharp needle held at a high positive voltage in the presence of a gas [206, 207]. A beam consisting of noble gas ions is preferred to minimize any chemical, electrical, or optical alteration of the sample. When helium is used as the noble gas, there is the additional benefit of minimal sputtering of the substrate [207]. An electron beam has a relatively large excitation volume in the substrate, due to the generation of many secondary electrons close to the surface of the sample, which are quite likely to generate even more electrons. This high number of secondary electrons able to escape the sample limits the resolution of a SEM regardless of the probe size. A helium ion does not suffer from this effect as the excitation volume "visible" to the secondary electron detector is much smaller than that of the SEM. As the penetration depth of the helium ions is higher than the penetration depth of the electrons [207], the majority of secondary electrons is generated deeper inside the sample, and therefore unable to escape and degrade the resolution. Furthermore, helium ion microscopy provides subnanometer resolutions for slow helium ions, as fast helium ion can penetrate cells. Thus, this technique is suitable for both, surface and subcellular imaging [208].

For this work a HeIM Zeiss Orion Plus (Carl Zeiss SMT, Oberkochen, Germany) was used. The imaging with this technique was conducted at the Bielefeld University with the support of PD Dr. André Beyer from the group of Prof. Dr. Armin Gölzhäuser.

RESULTS

4. Microfluidic shear stress assay

4.1. Evaluation of the results

4.1.1. Calculation of the shear stress

In order to quantify the adhesion of *Cobetia marina* on different coatings, the setup described in chapter 3.2 was used to apply a flow which consequently generates a defined hydrodynamic shear force to detach the bacteria. The wall shear stress τ created by a liquid flow can be calculated using the Poiseuille´s model [52] (see chapter 2.4.2) as:

$$\tau = \frac{6Q\mu}{h^2 w}$$

thereby Q is the volumetric flow rate, h and w are the height and width of the channel respectively, and μ is the viscosity of the medium ≈1 x 10^{-3} kg/m·s for seawater at 20°C [209]. When the term "critical shear stress" is mentioned in the following discussions, it refers to the wall shear stress needed to detach 50 % of adherent bacteria (τ_{50}).

For the present setup the size of the channels prior to the experiments is 1 mm x 0.150 mm x 13 mm (w x h x l). However channels are subjected to a slight compression by mounting the channel assembly, which leads to a small change of their dimensions and this must be taken into account when calculating the applied shear stress. Hence, the channel height and width were measured directly after each experiment (see chapter 3.2.3). The measurement of the height was performed at the position of the channel where the detachment process was recorded (middle position) using the same objective as for the detachment process (40xPh2). The width was determined from an image of the channel at the centre position with a 4xPh0 objective. The theoretical shear stress applied with these channel dimensions was calculated by knowing the volumetric flow which was induced by the syringe pump. The average measured dimensions of the channels were 0.9 mm x 0.140 mm x 13 mm (w x h x l). An explanation of the syringe setup and a detailed description of the assays can be found in chapter 3.2. The maximum applicable volume flow was Q≈90 ml/min, thus the maximum shear stress was ≈5,500 dyn/cm^2 (corresponding to 550 Pa). For seawater, the liquid density ρ is ≈1.02 x 10^{-3} g cm^{-3} [210] and the viscosity μ is about 1 x 10^{-3} kg/m·s [209] at 20°C. From these values the calculated maximum Reynolds number (Re ≈1700) indicates a laminar flow

($Re < 2300$) even at the highest shear stresses possible with this setup. This ensures that the theoretical model can be applied confidently. Besides, in previous work, the flow profile parallel to the surface and at medium height of the channel was experimentally measured using fluorescence correlation spectroscopy (FCS) [59]. The results showed that the experimentally measured velocity in the middle of the channel is in agreement with the theoretical mean flow velocity calculated from the formula described above.

The volume flow created by the syringe pump is progressively increased (see chapter 3.2.2). Since the increase of the flow with time is known, the time of the bacterial detachment video can be assigned to a certain volumetric flow which is directly correlated to the exerted wall shear stress. Thus, the number of bacteria which are still attached at a certain shear stress ($N(\tau)$) can be determined. After the incubation time, the initial number of bacteria (N) present in the recorded field of view was counted. After starting the syringe pump at a minimum speed, generating a flow of ≈0.01 dyn/cm^2, some bacteria detached from the surface. This fraction is called non adherent bacteria fraction.

Figure 24 shows a typical example of a detachment curve for *Cobetia marina* on DDT SAMs. From this detachment curve, two characteristic values for bacterial adhesion can be derived: the percentage of adherent bacteria and the critical shear stress (τ_{50}). To obtain the latter value the bacteria fraction ($N(\tau)/N$) was plotted against the applied shear stress (τ) as shown in Figure 24a. As the number of initially seeded bacteria varied between different sets of experiments (usually ≈ 400 cells), the adherent bacteria fraction ($N(\tau)/N_{ad}$) was plotted in the removal graphs in order to provide comparable results (Figure 24b). The y coordinate of the graph where 50 % of the adherent bacteria detached ($N(\tau)/N_{ad}$ =0.5) was magnified in order to determine the corresponding x coordinate which represents the τ_{50} value (Figure 24c). The percentage of adherent bacteria was calculated as the ratio of the number of adherent bacteria within the FOV and the total number of bacteria before applying any flow.

The applied laminar shear stress can be set into relation with the turbulent shear stress present at the surface of a moving ship 50 m downstream of the bow using calculations by Schultz *et al*. to give a rough idea of the range of shear stress used. These calculations reveal that a wall shear stress of 560 dyn/cm^2 is reached at a vessel velocity of ≈ 16 knots [211], as indicated at the top axis in Figure 24a. However, this interpretation of ship velocity needs to be used with some caution, as the flow situation at a ship hull is entirely different from the microfluidic

detachment experiment. Especially at low velocities deviations are likely, since a transition towards laminar conditions at the ship hull can be expected.

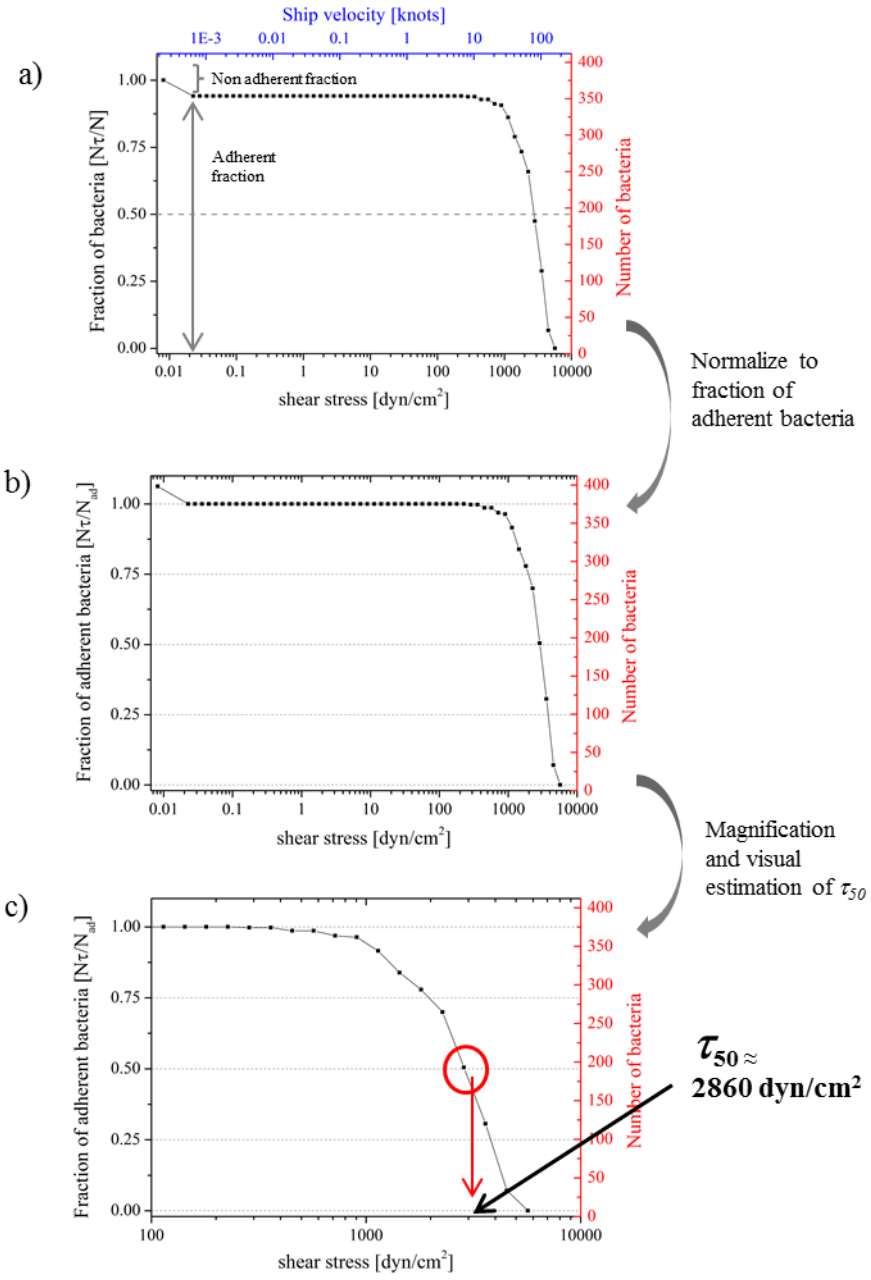

Figure 24. Visual determination of the critical shear stress.

Another method to determine the τ_{50} value was tested in previous work [59], and consisted of the application of a dose-response fit to the removal curve:

$$y = A_1 + \frac{A_2 - A_1}{1 + 10^{(log x_0 - x)p}} \quad (16)$$

The resulting curve was differentiated and the point of the curve where the maximum detachment rate of the cell fraction was reached was determined as the maximum of the Gauss-like curve. Both methods lead to nearly the same τ_{50} values. The visual analysis method has been applied in this thesis.

4.1.2. Statistics of the results and source of errors

The bacterial adhesion assays described in this work were conducted for each surface generally four times, if not stated otherwise. The values of the critical shear stress (τ_{50}) shown in this PhD thesis were determined by visual analysis (see chapter above) of the removal curves plotted for each experiment separately. Afterwards the mean and the standard deviation of the τ_{50} values and the percentage of adherent bacteria were calculated from the results of the repeated experiments. The error bars always show the standard deviation to indicate the variability of the data.

The random errors were mainly due to the bacteria themselves, as they are individual, living organisms and hence represent a population with natural variations in adhesion. However, the protocol on how to handle the bacteria prior to the detachment assays was optimized and always carefully followed in a uniform manner under sterile conditions to avoid contaminations and provide equal conditions for all experiments. All media and containers used for the assays which came in contact with the bacteria were previously sterilized. The streaking of the agar plates and the transfer of the bacteria to different containers was performed within 20 cm of a burning Bunsen burner. Only isolated and apparently healthy bacterial colonies growing on agar plates were chosen for the assays. New cultures from frozen stock solutions were seeded on fresh agar plates at least every four weeks to avoid possible mutations of the bacteria. After seeding the bacteria in MB, the optical density of the bacterial suspension was monitored during growth in the log phase until a value of 0.1 was reached in order to assure the same order of magnitude of the bacterial concentration for the experiments. After reaching the log phase the number of bacteria doubles approximately every two hours (from OD_{600}= 0.1 to 0.2 as shown in Figure 28). However, it is impossible to discriminate under the microscope between the ones that have already divided, the ones that have not yet divided and the ones have that have divided several times. This factor may

influence the adhesion of the bacteria. In spite of following the same procedure for the bacterial culture uncontrollable variations still remained.

The microfluidic system may also contribute random errors. The syringe used for defining the flow was a consumable so a different one was used for every experiment. As the flow was calculated from the linear speed of the syringe plunger, geometric variations of the syringe directly translate into an erroneous flow value.

A miscalibration of the linear translation stage results in a systematical deviation of the volumetric flow and consequently an error of the calculated shear stress. However, this systematic error affects only the absolute values, but does not impair the comparability of different experiments, as the translation stage was not exchanged during this work.

Furthermore, when opening a channel with the selector sometimes a flow pulse could be observed. This may represent a possible source of error for the experiments as the fraction of bacteria adhering weakly could be removed and attachment of adhered bacteria could be weakened. Both could affect the shear stress needed to remove the remaining bacteria.

Other sources of systematic errors are the dimensions of the channels, which are used to calculate the applied shear stress according to Poiseuille's model (see formula at the beginning of this chapter). To account for variations in the dimensions of the channels, the geometry of the mounted channels was determined after every experiment. Assuming an uncertainty of 5 µm in measurements of both height and width, and typical channel dimensions (height of 150 µm and width of 1000 µm), the systematic error of the applied shear stress as calculated with the formula above is approximately ± 7%.

$$\frac{\Delta\tau}{\tau} = \sqrt{\left(2 \times \frac{\Delta h}{h}\right)^2 + \left(\frac{\Delta w}{w}\right)^2} = \sqrt{\left(2 \times \frac{5\ \mu m}{150\ \mu m}\right)^2 + \left(\frac{5\ \mu m}{1000\ \mu m}\right)^2} \approx 0.07 = 7\ \%$$

In order to understand the difficulty in obtaining good statistics, it is important to point out the differences between the experiments performed during this PhD thesis and other biological studies. Our system applied a progressively increased shear stress covering a range of six orders of magnitude within 4.5 minutes. The number of bacteria present in the FOV of the microscope was usually above 400. The advantage of our system is that it is possible to observe all of these bacteria individually to gain more information about the whole detachment process, e.g. which shear stress is needed to detach the first bacteria, what shear stress is necessary to detach all of them and how steep is the decline of the detachment curve.

In contrast, other detachment studies count the number of organisms present in a defined area of a sample before and after applying only one value of shear stress. However, the additional information that can be obtained using our system comes at a price: Only one FOV per sample and incubation can be evaluated (n=1), while other detachment assays can evaluate much larger areas of a single sample after one incubation by acquiring images of many FOV, thus improving the statistics. Therefore, a direct comparison of the obtained statistics is not appropriate.

Thus, the observed variation of the results is due to various sources of error impairing the reproducibility of the results. In spite of these errors it was possible to obtain some data with good statistics. Consequently it can be suggested that the random errors might be more important than the systematic ones.

4.2. Optimization of parameters for bacterial assays

4.2.1. Influence of the incubation time and medium

For the experimental protocol, the choice of medium for the injection of the bacteria into the microfluidic system and the incubation time had to be optimized. Both parameters influence bacterial adhesion, thus they have to be chosen carefully. When the expression "incubation in MB or ASW" is mentioned in following discussions, it refers to the medium in which the bacteria were inoculated into the microfluidic system prior to the experiments with ASW as flow medium and after reaching the log phase in MB medium (see protocol described in chapter 3.1).

In order to find the optimal conditions for the assays, bacterial settlement and detachment were determined after 30 min, 1 h, 2 h and 4 h incubation time on glass surfaces. The bacteria were inoculated in both MB (bacterial growth medium) and ASW (flow medium). MB is a medium based on ASW but also contains peptone and yeast extract. For all time points, bacteria in ASW (Figure 25) clearly attached more strongly than in MB (Figure 26). This effect could also be observed in the average of the critical shear stress values (Figure 27a). In ASW the settlement time did not influence the shear stress if it was longer than 1 h.

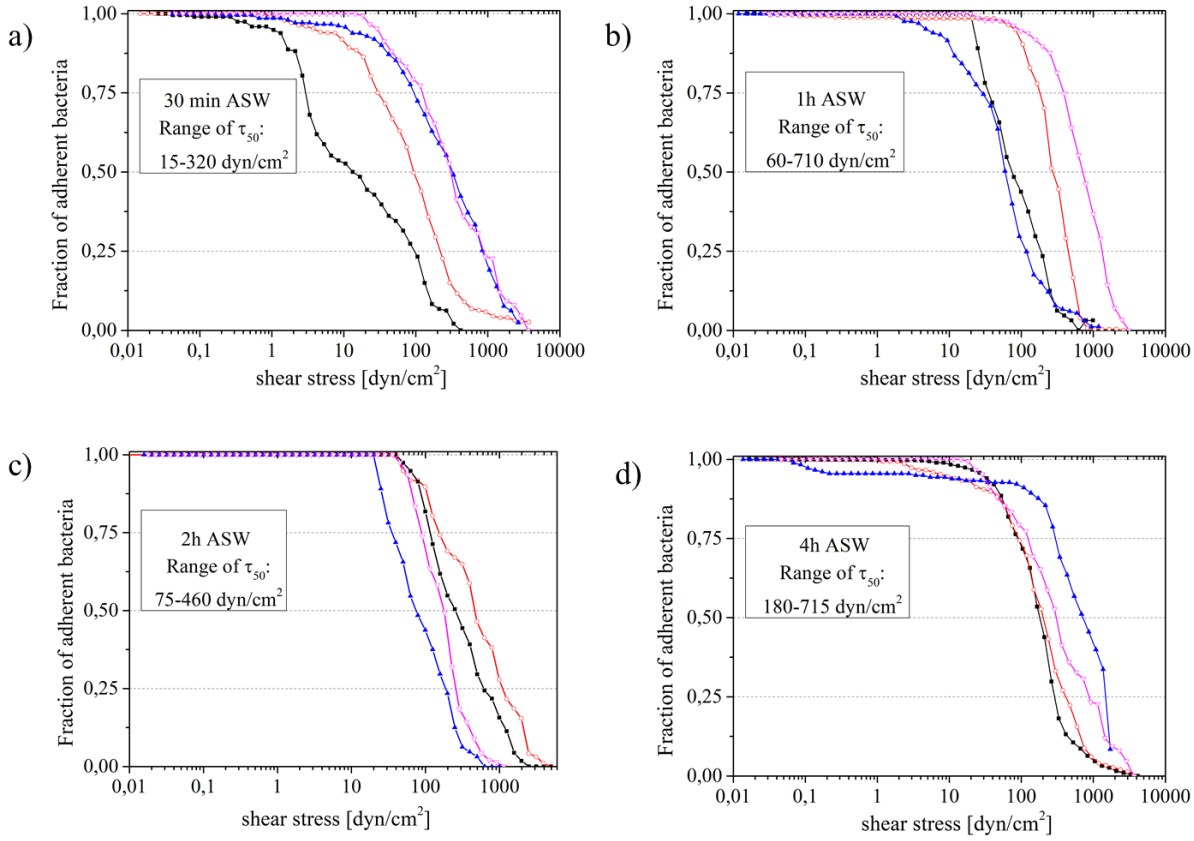

Figure 25. Detachment curves of *C. marina* in ASW from glass slides as a function of incubation time: 30 min (a), 1 h (b), 2 h (c) and 4 h (d). Each curve represents the detachment of ≈ 250 bacteria.

Figure 26 shows that the incubation time did not influence the detachment of the bacteria when they were incubated in MB. Besides it can be noticed that the bacterial detachment process of the samples incubated in MB occurred over a wide range of shear stresses as the failing edge of the removal curves for MB are not as steep as those for ASW. This observation indicates that when bacteria are incubated on the surface in MB they do not show a well-defined level of shear stress for detachment within the individual experiments.

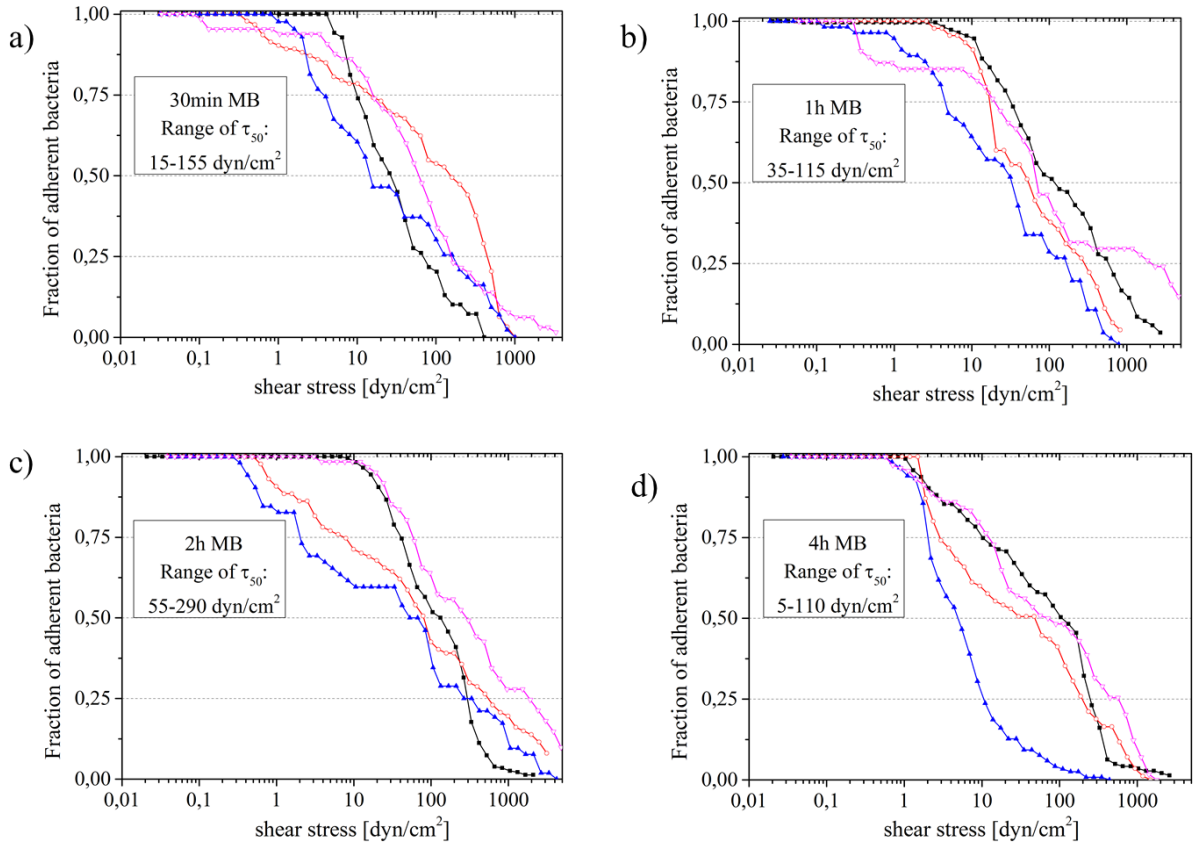

Figure 26. Detachment curves of *C. marina* in Marine broth (MB) from glass slides for different incubation times: 30 min (a), 1 h (b), 2 h (c) and 4 h (d). Each curve represents the detachment of ≈ 250 bacteria.

The experiments showed furthermore that the ratio of attached bacteria barely depended on incubation time or medium, since in all the cases ~ 40 % of the bacteria adhered (Figure 27b). Although this means that only a fraction of the bacteria was able to adhere, this fraction adhered rather quickly. In turn, complete establishment of adhesion as indicated by the τ_{50} values occurred on a longer timescale and strengthened over time. Such time-dependent adhesion is in general known as the transition from weak, temporary surface interaction of bacteria to a permanent bonding as established by extracellular polymeric substances (EPS) [212].

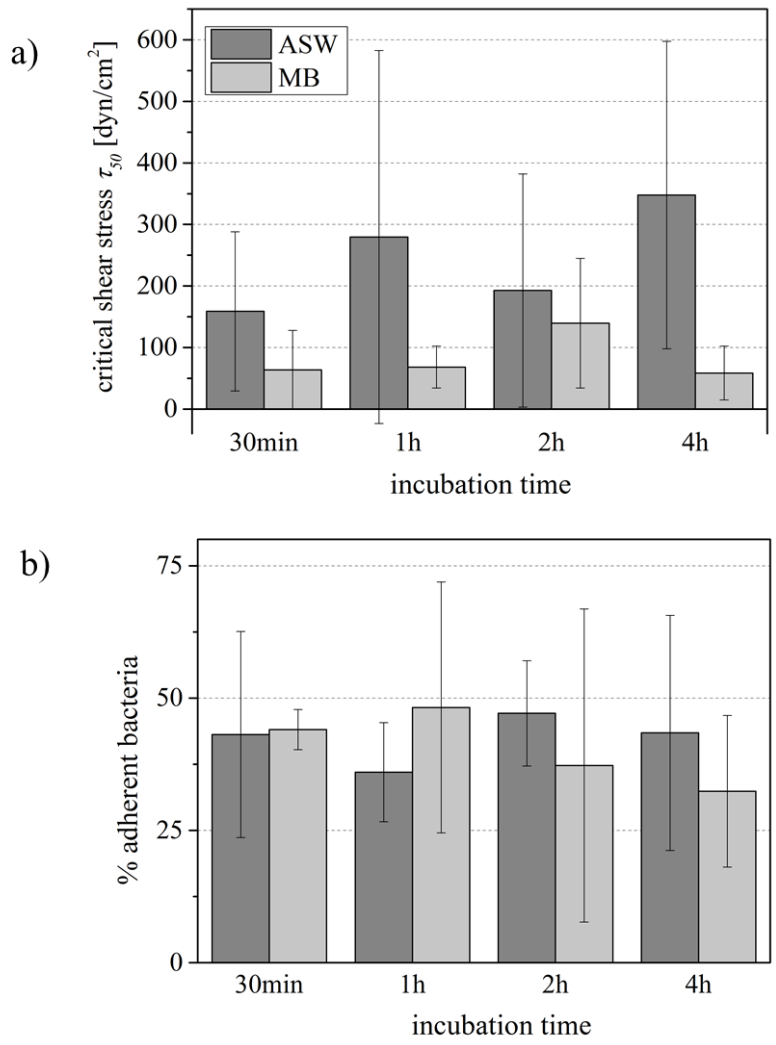

Figure 27. Average critical shear stress τ_{50} needed to detach 50 % of adherent bacteria (a) and fraction of adherent bacteria (b) settled on glass slides in ASW (dark gray) and MB (light gray) for different incubation times. Error bars represent the standard deviations.

It was desirable to keep the incubation time short in order to restrict the observations to the adhesion of individual bacteria. Simultaneously, the influence of incubation time and medium on the adhesion strength had to be as small as possible for maximum reproducibility. Thus, as a compromise for the microfluidic detachment assay 2 h settlement time in ASW was selected.

To confirm that the active bacterial physiological status was maintained in ASW, the bacteria were inoculated in ASW after reaching the log phase in MB and their growth was followed during 2 h by measuring the optical density at a wavelength of 600 nm. Figure 28 shows that despite the change of medium, the bacteria continued growing in ASW during the course of the experiment. Moreover, washing bacterial suspensions in ASW allowed removal of excess

EPS [108]. Consequently, ASW was used as both, incubation and removal medium for the detachment assays.

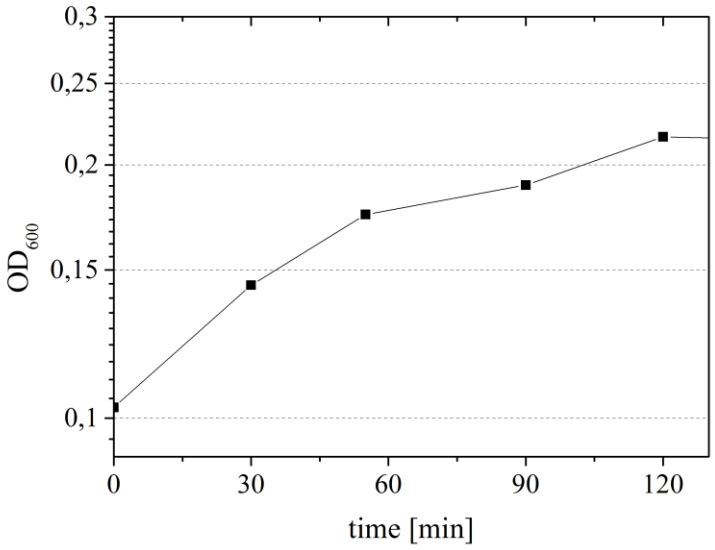

Figure 28. Growth curve of *C. marina* in ASW after reaching log phase in MB. The optical density was determined at a wavelength of 600 nm.

4.2.2. Influence of the rate of increase of the applied the shear stress

Fluid flow represents an important factor in microbial deposition [213] and consequently in bacterial adhesion on surfaces and biofilm formation. Shear stress is the dominant effect of fluid flow and can be well controlled in experimental systems like the microfluidic device used in this work. An increment of fluid flow velocity leads in first instance to a rise of microbial transport with regard to a substratum surface (convective diffusion) [34]. At the same time this increment of flow velocity causes a subsequent increase in hydrodynamic detachment forces as according to Poiseuille's model, the flow rate is directly proportional to the shear stress.

In order to investigate this effect and to find the optimal experimental parameters, the influence of the rate of increase of the applied shear stress with respect to the adhesion of *C. marina* was determined. Therefore the dwell time (5 s) and the shear stress reached at the end (≈5,500 dyn/cm^2) were kept constant, whereas the increment of applied shear stress every 5 s varied from 2 % to 8 %, 26 % and 90 % in relation to the shear stress applied during the previous step. As a consequence, the duration of the experiment differed resulting in 52 min,

14 min, 4.5 min and 1.7 min respectively. The applied shear stress as a function of time is represented in Figure 29.

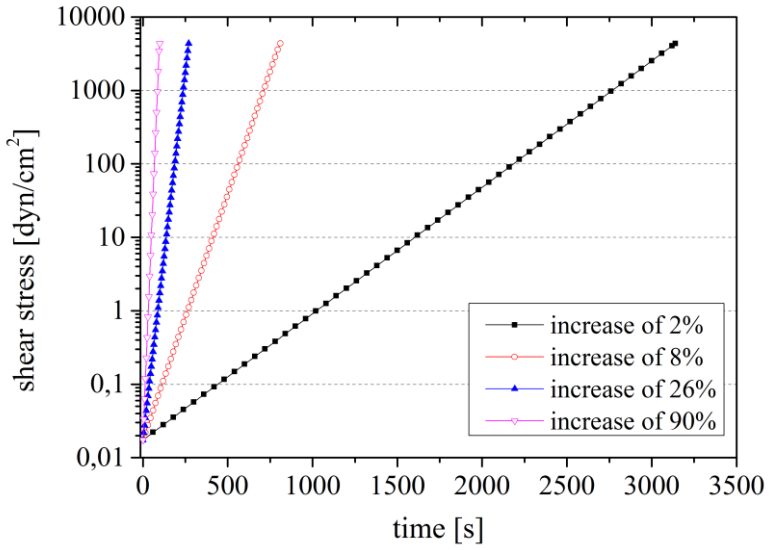

Figure 29. Shear stresses as a function of time as applied during the detachment assays.

For this study, the bacteria were incubated for 2 h on glass surfaces in ASW. The experiments were performed four times. The bacterial detachment curves are shown in Figure 30. Looking at the values of critical shear stress (τ_{50}, Figure 31) it can be noticed that with a faster increase of the applied flow and subsequently with decreased duration of experiments the shear stress necessary to detach the bacteria decreased. The explanation for that could be a potential adaptation of the bacteria to the flow by reinforcement of the adhesion. The only exception of this was for the 52 min experiment, where the τ_{50} value was similar to the one for the 1.7 min experiment although the experiments could not be analyzed without doubt because of their poor reproducibility.

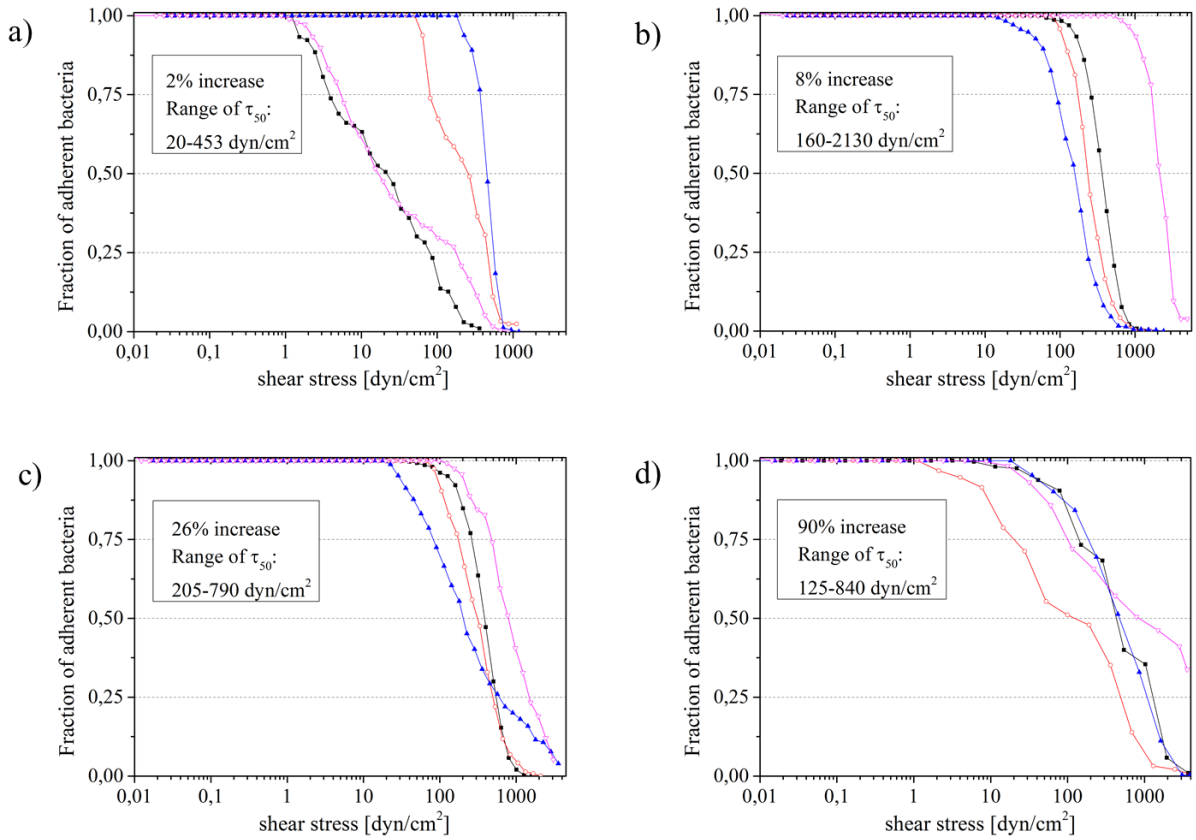

Figure 30. Bacterial detachment assays on glass performed with different increases of shear stress: 2 %, 8 %, 26 % and 90 %. Each curve represents the detachment of ≈ 400 bacteria.

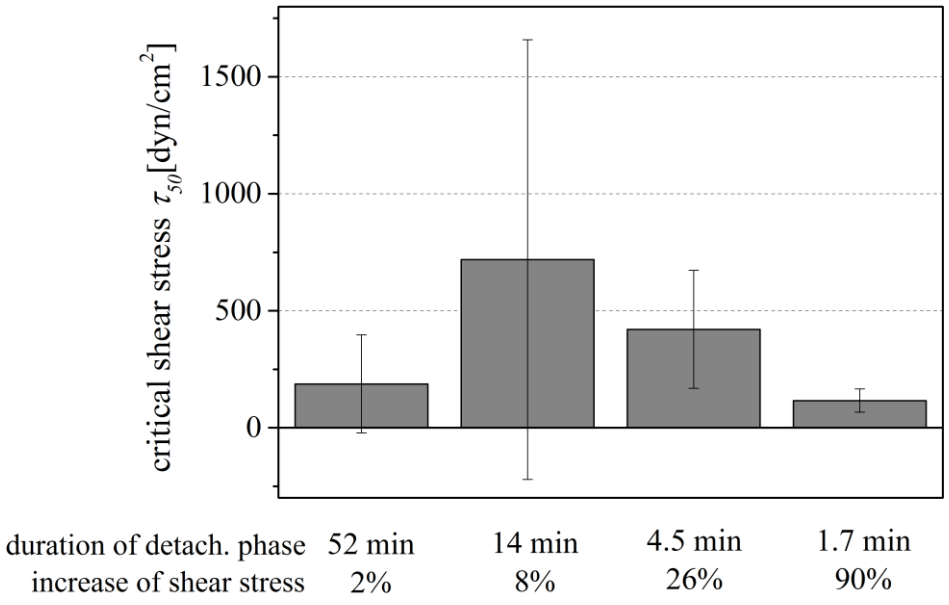

Figure 31. Average of the critical shear stress. Error bars are the standard deviation.

In order to choose the adequate parameter for the following detachment assays some criteria were taken into account. It was preferable to maintain a high reproducibility of the experiments and to keep the experimental duration short. Therefore, experiments with an increment of applied shear stress of 26 % or 90 % per 5 s seem to be the most suitable ones. A very fast rise of the applied hydrodynamic force (*e. g.* 90 %), on the other hand, leads to a removal curve with only few data points and accordingly to a rather coarse sampling. Besides, some of the removal curves of the experiment with a 90% increment per 5 s deviate from the others, as the detachment occurred over a wide range of shear stress resulting in a rather gently declining detachment curve.

Thus, detachment experiments with a 26 % per 5 s rate of increase of applied shear stress were found to be best suited to measure the adhesion of *C. marina* and were used for the experiments of this thesis.

4.3. Discussion

To determine the adhesion strength of the marine bacterium *Cobetia marina,* the critical shear stress to remove it from different surfaces was measured with a microfluidic shear stress setup. The assays conducted with this device provide two characteristic values for bacterial adhesion: the shear stress needed to detach 50 % of the adherent bacteria (τ_{50}), which was termed critical shear stress, and the percentage of adherent bacteria.

For the experimental protocol, the choice of the medium in which the bacteria were injected into the microfluidic system, incubation time, and rate of increase of the applied shear stress needed to be optimized. To find the optimal medium and incubation time, bacterial attachment and detachment were determined after 30 min, 1 h, 2 h and 4 h for bacteria inoculated in MB or ASW medium on glass surfaces. The results of these experiments showed a high variability and revealed that the ratio of adherent bacteria hardly depended on the incubation time or medium. It was observed for all time points that bacteria in ASW adhered more strongly than in MB, a medium containing peptides and yeast extract.

In ASW the settlement time did not influence the critical shear stress if it was longer than 1 h. In general the bacterial detachment process on the samples incubated in MB occurred over a wide range of shear stresses within individual experiments. For this reason ASW was the selected medium to carry out the experimental assays. Since it was desirable to keep

incubation time short and the influence of incubation time and medium on the adhesion strength as small as possible, 2 h settlement time in ASW inoculation medium was selected as the standard protocol for the detachment assays.

As fluid flow is an important factor in microbial adhesion, an optimization of its rate of increase was required. Consequently, the influence of the rate of increase of applied shear stress regarding bacterial adhesion was investigated. The dwell time (5 s) and the maximum shear stress (≈5,500 dyn/cm^2) were kept constant, while the increase of applied shear stress per step was varied from 2 % to 8 %, 26 % and 90 %. According to criteria such as experimental duration and sufficient sampling to accurately plot the removal curve, a rate of increase of applied shear stress of 26 % per 5 s was chosen as appropriate parameter for the detachment experiments.

Concluding, an incubation time of two hours in ASW and a rate of increase of applied shear stress of 26 %/5 s were found to be the optimal parameters to measure the critical shear stress of *C. marina*.

5. Influence of conditioning on the adhesion of bacteria

The formation of a conditioning film *i.e.* the adsorption of proteins and diverse macromolecules on submerged surfaces is commonly considered to be the first stage of the biofouling phenomenon [5] (see chapter 2.1). Such conditioning layers can mask the original surface chemistry [85] and affect bacterial adhesion [214] as natural sea water (NSW) and most growth media contain macromolecules that tend to form conditioning layers.

In order to further investigate this influence, the conditioning layer formed on ultrasmooth glass slides and DDT SAM was studied. These surfaces were selected since they have very different properties regarding wettability and chemistry. Glass substrates are unfunctionalized hydrophilic surfaces while DDT SAMs are hydrophobic methyl terminated SAMs. Furthermore, these surfaces are often used as a reference for biological assays.

5.1. Influence of conditioning on surfaces with different properties

5.1.1. Characterization of the samples incubated during different times

The most commonly used media in bacterial research are marine broth (MB) and artificial sea water (ASW), therefore they were chosen to investigate the influence of conditioning on surfaces with different properties: glass and DDT SAM. MB is a medium based on ASW with the addition of proteins (peptone and yeast extract). The surfaces were incubated in both media following a similar protocol to the established protein resistance assays [74, 75] for times ranging from 5 min up to 4 h. After immersion, the samples were characterized by contact angle goniometry and spectral ellipsometry or XPS for DDT SAMs and glass respectively. The characterization of the conditioning film formed on DDT SAMs after immersion for 30 min, 1 h, 2 h and 4 h in ASW or MB is shown in Figure 32. It was noticed that incubation of DDT in the different media had an influence on the wettability (Figure 32a), especially for substrates immersed in MB. The CA of DDT SAM after incubation on ASW barely varied during the first 2 h, nevertheless after 4 h it decreased from ≈95° to ≈80°. Incubation in MB caused a substantial change of the CA of DDT SAMs making the samples more hydrophilic with CA decreasing from 95° to 70°. This shift of CA occurred within the first 2 h, after which the CA hardly varied.

Figure 32b displays the thickness of the conditioning film on DDT SAM after incubation for different times in MB or ASW. After 30 min, a conditioning film of ≈ 4 Å was formed. This film on samples incubated in ASW barely changed during the first 2 h, nevertheless after 4 h its thickness increased to be 6 Å. Incubation of the samples in MB led to an important thickness increase of the conditioning film, especially for times longer than 2 h with the thickness reaching ≈ 14 Å after 2 h and ≈ 16 Å after 4 h immersion.

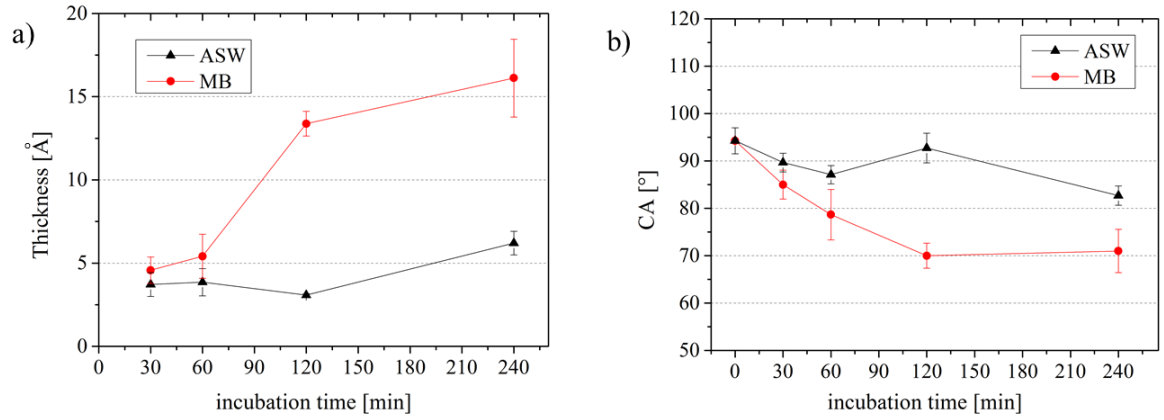

Figure 32. Characterization of the conditioning film on DDT SAMs formed after incubation in ASW or MB for 30 min, 1 h, 2 h and 4 h. CA (a) and thickness (b) were determined. Error bars are the standard errors of the mean.

Although the characterization of DDT SAM was not performed before a minimum incubation time of 30 min, additional time points after 5 min and 15 min were chosen for the evaluation of the film on glass substrates, in order to assure a gradual observation of the influence of the media in which the glass slides were immersed.

Characterization of the conditioning film formed on glass as a function of time exposed to ASW and MB media is represented in Figure 33. It was observed that the wettability of glass was influenced by conditioning (Figure 33a). After immersion in ASW, it became more hydrophilic as its CA decreased from ≈21° to ≈14°. In contrast, immersion in MB turned the substrates more hydrophobic causing a drastic change of the CA from ≈21° to ≈44°. These effects occurred within the first 30 min, afterwards the contact angles scarcely varied. The thickness of the conditioning layer (Figure 33b), determined by quantifying the attenuation of the XPS silicon Si2p spectrum (Figure 33c), and the nitrogen content (Figure 33d) were measured by XPS. For every time point, the thickness of the film on glass was significantly larger when incubated in MB. After 30 min the conditioning layer thicknesses were ≈2 Å and ≈8 Å for glass incubated in ASW and MB, respectively. These thicknesses remained nearly

constant and barely changed after longer incubation. N1s XPS signals (Figure 33d) indicated a high concentration of nitrogen present in all conditioning layers of samples incubated in MB likely due to the presence of yeast extract, a rich nitrogen source, which is an ingredient of the medium. In contrast, the samples immersed in ASW showed a nitrogen content nearly as low as the one found in the reference glass substrate. Previous work applied infrared reflection absorption spectroscopy (IRRAS) to investigate the chemistry of the conditioning films formed on SAMs with different wettabilities after incubation in spore water, a protein rich medium as MB. It was shown that the amide content was higher on hydrophilic surfaces (AUDT and HUDT SAMs) in comparison to hydrophobic surfaces (DDT and FUDT) [85]. These findings could explain the higher nitrogen content observed on the conditioning films from MB on glass slides, a very hydrophilic surface.

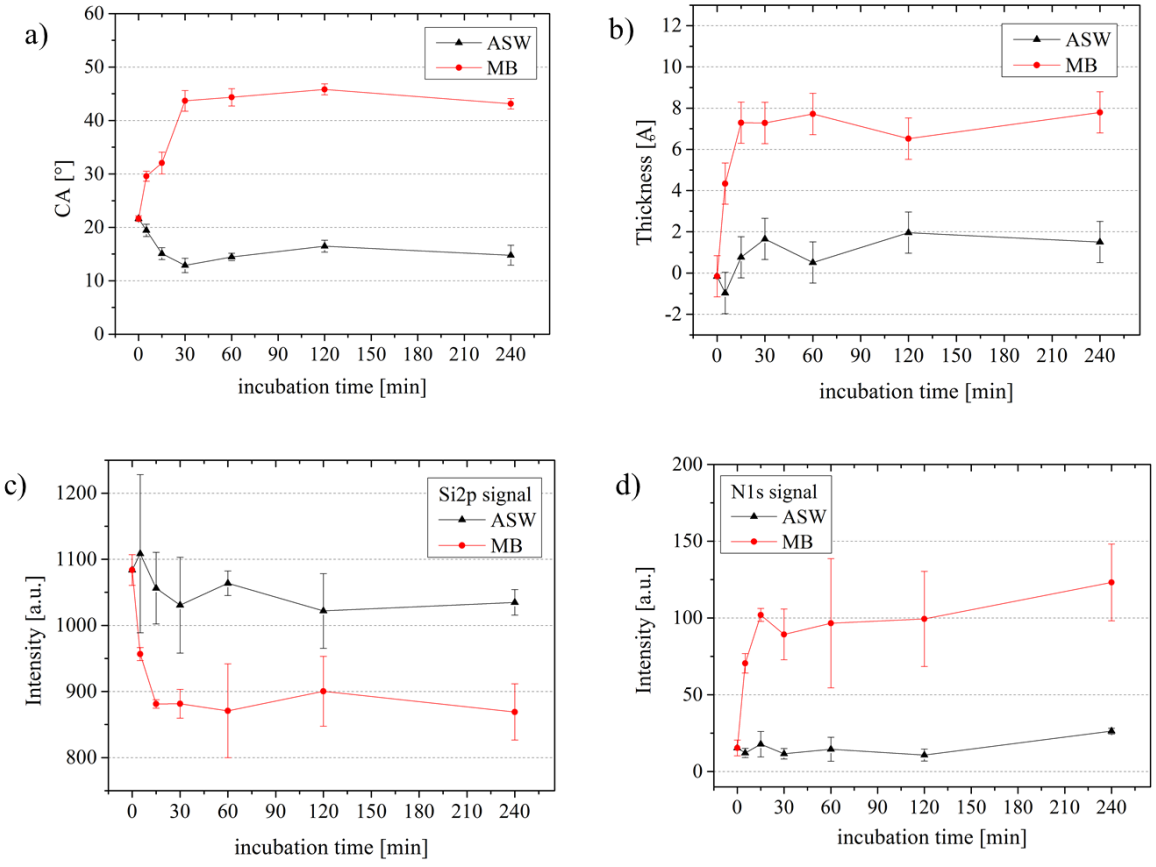

Figure 33. Characterization of the conditioning film formed on glass after incubation in ASW or MB for 0 min, 5 min, 15 min, 30 min, 1 h, 2 h and 4 h. CA (a), thickness (b), and silicon (c) and nitrogen (d) content as determined by XPS. Error bars are the standard error of the mean.

5.1.2. Characterization of samples after 2 h incubation in different media

The samples incubated for 2 h in MB, ASW and NSW media were characterized by contact angle (CA) goniometry and spectral ellipsometry in the case of DDT SAMs or XPS in the case of glass slides. The values represent the mean of three measurements. CA and thickness of the samples are shown in Figure 34. CA of samples incubated in ASW and NSW (Figure 34a) barely differed in comparison to pristine samples. Nevertheless after immersion in MB, the CA of the samples varied. DDT became more hydrophilic with the CA decreasing from ≈95° for pristine DDT to ≈70°. Submerging glass in MB caused a drastic increase of the CA which was at least twice as high as in the other samples. Figure 34b displays the thickness of the resulting conditioning film which was relative to the pristine surfaces. Some trends could be noted for both surfaces. A conditioning layer was formed on both surfaces, however the thicknesses after incubation in ASW and NSW were negligible in comparison to the one in MB, especially for DDT SAMs. The film found on the surfaces after immersion in ASW and NSW led to similar values. After submerging in MB, the resulting conditioning layer of DDT (≈13 Å) was nearly 5 times larger than after incubation in ASW and NSW (≈3 Å) [15]. The same trend was observed for glass substrates where the thickness values after immersion in MB (≈6.5 Å) were at least 3 times larger than after immersion in ASW (≈1.7 Å) and NSW (≈2.2 Å).

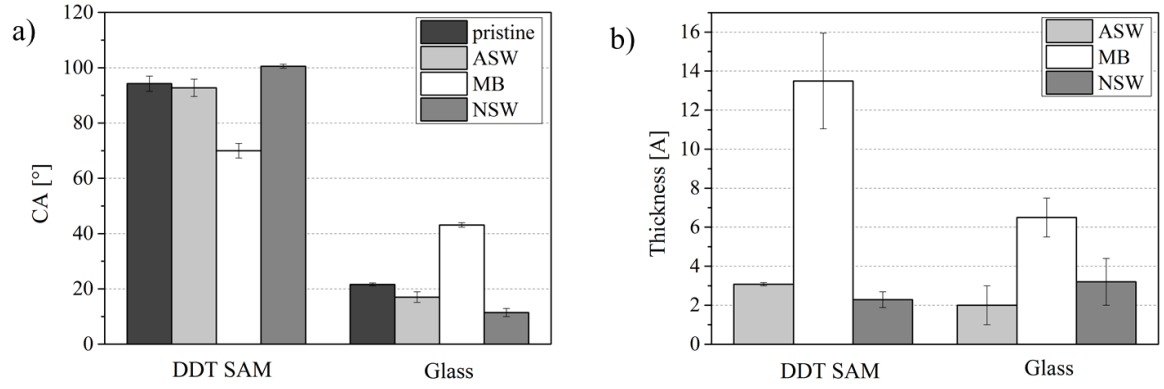

Figure 34. Characterization of glass slides and DDT SAMs after 2 h immersion into different media by measuring (a) CA and (b) conditioning layer thickness. The values represent the average of three samples. Thickness values are relative to a representative pristine surface. Error bars are the standard errors of the mean.

The high values of the thickness of the conditioning film for samples incubated in MB can be explained as protein rich media such as MB are known to cause thicker conditioning films [85].

5.2. Bacterial adhesion on conditioned surfaces

To understand in which manner the adsorbed overlayers affect bacterial adhesion, bacterial detachment assays were performed on pristine and conditioned surfaces. We focused on two factors: time and medium of the pre-incubation of the samples. Even though, the time of bacterial incubation was always kept constant: 2 hours.

5.2.1. Bacterial adhesion on DDT SAM pre-incubated in MB during different incubation times

In chapter 5.1.1 it was shown that immersion in MB changed the surface properties much more than immersion in ASW. Furthermore the conditioning film formed on DDT SAM was thicker than the one formed on glass. For this reason DDT SAM and MB were chosen to investigate the impact of the duration of the conditioning on bacterial adhesion. To this end, DDT samples were immersed 1 h, 2 h and 4 h in MB and subsequently used for the microfluidic bacterial assays. The removal curves obtained were compared to the ones for the pristine DDT SAM.

Figure 35 displays the removal curves and the range of critical shear stress (τ_{50}) for the bacterial detachment assays on pristine DDT SAM samples and those pre-incubated in MB for different times. The ranges of critical shear stress for pristine and 1 h pre-incubated DDT SAM were very similar indicating that 1 h incubation in MB did not influence the bacterial adhesion.

Looking at the range of critical shear stress a trend towards decreasing shear stress necessary to detach the bacteria with increasing duration of the pre-incubation was observed. As the ranges of critical shear stress for pristine and 1 h pre-incubated DDT SAM were very similar, this effect was noticed from 2 h on. At the same time, the critical shear stress ranges for 2 h and 4 h pre-incubated DDT SAMs were also similar.

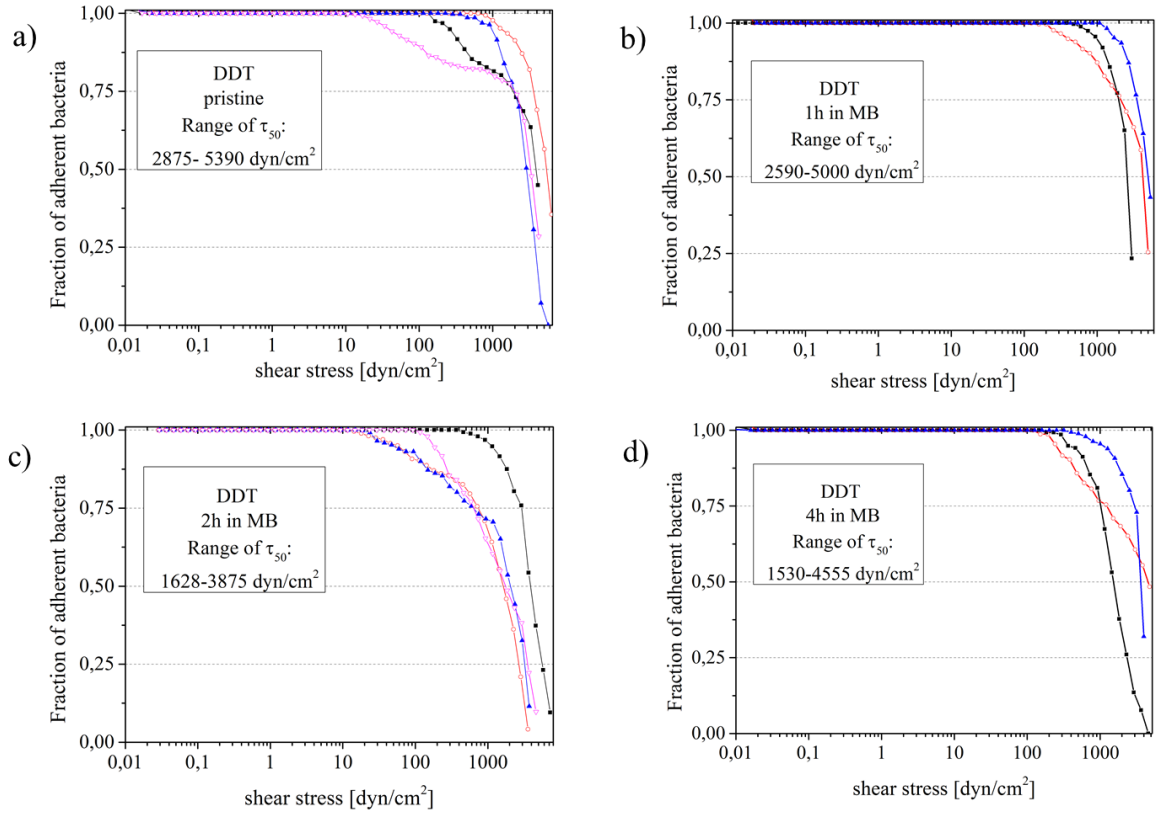

Figure 35. Removal curves and range of critical shear stress (τ_{50}) of the bacteria on DDT SAM and pre-incubated for 0 min (a), 1 h (b), 2 h (c) and 4 h (d) in MB. Each curve represents the detachment of ≈ 500 bacteria.

5.2.2. Bacterial adhesion assay on surfaces pre-conditioned 2h in different media

In order to determine whether the conditioning layer formed after incubation on different media affects bacterial adhesion, bacterial detachment assays were conducted on the samples described in the previous chapter. The resulting detachment curves were then compared to the ones for pristine surfaces. The selected media were artificial seawater (ASW), natural seawater (NSW) and the bacterial growth medium marine broth (MB). The samples were immersed in the media for 2 h, which corresponds to the time used for the biological experiments described previously (chapter 3.2.3).

Detachment curves of *C. marina* on DDT and on glass are shown in Figure 36 and Figure 37, respectively, for pristine samples (a) and samples conditioned in MB (b), ASW (c) and NSW (d). The critical shear stress and the percentage of adherent bacteria were determined in four independent experiments for each and their averages are shown in Figure 38.

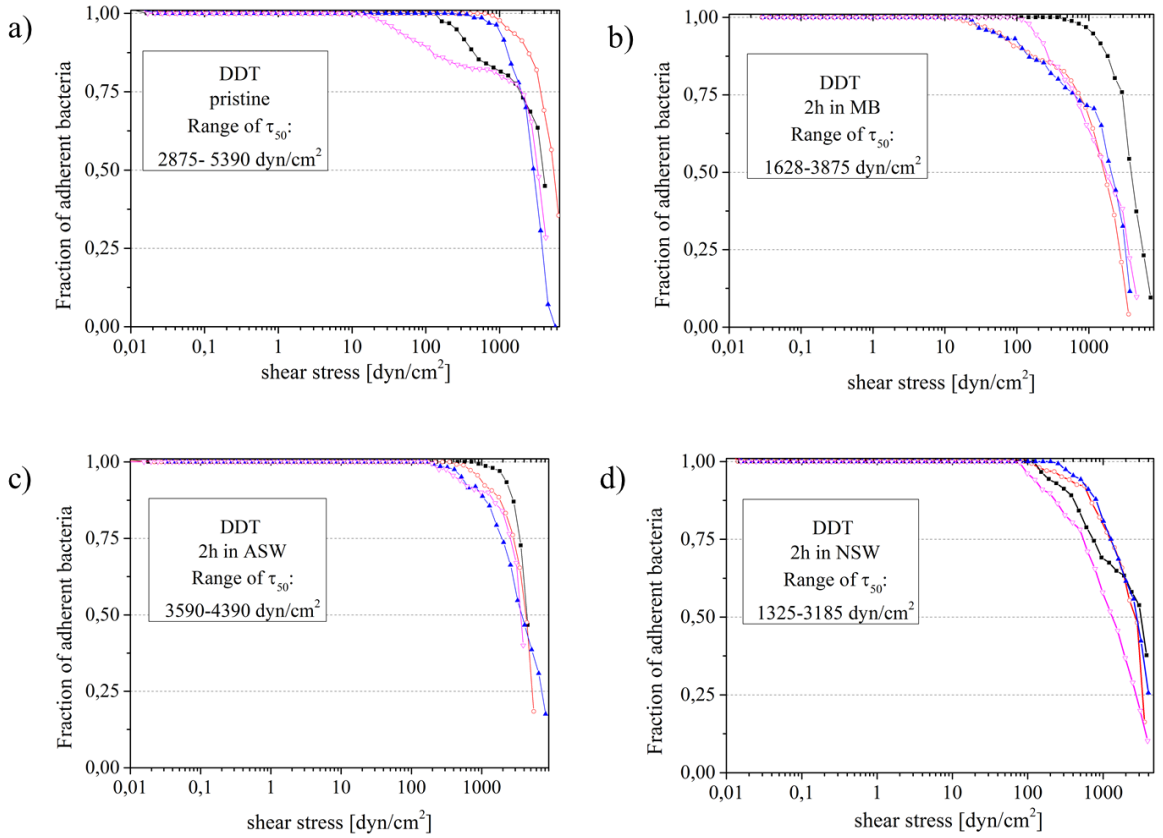

Figure 36. Detachment curves for *C. marina* on DDT SAM pristine (a) and after incubation in MB (b), ASW (c) and NSW (d) media. Each curve represents the detachment of ≈ 500 bacteria.

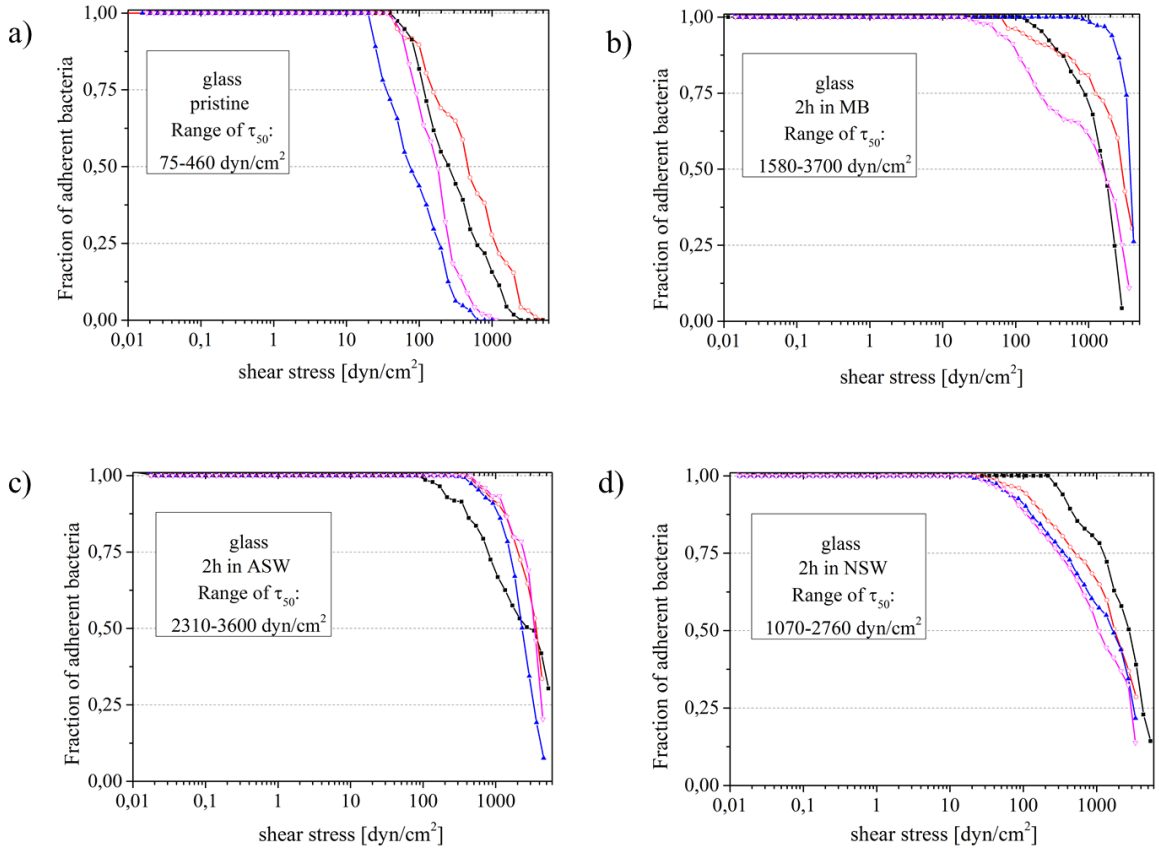

Figure 37. Detachment curves for *C. marina* on pristine glass (a) and after incubation in MB (b), ASW (c) and NSW (d) media. Each curve represents the detachment of ≈ 400 bacteria.

It was noticed that the shear stress needed to remove *C. marina* was affected by the conditioning film [15] as shown in Figure 38a. Incubation of DDT SAM in MB or NSW led to a similar critical shear stress value (≈2,300 dyn/cm^2). Simultaneously, such values were reduced by 30 % (from ≈3,400 dyn/cm^2 to ≈2,300 dyn/cm^2) in comparison to the pristine surfaces. In contrast, adhesion was barely enhanced when DDT SAM was incubated in ASW.

With regard to the influence of a conditioning film on bacterial adhesion on glass (Figure 37 and Figure 38a), all immersions strongly increased the critical shear stress of *C. marina* in comparison to the pristine surfaces. This value (≈250 dyn/cm^2) increased by a factor of 12, 8 and 5 when glass was incubated in ASW, MB or NSW respectively.

In general, after incubation in the same medium, the differences in critical shear stress between both surfaces diminished, compared to the values of pristine samples. An ANOVA test was performed between the critical shear stress (τ_{50}) values showing a statistically significant difference between the data (significance level of 0.05). Subsequently, a Tukey test was applied to compare pairs of the means as a post–hoc analysis in order to determine if the

pair of surfaces differed statistically. All of the coatings showed a statistically significant difference in comparison to glass. Besides, pristine DDT SAM compared to one incubated in NSW as well as glass immersed in NSW compared to DDT incubated in ASW also showed a statistical difference.

Figure 38b displays the percentage of adherent bacteria on glass and on DDT SAM. Incubation in all media hardly varied the percentage of adherent bacteria on DDT SAMs. Only incubation in NSW decreased the percentage of adherent bacteria by ~ 25 % in comparison to the other DDT SAMs. The conditioning film on glass immersed in MB strongly influenced the percentage of adherent bacteria in relation to the pristine glass. This value increased by at least 40 % with respect to the one for pristine surface when glass was incubated in any one of the media. It can be noticed that, after incubation in the same medium, the percentage of adherent bacteria on both surfaces was very similar.

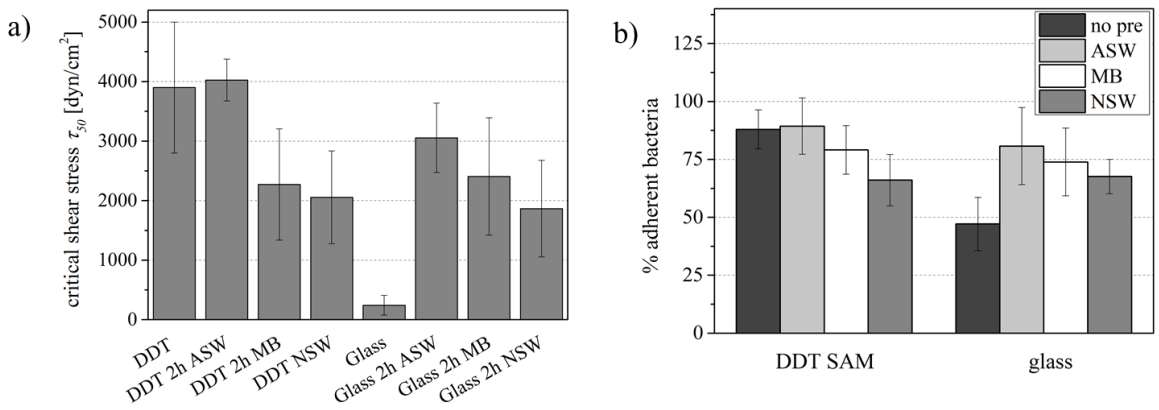

Figure 38. The average critical shear stress τ_{50} needed to detach 50 % of the adherent bacteria (a) and the fraction of adherent bacteria (b) on glass slides and DDT SAMs. Mean values were determined from four independent experiments. Error bars are the standard deviation.

5.3. Discussion

The influence of conditioning of surfaces with different properties, glass slides and DDT SAM, was evaluated in order to investigate the hypothesis that the conditioning film may influence the adhesion of bacteria. For this purpose, these surfaces were incubated in different media and characterized by contact angle goniometry and spectral ellipsometry, in the case of DDT SAM, or XPS for glass samples.

Surfaces were immersed in ASW or MB for durations ranging from 5 min up to 4 h and the resulting conditioning layers were characterized. At this point it is necessary to emphasize that MB is a protein rich medium as it contains peptone and yeast extract. The findings showed that only after 30 min a significant conditioning film was formed when incubated in MB. This observation was not surprising, as incubation in a protein containing medium led to the formation of a thicker conditioning film than immersion in salt water [85]. In the case of glass substrates, the film thicknesses after 30 min incubation in MB or ASW were ≈8 Å and ≈2 Å respectively and barely changed with time. Immersion of DDT SAMs in ASW for 30 min caused the formation of a conditioning film with a thickness of ≈4 Å. This value remained constant for the first 2 h and after 4 h it increased, reaching a value of ≈6 Å. Film thicknesses for DDT after incubation in MB strongly increased after 2 h (≈14 Å) and after 4 h the thickness was determined to be ≈16 Å. Thus, the film formed on DDT SAMs was thicker than the ones on glass substrates, which was in agreement with previous observations where hydrophobic surfaces, such as DDT, were able to readily adsorb a conditioning film [74, 75, 86].

The influence of the conditioning time of the surfaces on bacterial adhesion was investigated by immersing DDT SAMs for 1 h, 2 h and 4 h in MB, and subsequently performing bacterial detachment assays. A trend towards decreasing shear stress needed to detach the bacteria with increasing duration of the pre-incubation was observed. For pristine and 1 h pre-incubated SAM the range of critical shear stress was similar. That was the same case for the ranges of DDT SAM immersed 2 h and 4 h in MB. For this reason we suggest that the conditioning film formed during up to 2 h incubation in MB did not further influence the adhesion of *Cobetia marina.* These observations are in agreement with the experimental characterization of the formed conditioning film on DDT when incubated in MB as its thickness and CA hardly varied from up 2 h.

In order to evaluate the impact of the films formed on glass and DDT SAM after conditioning in diverse media on bacterial adhesion , the samples were immersed in ASW, NSW and MB media for 2 h, the same time span used for the bacterial detachment assays. These surfaces were characterized prior to being used for the assay with the microfluidic device. Thickness measurements showed that immersion of both surfaces in all media led to a formation of a conditioning film. The film thickness on both samples after submerging in ASW and NSW was very similar and nearly negligible in comparison to the results after submersion in MB, especially for DDT SAM. The wettability of both surfaces after immersion in ASW and NSW

hardly varied in relation to the one for pristine surfaces. Nonetheless the wettability of the surfaces after incubation in MB changed turning DDT SAM more hydrophilic and glass slides more hydrophobic. Consequently the conditioning film formed on samples incubated in MB was thicker than on those immersed in ASW and NSW.

Bacterial detachment assays revealed that conditioning exerted an influence on bacterial adhesion. Submerging DDT SAM on MB or NSW reduced the values of critical shear stress in comparison to those for pristine samples and those pre-incubated in ASW. In contrast to ASW, NSW contains some proteins since it was extracted from the nature and filtered with protein permeable filters. MB is a yeast and peptone culture medium. Thus, incubation in protein containing media clearly diminished the values of critical shear stress in comparison to the pristine surfaces.

Regarding the influence of the conditioning film on bacterial adhesion on glass, any incubation strongly altered the critical shear stress of *C. marina*. In comparison to the pristine surfaces, such value increased by a factor of 12, 8 and 5 when glass was incubated in ASW, MB or NSW respectively.

Conditioning also influenced the percentage of adherent bacteria on the surface although to a lesser degree than the critical shear stress. Submerging DDT SAMs in ASW or MB barely varied the percentage of adherent bacteria or led to a similar value in comparison to the pristine surfaces. However immersion in NSW decreased the percentage of adherent bacteria by ~ 25 % in comparison to the other DDT SAM samples. The conditioning film on glass strongly influenced the percentage of adherent bacteria. The value, when glass was incubated in any media, increased by at least 40 % with respect to the one of the pristine surfaces.

However, the most important finding was that after immersion in the same medium the values of critical shear stress and fraction of adherent bacteria of both samples were more similar than those of the pristine samples. Therefore we suggested that a conditioning of the samples leads to an equalization of both chemistries as the differences in critical shear stress and percentage of adherent bacteria diminished. This trend was observed for 2 h incubation time even though it can be speculated that after a certain time span, longer than 2 h, this effect could be even stronger.

Thus, it can be concluded that conditioning exerted an influence on bacterial adhesion. This influence was weaker for DDT SAM than for glass substrates and was minimized for the combination of DDT SAM and ASW. These observations support the choice of ASW as

medium for the bacterial assays (see chapter 4.2.1). In contrast, submerging glass in any media led to a strong increase of bacterial critical shear stress. These results suggest that glass substrates are not suitable surfaces to be used as references for bacterial adhesion assays.

6. Bacterial adhesion on differently terminated SAMs with different wettabilities

Numerous recent studies have revealed that the wettability of surfaces has an effect on their inert properties [75, 82, 93, 215-217]. While some studies showed a clear correlation between adhesion and contact angle [35, 50, 81, 82, 86, 96-99], other studies reported only a poor correlation between wettability and fouling behavior of selected species [100, 101].

The thesis that the wettability of the surfaces exerts an influence on the adhesion of the bacterium *C. marina* was investigated in this work. The evaluated surfaces, which cover a large range of wettabilities, were undecanethiol SAMs with different chemical end-groups namely $–CH_3$, $-NH_2$, $-CH_2OH$, $-OC_7F_{10}CF_3$ and polyethylene glycol (PEG) terminated SAMs (PEG 2000-OH).

6.1. Characterization of SAMs

The water contact angle and spectral film thickness of the analyzed SAMs are shown in Table 5. It can be observed that the coatings differ especially in their wettability. The values obtained are in good agreement with the ones found in the literature [83, 86, 103, 218, 219].

Label	Full name	Details	Contact angle [°]	Ellipsometric thickness [Å]
PEG	Hydroxy-PEG 2000-thiol	$SH-(CH_2)_2-(O-(CH_2)_2)_{44}-OH$	30	30
HUDT	11-Hydroxyl-1-undecanethiol	$SH-(CH_2)_{11}-OH$	38	10
DDT	11-Amino-1-undecanethiol	$SH-(CH_2)_{11}-NH_2$	106	13
AUDT	Dodecanethiol	$SH-(CH_2)_{11}-CH_3$	54	16
FUDT	11-(tridecafluorooctyloxy) undecanethiol	$SH-(CH_2)_{11}-O-(CH_2)_2-(CF_2)_5-CF_3$	113	16

Table 5. Properties of the different SAMs: water contact angle and film thickness as determined by spectral ellipsometry. The reported values are the average of three measurements (standard errors: ±2 °CA; ±2 Å ellipsometry).

Firstly it is important to point out that when the term PEG is mentioned during the follow discussions it refers to PEG 2000-OH SAMs. DDT and FUDT SAMs are hydrophobic (CA of 106° and 113° respectively). AUDT SAMs present an intermediate wettability with a CA of

54° while PEG and HUDT SAMs were hydrophilic with a CA of 30° and 38° respectively. As also shown in Table 5, all SAMs have a similar thickness, except for PEG, which is significantly thicker. According to some previous studies, the hydrophilic surfaces are supposed to present a weaker adhesion in comparison to the hydrophobic surfaces.

6.2. Bacterial adhesion on differently terminated SAMs

Bacteria were incubated on the surfaces for 2 h and their adhesion was determined using the microfluidic detachment assay [15]. The experiments were performed four times for each surface. Figure 39(a-e) shows the detachment curves for all surfaces. These curves revealed that at a shear stress of ≈5 dyn/cm^2, the adherent bacteria began to detach from PEG. For the other SAMs, the first bacteria were removed at a higher shear stress of ≈ 100 dyn/cm^2. For some samples, such as FUDT SAMs, it was not possible to remove all adherent bacteria before the maximal applied shear stress, as dictated by the setup, was reached.

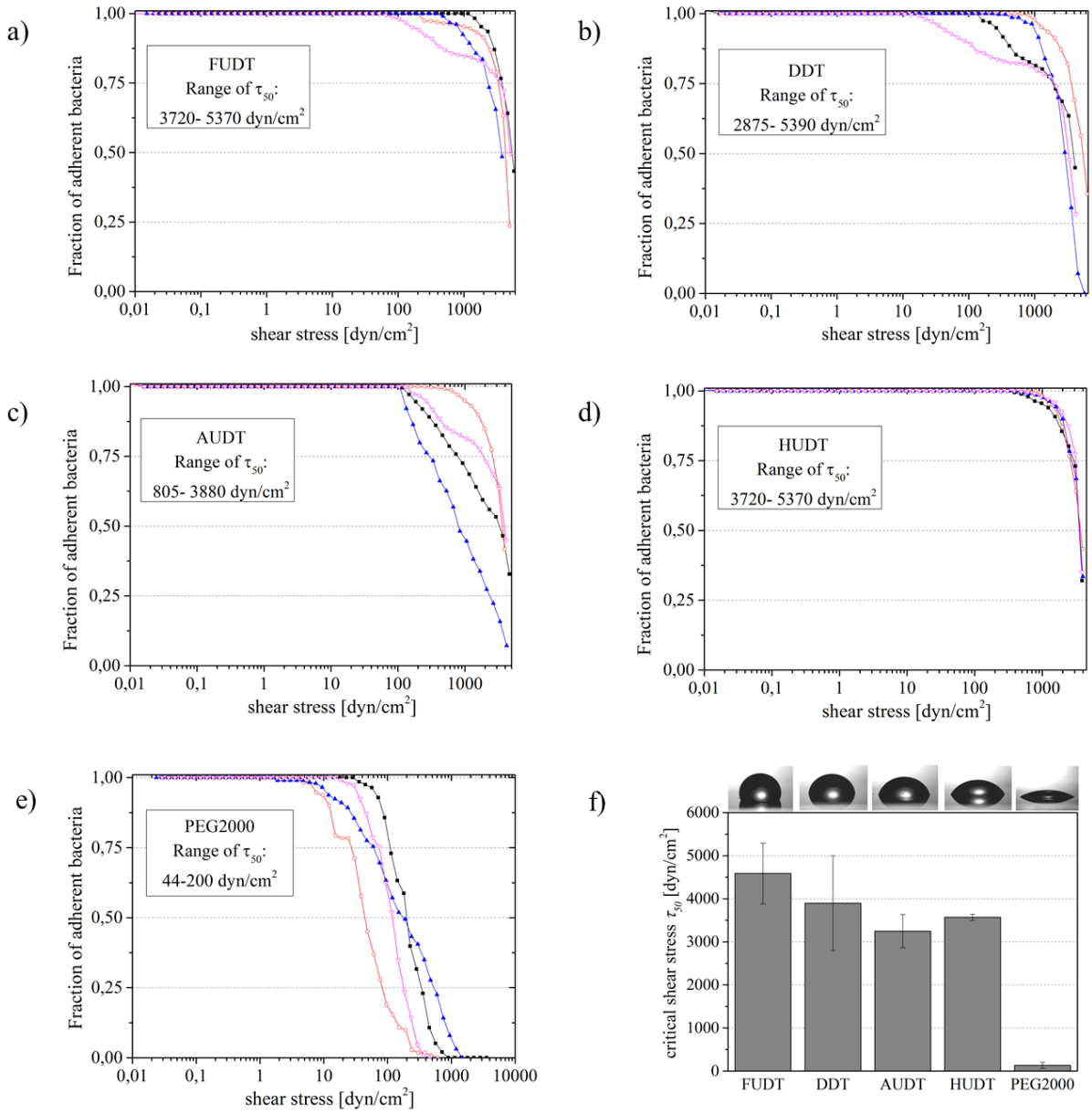

Figure 39. Detachment curves and range of critical shear stress (τ_{50}) for bacterial adhesion on chemically different terminated SAMs: FUDT (a), DDT (b), AUDT (c), HUDT (d), PEG2000-OH (e). Average critical shear stress needed for removal of 50 % of the adherent bacteria (f) SAMs vary in water contact angle. Each curve represents the detachment of ≈ 600 bacteria. Error bars are the standard deviation.

Figure 40f reveals that the chemical termination of the SAMs influenced the critical shear stress especially in the most hydrophobic and hydrophilic surfaces (FUDT and PEG SAMs). An ANOVA test was performed between the critical shear stress τ_{50} values showing a high statically significant difference of the data (significance level of 0.01). Furthermore, a Tukey test was applied to compare pairs of the means as a post-hoc analysis in order to determine if the pair of surfaces differed statistically. All the coatings showed a statistically significant difference in comparison to PEG SAM as well as FUDT compared to AUDT also showed a

statistically difference. Nevertheless, the influence of the chemical termination on bacterial adhesion hardly varied on SAMs with intermediate contact angles namely HUDT, DDT and AUDT SAMs.

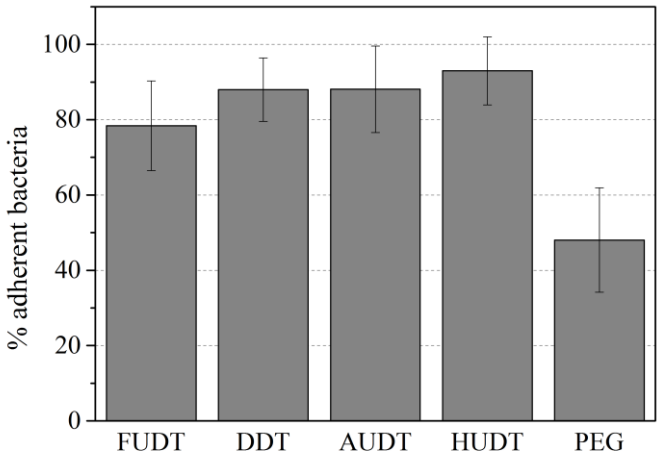

Figure 40. Bacterial attachment to DDT, FUDT, AUDT, HUDT and PEG SAMs after 2 h incubation in ASW. Fraction of adherent bacteria on the surfaces. Error bars are the standard deviation.

The wettability of the surfaces was found to influence the fraction of adherent bacteria on the samples to a lesser degree (Figure 40). However, PEG was a special case as its fraction of adherent bacteria and the critical shear stress were substantially reduced. The percentage of adherent bacteria on PEG was approximately half the value in comparison to the other SAMs.

6.3. Discussion

The influence of surface chemistry regarding the adhesion of *C. marina* was investigated. For this purpose, bacterial adhesion on chemically different terminated SAMs representing a range of wettabilities (PEG, HUDT, AUDT, DDT and FUDT SAMs, with increasing CA) was evaluated [15]. It was found that the chemical termination of the SAMs influenced the critical shear stress, particularly in the case of the most hydrophobic and hydrophilic SAMs (FUDT and PEG). Nonetheless, this influence on HUDT, DDT and AUDT SAMs scarcely varied. This observation was surprising especially for HUDT SAM, which has a wettability that is very similar to the one of PEG SAM. Therefore those coatings were expected to have better fouling-release properties, even though previous studies also showed the same trend of results [80]. The percentage of bacteria that adhered to the surface was affected to a lesser degree by the chemical termination. In the case of PEG, the fraction of adherent bacteria and the critical

shear stress were substantially reduced. The shear stress required to remove bacteria from the hydrophilic PEG-coated surfaces was only ~ 5 % of that needed for the other, more hydrophobic SAMs. These observations support the general notion that hydrophilic, highly hydrated surfaces have a good short term resistance and the ability to reduce the attachment of marine biofoulers [6, 108, 217, 220]. Nevertheless, the critical shear stress of the hydrophilic HUDT SAMs was similar to the one of SAMs with intermediate wettability which indicates that hydrophilicity is a necessary, but not sufficient criterion for resistance against biofoulers.

In the case of PEG bacterial adhesion was found to differ significantly from the other SAMs as the critical shear stress value on PEG (≈ 140 dyn/cm^2) was at least one order of magnitude lower than the value for the hydrophobic surfaces (≈ 3,500 – 4,000 dyn/cm^2). The fraction of the bacteria which adhered to the surface strongly decreased when the bacteria were incubated on PEG SAMs (~ 50 %) in relation to the other SAMs with approximately 85 % of adherent bacteria. These findings are in line with many previous studies reporting the good protein and biofouling resistance of PEG samples [6, 83, 108, 217].

7. Bacterial adhesion on ethylene glycol SAMs

Ethylene glycol (EG) based SAMs are well known protein resistant surfaces which have been investigated with respect to biomedical [55, 221] and antifouling applications [35, 83, 217, 222] (see chapter 2.7.2). The origin for this protein repelling property may be related to the ability of these surfaces to bind water since previous studies demonstrated that with an increasing number of EG units the hydration of the EG SAMs raises [102, 125, 128] and the fouling resistance increases [83, 222]. Furthermore, previous studies showed that the ability of these SAMs to resist protein adsorption depends on the molecular conformations [102, 127, 128] (see chapter 2.7.3). Thus another complementary explanation could be based on the adopted conformation of the oligomer chain of the EG SAMs. *Ab initio* calculations show that an optimized molecular conformation is a prerequisite for stable water binding [128]. In this chapter, the adhesion of the marine bacterium *C. marina* on EG SAMs with different chain lengths was investigated to test whether it is relevant to bacterial adhesion.

7.1. Characterization of EG SAMs

7.1.1. Contact angle goniometry and spectral ellipsometry

The wetting behaviour and the film thickness of the EG SAMs were characterized in order to verify the successful preparation of the samples. Figure 41 displays the structure of the molecules which were used for the EG_n (n = 1, 3 and 6) SAM preparation. The sessile water contact angles are listed in Table 6. All EG surfaces have similar sessile drop contact angles around 30° which indicates the hydrophilic character of the films.

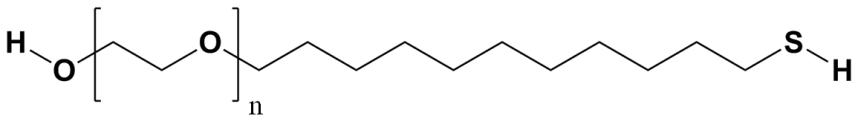

Figure 41. Structure of the EG_n molecules which were used to prepare the SAMs.

Label	Full name	Details	Contact angle [°]	Ellipsometric thickness [Å]
EG_1	Hydroxy-mono(ethylene glycol) undecanethiol	$SH-(CH_2)_{11}-(O-(CH_2)_2)-OH$	32	12
EG_3	Hydroxy-tri(ethylene glycol) undecanethiol	$SH-(CH_2)_{11}-(O-(CH_2)_2)_3-OH$	34	18
EG_6	Hydroxy-hexa(ethylene glycol) undecanethiol	$SH-(CH_2)_{11}-(O-(CH_2)_2)_6-OH$	32	27
PEG	Hydroxy-PEG 2000-undecanethiol	$SH-(CH_2)_2-(O-(CH_2)_2)_{44}-OH$	30	30

Table 6. Characterization results of EG SAMs: sessile water contact angle and film thickness as determined by spectral ellipsometry. The reported values are the average of three measurements each on at least three different surfaces (errors: ±2° CA; ±2 Å ellipsometry).

The EGs showed thicknesses of 15 Å up to 30 Å (Table 6) indicating an increase of the film thickness with an increasing number of EG units. Even though PEG contains an even higher number of ethylene glycol units, thicknesses are comparable to EG_6. The reason for the low value might be its short alkyl spacer (C_2) which promotes the mushroom-like constitution of the molecules preventing a closely packed brush-like surface [223].

7.1.2. XPS

The chemical composition of the EG_n SAMs with a short EG chain (n=1, 3 and 6) was characterized by XPS. Table 7 displays the thickness of the SAMs as measured by XPS compared to the data obtained by spectral ellipsometry. The thickness of the EG SAMs was calculated by the attenuation of the Au 4f signal. The increase of the SAMs thickness goes along with the rising number of EG units. The obtained values are in good agreement with literature values [83, 102, 224].

SAM	Thickness [Å]	
	XPS	ellipsometry
EG_1	15	12
EG_3	18	18
EG_6	26	27

Table 7. Thickness of the EG SAMs measured by XPS and spectral ellipsometry (standard errors: ±3 Å XPS; ±2 Å ellipsometry).

Figure 42 shows the O1s (a) and C1s (b) spectra of the EG SAMs. The formation of the EG part of the molecule can be confirmed by the growth of the O1s peak which corresponds to the increase of EG units. The C1s spectra consist of two peaks at 286.5 eV and 284.7 eV corresponding to the ether carbon and the alkyl carbon respectively [197]. The growth of the O1s and C1s ether carbon peaks with a rising number of EG units can be seen, confirming the formation of the EG part of the molecule. At the same time the C1s alkyl peak decreases. This decrease is due to the attenuation of the alkyl carbon signal by the growing chain length of the EG moieties above the alkyl chain.

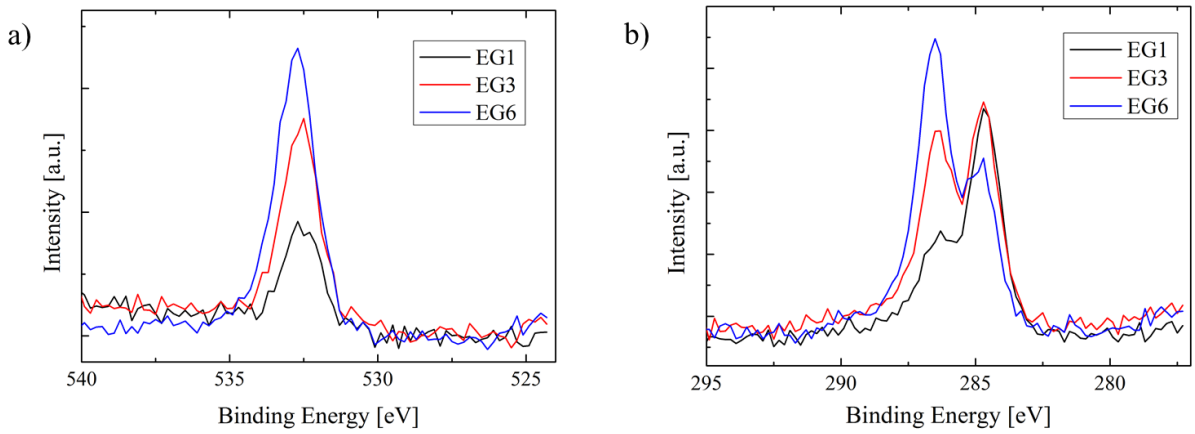

Figure 42. XPS spectra of the EG SAMs; O1s (a) and C1s (b) areas.

Table 8 shows the theoretical and the experimental C1s ether/C1s alkyl and C1s ether/O1s ether elemental ratios which were calculated from the O1s ether and C1s alkyl and ether carbon peak intensities. The procedure of these calculations is described in detail in chapter 3.11.4. The values are in agreement with previous measurements by Harder et al. [102]. As expected, the experimental values of C1s ether/C1s alkyl are higher than the theoretical ones confirming the attenuation of the buried alkyl carbon signal. The experimental C1s ether/O1s ether ratios are also larger than the theoretical ones but remained constant with the increase of EG units. The reason for the excess of carbon might be due to

carbon residues on the gold surface which could not be removed by UV cleaning or adsorbed carboxy species.

SAM	C1s ether/ C1s alkyl		C1s ether/ O1s ether	
	experimental	stoichiometric	experimental	stoichiometric
EG_1	0.4	0.3	2.3	2.0
EG_3	0.8	0.7	2.3	2.0
EG_6	1.6	1.3	2.2	2.0

Table 8. Experimental and stoichiometric ratios of C1s ether carbon to O1s oxygen and C1s ether carbon to C1s alkyl carbon.

7.1.3. FT-IRRAS

The IR spectra of the EG SAMs show mainly two characteristic spectral regions: the CH stretching modes from both alkyl and ethylene glycol parts of the molecules (3000-2800 cm^{-1}) and the different bending, wagging, twisting, rocking modes and skeletal vibrations of the oligomer parts (800-1600 cm^{-1}) [126].

Transmission IR spectra of neat liquid EG_n thiols (n=1, 3 and 6, Figure 43) were obtained as a control and to verify the purity of the chemicals used for the self-assembly process. The peaks were identified based on published data [102, 126, 225-228]. The bands at 1060, 1109 and 1119 cm^{-1} are associated to different C-O and C-C stretching vibrations. Bands at 1352 and 942 cm^{-1} are ascribed to ether CH_2 wagging and rocking modes. The CH_2 scissoring modes occur at 1458 cm^{-1}. The bands at 2856 and 2922 cm^{-1} are attributed to the symmetric and asymmetric CH_2 stretching bands respectively. These signals are indicative of crystalline alkane chains with an all-trans conformation such as in well-ordered alkanethiolate films. The spectra show a broad band at ~3460 cm^{-1} corresponding to the OH stretching mode.

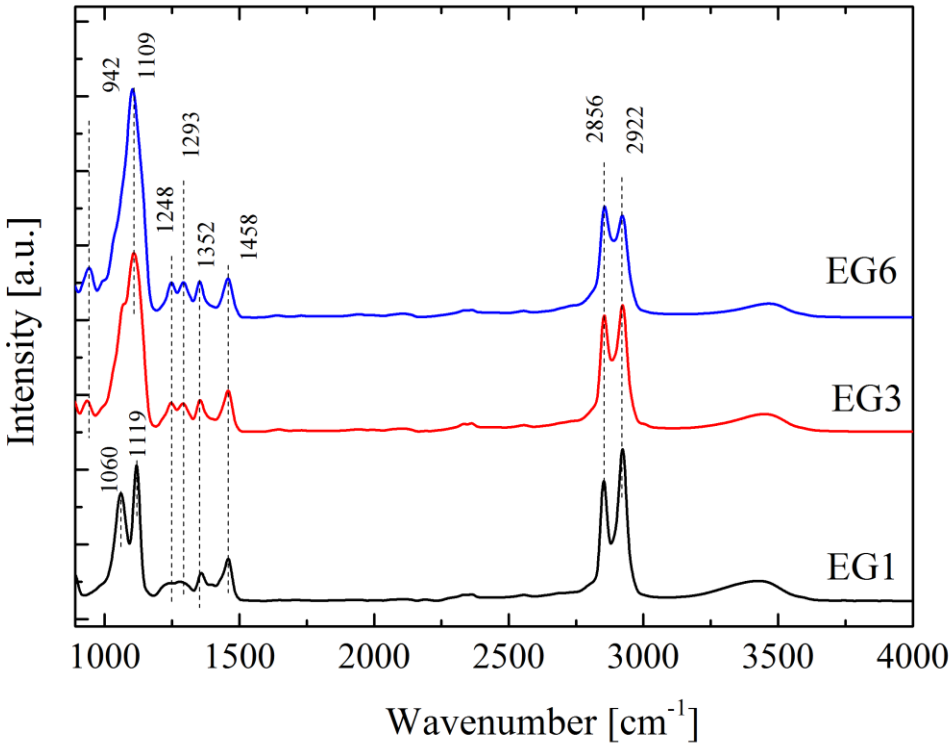

Figure 43. IR spectra of neat liquid EGn (n=1, 3 and 6) thiols.

Infrared Reflection-Absorption Spectroscopy (IRRAS) measurements of EG SAM samples from four different batches were conducted to verify the correct formation of the SAMs and to gain information about their molecular conformation (Figure 44, Figure 45 and Figure 46). The spectra were compared with the literature [102, 126, 131] to identify the molecular conformation of the EG chain of the molecule. The CH_2 stretching region indicates a good crystalline structure of the alkyl chains in all SAMs.

In contrast to the EG SAMs containing three or six EG units, the number of studies on SAMs with only one EG unit is limited. Liedberg et al. investigated the conformation of amide group containing EG_n SAMs (n=1 and 6) [126]. This work showed the featureless character of the EG_1 SAMs related to the one with six EG units. Figure 44 shows the obtained spectra for the EG_1 SAMs. All spectra contained a peak at 1136 or 1133 cm^{-1} attributed to the COC stretching modes. In general the fingerprint region of the spectra is not reproducible enough to perform a precise analysis. The reason might be the absence of many modes and the low intensity of the present ones complicating the assignation of the peaks.

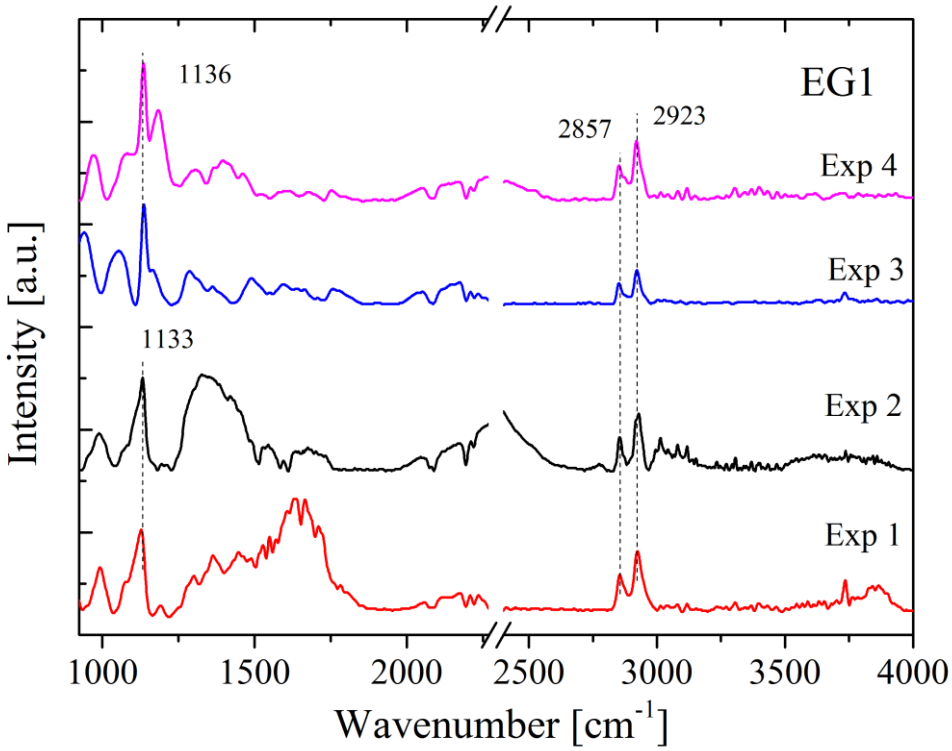

Figure 44. IRRAS spectra of four different replicates of EG_1 SAMs. The independent experiments are labeled Exp 1 to Exp 4.

Harder et al. studied the EG_6 and EG_3 SAMs in detail showing IR spectra of the three possible molecular conformations of the EG chain: helical, amorphous and all-trans [102, 131]. According to this work, molecular conformations were assigned to all spectra.

Figure 45 displays the IRRAS spectra for four different EG_3 SAMs. The position of the COC vibration modes (1132 and 1126 cm^{-1}) rejects the assumption of a planar conformation, and the behaviour between the CH_2 stretching peaks (the intensity of the peak at 2921 cm^{-1} is slightly greater than the one at 2859 cm^{-1}) indicates a helical conformation. The most important peaks can be interpreted and confirm a partial reproducibility of the samples however the remaining features cannot be assigned without doubt. In the same way as for EG_1 SAM the samples from the batch number one of both EG SAMs show some unclassified peaks between 1250 and 1800 cm^{-1}. The reason for that could be a contamination or poor quality of the slides.

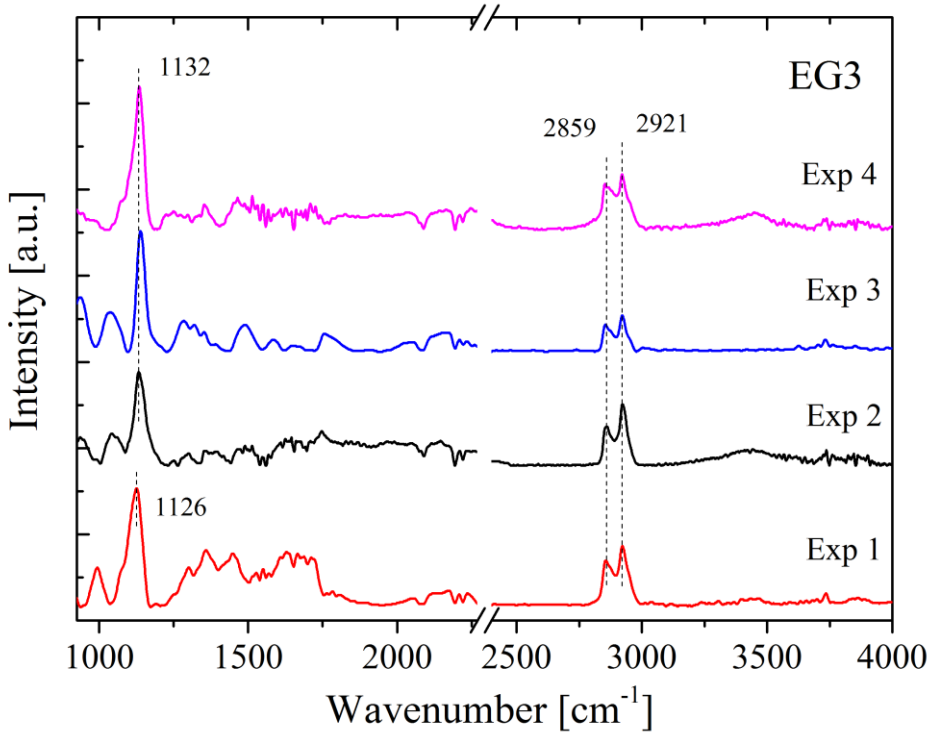

Figure 45. IRRAS spectra of four different replicates of EG_3 SAMs. The independent experiments are labeled Exp 1 to Exp 4.

The spectra of the EG_6 SAMs are shown in Figure 46. All of them are quite similar which confirm the reproducibility of the EG_6 samples. The presence of peaks at 2892 and 1348 cm^{-1} indicates the helical conformation of the samples from the experiments two, three and four, since such peaks are typical for a crystalline helical EG_6 SAMs [102]. However the absence of these signals suggests an amorphous conformation for the sample number one.

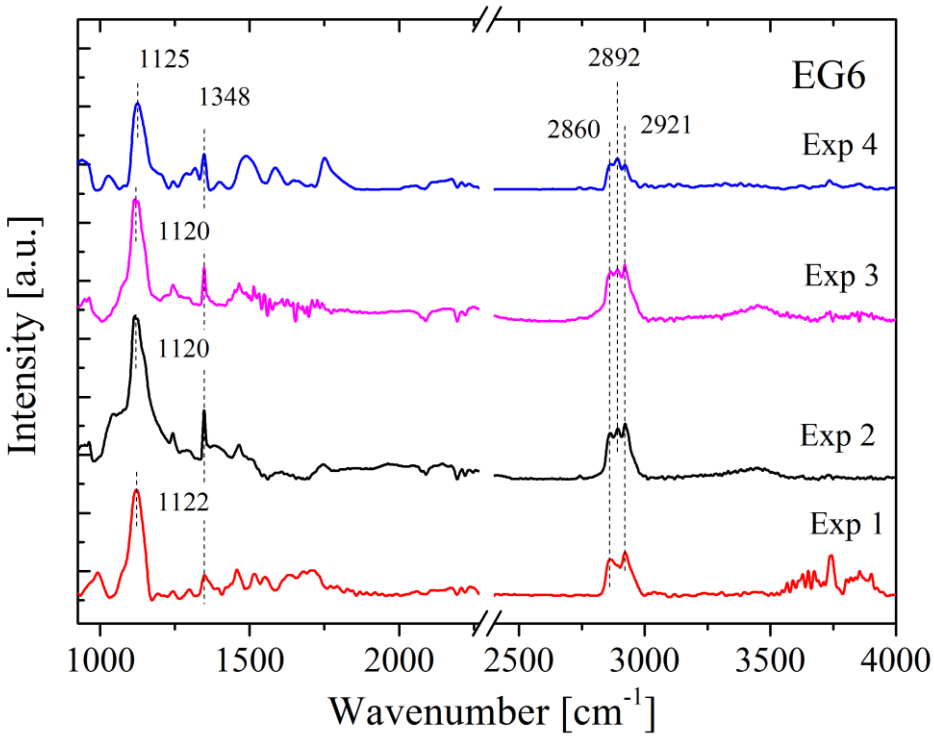

Figure 46. IRRAS spectra of four different replicates of EG_6 SAMs. The independent experiments are labeled Exp 1 to Exp 4.

The importance of the substrate on the shape of the spectrum was demonstrated since spectra of EG_6 SAMs on mica looked different than the ones on silicon [131]. Therefore the differences between the spectra of this thesis and the ones from the literature can be explained since the SAMs used in this work were synthesized on glass and not on silicon wafers.

In conclusion the spectra obtained of the CH_2 stretching region indicated a successful formation of all EG SAMs and verified a well ordered crystalline structure of their alkyl chains with an all-trans conformation. However spectra varied between samples especially for EG_1 which prohibits performing a precise analysis. This problem was already observed in other studies [131, 229] which confirms the difficulty to synthetize samples that show highly reproducible spectra. In spite of the variations between replicates it was possible to find some general trends in the features of the spectra of the different EG SAMs.

7.2. Bacterial adhesion on EG SAMs

The interaction of EG SAMs with proteins has been studied in detail [75] finding that water binding energy, the conformational degree of freedom and the lateral packing density affect protein resistance [102, 104, 130] (see chapter 2.7.2). Additionally to these protein resistance experiments the adhesion of diverse organisms such as algae [83], fibroblast cells [55] or bacteria [222] was investigated. A trend towards decreasing adhesion with an increasing number of EG units was observed. The samples containing one EG unit, EG_1 was found to be a non-resistant surface [55, 83, 103]. The reason for that may be the presence of at least two proton accepting oxygen atoms in the oligo(ethylene glycol) chain which allow for the formation of strong hydration bonds in a double hydrogen bridge configuration [125, 128]. Hence the question arises of in which degree the hydration of the surface may affect bacterial adhesion.

To investigate this hypothesis the adhesion of *C. marina* was quantified after 2 h incubation time on different hydrated EG SAMs. The assay was conducted at least four times for each surface. Figure 47 represents the removal curves for all EG SAMs.

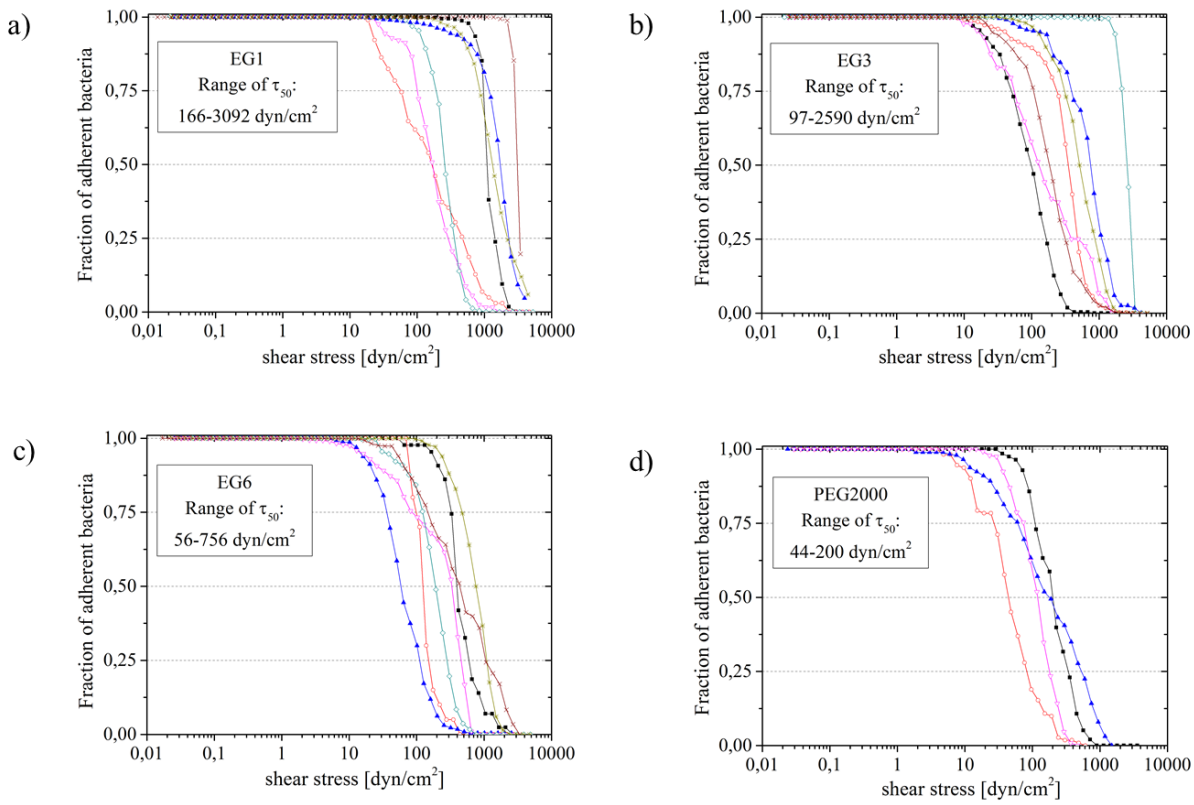

Figure 47. Range of obtained τ_{50} values and detachment curves of *C. marina* on different hydrated EG SAMs: EG_1 (a), EG_3 (b), EG_6 (c), PEG (d). Every curve represents the detachment of ≈300 bacterial cells for PEG and ≈600 bacteria for the other surfaces.

The detachment behavior strongly varied between experiments, especially for the EG short chains (EG_1, EG_3 and EG_6). Even when the assays were repeated seven times it was not possible to obtain good statistics. Despite the uncertainty of the results a trend could be observed towards lower shear stress values necessary to detach the bacteria with an increasing number of EG units (Figure 48a).

The percentage of adherent bacteria on the EG SAMs is shown in Figure 48. It was noticed that the hydration did not strongly influence the bacterial attachment since a similar percentage of bacteria adhered on all ethylene glycol short chains (EG_1, EG_3 and EG_6). Only the fraction of adherent bacteria on PEG decreased in comparison to the other surfaces (from ~ 90 % to ~ 60 %), however the variation is within the error bars.

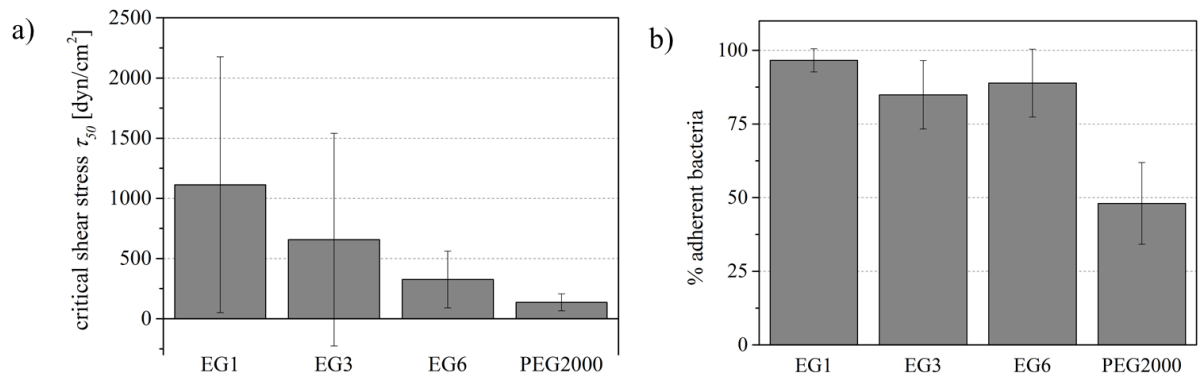

Figure 48. Influence of hydration on the adhesion of *C. marina*. Mean critical shear stress to detach 50 % of the adherent bacteria (a) and the percentage of adherent bacteria on the surfaces (b). Error bars are the standard deviation.

7.3. Discussion

EG SAMs with a different number of EG units (1, 3, 6 and 44) were characterized by spectral ellipsometry and contact angle goniometry. EG_n (n=1, 3 and 6) were additionally characterized by XPS and FT-IRRAS. The results indicate a successful formation of the surfaces as the values are in agreement with literature data. However, the IRRAS spectra revealed a varying quality of the prepared samples.

The adhesion of the marine bacterium *C. marina* on differently hydrated ethylene glycol SAMs was determined in order to investigate the hypothesis that hydration of the surfaces not only inhibits protein adsorption but also influences bacterial adhesion. The experiments were found to be not reproducible enough prohibiting a direct comparison between samples and thus a final conclusion about the influence of hydration on bacterial adhesion. The reason for this uncertainty of the results might be explained by taking into account the results of the surface characterization by IRRAS since the spectra varied between samples indicating the difficulty to obtain reproducible samples. Even though a trend could be found as the range of the τ_{50} values was shifted towards higher shear stresses with a decreasing number of EG units. This trend is in correlation to other observations for diverse organisms such as fibroblast cells or algae [55, 219].

The hydration did not strongly influence the bacterial attachment. Only the fraction of adherent bacteria on PEG decreased in comparison to the other SAMs with shorter EG chains

on which the percentage of adherent bacteria was similar, probably due to the strong steric repulsion of these long chain length molecules.

Although it is not possible to compare the performance of the different EG SAMs in a confident manner it is important to point out that in contrast to other results obtained in this PhD thesis, such as those for the SAMs with different wettabilities (see chapter 6.2), the bacteria adhered significantly weaker on EG SAMs than on the other surfaces. Based on this information it can be concluded that the hydration of the surfaces influences the bacterial detachment by decreasing the shear stress necessary to detach them.

8. Bacterial adhesion on polysaccharide coatings

Polysaccharides (PS) are, just like the EG SAMs, highly hydrated surfaces and considered to be a class of promising anti-fouling coatings (see chapter 2.7.2). They show a good resistance to proteins, freshwater bacteria and mammalian cells [114-117].

Due to their chemical composition with free hydroxyl groups, polysaccharides can interact with bivalent ions present in the marine environment causing a collapse of their structure which leads to a loss of hydration and thus of their inert properties. In order to avoid this collapse, the coatings were postmodified by capping their free carboxylic acid groups with a hydrophobic amine (TFEA). This hydrophobic capping adds amphiphilic properties to the hydrophilic polymer network [88, 121, 122] and shifts the contact angle towards the minimum in the Baier curve [94, 95].

This work investigates the performance of these coatings with respect to the bacterial adhesion towards the covalently immobilized hyaluronic acid (HA), alginic acid (AA) and chondroitin sulfate (CS) and if their performance can be enhanced by capping their free carboxylic acid groups with TFEA. Besides, the inert properties of the polysaccharides concerning the adhesion of early biofoulers were investigated to evaluate their performance when they are submerged into marine environment (see chapter 10.6.2).

8.1. Characterization of polysaccharides

The polysaccharide coatings were prepared and characterized by contact angle goniometry and spectral ellipsometry by Stella Bauer. Their contact angles and thicknesses are summarized in Table 9.

Surface	Contact angle [°]	Ellipsometric thickness [Å]
APTMS	35	11
HA	< 10	27
HA + TFEA	25	28
CS	11	26
CS + TFEA	28	29
AA	11	7
AA+TFEA	23	8

Table 9. Contact angles and thicknesses of APTMS, the pristine, and the capped polysaccharide coatings. Layer thicknesses of the PS were determined by spectral ellipsometry for coatings prepared on silicon wafers and are relative to the previous APTMS layer (standard errors: ±3° CA; ±3 Å ellipsometry).

As reported in previous publications, HA, CS and AA are hydrophilic [114, 120]. The thicknesses of all polysaccharides are in the range between 26 Å and 28 Å while the one of alginin coatings is only 7-8 Å. Obviously, they were slightly higher for the capped ones. Capping of the polysaccharides with TFEA slightly shifts the contact angles by 10-20°.

8.2. Bacterial adhesion on polysaccharides

8.2.1. Bacterial adhesion on capped and uncapped hyaluronans and chondroitins

HA and CS surfaces were chosen since they have a similar carbohydrate backbone but differ in the sulfate group only present in CS. The samples were stored in argon until being used for the bacterial assays. The bacterial adhesion was quantified after 2 h incubation time on the different polysaccharides. The assay was conducted four times for every surface. Figure 49 displays the removal curves for all polysaccharides. Except for the modified HA, the detachment behavior considerably varied between experiments. In spite of the uncertainty of the results, by observing the mean critical shear stress (Figure 50a) two effects could be confirmed. The bacterial critical shear stress was reduced when HA was protected by hydrophobic groups by almost a factor of five from ≈1,200 dyn/cm^2 on HA to ≈250 dyn/cm^2 on HA+TFEA. Nonetheless, capping CS led to a result contrary to that for HA. Bacteria

attached on CS+TFEA more than twice as strong as on CS as their critical shear stress values were ≈800 dyn/cm^2 and ≈300 dyn/cm^2 respectively.

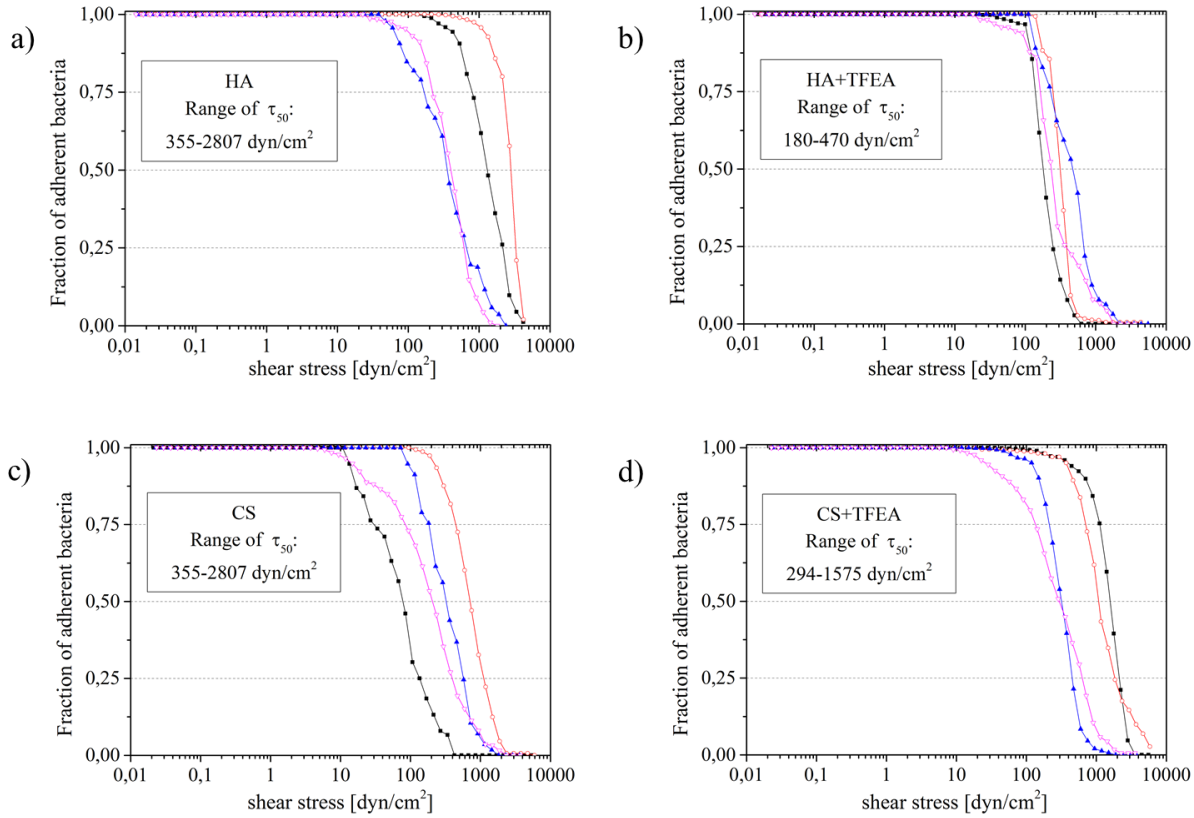

Figure 49. Range of obtained τ_{50} values and detachment curves of bacteria on the polysaccharide coatings: HA (a), HA+TFEA (b), CS (c) and CS+TFEA (d). Each curve represents the detachment of ≈ 500 bacteria.

Besides the detachment assays, the attachment strength of bacteria on different polysaccharides was also evaluated by quantifying the percentage of adherent bacteria on the surfaces. Figure 50b shows that the ratio of attached bacteria hardly depended on the characteristics of the PS. For HA, HA+TFEA, and CS+TFEA, a similar percentage of the bacteria adhered (~ 85 %). The only exception was CS on which the ratio of adherent bacteria slightly diminished; however this effect was not significant within the error bars.

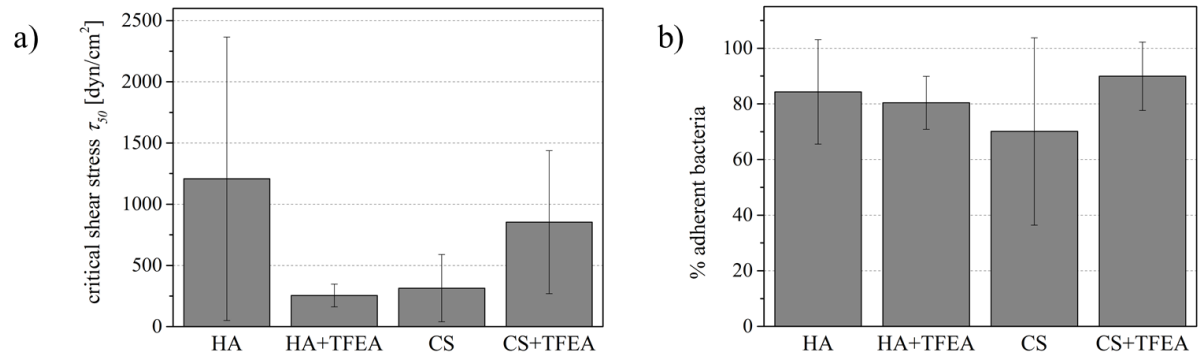

Figure 50. Mean critical shear stress (τ_{50}) (a) and percentage of adherent bacteria (b) on HA, HA+TFEA, CS, and CS+TFEA polysaccharide coatings. Error bars are the standard deviation.

8.2.2. Bacterial adhesion on capped and uncapped hyalurons and alginins

HA and AA surfaces have a similar carbohydrate backbone but differ in the number of carboxylic acid groups as HA contains one group and AA two. This way, the effect of the number of carboxylic acid groups on bacterial adhesion was investigated. The samples were stored in Milli-Q® water until being used for the bacterial assays. The bacterial detachment (Figure 51 and Figure 52a) and the percentage of adherent bacteria (Figure 52b) on AA, AA+TFEA, HA, and HA+TFEA polysaccharide coatings was determined after 2 h incubation. The assay was performed four times for each surface. The removal curves are shown in Figure 51. It was observed that the detachment behavior substantially varied between the assays with the exception of capped AA, which showed almost the same τ_{50} value in three of the four curves. Taking into account the average critical shear stress (Figure 52a) it was noticed that, despite these variations, bacterial adhesion on AA was much stronger than on the other polysaccharides. Capping AA with a hydrophobic amine confirms the efficacy of this modification by leading to a decrease of bacterial adhesion strength. Following the same trend, the bacterial critical shear stress on HA was higher than on HA+TFEA. However these effects could not be confirmed without doubt due to the high variation of the results.

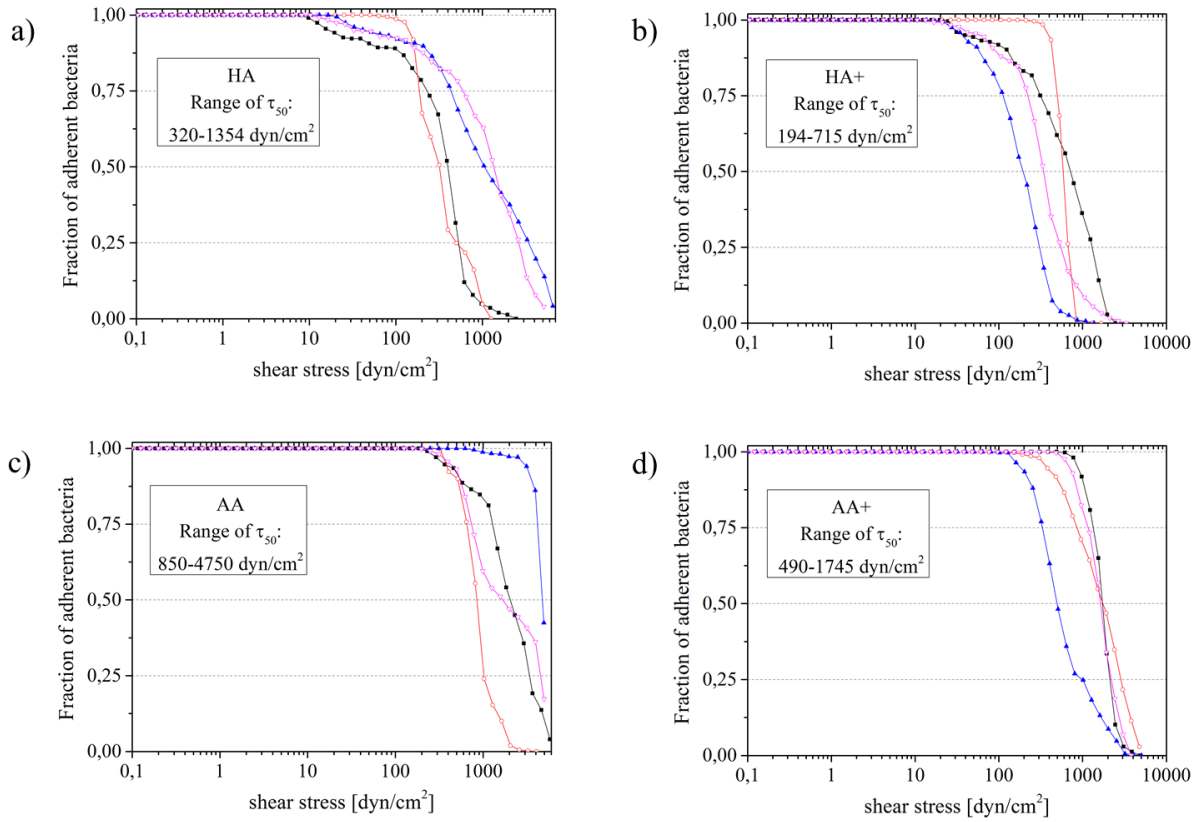

Figure 51. Range of τ_{50} values measured and removal curves for bacterial on HA (a), HA+TFEA (b), AA (c) and AA+TFEA (d) polysaccharides. Each curve represents the detachment of ≈ 600 bacteria.

Figure 52 displays the fraction of adherent bacteria on the coatings. It can be observed that the bacteria did not distinguish between polysaccharides and, as in the case of those containing a sulfate group, the ratio of adherent bacteria was similar (~ 80 % to 90 %).

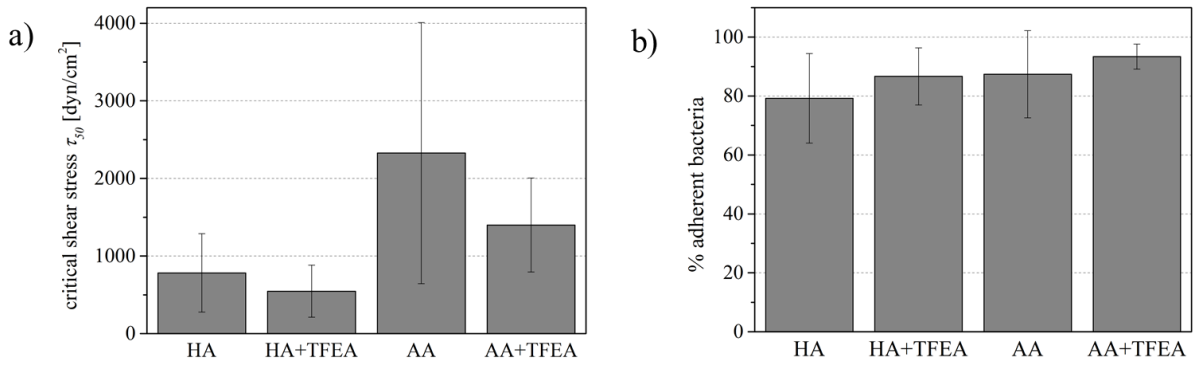

Figure 52. Average of the fraction of adherent bacteria on all polysaccharides. Error bars are the standard deviation.

8.3. Discussion

Polysaccharide coatings represent one class of promising anti-fouling coatings. They are highly hydrated and show a good resistance to proteins and bioorganisms [114-117].

In this work, the adhesion of *C. marina* on polysaccharide (PS) coatings with different chemical moieties was determined. The polysaccharides HA, CS, and AA were used. They are built up of a similar carbohydrate backbone but differ slightly in the composition of their functional moieties. HA has one carboxylic acid group per disaccharide unit, AA carries an additional carboxylic group and CS an additional sulfate group. The polysaccharides can interact with bivalent ions present in the marine environment by collapsing their film structure and thus losing their inert properties. In order to prevent this collapse, the polymers were modified by capping free-carboxyl groups with a hydrophobic fluorinated alkylamine (TFEA).

The microfluidic results demonstrated that critical shear stress needed for bacterial removal was diminished when HA was protected by hydrophobic groups. This trend could be observed for both series of experiments. The difference between the values of HA and HA+TFEA coatings between both series of experiments may be due to their different storage. For the first series of experiments, the polysaccharides were stored under argon and for the second one they were stored in Milli-Q® water. Since PS are hydrogels, the storage in water maintains their degree of hydration and thus, more water can be bound which leads to an increase of antifouling properties as shown in the second series of experiments.

Following the same trend as for capped HA, capping AA led to a considerable decrease of bacterial adhesion strength. These findings indicate that polysaccharides present a good resistance to adhesion of marine bacteria and TFEA modification indeed has the desired effect. The high critical shear stress on AA compared to the other polysaccharides was expected, since this molecule contains more carboxylic acid groups. Thus, it is more prone to complexation by bivalent ions, the associated collapse of the polysaccharide hydrogel leading to a loss of its inert properties [114]. X. Cao verified that indeed the interaction between the polysaccharide structures and bivalent ions was higher on AA than on HA [230] which explains the different bacterial resistance of HA and AA. He investigated the adsorption of calcium on polysaccharides and its influence on protein adsorption. XPS results show that in contrast to AA, there was no calcium adsorption on HA. Nevertheless, the adsorbed Ca^{2+} could be removed with an EDTA solution. Regarding lysozyme adsorption tests, the

resistance of AA after adsorption of the cations from ASW significantly decreased in comparison to the freshly prepared coatings, even if the cations were removed by EDTA. In contrast, the resistance of HA barely varied compared to the pristine surfaces. This effect was prevented in this thesis by capping AA polysaccharides with TFEA.

Nonetheless, modifying CS led to the contrary result as for HA and AA. Bacteria attached on CS+TFEA more strongly than on uncapped CS. The inert properties of CS could be related to the sulfate group causing good fouling-release properties and may be the reason why it is part of the mucus on the skin of fish [113].

The attachment of bacteria on these coatings was also evaluated. The results showed that the ratio of attached bacteria scarcely depended on the characteristics of PS. For all PS a similar percentage of the bacteria adhered (~ 85 %). The only exception was CS on which the ratio of adherent bacteria was slightly diminished (~ 75 %), however this effect was not significant within the error bars.

The polysaccharides showed a common feature with the EG SAMs, the other kind of hydrogel examined in this thesis (see chapter 7). Although it is generally not possible to compare the performance of the different surfaces in a confident manner, it can be observed that the bacteria adhered more weakly on the highly hydrated surfaces, polysaccharides and EG SAMs, than on other surfaces investigated during this PhD thesis (for example those in chapter 6.2). The results are summarized in the Table 10.

Surface	CA [°]	Mean critical shear stress [dyn/cm^2]
HA	< 10	780
HA + TFEA	25	545
CS	11	315
CS + TFEA	28	850
AA	11	2325
AA+TFEA	23	1400
EG1	28	790
EG3	30	330
EG6	32	135
PEG	30	130
HUDT	38	3570
DDT	106	3900
AUDT	54	3250
FUDT	113	4600

Table 10. Summary of the contact angle (CA) and the obtained critical shear stress values for all SAMs and PS surfaces investigated in this thesis. Data were collected from 6.1, 7.1 and 8.1.

The data listed in Table 10 is plotted in Figure 53. This figure summarizes the trends found in this thesis. In general, a lower CA is a good indicator for better fouling-release properties. The datasets fitting the least into this trend are the polysaccharide AA and the HUDT SAM. The high critical shear stress value for AA could be expected, though, since this PS contains two free-carboxylic groups and thus it is more prone to be collapsed by the interaction with bivalent ions present in the sea water, leading to a decrease of hydration and consequently a loss of the inert properties. Nevertheless, the result for the hydroxyl-terminated HUDT SAM is more surprising. This data proves the importance of hydration to reduce the shear stress needed to detach the bacteria, as the EG SAMs, the other samples with a hydroxyl termination and a CA similar to the one of the HUDT SAM, performed much better. The graphic also shows the good fouling-release properties of all PS and a further improvement through capping them with a hydrophobic amine. CS is the only exception from this trend.

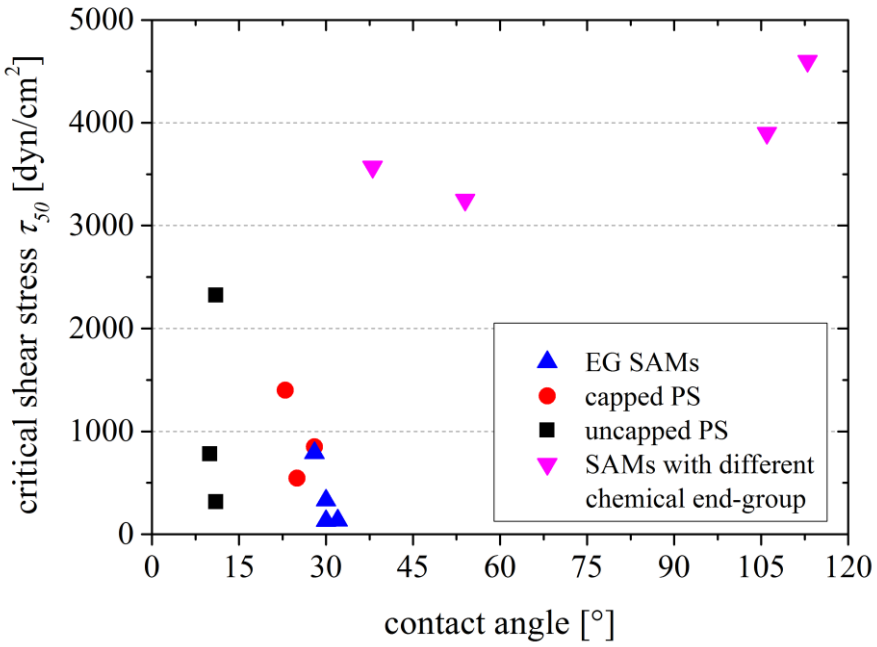

Figure 53. Plot of the mean critical shear stress of the investigated surfaces against their sessile water contact angle.

According to these findings we suggest that the adhesion strength of the bacteria is effectively weakened by hydrogels facilitating detachment of the bacteria while simultaneously making the adhesion strength more susceptible to small variations between different replicates of a surface increasing the variability of the results.

9. Metal organic coatings with controlled release properties: Bacterial adhesion on Cu-SURMOF 2

Surface oriented highly porous and ordered metal-organic frameworks (MOFs) have high potential for many microbiological, cell culture and biomedical applications, especially those which are related to the storage of biomacromolecules within the MOF structures (see chapter 2.7.5).

To this day, copper based coatings have been applied frequently on ship hulls as antifouling coatings. Nevertheless, the damaging effect of their copper release on the marine ecosystem has been demonstrated repeatedly [155-158] (see chapter 2.8). Consequently a coating which only affects the target organisms avoiding the uncontrolled release of metal ions into the environment is desired.

Recently a homogeneous MOF based on a $(Cu^{2+})_2$ or $(Zn^{2+})_2$ paddle-wheel based 2D structure $[M_2(bcd)_2]_n$ (M= Cu^{2+} or Zn^{2+}) with bcd (benzene-1,4-dicarboxylic acid) as linker and grown using liquid phase epitaxy (LPE) has been developed [149]. Such coatings are referred to as Cu- or Zn-SURMOF 2. Three copper based surfaces differing in thickness (≈80, 120 and 160 nm) were tested. Figure 54 displays the 3D structure of Cu-SURMOF 2. Since previous work showed the instability of the coatings in protein rich media [150], at this point we hypothesized that there is some kind of interaction between the coating and the bacteria which leads to a stimulus response and hence, a controlled copper release ultimately resulting in the collapse of the MOF.

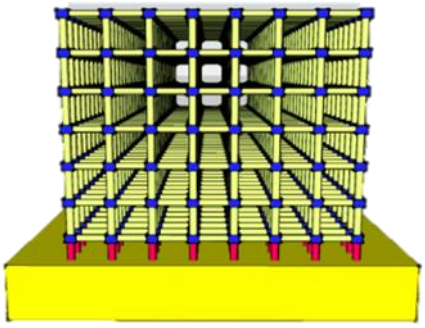

Figure 54. 3D structure of the Cu-SURMOF 2. Layers of copper cations (blue circle) connected by organic linkers (bcd, yellow rods) grown on a MHDA SAM on gold (red rods). Image was taken from [231].

Therefore the adhesion of the marine bacterium *C. marina* on surfaces covered with Cu-SURMOF 2 was evaluated. Besides, the stability of these coatings after incubation in

bacterial solution was examined to determine if the bacteria exert any influence on the Cu-SURMOF 2.

9.1. Stability of Cu-SURMOF 2

9.1.1. Stability of Cu-SURMOF 2 in different media

Prior to the determination whether bacteria provoke a stimulus response of the coatings, it is necessary to assess the stability of these surfaces in aqueous media. Accordingly XPS and XRD measurements, performed by Stella Bauer and Zhengbang Wang respectively, were conducted to evaluate the stability of Cu-SURMOF 2 (thickness ≈120 nm) in deionized water (Milli-Q®) and artificial seawater (ASW).

XPS measurements of these surfaces after immersion in the media were conducted in order to obtain information about changes in the chemical composition by examination of the C1s and Cu2p peak regions (Figure 55a and b). Additionally to previous work, which demonstrated the sturdiness of these coatings after immersion in ASW for 1 h [150], the stability of the coatings was investigated after immersion for 2 h, *i.e.* the duration of the bacterial assays. The intensity of the Cu2p peak increased slightly, while the C1s peak showed a minimal decrease. This could be due to a possible disassembly at the top layers of the SURMOF structure leading to a loss of some bcd linkers facilitating the accessibility of the Cu^{2+} building units. Despite these intensity changes it can be concluded that Cu-SURMOF 2 remained stable after 2 h incubation in ASW.

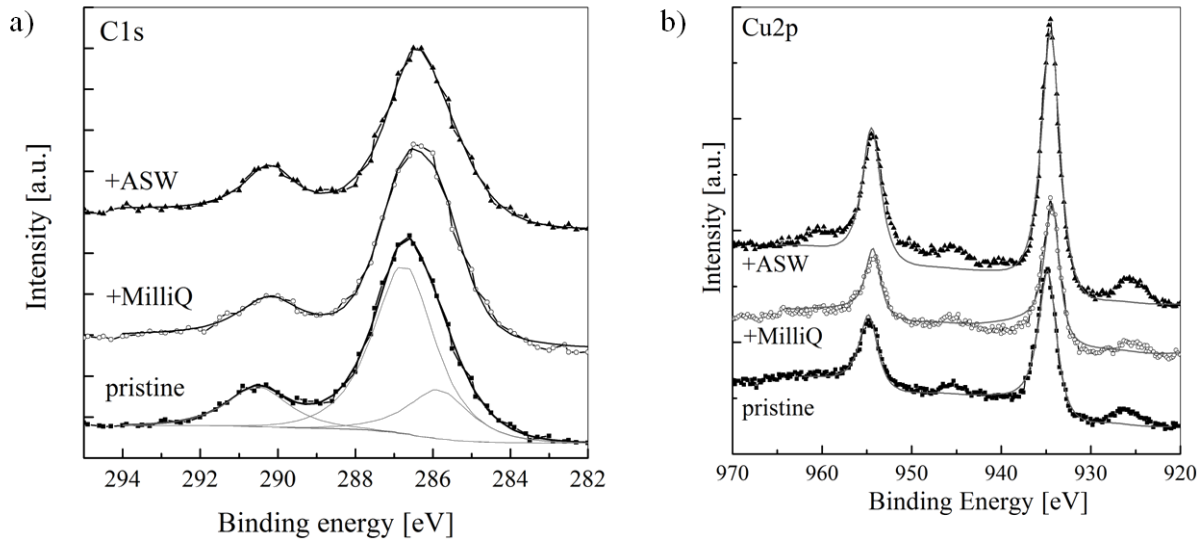

Figure 55. XPS spectra of the C1s (a) and Cu2p region (b) of Cu-SURMOF 2 of the pristine samples and after immersion for 2 h in Milli-Q® and ASW.

Additionally, the stability of Cu-SURMOF 2 in ASW was analyzed after 2 h incubation in ASW and Milli-Q® water (Figure 56) which corresponds to the time used for the biological assays. The XRD spectra showed unchanged peaks. The good stability of Cu-SURMOF 2 in ASW is in agreement with earlier findings [150].

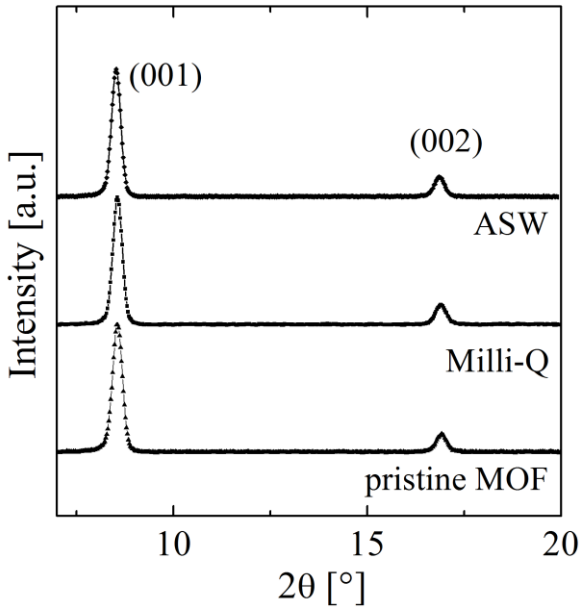

Figure 56. XRD spectra for Cu-SURMOF 2 before and after 2 h incubation in Milli-Q® and ASW

9.1.2. Stability of Cu-SURMOF 2 after bacterial incubation

The observation that the Cu-SURMOF 2 is stable in Milli-Q® water and ASW but disassembles in phosphate buffer and protein rich media [150] stimulated the hypothesis that the presence of the extracellular polymeric substances (EPS) secreted by bacteria could lead to a similar effect by degrading the SURMOF 2. As shown in Figure 57, the crystallinity of Cu-SURMOF 2 decreased gradually after incubation for 15, 30, 60, 90, 120 and 180 min in bacterial ASW suspension. However the structural integrity was maintained after immersion in ASW without bacteria. The fact that this decrease of crystallinity can only be observed after incubation in the bacterial suspension indicates that the Cu-SURMOF 2 is degraded in the presence of bacteria.

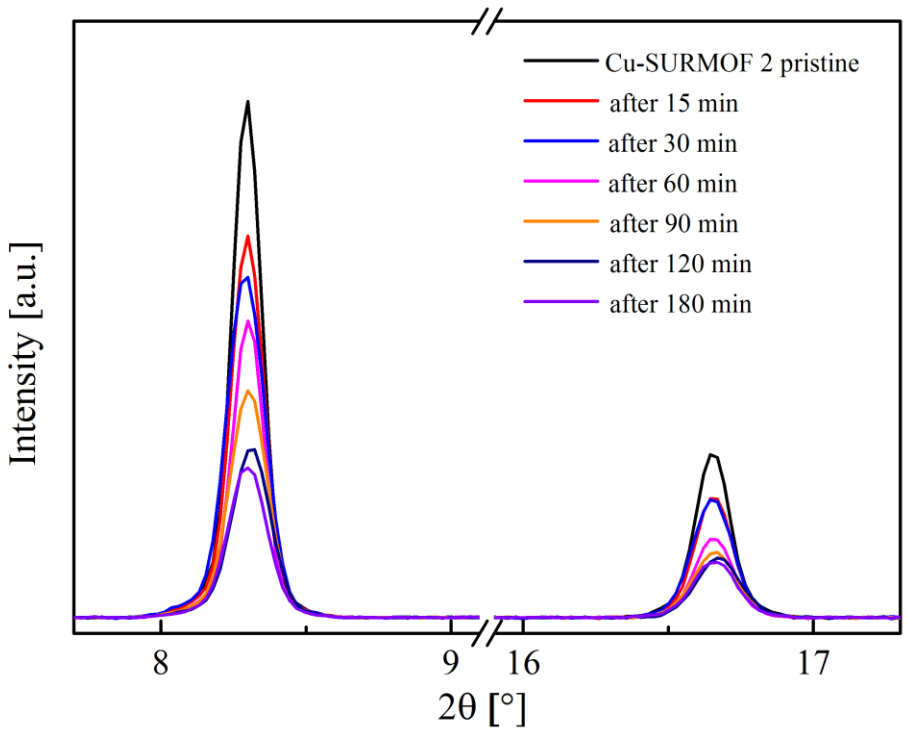

Figure 57. XRD spectra of Cu-SURMOF 2 after different incubation times in ASW containing bacteria.

The bacteria attach to the surfaces by means of their EPS [28]. This substance is excreted during growth and is composed of mostly polysaccharides [36] such as alginic acid (AA) [41]. Based on this knowledge in relation to the latter results the question arises of whether the stability of the coating changes after immersion in different solutions related to bacterial growth. To this end, the coatings were incubated 2 h in diverse media and XRD measurements were conducted. The spectra are shown in Figure 58.

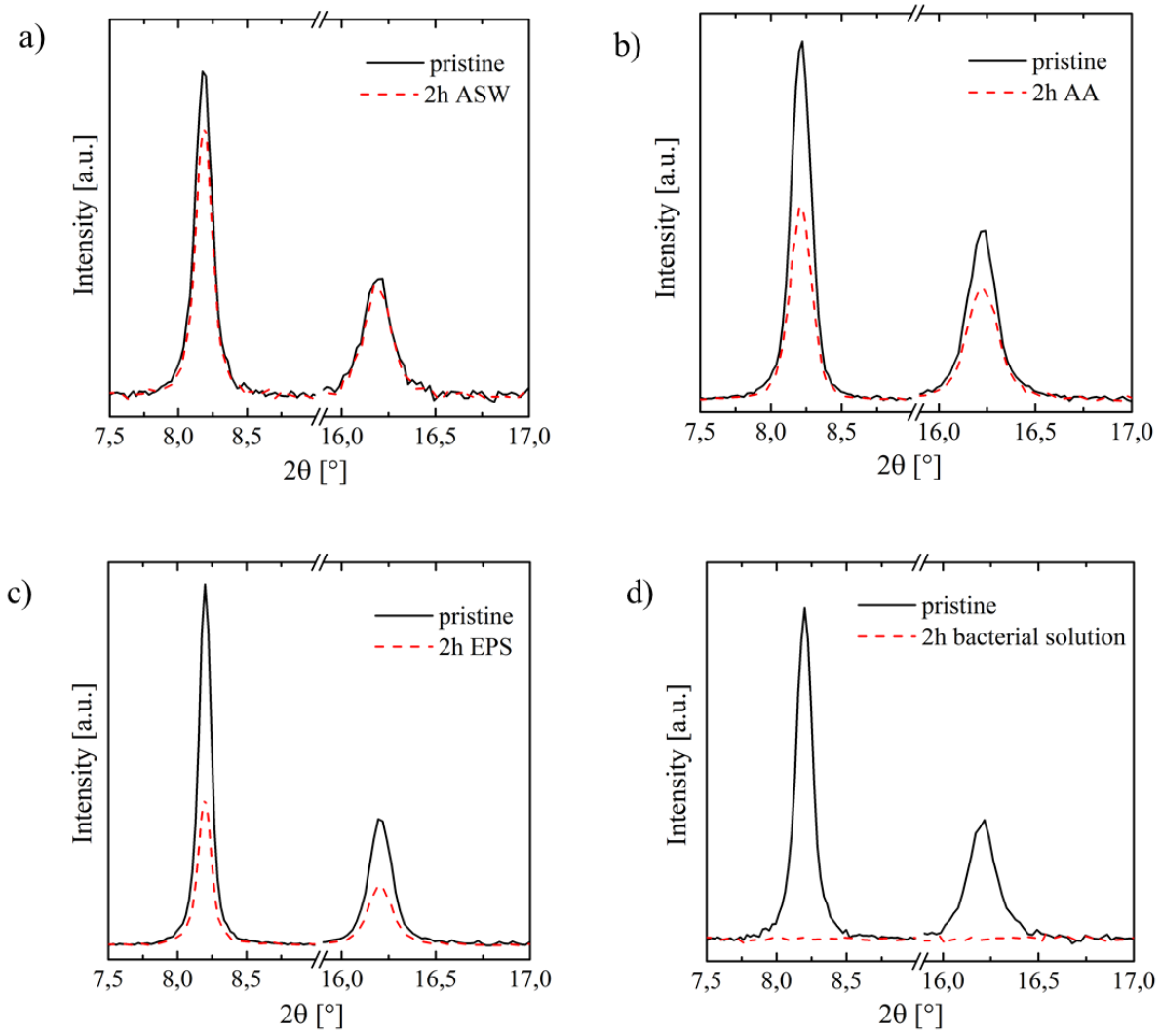

Figure 58. XRD spectra of pristine Cu-SURMOF 2 (black line) and after 2 h incubation in ASW (a), AA 0.5 mg/ml solution (b), EPS solution secreted from the bacteria in ASW (c) and ASW in which bacteria were cultured, filtered to remove the bacteria (d).

The selected solutions were: ASW as reference (Figure 58a), 0.5 mg/ml AA solution in Milli-Q® water (Figure 58b), EPS solution from *C. marina* in ASW (Figure 58c) and ASW in which the bacteria were cultured filtered through a syringe filter (0.45 µm pore size) to remove the bacteria. For the latter two, the bacteria were first inoculated in ASW after reaching the log phase (as described in chapter 3.1) and subsequently incubated in an Erlenmeyer flask for 2 h. The supernatant solution was filtered and directly used for incubation. The EPS from the remaining solution was separated from the bacteria following published protocols [28] and dissolved in ASW prior to the experiments. Spectra showed that after all incubations, with the only exception of ASW in which the integrity of the coatings was almost preserved (Figure 58a), the peak intensity strongly decreased (Figure 58b-d). This effect was especially remarkable when samples were incubated in ASW in which the bacteria

were cultured leading to a complete loss of crystallinity. These findings demonstrate that the loss of crystallinity is closely related to substances excreted by the bacteria.

AFM and SEM measurements were conducted in order to determine how localized the degradation of the coatings were when bacteria were present on the surface. Cu-SURMOF 2 (≈120 nm) was incubated in bacterial solution for 2 h. Subsequently the samples were removed from the suspension, gently washed with Milli-Q® water and fixed with ice cold methanol. This protocol was chosen to observe the morphology of the bacteria without deterioration by the fixation process as demonstrated in the chapter 12.1. Figure 59 displays SEM images at magnification of 10,000x (a) and 20,000x (b) of partially removed bacteria on Cu-SURMOF 2 (≈120 nm). The original attachment position of the bacterium could easily be determined as a dark spot on the surface. Thus the surface was only changed at the initial attachment position. This impression was supported by tilted SEM images after fracturing the samples (Figure 59c).

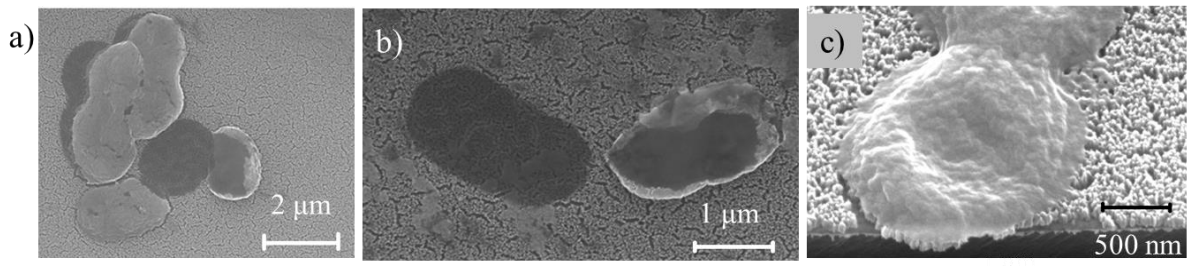

Figure 59. SEM images of removed bacteria on Cu-SURMOF 2 with 10,000x magnification (a) and 20,000x magnification (b). Tilted view after fracturing the sample to provide a cross section of the Cu-SURMOF 2 beneath the bacterium (c).

The thickness of the Cu-SURMOF 2 (≈160 nm) was not affected in the direct vicinity of the bacterium. Figure 60 shows an AFM image of this coating (a) and its height profile (b) from which the thickness was determined. It can be noticed in Figure 60b that the thickness after the bacterial incubation was ≈ 160 nm, the typical thickness of 20 layers of Cu-SURMOF 2. Thus the hypothesis that the degradation of the coating is very localized could be verified.

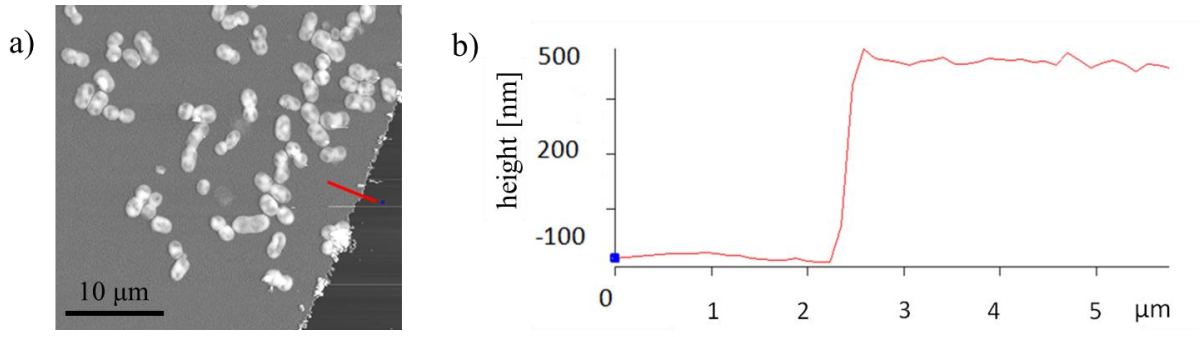

Figure 60. AFM image of the Cu-SURMOF 2 (≈160 nm) after 2 h incubation with *C. marina* suspension (a), and height profile along the red line (b).

9.2. Bacterial adhesion on SURMOF 2

Microfluidic detachment assays were conducted to reveal the influence of the active degradation of the Cu-SURMOF 2 on bacterial adhesion. After 2 h incubation the critical shear stress of the bacteria on these coatings (≈120 nm and ≈80 nm thicknesses) and hexadecanethiol (HDT) and mercaptohexadecanoid acid (MHDA) SAMs as copper free controls was determined. Additionally, one surface with known resistance to protein and organism adhesion was included. This surface, polyethylene glycol (PEG) [15] (see chapter 6.2), provided a suitable control as typical inert surface. Figure 61a displays representative removal curves, showing the fraction of adherent bacteria plotted against the applied shear stress (τ) (Figure 61a) and the critical shear stresses (τ_{50}) as determined from the removal curves (Figure 61b). The shear stress needed to detach the bacteria was significantly lower for both Cu-SURMOF 2 coatings compared to the controls HDT and MHDA SAMs. Even though the trend was nearly negligible within the standard deviation, the 120 nm thick SURMOFs seemed to reduce adhesion more effectively compared to the 80 nm thick one. An ANOVA test was performed between the critical shear stress τ_{50} values showing a high significance of the data (significance level of 0.01). Further, a Tukey test was applied to compare pairs of the means as a post-hoc analysis in order to determine the pairs of surfaces that statistically differ. PEG SAMs and both Cu-SURMOF 2 showed a statistically significant difference in comparison to MHDA and HDT SAMs. These results indicate that Cu-SURMOF 2 led to a statistically significant reduction of the adhesion strength to a degree comparable to the one of an established protein and biofouling resistant surface.

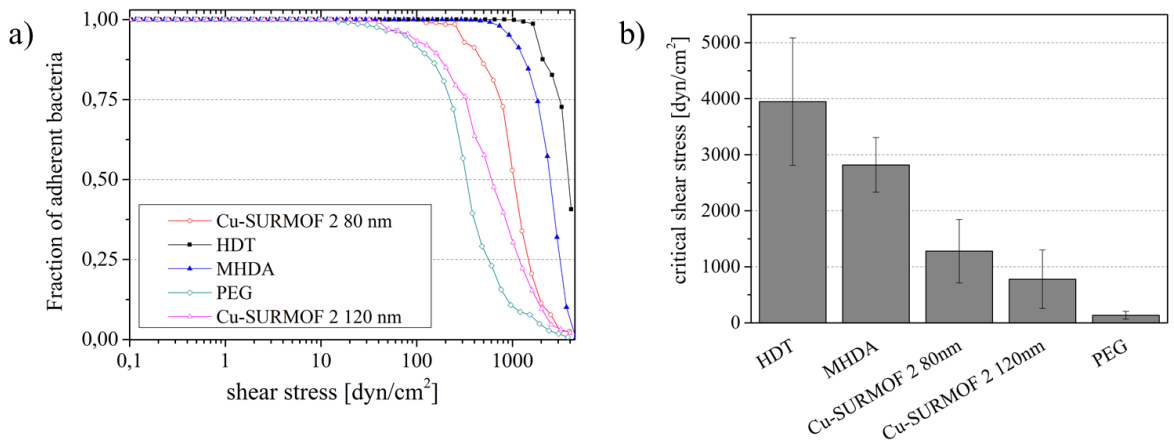

Figure 61. Typical detachment curves of *Cobetia marina* from the different surfaces. Critical shear stress (τ_{50}) required to remove the bacteria from different surfaces including different controls (a). Error bars are the standard deviation of five experiments (both Cu-SURMOF 2 and HDT SAM), and four experiments (all other surfaces) (b). Every curve represents the detachment of ≈ 300 bacteria for both Cu-SURMOF 2 and PEG and ≈ 700 bacteria fot the other surfaces.

9.3. Bacterial viability assay on Cu-SURMOF 2

The reduced critical shear stress on the Cu-SURMOF 2 suggests that the viability of the bacteria is affected during adhesion. Bacterial viability was determined by a live/dead viability assay on the Cu-SURMOF 2 (≈120 nm thickness) and MHDA SAM as non-copper containing control, after 2 h immersion in bacterial ASW solution. All bacteria were labelled by the green-fluorescent nucleic acid stain while only bacteria with damaged membranes were stained by red-fluorescent dye. The ratio of damaged versus all bacteria was determined by evaluation of the fluorescence signals (stained areas) in the fluorescent microscopy images (Figure 62). More than half of the bacterial population was found to be damaged on the Cu-SURMOF 2 (~ 88 %). In contrast, this fraction was only 0.9 % on the MHDA SAM. These findings show that the Cu-SURMOF 2 did not only decrease the critical shear stress of the bacteria but also affected their viability since it was able to damage their membranes.

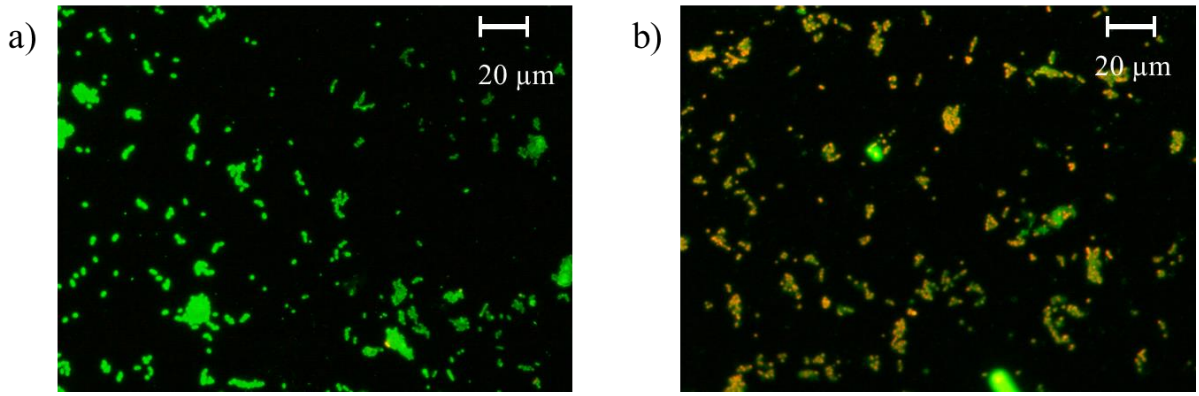

Figure 62. Fluorescence microscopy images of adherent bacteria on MHDA SAM (a) and Cu-SURMOF 2 (≈120 nm thickness) (b).

9.4. Evaluation of bacterial morphological changes on Cu-SURMOF 2

In addition to adhesion and viability assays, atomic force microscopy (AFM), scanning electron microscopy (SEM) and helium ion microscopy (HeIM) were used to analyze whether adhesion on the Cu-SURMOF 2 changes the morphology of the bacteria.

SEM images of the bacteria after 2 h incubation (see appendix Figure 81) on Cu-SURMOF 2 (b and d) and HDT SAM (a and c) as a non-toxic control were acquired.

The images reveal that bacteria on Cu-SURMOF 2 (≈120 nm, d) appeared to be relatively flat and with apparent protrusions in the middle of the bacteria in comparison to those incubated on HDT SAM (c).

9.4.1. Evaluation of bacterial morphological changes on Cu-SURMOF 2 by AFM

The AFM evaluations were carried out with the help of Carlos Azucena. In order to quantitatively evaluate the bacterial morphological change on Cu-SURMOF 2 (≈120 nm), AFM measurements were conducted. This coating and HDT SAM as a non-toxic reference

were incubated into a bacterial solution for 2 h. For these experiments, the samples were air dried. The following AFM evaluations were done based on certain numbers of bacteria, nevertheless their morphology was very homogeneous on every kind of surface, and thus the obtained observations represent the total population of the bacteria. Figure 63 shows AFM images of bacteria on Cu-SURMOF 2 (Figure 63c and d) and HDT (Figure 63a and b). The bacteria seemed to be more buckled on the Cu-SURMOF 2. This visual impression is supported by height profiles along the long axis (Figure 63e), which reveal an irregular and lower average height for bacteria adherent on this surface.

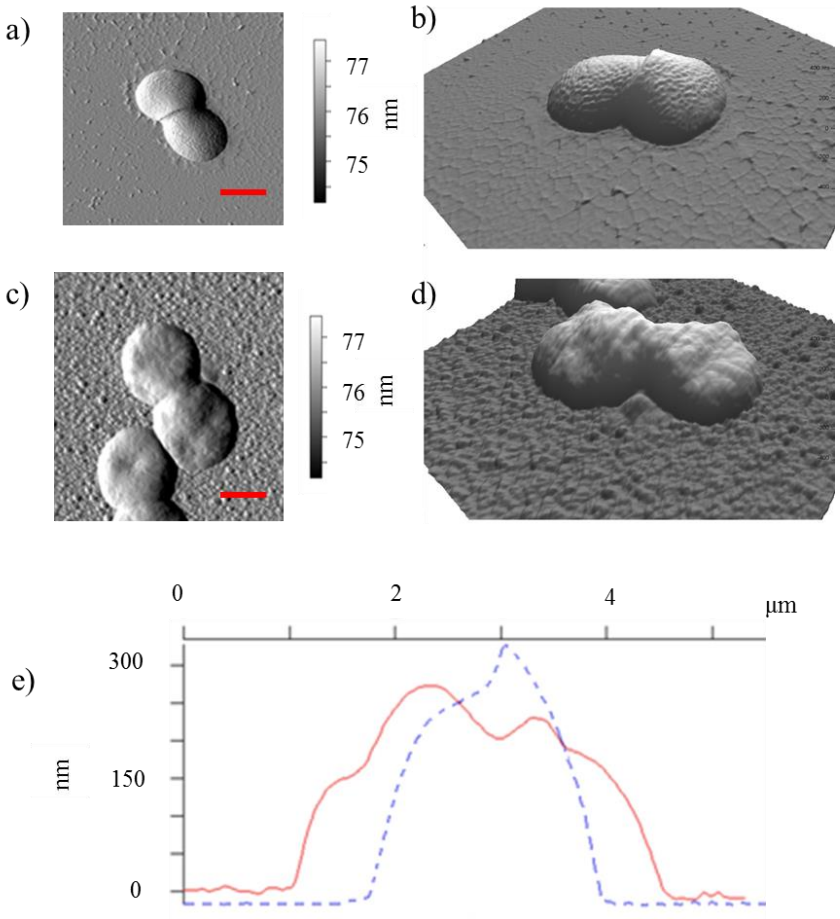

Figure 63. AFM phase images and 3D images of the bacteria on HDT SAM (a and b) and Cu-SURMOF 2 (c and d), and height profiles along the long axis of the bacteria (e, continuous line Cu-SURMOF 2, dashed line HDT control). Scale bars represent 1 µm.

3D visualization of the AFM images (Figure 63b and d) shows that the bacteria appeared crumpled and wrinkled-up when incubated on Cu-SURMOF 2 (Figure 63d). In contrast, the bacteria incubated on HDT SAM had a smooth morphology (Figure 63b).

To demonstrate morphological changes quantitatively, the roughness and width of the bacteria on the surfaces were determined. Figure 64a shows the mean roughness which was 50 % larger for the bacteria on Cu-SURMOF 2 than for the ones on HDT SAM. Bacteria on the Cu-SURMOF 2 appeared to be flatter and broader compared to the HDT control. To quantitatively demonstrate this observation, the mean width of the bacteria (Figure 64c-d) as determined by line profiles (Figure 64e-f) was calculated (Figure 64b). Bacteria on Cu-SURMOF 2 were 25 % wider than on HDT SAM.

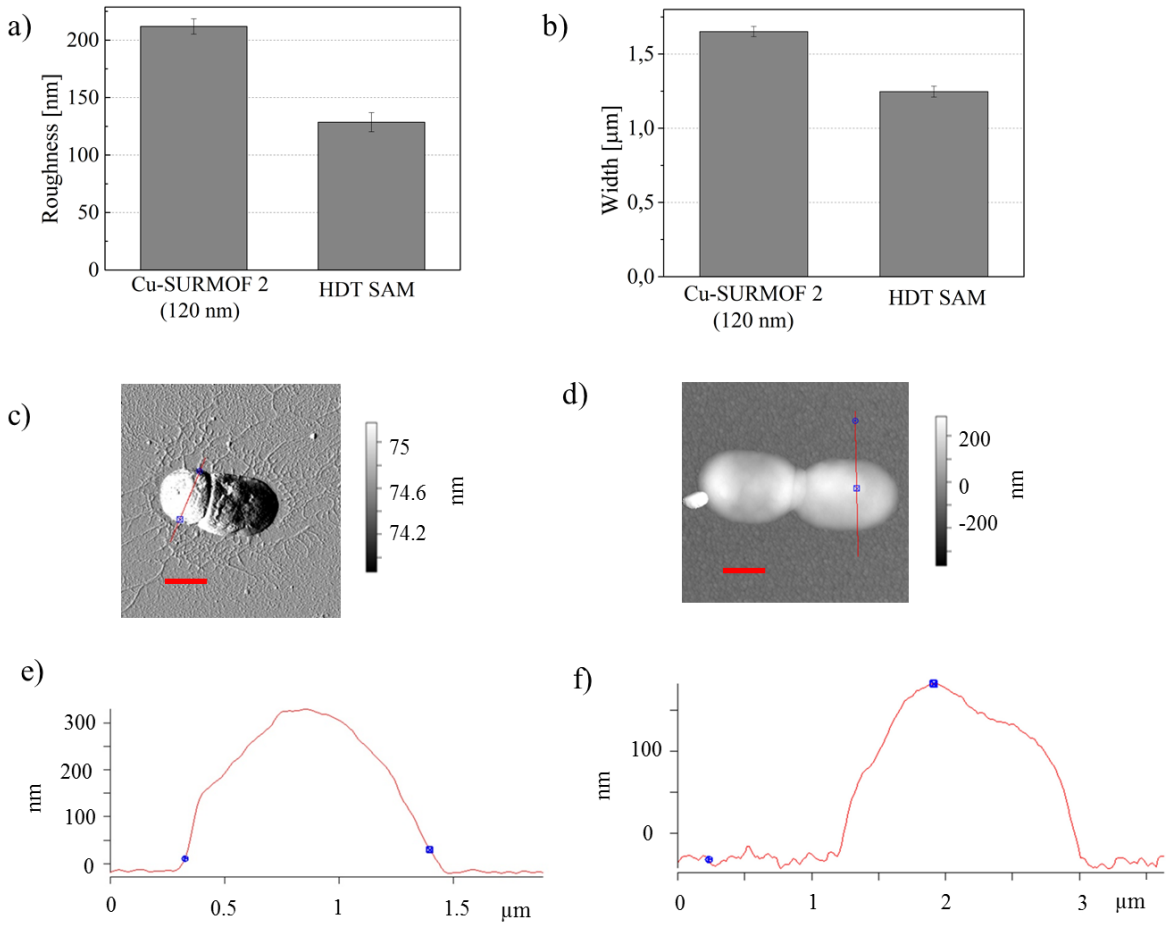

Figure 64. Mean values of roughness (a) and width (b) of the bacteria on Cu-SURMOF 2 (≈120 nm) and HDT SAM. Measurements were done on seven individual bacteria. Error bars are the standard error. AFM images of a bacterium on HDT SAM (c) and Cu-SURMOF 2 (d) and their width profiles along the transverse axis (e-f) respectively. Scale bars represent 1 µm.

9.4.2. Evaluation of bacterial morphological changes on Cu-SURMOF 2 by HeIM

At this point, the suggested hypothesis that the morphological change can be observed after shorter incubation times was investigated. Consequently, bacteria were incubated on Cu-SURMOF 2 (≈160 nm) for 30 min and 60 min and subsequently fixed by immersion in ice cold methanol. Helium ion microscopy (HeIM) was employed for such evaluation in collaboration with the University of Bielefeld. As shown in HeIM images (Figure 65), the morphological change occurred within the first 30 min (Figure 65a).

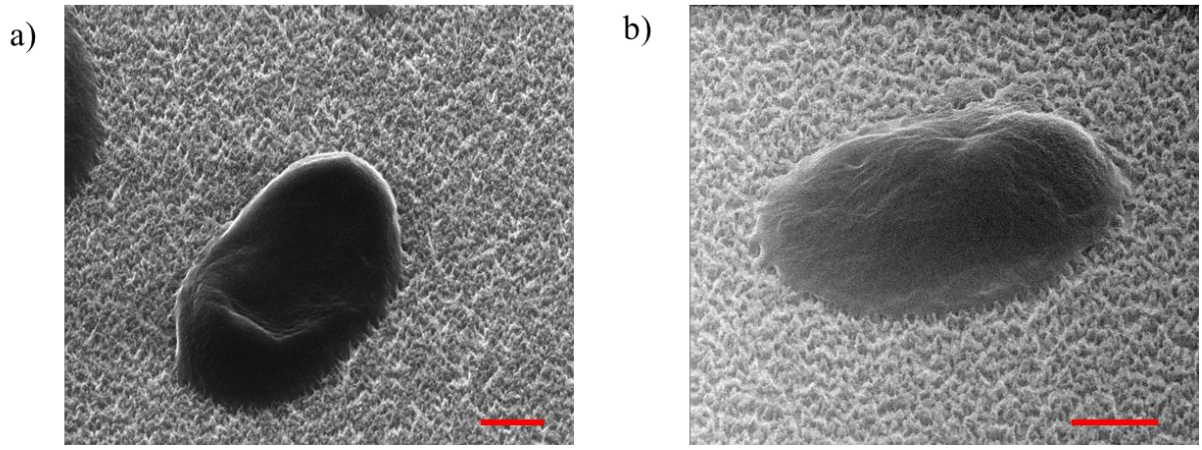

Figure 65. HeIM images of the bacteria on Cu-SURMOF 2 (≈160 nm) after 30 min (a) and 1 h incubation time. Scale bars represent 500 µm.

9.5. Comparison of adhesion strength of *C. marina* on Cu- and Zn-SURMOF 2

To confirm that copper was the active component which caused the harmful effect on the bacteria, Zn-SURMOF 2 was tested as additional control surface to reveal potential effects of the bdc linker on the bacteria. For this purpose, the critical shear stress of *Cobetia marina* on the different surfaces was measured using the microfluidic detachment assay. Figure 66 shows the critical shear stress (τ_{50}) of the bacteria on the different surfaces (data from Figure 61a) in comparison to the one on the Zn-SURMOF 2. The bacteria adhered significantly more weakly (three to six times) on both Cu-SURMOF 2 (≈120 nm and ≈80 nm) compared to the Zn based SURMOF 2 and SAM controls. According to an ANOVA test the differences between the τ_{50} of the surfaces are significant. The results indicate that the bdc linker does not negatively

affect the bacteria and the effect observed on Cu-SURMOF 2 is most likely related to the released copper ions.

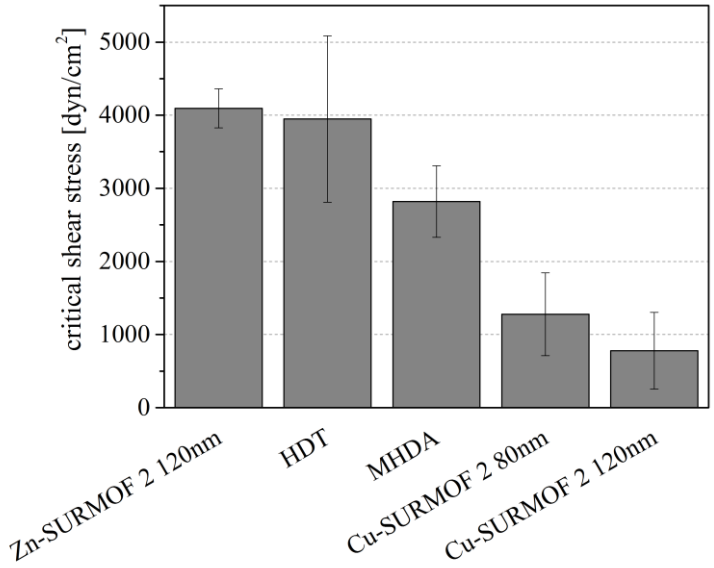

Figure 66. Critical shear stress (τ_{50}) of the bacteria for the different surfaces. Error bars are the standard deviation.

9.6. Discussion

The stability of Cu-SURMOF 2 after immersion in ASW was analyzed in detail by XPS and XRD. The data revealed that the integrity of Cu-SURMOF 2 was preserved for at least 2 h incubation in ASW. However, when bacteria were added to ASW, a gradual decrease of crystallinity of the Cu-SURMOF 2 occurred. The decrease of crystallinity of the coatings after 2 h incubation in different mixtures of ASW with substances secreted by *C. marina* demonstrated that the lost of crystallinity is closely related to substances excreted by the bacteria.

Both, SEM and AFM images showed that the presence of the bacteria triggered the active degradation of these coatings which was highly localized where the bacteria attached. Nonetheless, it could be observed that the Cu-SURMOF 2 film in the vicinity of the bacteria was preserved after the incubation with *C. marina* for 2 h. These results confirm the hypothesis that only the interface of interaction between bacteria and Cu-SURMOF 2 was affected by incubation with *C. marina*.

The critical shear stress of the bacteria was measured on Cu-SURMOF 2 (80 nm and 120 nm) and non-toxic control coatings (HDT and MHDA SAM). Such values were compared to PEG SAM, a typical inert surface. The bacteria adhered substantially more weakly on the Cu-SURMOF 2 than on the control, particularly on the one of 120 nm thickness. The results were comparable to the protein and biofouling resistant surface PEG.

The integrity of Cu-SURMOF 2 after immersion in bacterial suspension was determined using XRD. The spectra revealed a gradual degradation of its crystallinity with time. This observation was connected with the considerable diminution in critical shear stress.

Furthermore a viability assay showed that the majority of bacteria adhering on the SURMOF 2 were damaged whereas bacteria on a control remained viable. This difference of viability was connected with an alteration in cell morphology as shown by SEM and AFM. This effect could not only be observed for a Cu-SURMOF 2 with ≈160 nm thickness but also for a ≈120 nm thick surface with corresponding lower copper content. Roughness and width measurements of the bacteria on Cu-SURMOF 2 and HDT SAM verified these morphological changes quantitatively showing that bacteria incubated on Cu-SURMOF 2 were 25 % wider and their roughness 50 % larger than those on HDT SAM. These alterations of the physiology of the bacteria could be noticed even after 30 min incubation as shown in HeIM images. This observation is in agreement with the XRD data, which indicated a loss of crystallinity even after 15 min in bacterial solution.

Experiments using zinc based SURMOF 2 as additional control, were performed to reveal potential effects of the bdc linker on the bacteria. The bacterial critical shear stress was similar on Zn-SURMOF 2 compared to the other controls HDT and MHDA, and significantly larger compared to Cu-SURMOF 2. These observations demonstrate that the bdc linker did not negatively affect the bacteria.

Thus, the effects observed on Cu-SURMOFs, namely the reduction of the critical shear stress and the alterations in bacterial viability and morphology are most likely related to the release of copper ions caused by an active degradation of the SURMOF structure by the bacteria.

Especially, the stability in the absence of bacteria proves the stimulus response of the coatings as regards the bacteria. Despite the challenge of incorporating our findings into a commercial product, a fundamentally promising approach for a smart class of materials has been presented.

Furthermore, these results in connection with previous findings that the release of Cu^{2+} did not affect cell integrity [150] demonstrate the usefulness of this class of coatings for biomedical applications.

10. Field tests: comparison between laboratory assays and the real marine world

Numerous studies have shown that the colonization by marine organisms depends on the chemical and physical properties of the submerged surfaces [12, 67, 87-91]. However, there is a lack of investigations supporting these hypotheses by means of field tests.

The goal of this investigation was to correlate the results obtained in previous laboratory assays with *C. marina* with field experiments. The tested samples covered a range of well-defined model surfaces previously investigated by conventional laboratory assays. The selection of the samples was not by chance. The surfaces were rather chosen to comprise a wide range of surface properties as the aim of this PhD thesis was to investigate the influence of those properties on the adhesion of the marine bacterium *Cobetia marina*. Thus the theory that the influence of surface properties plays a role in the natural environment of marine organisms was suggested.

The evaluated surfaces and accordingly the property investigated were: different terminated SAMs with different wettability (chemistry), ethylene glycol (EG) SAMs with different numbers of EG units and polysaccharide coatings (hydration) and different EG based polymers (transition from monolayers to polymeric EG surfaces). The surface characterization is described in previous chapters (6.1 and 7.1 for the SAMs and 8.1 for the polysaccharides).

10.1. Environmental conditions during the immersion

In contrast to laboratory assays, which ensure constant environmental conditions (temperature, salinity, humidity, light), field experiments bear the complication of weather and water composition dependence. Thus, results can change with temperature, salinity, humidity, wind, rain, sun hours, and concentration of salt, proteins and chemicals present in the water. As the experiments were a snapshot in time, the temperature of water and air and water conductivity under which the results were obtained are summarized in Table 11. They were measured immediately after immersing the collection of samples (t=0 h) and each time the samples were removed from the water. After immersion on day one of experiment N1, the weather was mild and with light rain during the first hours. Experiment N2 started with cloudy conditions without rain.

Experiment N1: date of immersion: November 30th at 08:00 am.				
Immersion time [h]	Submerged samples	Temperature [°C]		Water conductivity [mS/cm]
		air	water	
0	Every sample	23	22	42.8
2	DDT, AUDT, FUDT, HUDT, PEG and EGx (x=1, 3 and 6) SAMs and glass slide	24	22	42.8
6		25	23	
12		24	22	
48	DDT, AUDT, FUDT, HUDT and PEG SAMs, glass slide and –OH and $–OCH_3$ POEGMAs	8	16	42.8

Experiment N2: date of immersion: December 1st at 08:00 am.				
Immersion time [h]	Submerged samples	Temperature [°C]		Water conductivity [mS/cm]
		Air	Water	
0	Every sample	18	22	41.9
2	DDT, AUDT, FUDT, HUDT, PEG and EGx (x=1, 3 and 6) SAMs and glass slide	18	22	41.9
6		19	22	
12		13	18	
24	AA, AA+TFEA, HA, HA+TFEA, CS and CS+TFEA polysaccharides, glass slide and –OH and $–OCH_3$ POEGMAs	8	16	42.8
48	DDT, AUDT, FUDT, HUDT and PEG SAMs, glass slide and –OH and $–OCH_3$ POEGMAs	9	14	40.8

Table 11. Summary of immersion times, submerged samples and environmental conditions under which the experiments were realized.

10.2. Organism identification

During the analysis of the microscopy data, several organisms were observed and the most common ones sized larger than 10 µm were classified and counted. Mainly, nine diatom genera and one subclass of protozoa were found. The different genera of the diatoms were: *Mastogloia*, *Cocconeis*, *Navicula*, *Grammatophora*, *Bacillaria*, *Amphora*, *Triceratium*, *Melosira* and *Coscinodiscus* (Figure 67 a-i). The genera *Coscinodiscus*, *Triceratium*, and *Melosira* were grouped together as "others" since they were only seldom encountered. The subclass of protozoa found was *Peritrich* occurred frequently (Figure 67 j).

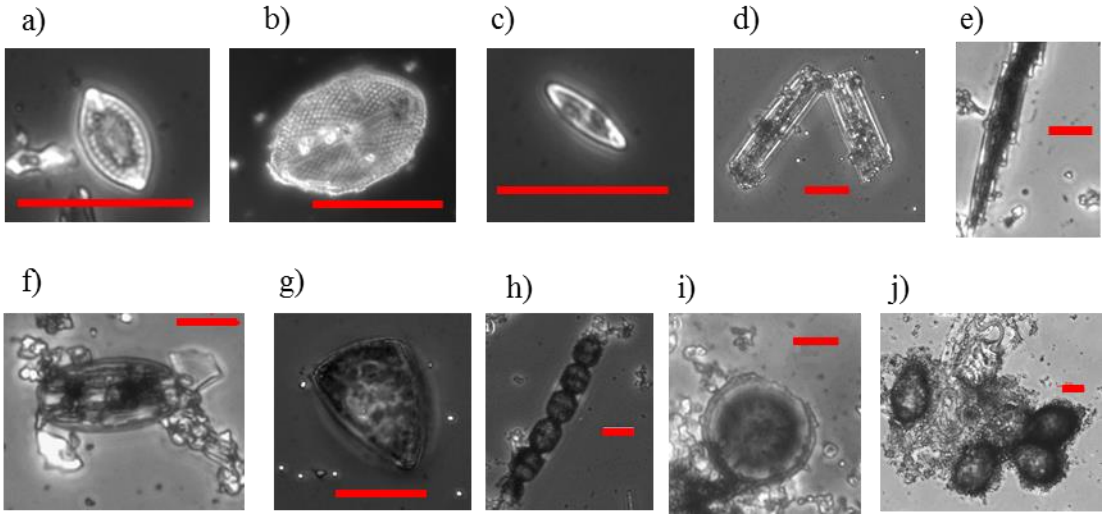

Figure 67. Most frequently observed organisms on the tested surfaces: (a) *Mastogloia*, (b) *Cocconeis*, (c) *Navicula*, (d) *Grammatophora*, (e) *Bacillaria*, (f) *Amphora*, (g) *Triceratium*, (h) *Melosira*, (i) *Cocinodiscus*, (j) *Peritrich*. Scale bars represent 20 µm. Images were acquired with a Nikon, TE-2000-U microscope.

Even though the presence and importance of these species has been pointed out previously [154], it was interestingly that diatoms were amongst the earliest species found, since they are known to not be very motile.

10.3. Percentage of relative abundance at all time points

The percentage of relative abundance of the most commonly observed organisms (Figure 67) was determined for both experiments across all time points (Figure 68).

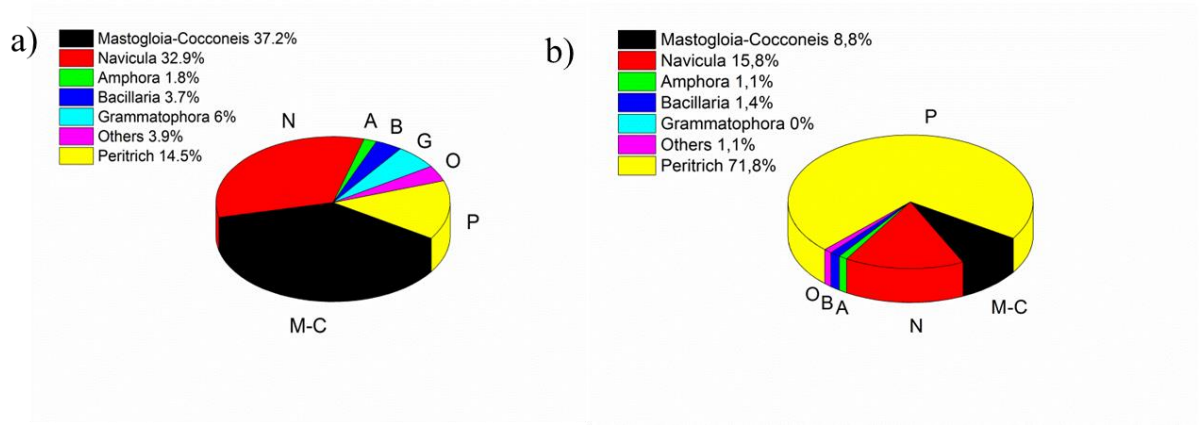

Figure 68. Percentage of the relative abundance of the most frequently found organisms on the coatings after immersion across all time points for experiments N1 (a) and N2 (b). Values are calculated from the sum of absolute occurrence on all samples and for all immersion durations.

The diatoms *Mastogloia*, *Cocconeis* and *Navicula* and the protozoa *Peritrich* were most frequently observed in both experiments. The diversity in species was slightly higher for experiment N1 than for N2 since *Grammatophora* was not found in the latter one. Important differences were observed between the abundance of the different organisms in both experiments. The most common organisms found for N1 were *Mastogloia* and *Cocconeis* with ~ 37 % abundance. Their occurrence was reduced by approximately by a factor of 4 in experiment N2 to ~ 9 %. The situation was similar for *Navicula*, its abundance of ~ 33 % for N1 was reduced to ~ 16 % in N2. For all other diatom species the abundance was also decreased from N1 to N2. In contrast, the occurrence of the protozoa *Peritrich* increased nearly five times from ~ 14 % for N1 to ~ 72 % for N2. As shown in Table 11, the weather changed between experiments N1 and N2 and especially the temperature differed. During the experiments N2 the water temperature was significantly lower than during N1 (Table 11), so the population seemed to be influenced by the environmental conditions.

10.4. Influence of wettability on marine settlement

Surfaces with different wettability have been investigated in this work concerning bacterial adhesion [15] by controlled laboratory assays. In this context the question emerges of whether the wettability character of the surfaces can exert an influence on diverse marine organisms present in their natural environment just as it is the case for the bacteria used in the laboratory assays. The SAMs used during the field tests were prepared by Isabel Thomé following

published protocols [85]. EG and PEG SAMs were prepared on-site at the marine corrosion laboratory of the Florida Institute of Technology (FIT) in Melbourne, Florida, in order to ensure perfect quality of the SAMs and avoid possible alterations of their chemistry during transport.

Results for the SAMs with different wettability and glass slides are shown in Figure 69. During the first 6 h, the settlement barely varied. After 12 h there were roughly four times more organisms on the surfaces immersed in the experiment N1 (Figure 69a) compared to experiment N2 (Figure 69b). This effect disappeared after 48 h and the settlement was similar in both sets. Most remarkable was the abundance of *Peritrich* which significantly increased at lower water temperatures (N2, Figure 69b).

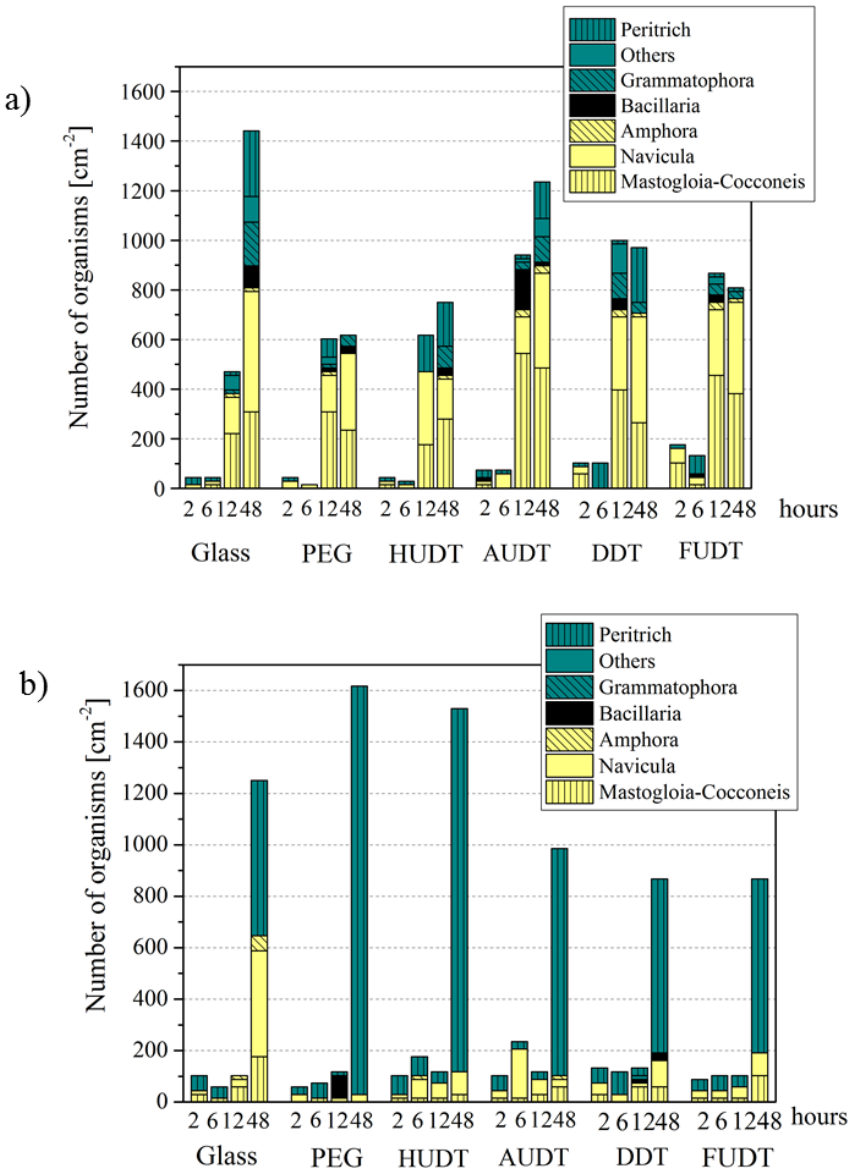

Figure 69. Number of organisms of each species on the diverse SAMs and glass incubated 2 h, 6 h, 12 h and 48 h for experiment N1 (a) and N2 (b).

10.5. Influence of the transition from polymeric EG to methacrylate polymers

Besides oligomeric and polymeric ethylene glycol SAMs, a range of methacrylate-based polymers brushes with oligoethylene side chains was additionally submerged. Poly[oligo(ethylene glycol)methacrylate] (POEGMA) brushes are ethylene glycol hydrogels with a methacrylate backbone (see chapter 2.7.4). The hypothesis behind this experiment was

whether thick, dense coatings with OEG side-chains would provide long-term resistance to colonization.

For this study two different (POEGMA) brushes, prepared by Angus Hucknall, were used: methoxy and hydroxy terminated POEGMA. Wettability of the POEGMA brushes was characterized by a measurement of the contact angle. Both POEGMA surfaces have a similar contact angle, 45° and 50° for methoxy (-OCH_3) and hydroxy (-OH) termination respectively. The values are slightly higher compared to the polyethylene glycol SAMs and the oligoethylene glycol SAMs, most likely because of the methacrylate backbone of the polymers.

Figure 70 shows the results and surprisingly the number of organisms after 48 h immersion on the POEGMA brushes even exceeded the one on the PEG SAMs. The different environmental conditions during the immersion of the two sets did not majorly influence the general trend of these results and in all cases more organisms were found on the methoxy-terminated POEGMA than on the hydroxy-terminated POEGMA.

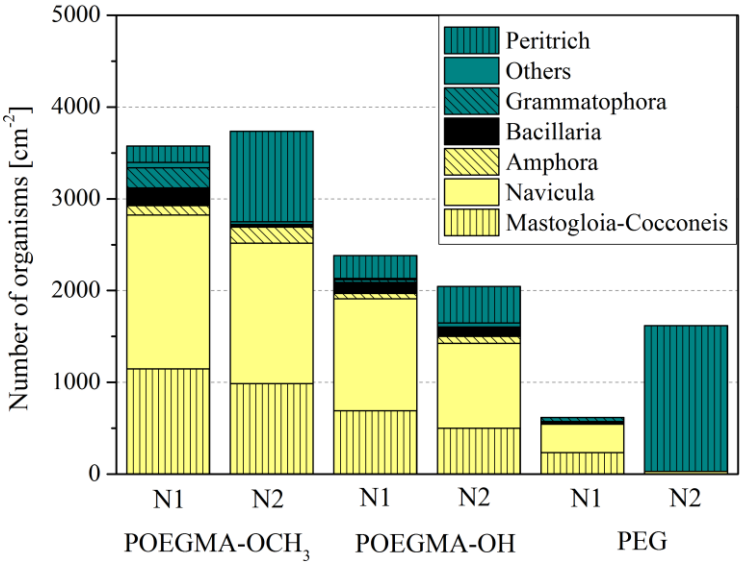

Figure 70. Number of organisms on a range of ethylene glycol containing polymer coatings: POEGMA brushes and PEG SAMs after 48 h immersion for experiments N1 and N2.

10.6. Influence of hydration on marine settlement

10.6.1. Ethylene glycol SAMs

Furthermore the hypothesis that surface hydration is able to affect the settlement of microorganisms as shown in previous bacterial assays was investigated with regard to field experiments. For this purpose, an established series of EG terminated SAMs with different abilities to bind water [6, 83] was used. In general, water can be displaced more easily if less moieties of EG are present while with increasing EG chain length, water can be bound more strongly.

Figure 71 shows the results and, especially for set N1 (a), a trend towards fewer organisms with increasing hydration (more EG units) was observed. These results are in line with former *Ulva* spore adhesion experiments [83].

PEG showed the expected resistance during the first 6 h. Nonetheless, in the N1 series settlement on PEG drastically increased for the 12 h time point and even exceeded the values for the oligoethylene glycol surfaces by a factor of two, five and ten when they contain one, three or six EG units respectively.

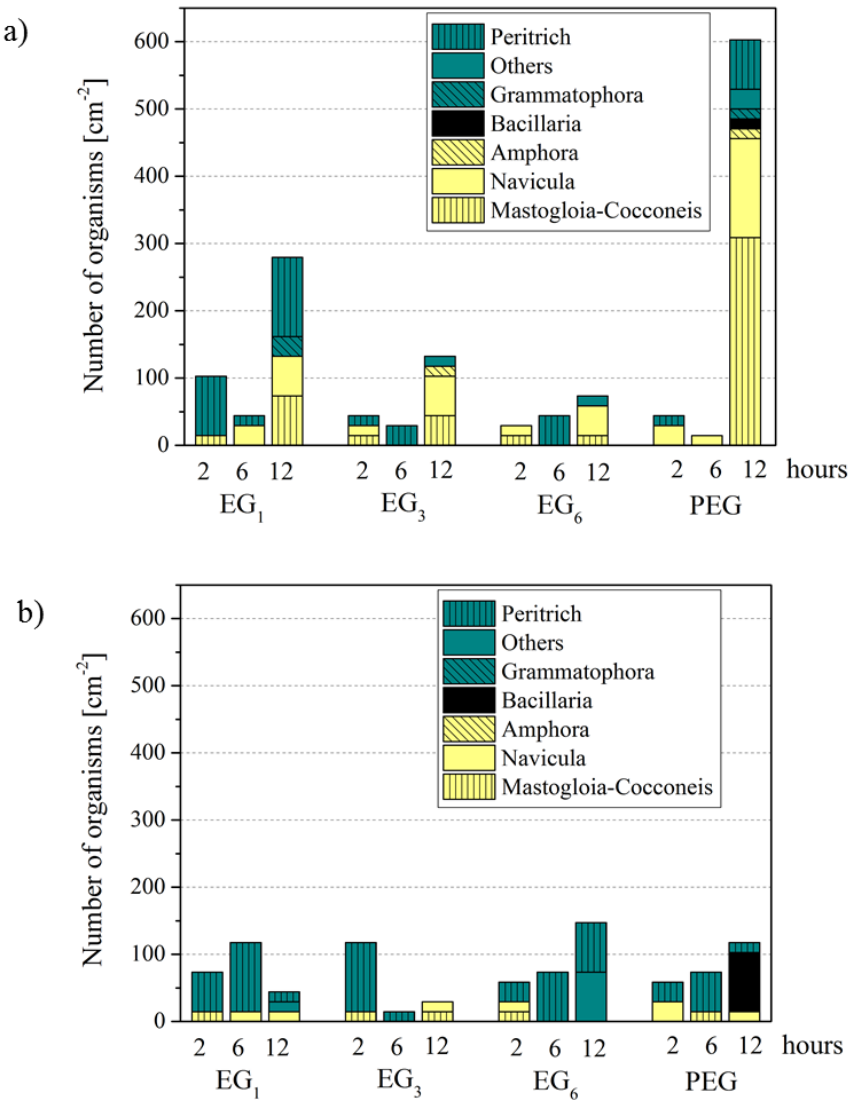

Figure 71. Number of organisms of each species on EGs and PEG SAMs for experiment N1 (a) and N2 (b).

10.6.2. Polysaccharide coatings

Polysaccharide coatings have shown a good performance in previous laboratory assays with different fouling organisms [114, 120], however they have never been tested in the field. Similar to the POEGMA brushes, they combine the advantage of being highly hydrated with being less prone to degradation compared to EG moieties.

As the free-carboxyl groups of the PS may react with the bivalent ions present in the marine environment leading to a collapse of their structures, they were modified by capping free-carboxyl groups with a hydrophobic fluorinated alkylamine to prevent complexation of

bivalent ions by the carboxylates It was investigated whether these surfaces maintain their resistance against marine adhesion even in the ocean, where the chance of collapse of their structures is increased. Alginic acid (AA), hyaluronic acid (HA) and chondroitin sulfate (CS) were tested as acidic polysaccharides which consist of a similar carbohydrate backbone but differ slightly in the composition of their functional moieties. HA contains one carboxylic acid group per disaccharide unit, AA carries an additional carboxylic group and CS an additional sulfate group.

As shown in Figure 72, polysaccharide coatings clearly outperformed POEGMA and except for AA, their settlement decreased by a factor of ten in comparison to the POEGMA brushes. Population on pristine glass was roughly three times larger than on the polysaccharide coatings, again with the only exception of AA. On alginic acid terminated surfaces, the effect of capping of the carboxylic groups became very visible. Capping of the PS led to very low settlements, which was comparable to the one on pristine HA and CS surfaces.

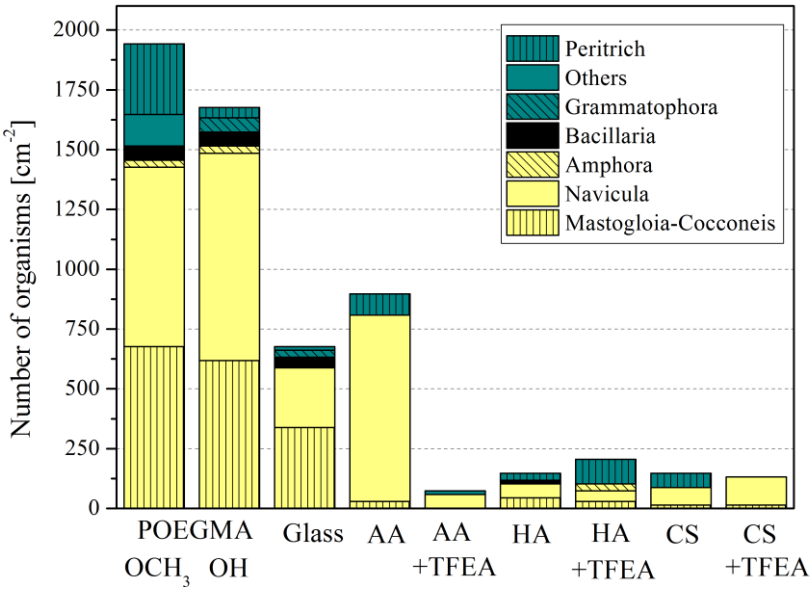

Figure 72. Number of organisms of each species detected on POEGMA brushes, polysaccharide coatings and glass as a reference after 24 h immersion.

10.7. Discussion of the field tests

The major goal of this study was to investigate the influence of surface properties on the early colonization of a range of model surfaces by a natural mix of species in their marine

environment and correlate the results with the ones obtained in previous laboratory assays. The tested surfaces were selected as they comprise a wide range of different surfaces properties. The surface samples were submerged for incubation times ranging from 2 h up to 48 h. In standard immersion tests, the samples are usually submerged for several months or years [154, 160], nevertheless there is a lack of such studies concentrating on the first hours of the surface colonization.

The dominant organisms sized larger than 10 μm on the surfaces were mainly diatoms of the genera *Navicula, Mastogloia, Cocconeis* and *Amphora* and the protozoa *Peritrich*. The abundance and composition of these organisms varied between both experiments reflecting the significantly changed weather conditions. Thus, it can be suggested that temperature of air and water are an important factor for the colonization of the surfaces, particularly during the first 12 h. The notion that water temperature can induce a shift in species occurrence on surfaces, and thus the composition of diatom communities, is in agreement with the literature [170, 232].

The influence of the surface wettability was evaluated using SAMs with different chemistries. In general, the experiments showed that the water contact angle can slightly influence the population density at a given time point. Nevertheless, the composition of the community was similar and did not appear to be systematically affected by the wettability of the surfaces.

The influence of hydration was also investigated, utilizing two kinds of surfaces: EG SAMs and polysaccharide coatings. Hydration seemed to be more important than the wettability. Especially in set N1, EG SAMs showed an increasing resistance with longer chain length, an effect attributed to the enhanced ability to bind water. These results are in line with recent observations for *Ulva* zoospores and eukaryotic cells [55, 83].

The field tests revealed a similar resistance of PEG and the EGs after 2 h and 6 h (Figure 71). However, the settlement of polymeric surfaces increased after 12 h in data set N1 in comparison to the shorter homologues, indicating a faster degradation of the polymeric PEG. This was surprising as PEG coatings are thicker (7 nm) than EG_x (1-3 nm). One possible reason could be that the packing density of the EG chains in a polymer is in general much lower compared to a SAM surface and thus the exchange of water, ions and oxidizing components is promoted.

Recent experiments with *Ulva* zoospores indicated that in short term experiments (45 min settlement assays) PEG surfaces were highly resistant and spores did not even attempt to

settle [85]. As the duration of the experiments in the ocean was much longer (several hours), it is likely that degradation of the PEG surfaces contributed to the unexpected accumulation after long times. Such degradation of EGs in aqueous environments is a well known issue [85, 106, 144, 233].

As a further class of highly hydrated non-fouling surfaces, polysaccharide coatings were examined. The three anionic coatings AA, HA and CS were compared to their TFEA modifications which capped the free-carboxyl groups. AA coatings, which carried an additional carboxylic group, accumulated the most biomass. That is likely due to the loss of the inert properties when applied in the marine environment as complexation of the bivalent ions leads to a collapse of the hydrogels [114]. Capping of AA drastically enhanced the inert properties. HA and CS performed also very well as the settlement on them was considerably lower in comparison to the other surfaces. Interestingly, CS with a lower number of carboxylic acid groups compared to AA, but a similar net charge under the pH of sea water due to additional sulfate groups, seemed to be able to maintain inertness in saltwater while AA did not. These inert properties of CS could be the reason why it is part of the mucus on the skin of many fish [113]. In extension to the short time assays conducted under laboratory conditions [120], these mixed species experiments also demonstrated the inert properties of amphiphilic polysaccharide coatings and the desired effect of the TFEA modification.

Furthermore, a range of methacrylate polymers with oligoethylene side chains was examined to evaluate the influence of the transition from polymeric EG to methacrylate polymers. Despite the methacrylate backbone in POEGMA brushes, the degradation of these surfaces was even faster and resistance was significantly lower compared to PEG, presumably because of the hydrolysis of the ester moieties in the side chain. This result was contrary to the high protein resistance and lack of attachment of mammalian cells previously observed on these interfaces [142, 176, 234-236].

In conclusion, the experiments represent a pioneer study which showed that the short-term immersion of well-defined model surfaces provides useful information on the resistance of the surfaces against biofouling.

10.8. Comparison between laboratory and real marine world

In the course of this PhD thesis, the influence of surface properties on the adhesion of the marine bacterium *Cobetia marina* was investigated. These bacterial assays were realized at least four times and were always performed under the same specific conditions. The bacteria were incubated at room temperature (22-24 C) for 2 h to allow settlement, whereas the field tests were executed twice (N1 and N2) in the natural environment with incubation times ranging from 2 h up to 48 h. Because of these different experimental conditions a direct comparison of all field results to the ones obtained in the laboratory has to be done with caution, even though a general correlation can be achieved. The weather varied between both field experiments, thus their environmental conditions differed, especially the water and air temperature. During the experiments N1 the water was significantly warmer than during N2. Despite small variations during the two field experiments, some trends found in previous laboratory experiments could be reproduced in the field.

In general, the experiments revealed that the water contact angle hardly influenced the population density or the composition of the settled organisms and they did not appear to be systematically affected by the wettability of the surfaces. The bacterial lab assays are in line with these finding (see chapter 6), except for PEG, on which a considerable lower bacterial adhesion was found in comparison to the other SAMs. However, by observing in detail the field results of PEG it was noticed that during the first 6 h the total number of settled organisms was indeed slightly lower than for the other SAMs, especially in set N1.

In field tests as well as in bacterial assays hydration seemed to be more important than the wettability. Particularly in set N1, EG SAMs showed an increasing resistance with higher chain length during the first 6 h. This effect can be attributed to the enhanced ability of longer EGs to bind water. These results are in line with the bacterial assays and recent observations for *Ulva* zoospores and eukaryotic cells [55, 83]. Nonetheless, the polymeric surfaces, in comparison to the shorter homologues, presented an increase in settlement after 12 h in data set N1, indicating a faster degradation of the polymeric PEGs. The packing density of the EG chains in a polymer is much lower, compared to the monolayers of EG SAMs, promoting the exchange of water. Such degradation in aqueous environments has been described in previous laboratory assays [85, 106, 144, 233]. As the incubation time employed for the bacterial assays was only 2 h, this effect was not observed.

The performance of the three highly hydrated polysaccharide coatings AA, HA and CS was compared to their TFEA modifications with capped free-carboxyl groups. For the AA coatings, the same trend of enhanced performance after capping was found in field and bacterial laboratory tests. The uncapped AA presented the highest accumulation of biomass, whereas its capped homologue had drastically enhanced inert properties. The high settlement found on AA can be explained as this coating carries an additional carboxylic group compared to the other polysaccharides, thus its structure is more prone to be collapsed by complexation of bivalent ions present in the marine environment [114]. HA and CS, both pristine and modified, performed similarly in a good manner. In the laboratory assays, the capping of these polysaccharides led to a slightly different critical shear stress compared to the corresponding pristine surfaces. Since the performance of HA and CS in relation to the one of AA was substantially better in the field tests than in the laboratory assays, the field results can still be considered to be successful.

In conclusion, some trends which were found in previous laboratory experiments could be verified in the field, even if the surfaces were submerged in the natural marine environment, with a natural mix of species and under variable and uncontrolled conditions. Despite the fact that the performance of the coatings in the field tests did not always match the expectations based on the laboratory results, the findings of this PhD work clearly point out, that the results obtained by laboratory assays are nevertheless a valuable indicator of the resistance of surfaces to biofouling.

11. Summary and Outlook

In the course of this thesis the influence of surface properties relevant for bioadhesion was evaluated with regard to adhesion and the unwanted colonization of submerged surfaces, also referred to as marine biofouling. The investigated samples comprised a wide range of surface properties namely wettability, chemistry, hydration, transition from monolayers to polymeric coatings and controlled release properties.

In order to measure the adhesion of the marine bacterium *Cobetia marina* on a variety of model surfaces a microfluidic shear stress assay based on the principle of a parallel plate flow chamber was employed. After injection of the bacteria into the microfluidic system and incubation on the desired samples, a controlled flow was applied and stepwise increased covering a shear stress range of nearly six orders of magnitude (from ≈0.01 dyn/cm^2 to 5,500 dyn/cm^2). The resulting detachment curves provided two values for the quantification of adhesion: the critical shear stress needed to detach 50 % of the adherent bacteria (τ_{50}) and the percentage of bacteria initially attached to the surface. Experimental parameters for this assay such as incubation time, medium, and flow increment rate were optimized showing that two hours of incubation in artificial seawater (ASW) and an increment of flow of 26 % every 5 s were a suitable set of parameters (see chapter 4).

The impact of the conditioning films formed on DDT self-assembled monolayers (SAMs) and glass slides after immersion in various media on bacterial adhesion was evaluated. The film formed after two hours of incubation in ASW, natural seawater (NSW) and MB was found to shift the wettability of the samples and it was thicker in the case of MB compared to ASW. The conditioning of films strongly influenced both critical shear stress and percentage of adherent bacteria. The differences between pristine samples of different coatings generally diminished after incubation in either MB, ASW or NSW, in particular the percentage of adherent bacteria reached almost the same value for all samples after immersion. These findings suggest that, after immersion, all surface chemistries may be equalized showing similar values for bacterial adhesion. Although these results were conclusive in this study, further investigations of surfaces pre-incubated longer than 2 h should be considered to verify this hypothesis (see chapter 5).

Bacterial adhesion on a variety of SAMs with different wettabilities (chapter 6) and hydration levels (chapter 7) was tested in order to investigate their influence on bacterial adhesion. Results showed that in general these properties had an impact on bacterial detachment.

However, they had only a minor influence on the fraction of adherent bacteria with the polymeric hydrated PEG SAM being the only surface where settlement was significantly reduced.

Even though the results showed a high variability, hydration was found to be an especially important surface property, since the critical shear stress of the bacteria decreased with every addition of an ethylene glycol (EG) unit and consequently with an increasing amount of bound water. This observation is in line with previous findings for mammalian cells and algae [55, 83]. The reason for the high variability of the results seems to be a combination of biological variability, experimental errors and slightly different surface properties as the IRRAS spectra varied between replicates to some degree.

Polysaccharide coatings with different chemical moieties, hyaluronic acid (HA), chondroitin sulfate (CS), and alginic acid (AA) were tested as highly hydrated model surfaces to investigate the influence of hydration on the adhesion of the bacteria. Since the structures of the polysaccharides might collapse due to interaction with bivalent ions present in sea water, their free-carboxyl groups were capped with a hydrophobic amine (TFEA). If AA and HA were modified, it was noticed that the bacterial critical shear stress was substantially reduced, particularly in the case of AA as this molecule contains more carboxylic acid groups. These observations indicate that TFEA modifications really did cause the desired effect. Modifying CS led to the opposite result as it performs very well by itself, which might be the reason for it being a component of the mucus on the skin of fish [113] (see chapter 8). Nevertheless, just as in the case of EG SAMs, the ratio of adherent bacteria was scarcely influenced by the characteristics of polysaccharides. As in the case of the EG SAMs, the variability of the results was remarkable prohibiting the direct comparison of the performance of the samples in a confident manner. Despite this observation, it was confirmed that bacteria adhered to these hydrogels considerably more weakly than on the other SAMs investigated during this thesis by more than one order of magnitude.

The variability of the results obtained for some sets of surfaces investigated during this PhD thesis was explained in chapter 4.1.2. Our system observed the detachment of all bacteria present in the FOV - usually more than 400 - individually. This way it was possible to gain more information than in other biological detachment assays which solely count the number of bacteria before and after rinsing the surface. However, this detailed observation comes at a price: it is not possible to acquire data from multiple FOVs after one incubation. Therefore, a

direct comparison of the obtained statistics in this work to those showed for other biological assays does not seem appropriate.

As a further antifouling concept, copper based metal-organic frameworks (Cu-SURMOF 2) were tested in order to investigate the influence of copper release on bacterial adhesion. The motivation for this study was based on the desire to develop coatings which only act when target organisms are present, thus avoiding the uncontrolled release of metal ions into the environment. Numerous damaging effects on bacteria could be observed when incubated on these coatings, such as the reduction of the critical shear stress and alterations in bacterial viability and morphology. Such observations are presumably due to the effect of copper ions released after degradation of the coatings, manifested by the loss of crystallinity. In particular, the fact that the coatings were stable in ASW in the absence of bacteria proves the stimulus response of such samples with regard to the bacteria (see chapter 9).

Finally, a variety of model surfaces covering a wide range of surface properties and previously tested in conventional laboratory assays were submerged into the ocean. The aim of this study was to investigate their influence on the early colonization by biofoulers in the natural marine environment and correlate these results to the ones obtained in the laboratory assays performed under controlled conditions. Despite the fact that the samples were exposed to a natural mix of species under variable and poorly controlled conditions, some trends which were found in the laboratory could be confirmed in the field. Results from the field tests confirmed that hydration appeared to be more important than the wettability, as the EG SAMs showed an increased resistance with more EG units. The good performance of the polysaccharide coatings and the desired effect achieved by capping their free-carboxyl groups could be verified in the field as well. In spite of the observed trends, it is necessary to point out that this study, described in chapter 10, was pioneer work, thus some optimization of the experimental layout is required to confirm the results. For the future, more replicates immersed exactly under the same conditions are needed to obtain better statistics. In parallel to the improvement of the reproducibility, it would be advisable to evaluate the stability of the samples in the seawater at the site of the experiments by XPS measurements to ensure that the performance of the samples is due to their surface chemistry.

This work comprised a range of surface properties which were studied by a newly established microfluidic assay and a new field test protocol. It opens the possibility to address many future questions such as topography or charge.

Further future experiments could be the study of detachment of micro-particles on glass, in order to perform a thorough calibration of the system, minimize systematic errors and optimize the reproducibility of the data.

In conclusion, this thesis investigated the influence of various surface properties on the adhesion of the marine bacterium *Cobetia marina* and correlated the results to the performance of samples in the "real marine world". Some observations were found for both studies as in general the adherent fraction of the bacteria was independent from surface chemistry and hydration strongly reduced adhesion. Thus, this work provides both a new method and fundamentally new knowledge that could contribute to the development of new coatings to tackle the challenge of marine biofouling.

12. Appendix

12.1. Morphology of the bacteria on Cu-SURMOF 2

12.1.1. Procedure to optimize sample preparation and imaging

An immediate occurring question was if the morphology of the bacteria changed during incubation on Cu-SURMOF 2.

The bacterium *Cobetia marina* incubated on DDT and HDT SAMs and glass slides was visualized in greater detail using several methods. To optimize the sample preparation and imaging different fixation procedures and analytical methods were compared: light microscopy, helium ion microscopy (HeIM), atomic force microscopy (AFM) and scanning electron microscopy (SEM) as analytical devices and critical point drying (CPD), freeze drying of plunge-frozen samples (FDPFS) and immersion in ice cold methanol (ICM) as fixation methods. Nonetheless, bacteria were air dried overnight as well to avoid possible alterations of the test surfaces by the fixation process. Although this procedure is not among the most commonly used preparation techniques for SEM characterization, it has been used as an alternative drying method in previous studies [201, 237].

Figure 73 displays *in-situ* light microscopy images of bacteria incubated for 15 min, 1 h and 4 h on DDT SAM (a, b and c) and glass slides (d, e and f). These images were acquired with a TE-2000-U (Nikon, Tokyo, Japan) with a 40x Ph2 objective (NA = 0.6) with a resulting field of view of 256 µm by 192 µm. Obviously, the number of bacteria increased with time. It could be noticed that bacteria prefer to attach on DDT SAM, which was not surprising since *C. marina* attached preferentially to hydrophobic surfaces [35, 37, 82].

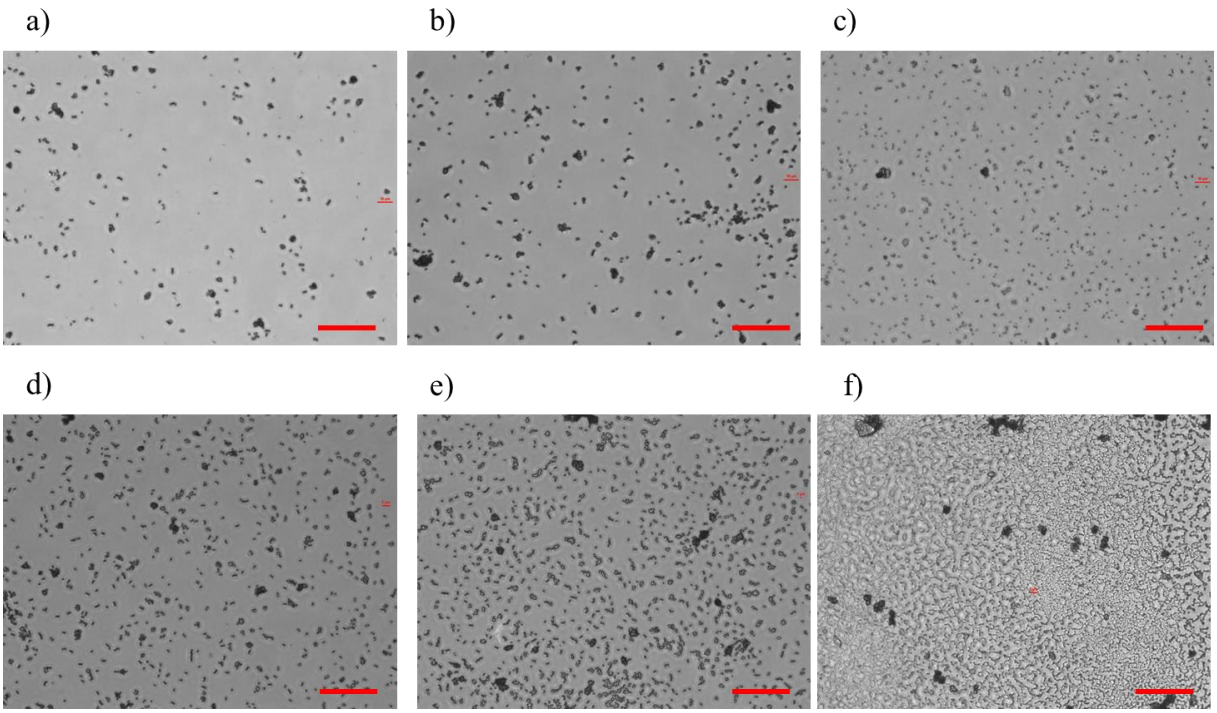

Figure 73. Light microscopy images of bacteria incubated on DDT SAM (a, b and c) and on glass slides (d, e and f) for 15 min, 1 h and 4 h Field of view: 256 µm by 192 µm. Scale bars represent 50 µm.

SEM is probably the most commonly used technique, besides light microscopy, to image biological tissues (see chapter 3.11.6). The SEM images of the bacteria on HDT incubated for 2 h and then air dried without previous fixation (Figure 74b), and the images of the bacteria incubated on glass and DDT SAM for 15 min, 1 h and 4 h, fixed with glutaraldehyde and subsequently CPD (Figure 75 and Figure 76) were obtained with a LEO 1530 (Zeiss, Oberkochen, Germany) SEM. The SEM images of the air dried bacteria incubated for 2 h on HDT SAM (Figure 74b) were acquired using a FEI Philips XL 30 FEG-ESEM operated in SEM-Mode.

It could be observed that drying the samples by immersion in ICM and by air drying overnight lead to similar results showing the bacteria with a smooth normal morphology (Figure 74a and b respectively).

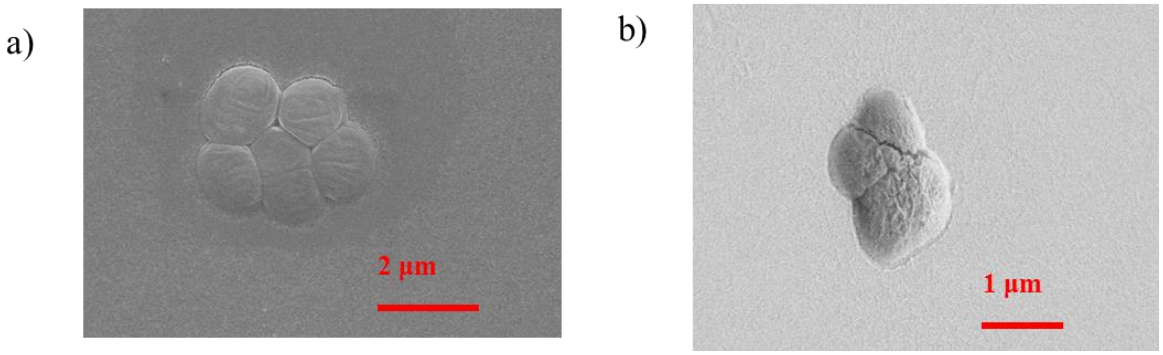

Figure 74. SEM images of bacteria incubated on HDT SAM for 2 h. The bacteria were either fixed and dried by immersion in ice cold methanol and sputtered prior to imaging at 10,000x magnification (a), or air dried without fixation (15,000x magnification) (b).

Figure 75 displays SEM images of bacteria which were fixed with glutaraldehyde, dried by CPD and subsequently sputtered (detailed protocol in chapter 3.8). The bacteria were incubated on DDT SAM (a-c) and glass slides (d-f) for 15 min (a and d), 1 h (b and e) and 4 h (c and f). The images after 15 min and 4 h were recorded with 1,000x magnification, whereas the ones incubated 1 h were recorded with 3,000x and 5,000x respectively. It could be noticed that the number of bacteria increased with time and that bacteria prefer to attach to the DDT SAMs. These results are in line with observations using light microscopy (Figure 73). In order to evaluate the morphology of the bacteria on these samples in greater detail, SEM images with higher magnifications were recorded. In contrast to the SEM images of air dried bacteria and those dried by immersion in ICM (Figure 74), the bacteria fixed with glutaraldehye and dried by CPD appeared crumpled and wrinkled up (Figure 76). That was unexpected since this protocol is routinely used in sample preparation for SEM imaging of diverse organisms. These results suggest that drying the bacteria under extreme conditions such as high pressures may affect their morphology.

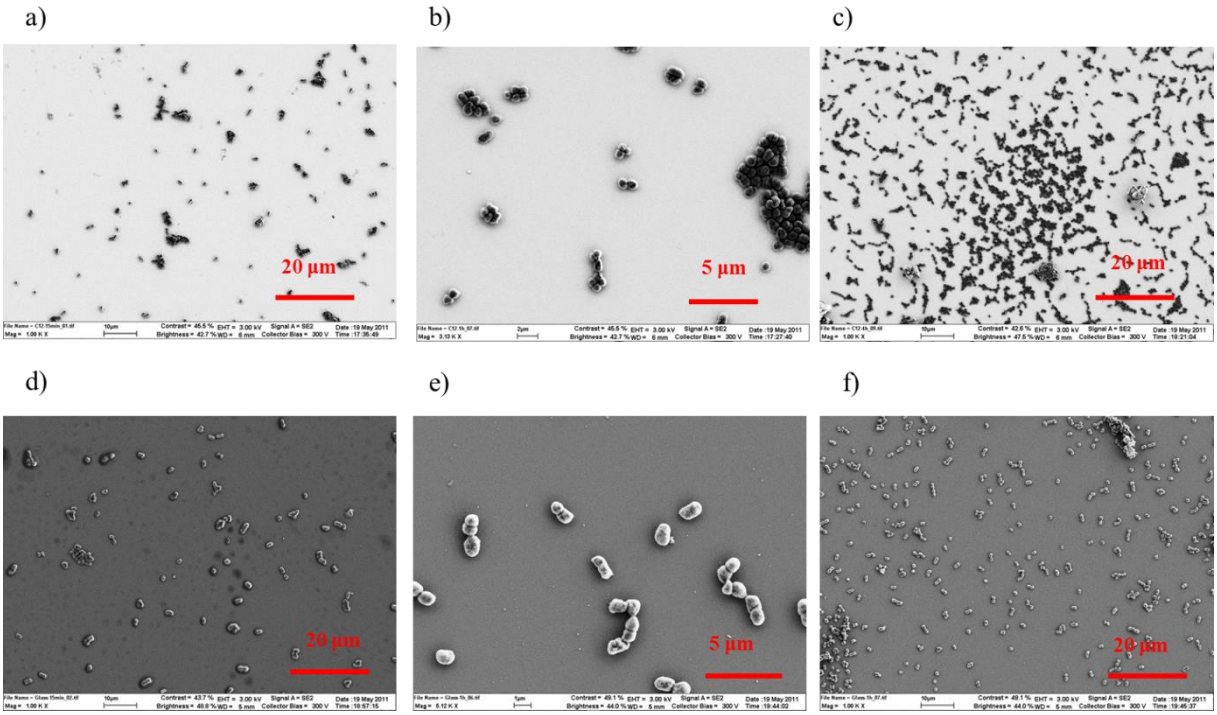

Figure 75. SEM images of bacteria fixed with glutaraldehyde and then dried by CPD. Bacteria were incubated on DDT SAM for 15 min, 1 h and 4 h (a, b and c) and on glass slides for 15 min, 1 h and 4 h (d, e and f).

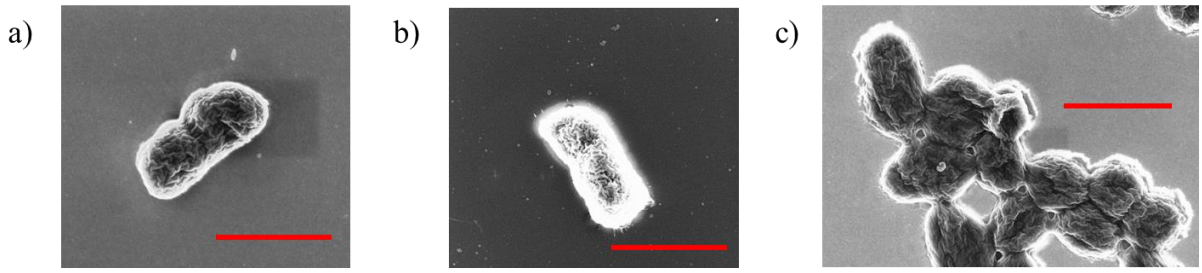

Figure 76. SEM images of bacteria fixed with glutaraldehyde and then dried by CPD in greater detail. Bacteria were incubated on DDT SAM for 15 min (a), on glass 1 h and on DDT SAM 4 h (c). SEM images were taken with a magnification of 25,000x, 25,000x and 20,000x respectively.

As a further technique to visualize the bacteria, HeIM was used. Samples for these experiments were prepared by freeze-drying plunge-frozen samples. Droplets of bacterial solution were placed on TEM grids coated with a holey carbon film (Quantifoil® R 2/4). After a few minutes, during which a number of bacteria adhered to the surface, the samples were plunge-frozen using an ethane/propane mixture as a cryogen and afterwards dried by freeze drying. Figure 77 shows HeIM images of the freeze-dried bacteria. Although these bacteria did not appear as much crumpled as the ones dried by CPD, they did not present the same morphology as the ones dried by immersion in ice cold ethanol or the air dried ones (Figure 74). Even though the method of freeze-drying plunge-frozen samples is known to preserve the

morphology of biological specimen very well, in this case it seemed to fail. It can be speculated that the preservation of the cell wall after freeze-drying caused the bacteria to crumple during the fixation and dehydration.

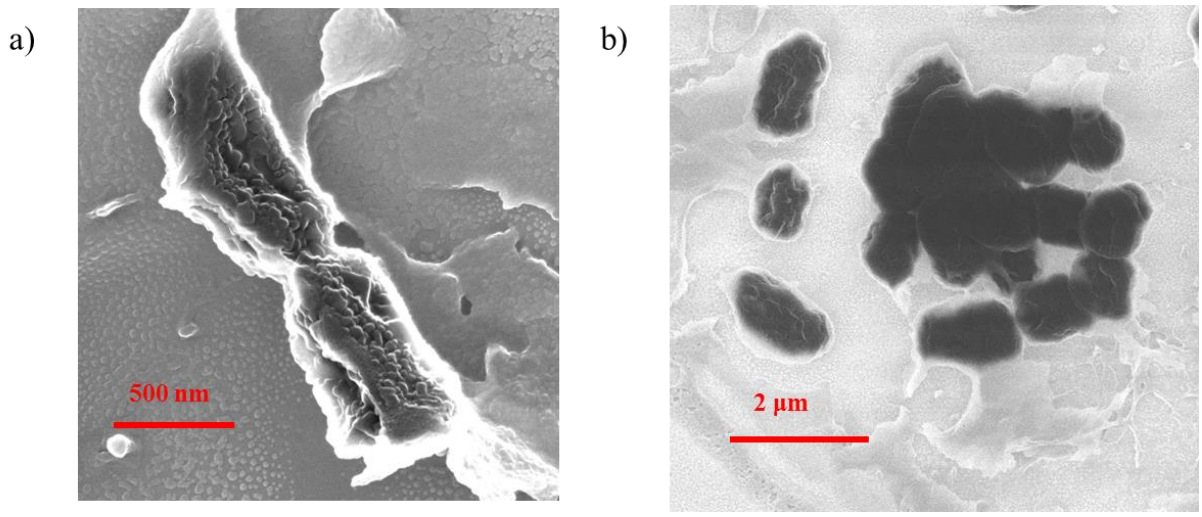

Figure 77. HeIM images of bacteria fixed by plunge drying and dried by freeze drying.

Figure 78 shows images of the dried bacteria at the same scale providing a direct comparison of the different techniques: critical point drying (a), freeze drying (b), immersion in ice cold methanol (c) and air drying (d). It can be seen that the bacterial morphology appears smoother for samples dried by immersion in ICM or air dried than for those prepared by critical point drying or freeze drying.

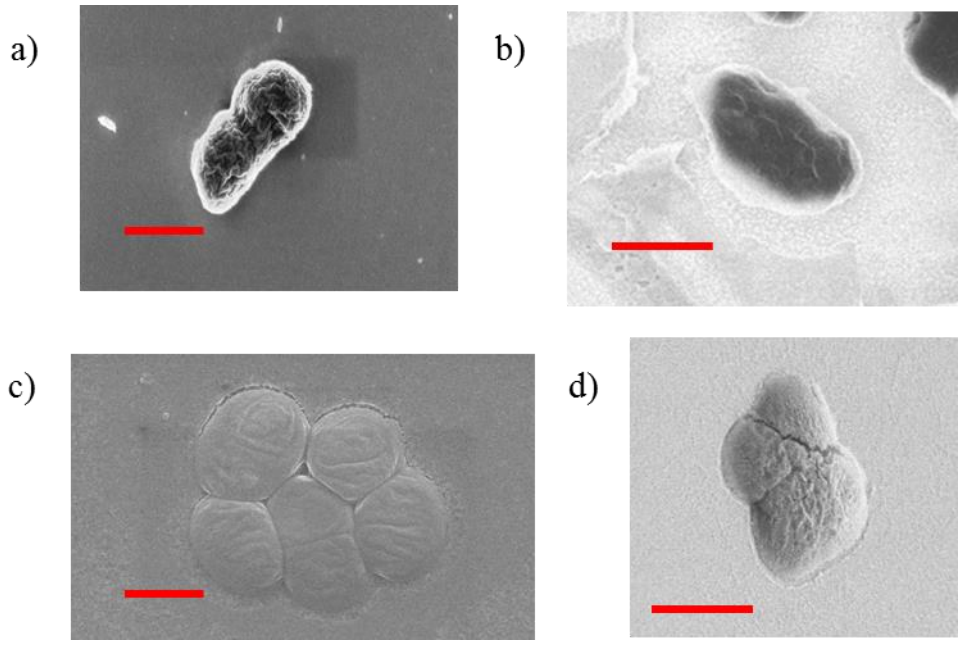

Figure 78. Images of *Cobetia marina* dried with different methods: critical point drying (a), freeze drying (b), immersion in ice cold methanol (c) and air drying (d). Scale bars are 1 μm.

AFM was employed to gather complementary information of the bacteria such as their roughness or height. Figure 79 and Figure 80 show AFM images (a), with the corresponding rendered 3D AFM images (b) and the height profile across the long axis (c) of bacteria incubated on HDT SAM for 2 h and subsequently dried by immersion in ice cold methanol (Figure 79) or air dried (Figure 80). It can be noticed that as previously shown by SEM (Figure 74), the morphology of the bacteria appeared smooth and it was similar in both cases.

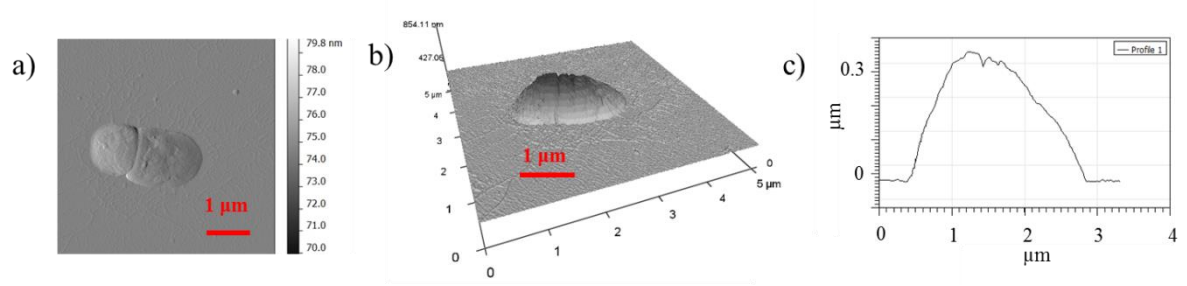

Figure 79. Bacteria incubated for 2 h on HDT SAM and dried by immersion in ice cold methanol for 3 min. AFM image (a), resulting 3D rendering (b) and the corresponding height profile across the long axis (c).

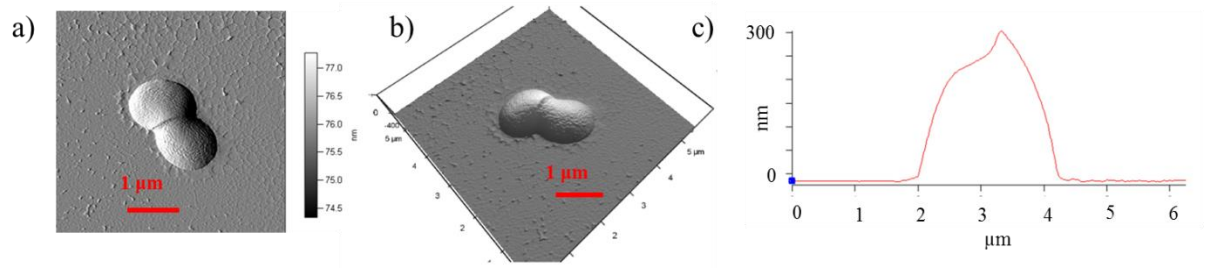

Figure 80. Bacteria incubated for 2 h on HDT SAM without fixation and air dried. AFM image (a), resulting 3D rendering (b) and the corresponding height profile across the long axis (c).

12.1.2. Discussion about the methods used for bacterial imaging

During the course of this investigation it was realized how important it is to establish the ideal protocol for the further evaluation of the morphology of the bacteria when incubated on Cu-SURMOF 2. Therefore images of bacteria on different surfaces and dried with various methods were acquired using several analytical techniques, namely light microscopy, SEM, AFM and HeIM. The chosen surfaces were DDT and HDT SAM, glass slides and TEM grids coated with a holey carbon film (Quantifoil® R 2/4). Diverse fixation and drying methods were used such as FDPFS, immersion in ICM, air drying without previous fixation and fixation with glutaraldehyde followed by CPD.

Bacteria incubated for 15 min, 1 h and 4 h on DDT SAMs and glass slides were visualized by *in-situ* light microscopy and by SEM when bacteria were fixed with glutaraldehyde and critical point dried after incubation. These results revealed that bacteria preferred to attach on DDT SAM which was not surprising since *C. marina* attached preferentially to hydrophobic surfaces [35, 37, 82], besides the obvious observation that the attachment of bacteria

increased with the time. Nevertheless light microscopy is not suitable for a detailed evaluation of the morphology of the bacteria.

AFM and SEM visualization showed a smooth morphology of the bacteria attached on HDT SAM when the samples were dried by immersion in ICM or air drying. However if the bacteria on DDT and glass slides were fixed with glutaraldehyde and CPD afterwards, they appeared crumpled and wrinkled up. Furthermore, the bacteria were freeze-dried and visualized with HeIM. Although these bacteria did not appear as much crumpled as the ones after CPD, they did not show the same morphology as the ones dried by ICM or the air dried.

Concluding, the techniques AFM, SEM and HeIM and the fixation methods air drying and immersion in ICM appear to be best suited for the evaluation of the morphology of *Cobetia marina*.

12.1.3. Evaluation of bacterial morphological changes on Cu-SURMOF 2 by SEM

SEM images of the bacteria after 2 h incubation on Cu-SURMOF 2 (Figure 81b and d) and HDT SAM (Figure 81a and c) as a non-toxic control were acquired. The bacteria were fixed by immersion in ice cold methanol following the optimized protocol described in chapter 12.1. The images revealed that the bacteria on Cu-SURMOF 2 (≈160 nm) appeared to be relatively flat (Figure 81b) in comparison to those incubated on HDT SAM (Figure 81a).

The samples shown in Figure 81c and d were removed from the solution after immersion for 2 h in bacterial suspension, rinsed with Milli-Q® water and air dried overnight. Although this protocol is not among the most commonly used for SEM characterization, it has been employed as an alternative drying method in previous studies [201, 237]. Besides, the morphology of the bacteria on Cu-SURMOF 2 ≈120 nm thick (Figure 81) was also imaged to evaluate whether these coatings containing less copper, in comparison to the 160 nm ones, were able to cause a morphology change on the bacteria as well. The images reveal that bacteria on Cu-SURMOF 2 (≈120 nm, Figure 81d) appeared to be relatively flat and with apparent protrusions in the middle of the bacteria in comparison to those incubated on HDT SAM (Figure 81c).

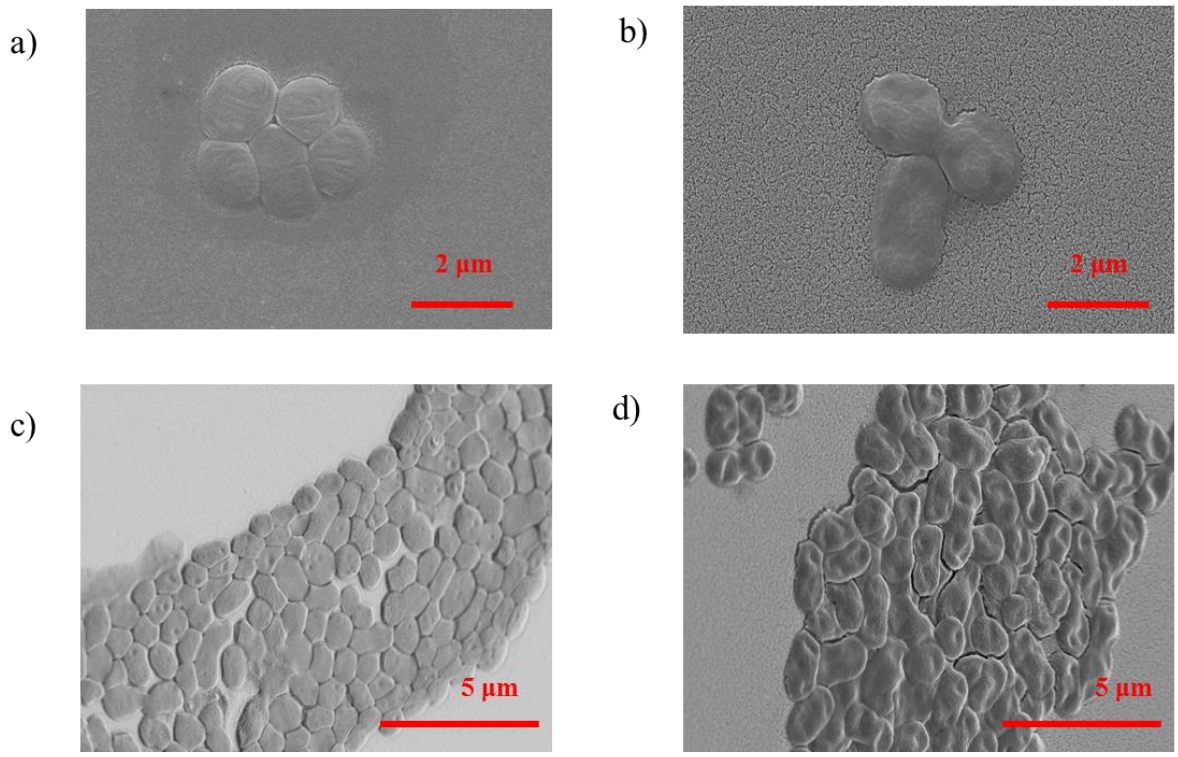

Figure 81. SEM images of *C. marina* after 2 h incubation on HDT SAM (a and c) and on Cu-SURMOF 2 (b and d). The bacteria shown in a and b were fixed by immersion in ice cold methanol for 3 min and visualized with 10,000x magnification, while those shown in c and d were air dried and visualized with a magnification of 5,000x.

12.2. Bibliography

1. Callow, M.E. and J.A. Callow, *Marine biofouling: a sticky problem.* Biologist, 2002. **49**: p. 1-5.

2. Bers, A.V. and M. Wahl, *The influence of natural surface microtopographies on fouling.* Biofouling, 2004. **20**(1): p. 43-51.

3. Yebra, D.M., S. Kiil, and K. Dam-Johansen, *Antifouling technology - past, present and future steps towards efficient and environmentally friendly antifouling coatings.* Progress in Organic Coatings, 2004. **50**(2): p. 75-104.

4. Corbett, J.J. and H.W. Koehler, *Updated emissions from ocean shipping.* Journal of Geophysical Research-Atmospheres, 2003. **108**(D20).

5. Callow, J.A. and M.E. Callow, *Trends in the development of environmentally friendly fouling-resistant marine coatings.* Nature Communications, 2011. **2**.

6. Rosenhahn, A., et al., *The role of "inert" surface chemistry in marine biofouling prevention.* Physical chemistry chemical physics, 2010. **12**(17): p. 4275-4286.

7. Abbott, A., et al., *Cost-benefit analysis of the use of TBT: the case for a treatment approach.* Science of the Total Environment, 2000. **258**(1-2): p. 5-19.

8. Reise, K., S. Gollasch, and W. Wolff, *Introduced marine species of the North Sea coasts.* Helgoland Marine Research, 1998. **52**(3): p. 219-234.

9. Qian, P.Y., et al., *Marine biofilms as mediators of colonization by marine macroorganisms: Implications for antifouling and aquaculture.* Marine Biotechnology, 2007. **9**(4): p. 399-410.

10. Videla, H.A. and L.K. Herrera, *Microbiologically influenced corrosion: looking to the future.* International Microbiology, 2005. **8**(3): p. 169-180.

11. Palmer, J., S. Flint, and J. Brooks, *Bacterial cell attachment, the beginning of a biofilm.* Journal of Industrial Microbiology & Biotechnology, 2007. **34**(9): p. 577-588.

12. Rosenhahn, A., T. Ederth, and M.E. Pettitt, *Advanced nanostructures for the control of biofouling: The FP6 EU Integrated Project AMBIO.* Biointerphases, 2008. **3**(1): p. IR1-IR5.

13. Monod, J., *The Growth of Bacterial Cultures.* Annual Reviews in Microbiology, 1949. **3**(1): p. 371-394.

14. D'Souza, F., et al., *Bacterial assay for the rapid assessment of antifouling and fouling release properties of coatings and materials.* Journal of Industrial Microbiology & Biotechnology, 2010. **37**(4): p. 363-370.

15. Arpa-Sancet, M., C. Christophis, and A. Rosenhahn, *Microfluidic Assay to Quantify the Adhesion of Marine Bacteria*. Biointerphases, 2012. **7**(1): p. 1-9.

16. Zobell, C.E., *The Effect of Solid Surfaces upon Bacterial Activity.* Journal of Bacteriology, 1943. **46**(1): p. 39-56.

17. Donlan, R.M., *Biofilm Formation: A Clinically Relevant Microbiological Process.* Clinical Infectious Diseases, 2001. **33**(8): p. 1387-1392.

18. Monroe, D., *Looking for chinks in the armor of bacterial biofilms.* Plos Biology, 2007. **5**(11): p. 2458-2461.

19. Hall-Stoodley, L., J.W. Costerton, and P. Stoodley, *Bacterial biofilms: From the natural environment to infectious diseases.* Nature Reviews Microbiology, 2004. **2**(2): p. 95-108.

20. Tsuneda, S., et al., *Extracellular polymeric substances responsible for bacterial adhesion onto solid surface.* Fems Microbiology Letters, 2003. **223**(2): p. 287-292.

21. Flemming, H.-C., T.R. Neu, and D.J. Wozniak, *The EPS Matrix: The "House of Biofilm Cells".* Journal of Bacteriology, 2007. **189**(22): p. 7945-7947.

22. Akiyama, H., et al., *Confocal laser scanning microscopic observation of glycocalyx production by Staphylococcus aureus in mouse skin: does S. aureus generally produce a biofilm on damaged skin?* British Journal of Dermatology, 2002. **147**(5): p. 879-885.

23. Shikuma, N.J. and M.G. Hadfield, *Temporal variation of an initial marine biofilm community and its effects on larval settlement and metamorphosis of the tubeworm Hydroides elegans.* Biofilms, 2005. **2**(4): p. 231-238.

24. Hadfield, M.G., *Biofilms and Marine Invertebrate Larvae: What Bacteria Produce That Larvae Use to Choose Settlement Sites*, in *Annual Review of Marine Science, Vol 3*, C.A. Carlson and G.S. J., Editors. 2011. p. 453-470.

25. Huang, S.Y. and M.G. Hadfield, *Composition and density of bacterial biofilms determine larval settlement of the polychaete Hydroides elegans.* Marine Ecology-Progress Series, 2003. **260**: p. 161-172.

26. Marshall, K., et al., *Effect of marine bacterial isolates on the growth and morphology of axenic plantlets of the green alga Ulva linza.* Microbial ecology, 2006. **52**(2): p. 302-310.

27. Patel, P., et al., *Specificity in the settlement - modifying response of bacterial biofilms towards zoospores of the marine alga Enteromorpha.* Environmental Microbiology, 2003. **5**(5): p. 338-349.

28. Mayer, C., et al., *The role of intermolecular interactions: studies on model systems for bacterial biofilms.* International Journal of Biological Macromolecules, 1999. **26**(1): p. 3-16.

29. Joint, I., et al., *Cell-to-cell communication across the prokaryote-eukaryote boundary.* Science, 2002. **298**(5596): p. 1207-1207.

30. Dobretsov, S., M. Teplitski, and V. Paul, *Mini-review: quorum sensing in the marine environment and its relationship to biofouling.* Biofouling, 2009. **25**(5): p. 413-427.

31. Bos, R., H.C. van der Mei, and H.J. Busscher, *Physico-chemistry of initial microbial adhesive interactions – its mechanisms and methods for study.* FEMS Microbiology Reviews, 1999. **23**(2): p. 179-230.

32. Hermansson, M., *The DLVO theory in microbial adhesion.* Colloids and Surfaces B: Biointerfaces, 1999. **14**(1–4): p. 105-119.

33. An, Y.H. and R.J. Friedmann, eds. *Handbook of bacterial adhesion- principles, methods, and applications*. 2000, Humana Press: Totowa, NJ.

34. Boks, N.P., et al., *Forces involved in bacterial adhesion to hydrophilic and hydrophobic surfaces.* Microbiology, 2008. **154**(10): p. 3122-3133.

35. Ista, L.K., et al., *Attachment of bacteria to model solid surfaces: Oligo(ethylene glycol) surfaces inhibit bacterial attachment.* Fems Microbiology Letters, 1996. **142**(1): p. 59-63.

36. Shea, C., L.J. Lovelace, and H.E. Smithsomerville, *Delaya Marina as a model organism for studies of bacterial-colonization and biofilm formation.* Journal of Industrial Microbiology, 1995. **15**(4): p. 290-296.

37. Ista, L.K., V.H. Perez-Luna, and G.P. Lopez, *Surface-grafted, environmentally sensitive polymers for biofilm release.* Applied and Environmental Microbiology, 1999. **65**(4): p. 1603-1609.

38. Mata, J.A., et al., *A detailed phenotypic characterisation of the type strains of Halomonas species.* Systematic and Applied Microbiology, 2002. **25**(3): p. 360-375.

39. Cobet, A.B., et al., *The effect of Nickel on a marine bacterium Arthrobacter-Marinus new species* Journal of General Microbiology, 1970. **62**(2): p. 159-169.

40. Baumann, L., et al., *Taxonomy of aerobic marine eubacteria.* Journal of Bacteriology, 1972. **110**(1): p. 402-429.

41. Baumann, L., R.D. Bowditch, and P. Baumann, *Description of Deleya gen. nov. Created to Accommodate the Marine Species Alcaligenes aestus, A. pacificus, A. cupidus, A. venustus, and Pseudomonas marina.* International Journal of Systematic Bacteriology, 1983. **33**(4): p. 793-802.

42. Dobson, S.J. and P.D. Franzmann, *Unification of the genera Deleya (Baumann et al 1983), Halomonas (Vreeland et al 1980), and Halovibrio (Fendrich 1988) and the species Paracoccus halodenitrificans (Robinson and Gibbons 1952) into a single genus, Halomonas, and placement of the genus Zymobacter in the family Halomonadaceae.* International Journal of Systematic Bacteriology, 1996. **46**(2): p. 550-558.

43. Arahal, D.R., et al., *Phylogeny of the family Halomonadaceae based on 23S and 16S rDNA sequence analyses.* International Journal of Systematic and Evolutionary Microbiology, 2002. **52**: p. 241-249.

44. Arahal, D.R., et al., *Proposal of Cobetia marina gen. nov., comb. nov., within the Family Halomonadaceae, to Include the Species Halomonas marina.* Systematic and Applied Microbiology, 2002. **25**(2): p. 207-211.

45. Swain, G.W., W.G. Nelson, and S. Preedeekanit, *The influence of biofouling adhesion and biotic disturbance on the development of fouling communities on non-toxic surfaces.* Biofouling, 1998. **12**(1-3): p. 257-269.

46. Christ, K.V. and K.T. Turner, *Methods to Measure the Strength of Cell Adhesion to Substrates.* Journal of Adhesion Science and Technology, 2010. **24**(13-14): p. 2027-2058.

47. Butt, H.J., et al., *Impact of atomic force microscopy on interface and colloid science.* Advances in Colloid and Interface Science, 2007. **133**(2): p. 91-104.

48. Yongsunthon, R., et al., *Correlation between fundamental binding forces and clinical prognosis of Staphylococcus aureus infections of medical implants.* Langmuir : the ACS journal of surfaces and colloids, 2007. **23**(5): p. 2289-2292.

49. Waar, K., et al., *Atomic force microscopy study on specificity and non-specificity of interaction forces between Enterococcus faecalis cells with and without aggregation substance.* Microbiology (Reading, England), 2005. **151**(Pt 7): p. 2459-2464.

50. Busscher, H.J., et al., *Measurement of the surface free energy of bacterial cell surfaces and its relevance for adhesion.* Applied and Environmental Microbiology, 1984. **48**(5): p. 980-3.

51. Chaw, K.C., M. Manimaran, and F.E. Tay, *Role of Silver Ions in Destabilization of Intermolecular Adhesion Forces Measured by Atomic Force Microscopy in Staphylococcus epidermidis Biofilms.* Antimicrobial Agents and Chemotherapy, 2005. **49**(12): p. 4853-4859.

52. Deen, W.M., *Analysis of Transport Phenomena.* Oxford University Press, New York, 1998.

53. Truskey, G.A. and J.S. Pirone, *The effect of fluid shear stress upon cell adhesion to fibronectin-treated surfaces.* Journal of Biomedical Materials Research, 1990. **24**(10): p. 1333-1353.

54. Lu, H., et al., *Microfluidic shear devices for quantitative analysis of cell adhesion.* Analytical Chemistry, 2004. **76**(18): p. 5257-5264.

55. Christophis, C., M. Grunze, and A. Rosenhahn, *Quantification of the adhesion strength of fibroblast cells on ethylene glycol terminated self-assembled monolayers by a microfluidic shear force assay.* Physical Chemistry Chemical Physics, 2010. **12**(17): p. 4498-4504.

56. Christophis, C., Taubert, I., Meseck, G., *et al.*, *Shear Stress Regulates Adhesion and Rolling of CD44D Leukemic and Hematopoietic Progenitor Cells on Hyaluronan.* Biophysical Journal, 2011. **101**: p. 585-593.

57. Christophis, C., et al., *Fibroblast adhesion on unidirectional polymeric nanofilms.* Biointerphases, 2011. **6**(4): p. 158-163.

58. Whitesides, G.M., *The origins and the future of microfluidics.* Nature, 2006. **442**(7101): p. 368-373.

59. Christophis, C., *Quantification of cell adhesion strength on artifical surfaces with a microfluidic shear force device*, 2011, University of Heidelberg.

60. Hohne, D.N., J.G. Younger, and M.J. Solomon, *Flexible Microfluidic Device for Mechanical Property Characterization of Soft Viscoelastic Solids Such as Bacterial Biofilms.* Langmuir, 2009. **25**(13): p. 7743-7751.

61. Martinez, A.W., et al., *Diagnostics for the developing world: microfluidic paper-based analytical devices.* Analytical chemistry, 2010. **82**(1): p. 3-10.

62. Vella, S.J., et al., *Measuring markers of liver function using a micropatterned paper device designed for blood from a fingerstick.* Analytical chemistry, 2012. **84**(6): p. 2883-2891.

63. Chiovitti, A., T.M. Dugdale, and R. Wetherbee, eds. *Diatom adhesives: molecular and mechanical properties, In: Biological Adhesives.* 2007, Springer: Heidelberg 79-103.

64. Molino, P.J. and R. Wetherbee, *The biology of biofouling diatoms and their role in the development of microbial slimes.* Biofouling, 2008. **24**(5): p. 365-379.

65. Wetherbee, R., et al., *The first kiss: Establishment and control of initial adhesion by raphid diatoms.* Journal of Phycology, 1998. **34**(1): p. 9-15.

66. Wu, A.H.F., et al., *Hierarchical surfaces: an in situ investigation into nano and micro scale wettability.* Faraday Discussions, 2010. **146**: p. 223-232.

67. Scardino, A.J., E. Harvey, and R. De Nys, *Testing attachment point theory: diatom attachment on microtextured polyimide biomimics.* Biofouling, 2006. **22**(1): p. 55-60.

68. Schumacher, J.F., et al., *Engineered antifouling microtopographies - effect of feature size, geometry, and roughness on settlement of zoospores of the green alga Ulva.* Biofouling, 2007. **23**(1): p. 55-62.

69. Fishelson, L., *A comparative study of ridge-mazes on surface epithelial cell-membranes of fish scales pisces teleostei.* Zoomorphology (Berlin), 1984. **104**(4): p. 231-238.

70. Nuzzo, R.G. and D.L. Allara, *Adsorption of bifunctional organic disulfides on gold surfaces.* Journal of the American Chemical Society, 1983. **105**(13): p. 4481-4483.

71. Kind, M. and C. Woell, *Organic surfaces exposed by self-assembled organothiol monolayers: Preparation, characterization, and application.* Progress in Surface Science, 2009. **84**(7-8): p. 230-278.

72. Love, J.C., et al., *Self-assembled monolayers of thiolates on metals as a form of nanotechnology.* Chemical Reviews, 2005. **105**(4): p. 1103-1169.

73. Ulman, A., *Formation and structure of self-assembled monolayers.* Chemical Reviews, 1996. **96**(4): p. 1533-1554.

74. Prime, K.L. and G.M. Whitesides, *Self-assembled organic monolayers: model systems for studying adsorption of proteins at surfaces* Science, 1991. **252**(5009): p. 1164-1167.

75. Prime, K.L. and G.M. Whitesides, *Adsorption of proteins onto surfaces containing end-attached oligo(ethylene oxide): a model system using self-assembled monolayers.* Journal of the American Chemical Society, 1993. **115**(23): p. 10714-10721.

76. Chelmowski, R., et al., *Peptide-Based SAMs that Resist the Adsorption of Proteins.* Journal of the American Chemical Society, 2008. **130**(45): p. 14952-14953.

77. Chen, S., L. Liu, and S. Jiang, *Strong Resistance of Oligo(phosphorylcholine) Self-Assembled Monolayers to Protein Adsorption.* Langmuir, 2006. **22**(6): p. 2418-2421.

78. Faucheux, N., et al., *Self-assembled monolayers with different terminating groups as model substrates for cell adhesion studies.* Biomaterials, 2004. **25**(14): p. 2721-2730.

79. Steinberg, P.D., R. De Nys, and S. Kjelleberg, *Chemical cues for surface colonization.* Journal of Chemical Ecology, 2002. **28**(10): p. 1935-1951.

80. Finlay, J.A., et al., *The influence of surface wettability on the adhesion strength of settled spores of the green alga Enteromorpha and the diatom Amphora.* Integrative and Comparative Biology, 2002. **42**(6): p. 1116-1122.

81. Callow, M.E., et al., *Use of self-assembled monolayers of different wettabilities to study surface selection and primary adhesion processes of green algal (Enteromorpha) zoospores.* Applied and Environmental Microbiology, 2000. **66**(8): p. 3249-3254.

82. Ista, L.K., et al., *Effect of substratum surface chemistry and surface energy on attachment of marine bacteria and algal spores.* Applied and Environmental Microbiology, 2004. **70**(7): p. 4151-4157.

83. Schilp, S., et al., *Physicochemical Properties of (Ethylene Glycol)-Containing Self-Assembled Monolayers Relevant for Protein and Algal Cell Resistance.* Langmuir, 2009. **25**(17): p. 10077-10082.

84. Love, J.C., et al., *Self-assembled monolayers of alkanethiolates on palladium are good etch resists.* Journal of the American Chemical Society, 2002. **124**(8): p. 1576-1577.

85. Thome, I., et al., *Conditioning of surfaces by macromolecules and its implication for the settlement of zoospores of the green alga Ulva linza.* Biofouling, 2012. **28**(5): p. 501-510.

86. Schilp, S., et al., *Settlement and adhesion of algal cells to hexa (ethylene glycol)-containing self-assembled monolayers with systematically changed wetting properties.* Biointerphases, 2007. **2**(4): p. 143-150.

87. Ekblad, T., et al., *Lateral Control of Protein Adsorption on Charged Polymer Gradients.* Langmuir, 2009. **25**(6): p. 3755-3762.

88. Krishnan, S., C.J. Weinman, and C.K. Ober, *Advances in polymers for anti-biofouling surfaces.* Journal of Materials Chemistry, 2008. **18**(29): p. 3405-3413.

89. Cao, X., et al., *Interaction of Zoospores of the Green Alga Ulva with Bioinspired Micro- and Nanostructured Surfaces Prepared by Polyelectrolyte Layer-by-Layer Self-Assembly.* Advanced Functional Materials, 2010. **20**(12): p. 1984-1993.

90. Scardino, A.J. and R. de Nys, *Mini review: Biomimetic models and bioinspired surfaces for fouling control.* Biofouling, 2010. **27**(1): p. 73-86.

91. Magin, C.M., S.P. Cooper, and A.B. Brennan, *Non-toxic antifouling strategies.* Materials Today, 2010. **13**(4): p. 36-44.

92. Rosenhahn, A. and G.H. Sendra, *Surface Sensing and Settlement Strategies of Marine Biofouling Organisms.* Biointerphases, 2012. **7**(1-4): p. 1-13.

93. Baier, R.E.D., V.A. DePalma, ed. *The Relation of the Internal Surface of Grafts to Thrombosis*. Management of Arterial Occlusive Disease 1971, W. A. Dale.: Chicago. 147-163.

94. Vogler, E.A., *Structure and reactivity of water at biomaterial surfaces.* Advances in Colloid and Interface Science, 1998. **74**: p. 69-117.

95. Berg, J.M., et al., *Three-Component Langmuir-Blodgett Films with a Controllable Degree of Polarity.* Langmuir, 1994. **10**(4): p. 1225-1234.

96. Dexter, S.C., et al., *Influence of substrate wettability on the attachment of marine bacteria to various surfaces.* Applied microbiology, 1975. **30**(2): p. 298-308.

97. Van Loosdrecht, M.C.M., et al., *Electrophoretic mobility and hydrophobicity as a measure to predict the initial steps of bacterial adhesion.* Applied and Environmental Microbiology, 1987. **53**(8): p. 1898-1901.

98. Wiencek, K.M. and M. Fletcher, *Effects of substratum wettability and molecular topography on the initial adhesion of bacteria to chemically defined substrata.* Biofouling, 1997. **11**(4): p. 293-311.

99. Wigglesworth-Cooksey, B., et al., *The influence of surface chemistry on the control of cellular behavior: studies with a marine diatom and a wettability gradient.* Colloids and Surfaces B-Biointerfaces, 1999. **15**(1): p. 71-80.

100. Grozea, C.M. and G.C. Walker, *Approaches in designing non-toxic polymer surfaces to deter marine biofouling.* Soft Matter, 2009. **5**(21): p. 4088-4100.

101. Petrone, L., et al., *Effects of surface charge and Gibbs surface energy on the settlement behaviour of barnacle cyprids (Balanus amphitrite).* Biofouling, 2011. **27**(9): p. 1043-1055.

102. Harder, P., et al., *Molecular conformation in oligo(ethylene glycol)-terminated self-assembled monolayers on gold and silver surfaces determines their ability to resist protein adsorption.* Journal of Physical Chemistry B, 1998. **102**(2): p. 426-436.

103. Herrwerth, S., et al., *Factors that determine the protein resistance of oligoether self-assembled monolayers - Internal hydrophilicity, terminal hydrophilicity, and lateral packing density.* Journal of the American Chemical Society, 2003. **125**(31): p. 9359-9366.

104. Ostuni, E., et al., *Self-assembled monolayers that resist the adsorption of proteins and the adhesion of bacterial and mammalian cells.* Langmuir, 2001. **17**(20): p. 6336-6343.

105. Luk, Y.Y., M. Kato, and M. Mrksich, *Self-assembled monolayers of alkanethiolates presenting mannitol groups are inert to protein adsorption and cell attachment.* Langmuir, 2000. **16**(24): p. 9604-9608.

106. Nelson, C.M., et al., *Degradation of micropatterned surfaces by cell-dependent and -independent processes.* Langmuir, 2003. **19**(5): p. 1493-1499.

107. Larsson, A., et al., *Photografted poly(ethylene glycol) matrix for affinity interaction studies.* Biomacromolecules, 2007. **8**(1): p. 287-295.

108. Ekblad, T., et al., *Poly(ethylene glycol)-Containing Hydrogel Surfaces for Antifouling Applications in Marine and Freshwater Environments.* Biomacromolecules, 2008. **9**(10): p. 2775-2783.

109. Jeon, S.I. and J.D. Andrade, *Protein surface interactions in the presence of polyethylene oxide. 2. Effect of protein size.* Journal of Colloid and Interface Science, 1991. **142**(1): p. 159-166.

110. Wloka, M., et al., *Rheological properties of viscoelastic biofilm extracellular polymeric substances and comparison to the behavior of calcium alginate gels.* Colloid and Polymer Science, 2004. **282**(10): p. 1067-1076.

111. Fraser, J.R.E., T.C. Laurent, and U.B.G. Laurent, *Hyaluronan: Its nature, distribution, functions and turnover.* Journal of Internal Medicine, 1997. **242**(1): p. 27-33.

112. Schiraldi, C., D. Cimini, and M. De Rosa, *Production of chondroitin sulfate and chondroitin.* Applied Microbiology and Biotechnology, 2010. **87**(4): p. 1209-1220.

113. Shephard, K.L., *Functions for fish mucus.* Reviews in Fish Biology and Fisheries, 1994. **4**(4): p. 401-429.

114. Cao, X., et al., *Resistance of Polysaccharide Coatings to Proteins, Hematopoietic Cells, and Marine Organisms.* Biomacromolecules, 2009. **10**(4): p. 907-915.

115. Morra, M. and C. Cassineli, *Non-fouling properties of polysaccharide-coated surfaces.* Journal of Biomaterials Science-Polymer Edition, 1999. **10**(10): p. 1107-1124.

116. Morra, M. and C. Cassinelli, *Surface studies on a model cell-resistant system.* Langmuir, 1999. **15**(13): p. 4658-4663.

117. McArthur, S.L., et al., *Effect of polysaccharide structure on protein adsorption.* Colloids and Surfaces B-Biointerfaces, 2000. **17**(1): p. 37-48.

118. Grant, G.T., et al., *Biological interactions between polysaccharides and divalent cations the egg box model.* Febs Letters, 1973. **32**(1): p. 195-198.

119. Braccini, I. and S. Pérez, *Molecular Basis of Ca2+-Induced Gelation in Alginates and Pectins: The Egg-Box Model Revisited.* Biomacromolecules, 2001. **2**(4): p. 1089-1096.

120. Bauer, S., et al., *Adhesion of Marine Fouling Organisms on Hydrophilic and Amphiphilic Polysaccharides.* Langmuir, 2013.

121. Krishnan, S., et al., *Comparison of the fouling release properties of hydrophobic fluorinated and hydrophilic PEGylated block copolymer surfaces: Attachment strength of the diatom Navicula and the green alga Ulva.* Biomacromolecules, 2006. **7**(5): p. 1449-1462.

122. Gudipati, C.S., et al., *The antifouling and fouling-release perfomance of hyperbranched fluoropolymer (HBFP)-poly(ethylene glycol) (PEG) composite coatings evaluated by adsorption of biomacromolecules and the green fouling alga Ulva.* Langmuir, 2005. **21**(7): p. 3044-3053.

123. Valiokas, R., et al., *Structural and kinetic properties of laterally stabilized, oligo(ethylene glycol)-containing alkylthiolates on gold: A modular approach.* Biointerphases, 2006. **1**(1): p. 22-34.

124. Malysheva, L., A. Onipko, and B. Liedberg, *Orientation of OH terminal groups in oligo(ethylene glycol)-terminated self-assemblies: results of ab initio modeling.* Physica Status Solidi B-Basic Solid State Physics, 2006. **243**(13): p. 3489-3493.

125. Wang, R., H. Kreuzer, and M. Grunze, *The interaction of oligo(ethylene oxide) with water: a quantum mechanical study.* Physical Chemistry Chemical Physics, 2000. **2**(16): p. 3613-3622.

126. Valiokas, R., et al., *Self-assembled monolayers of oligo(ethylene glycol)-terminated and amide group containing alkanethiolates on gold.* Langmuir, 1999. **15**(10): p. 3390-3394.

127. Harder, P., M. Grunze, and J. Waite, *Interaction of the adhesive protein Mefp-1 and fibrinogen with methyl and oligo(ethylene glycol)-terminated self-assembled monolayers.* Journal of Adhesion, 2000. **73**(2-3): p. 161-177.

128. Wang, R.L.C., H.J. Kreuzer, and M. Grunze, *Molecular conformation and solvation of oligo(ethylene glycol)-terminated self-assembled monolayers and their resistance to protein adsorption.* Journal of Physical Chemistry B, 1997. **101**(47): p. 9767-9773.

129. Pertsin, A.J., T. Hayashi, and M. Grunze, *Grand Canonical Monte Carlo Simulations of the Hydration Interaction between Oligo(ethylene glycol)-Terminated Alkanethiol Self-Assembled Monolayers.* The Journal of Physical Chemistry B, 2002. **106**(47): p. 12274-12281.

130. Kreuzer, H.J., R.L.C. Wang, and M. Grunze, *Hydroxide ion adsorption on self-assembled monolayers.* Journal of the American Chemical Society, 2003. **125**(27): p. 8384-8389.

131. Harder, P., *Oligo(ethylenglykol)-terminierte Alkanthiolatmonolagen auf Gold und Silber*, 1999, Heidelberg.

132. Valiokas, R., et al., *Influence of specific intermolecular interactions on the self-assembly and phase behavior of oligo(ethylene glycol)-terminated alkanethiolates on gold.* Journal of Physical Chemistry B, 2001. **105**(23): p. 5459-5469.

133. Ostblom, M., et al., *Ice nucleation and phase behavior on oligo(ethylene glycol) and hydroxyl self-assembled monolayers: Simulations and experiments.* Journal of Physical Chemistry B, 2006. **110**(4): p. 1830-1836.

134. Valiokas, R., et al., *Thermal stability of self-assembled monolayers: Influence of lateral hydrogen bonding.* Journal of Physical Chemistry B, 2002. **106**(40): p. 10401-10409.

135. Hoipkemeier-Wilson, L., et al., *Antifouling potential of lubricious, micro-engineered, PDMS elastomers against zoospores of the green fouling alga Ulva (Enteromorpha).* Biofouling, 2004. **20**(1): p. 53-63.

136. Callow, M.E., et al., *Microtopographic cues for settlement of zoospores of the green fouling alga Enteromorpha.* Biofouling, 2002. **18**(3): p. 237-245.

137. Granhag, L.M., et al., *Roughness-dependent removal of settled spores of the green alga Ulva (syn. Enteromorpha) exposed to hydrodynamic forces from a water jet.* Biofouling, 2004. **20**(2): p. 117-122.

138. Ista, L.K., et al., *Synthesis of poly(N-isopropylacrylamide) on initiator-modified self-assembled monolayers.* Langmuir, 2001. **17**(9): p. 2552-2555.

139. Rühe, J., *Polymers grafted from solid surfaces.* Macromolecular Symposia, 1998. **126**(1): p. 215-222.

140. Ista, L.K., S. Mendez, and G.P. Lopez, *Attachment and detachment of bacteria on surfaces with tunable and switchable wettability.* Biofouling, 2010. **26**(1): p. 111-118.

141. Ahmad, S.A., et al., *Micro- and nanostructured poly oligo(ethylene glycol)methacrylate brushes grown from photopatterned halogen initiators by atom transfer radical polymerization.* Biointerphases, 2011. **6**(1): p. 8-15.

142. Ma, H.W., et al., *Surface-initiated atom transfer radical polymerization of oligo(ethylene glycol) methyl methacrylate from a mixed self-assembled monolayer on gold.* Advanced Functional Materials, 2006. **16**(5): p. 640-648.

143. Hucknall, A., S. Rangarajan, and A. Chilkoti, *In Pursuit of Zero: Polymer Brushes that Resist the Adsorption of Proteins.* Advanced Materials, 2009. **21**(23): p. 2441-2446.

144. Crouzet, C., C. Decker, and J. Marchal, *Characterization of primary reactions of oxidative-degradation in course of autoxidation of poly(oxyethlene)s at 25°C: Study in aqueous-solution with initiation by irradation of solvent, 8. Kinetic studies at pH between 1 and 13.* Makromolekulare Chemie-Macromolecular Chemistry and Physics, 1976. **177**(1): p. 145-157.

145. Horcajada, P., et al., *Flexible porous metal-organic frameworks for a controlled drug delivery.* Journal of the American Chemical Society, 2008. **130**(21): p. 6774-6780.

146. Horcajada, P., et al., *Porous metal-organic-framework nanoscale carriers as a potential platform for drug delivery and imaging.* Nature Materials, 2010. **9**(2): p. 172-178.

147. An, J., S.J. Geib, and N.L. Rosi, *Cation-Triggered Drug Release from a Porous Zinc-Adeninate Metal-Organic Framework.* Journal of the American Chemical Society, 2009. **131**(24): p. 8376-8377.

148. Rowsell, J.L.C. and O.M. Yaghi, *Metal-organic frameworks: a new class of porous materials.* Microporous and Mesoporous Materials, 2004. **73**(1-2): p. 3-14.

149. Arslan, H.K., et al., *High-Throughput Fabrication of Uniform and Homogenous MOF Coatings.* Advanced Functional Materials, 2011. **21**(22): p. 4228-4231.

150. Hanke, M., et al., *The Biocompatibility of Metal-Organic Framework Coatings: An Investigation on the Stability of SURMOFs with Regard to Water and Selected Cell Culture Media.* Langmuir, 2012. **28**(17): p. 6877-6884.

151. Swain, G.E., *Redefining antifouling coatings.* Paint Coatings Europe, 1999. **4**: p. 18-25.

152. Brooks, S. and M. Waldock, eds. *in Advances in marine antifouling coatings and technology, eds. C. Hellio and D. Yebra*. Vol. ch. 19. 2009, Woodhead Publishing Limited: Cambridge. 492-521.

153. Tribou, M. and G. Swain, *The use of proactive in-water grooming to improve the performance of ship hull antifouling coatings.* Biofouling, 2010. **26**(1): p. 47-56.

154. Zargiel, K., J. Coogan, and G. Swain, *Diatom community structure on commercially available ship hull coatings.* Biofouling, 2011. **27**(9): p. 955-65.

155. Gledhill, M., et al., *The toxicity of copper (II) species to marine algae, with particular reference to macroalgae.* Journal of Phycology, 1997. **33**(1): p. 2-11.

156. Morán, A.C., et al., *Changes in bacterial community structure associated with coastal copper enrichment.* Environmental toxicology and chemistry / SETAC, 2008. **27**(11): p. 2239-2245.

157. Correa, J., et al., *Copper, copper mine tailings and their effect on marine algae in Northern Chile.* Journal of Applied Phycology, 1999. **11**(1): p. 57-67.

158. Peden, J.D., et al., *Heavy metals in somerset marine organisms.* Marine Pollution Bulletin, 1973. **4**(1): p. 7-9.

159. Thomas, K., et al., *The effects of short-term changes in environmental parameters on the release of biocides from antifouling coatings: cuprous oxide and tributyltin.* Applied Organometallic Chemistry, 1999. **13**(6): p. 453-460.

160. Swain, G.W. and M.P. Schultz, *The testing and evaluation of non-toxic antifouling coatings.* Biofouling, 1996. **10**(1-3): p. 187-197.

161. Swain, G., et al., *Biofouling and barnacle adhesion data for fouling-release coatings subjected to static immersion at seven marine sites.* Biofouling, 2000. **16**(2-4): p. 331-344.

162. Swain, G., et al., *Short-term testing of antifouling surfaces: the importance of colour.* Biofouling, 2006. **22**(6): p. 425-429.

163. Casse, F. and G.W. Swain, *The development of microfouling on four commercial antifouling coatings under static and dynamic immersion.* International Biodeterioration & Biodegradation, 2006. **57**(3): p. 179-185.

164. Siqueiros-Beltrones, D., F.O. López-Fuerte, and I. Gárate-Lizárraga, *Structure of Diatom Assemblages Living on Prop Roots of the Red Mangrove (Rhizophora mangle) from the West Coast of Baja California Sur, México1.* Pacific Science, 2005. **59**(1): p. 79.

165. Ortigosa, M., E. Garay, and M.-J. Pujalte, *Numerical Taxonomy of Aerobic, Gram-negative Bacteria associated with Oysters and Surrounding Seawater of the Mediterranean Coast.* Systematic and Applied Microbiology, 1995. **17**(4): p. 589-600.

166. Phlips, E.J., et al., *The occurrence of potentially toxic dinoflagellates and diatoms in a subtropical lagoon, the Indian River Lagoon, Florida, USA.* Harmful Algae, 2004. **3**(1): p. 39-49.

167. Quinlan, E.L. and E.J. Phlips, *Phytoplankton assemblages across the marine to low-salinity transition zone in a blackwater dominated estuary.* Journal of Plankton Research, 2007. **29**(5): p. 401-416.

168. Bannister, R.J., C.N. Battershill, and R. de Nys, *Demographic variability and long-term change in a coral reef sponge along a cross-shelf gradient of the Great Barrier Reef.* Marine and Freshwater Research, 2010. **61**(4): p. 389-396.

169. Huggett, M.J., B.T. Nedved, and M.G. Hadfield, *Effects of initial surface wettability on biofilm formation and subsequent settlement of Hydroides elegans.* Biofouling, 2009. **25**(5): p. 387-399.

170. Vinson, D.K. and S.R. Rushforth, *Diatom species composition along a thermal-gradient in the Portneuf River, Idaho, USA.* Hydrobiologia, 1989. **185**(1): p. 41-54.

171. Plisova, E.Y., et al., *A highly active alkaline phosphatase from the marine bacterium Cobetia.* Marine Biotechnology, 2005. **7**(3): p. 173-178.

172. Li, S. and S. Chen. *Polydimethylsioxane fluidic interconnects for microfluidic systems*. 2003. Piscataway: IEEE-Inst Electrical Electronics Engineers Inc.

173. Albert, G., *Herstellung und charakterisierung polykristalliner Goldschichten zur verwendung in der nanolithographie.* Diplom thesis, Ruprecht Karls University, 1996.

174. Arnold, R., et al., *Preparation, modification, and crystallinity of aliphatic and aromatic carboxylic acid terminated self-assembled monolayers.* Langmuir, 2002. **18**(10): p. 3980-3992.

175. Bauer, S.V., *Inerte Oberflächen auf Basis von immobilisierten Polysacchariden*, in *Institute of Physical Chemistry, University of Heidelberg*2011.

176. Ma, H.W., et al., *Protein-resistant polymer coatings on silicon oxide by surface-initiated atom transfer radical polymerization.* Langmuir, 2006. **22**(8): p. 3751-3756.

177. Berney, M., et al., *Assessment and interpretation of bacterial viability by using the LIVE/DEAD BacLight kit in combination with flow cytometry.* Applied and Environmental Microbiology, 2007. **73**(10): p. 3283-3290.

178. Boulos, L., et al., *LIVE/DEAD® BacLight™: application of a new rapid staining method for direct enumeration of viable and total bacteria in drinking water.* Journal of Microbiological Methods, 1999. **37**(1): p. 77-86.

179. Singh, A., B.H. Pyle, and G.A. McFeters, *Rapid enumeration of viable bacteria by image analysis.* Journal of Microbiological Methods, 1989. **10**(2): p. 91-101.

180. Davey, H.M., *Life, Death, and In-Between: Meanings and Methods in Microbiology.* Applied and Environmental Microbiology, 2011. **77**(16): p. 5571-5576.

181. Lide, R.D., ed. *Handbook of Chemistry and Physics*. Vol. 89. 2008.

182. Braet, F., R. deZanger, and E. Wisse, *Drying cells for SEM, AFM and TEM by hexamethyldisilazane: A study on hepatic endothelial cells.* Journal of Microscopy-Oxford, 1997. **186**: p. 84-87.

183. Hendey, N.I., *Littoral diatoms of Chichester Harbour with special reference to fouling.* Jour Roy Microsc Soc, 1951. **71**(1): p. 1-86.

184. Hargraves, P., *Diatoms of the Indian River Lagoon, Florida: An annotated account.* Florida Scientist, 2002. **65**(4): p. 225-244.

185. Lange-Bertalot, H., ed. *Iconographia diatomologica: annotated diatom micrographs.* 2000, ARG Gantner Verlag KG.: Königstein (Germany).

186. Linne von Berg, K.H. and M. Melkonian, eds. *Der Kosmos-Algenfuehrer*. 2004, Kosmos.

187. Round, F., R. Crawford, and D. Mann, eds. *The diatoms: biology and morphology of the genera.* 1990, Cambridge University Press.: Cambridge (UK).

188. Zisman, W.A., *Relation of the Equilibrium Contact Angle to Liquid and Solid Constitution*, in *Contact Angle, Wettability, and Adhesion*1964, American Chemical Society. p. 1-51.

189. Young, T., *An Essay on the Cohesion of Fluids.* Philosophical Transactions of the Royal Society of London, 1805. **95**: p. 65-87.

190. Marmur, A., *Super-hydrophobicity fundamentals: implications to biofouling prevention.* Biofouling, 2006. **22**(2): p. 107-115.

191. Wenzel, R.N., *Resistance of solid surfaces to wetting by watter.* Industrial & Engineering Chemistry, 1936. **28**(8): p. 988-994.

192. Cassie, A.B.D. and S. Baxter, *Wettability of porous surfaces.* Transactions of the Faraday Society, 1944. **40**: p. 546.

193. Bordo, V.G. and H.-G. Rubahn, eds. *Optics and Spectroscopy at Surface and Interfaces*. 2005, WILEY-VCH: Weinheim, Germany.

194. http://www.jawoollam.com/tutorial_2.html. 09.10.2012.

195. Tompkins, H.G., ed. *A User´s Guide to Ellipsometry*. 2006, Academic Press Inc.: San Diego, CA.

196. Rissanen, K., ed. *Advanced X-ray crystallography*. Topics in Current Chemistry ; 315. Vol. 315. 2012, Springer: Berlin ; Heidelberg. XI, 181 S.

197. Ratner, B. and D. Castner, *Electron Spectroscopy for Chemical Analysis*. 2 ed. Surface analysis : the principal techniques, ed. J.C. Vickerman and I. Gilmore2009, Chichester [England]; New York: John Wiley.

198. Klein, A., et al., *Photoelectron Spectroscopy in Materials Science and Physical Chemistry: Analysis of Composition, Chemical Bonding, and Electronic Structure of Surfaces and Interfaces*, in *Methods in Physical Chemistry*2012, Wiley-VCH Verlag GmbH & Co. KGaA. p. 477-512.

199. Scofield, J.H., *Hartree-Slater subshell photoionization cross-sections at 1254 and 1487 eV.* Journal of Electron Spectroscopy and Related Phenomena, 1976. **8**(2): p. 129-137.

200. Meyerbröker, N., *Präparation und Charakterisierung ultradünner, biokompatibler Filme und Membranen auf Basis von Polyethylenglykolen*, 2012, Heidelberg.

201. Nishino, T., E. Ikemoto, and K. Kogure, *Application of atomic force microscopy to observation of marine bacteria.* Journal of Oceanography, 2004. **60**(2): p. 219-225.

202. Bolshakova, A.V., et al., *Comparative studies of bacteria with an atomic force microscopy operating in different modes.* Ultramicroscopy, 2001. **86**(1-2): p. 121-128.

203. Braga, P.C. and D. Ricci, *Atomic Force Microscopy: Application to Investigation of Escherichia coli Morphology before and after Exposure to Cefodizime.* Antimicrobial Agents and Chemotherapy, 1998. **42**(1): p. 18-22.

204. Giessibl, F.J., *Advances in atomic force microscopy.* Reviews of Modern Physics, 2003. **75**(3): p. 949-983.

205. Sluder, G. and J.J. Nordberg, *Microscope Basics*, in *Methods in Cell Biology*, S. Greenfield and E.W. David, Editors. 2007, Academic Press. p. 1-10.

206. Bell, D.C., *Contrast mechanisms and image formation in helium ion microscopy.* Microscopy and microanalysis : the official journal of Microscopy Society of America, Microbeam Analysis Society, Microscopical Society of Canada, 2009. **15**(2): p. 147-153.

207. Notte, J., et al., *An Introduction to the Helium Ion Microscope.* AIP Conference Proceedings, 2007.

208. Chen, X., et al., *Whole-Cell Imaging at Nanometer Resolutions Using Fast and Slow Focused Helium Ions.* Biophysical journal, 2011. **101**(7): p. 1788-1793.

209. Siedler, G. and H. Peters, eds. *Numerical data and functional relationships in scince and technology, chapter 3.1: properties of seawater*. Landolt-Börnstein New Series V/3a, ed. J. Sündermann. Vol. 3a. 1986, Springer: Berlin. 233-264.

210. Sharqawy, M.H., J.H. Lienhard, and S.M. Zubair, *The thermophysical properties of seawater: A review of existing correlations and data.* 2009.

211. Schultz, M.P., et al., *Three models to relate detachment of low form fouling at laboratory and ship scale.* Biofouling, 2003. **19**: p. 17-26.

212. Stoodley, P., et al., *Biofilms as complex differentiated communities.* Annual Review of Microbiology, 2002. **56**: p. 187-209.

213. Bakker, D.P., H.J. Busscher, and H.C. van der Mei, *Bacterial deposition in a parallel plate and a stagnation point flow chamber: microbial adhesion mechanisms depend on the mass transport conditions.* Microbiology (Reading, England), 2002. **148**(Pt 2): p. 597-603.

214. Jain, A. and N.B. Bhosle, *Biochemical composition of the marine conditioning film: implications for bacterial adhesion.* Biofouling, 2009. **25**(1): p. 13-19.

215. Berg, J.M., et al., *Three-Component Langmuir-Blodgett Films with a Controllable Degree of Polarity.* Langmuir, 1994. **10**(4): p. 1225-1234.

216. Khan, M.M.T., et al., *Experimental and theoretical examination of surface energy and adhesion of nitrifying and heterotrophic bacteria using self-assembled monolayers.* Environmental science & technology, 2011. **45**(3): p. 1055-1060.

217. Finlay, J.A., et al., *Settlement of Ulva zoospores on patterned fluorinated and PEGylated monolayer surfaces.* Langmuir : the ACS journal of surfaces and colloids, 2008. **24**(2): p. 503-510.

218. Bain, C.D., et al., *Formation of monolayer films by the spontaneus assembly of organic thiols from solution onto gold.* Journal of the American Chemical Society, 1989. **111**(1): p. 321-335.

219. Zhu, B., et al., *Chain-length dependence of the protein and cell resistance of oligo(ethylene glycol)-terminated self-assembled monolayers on gold.* Journal of Biomedical Materials Research, 2001. **56**(3): p. 406-416.

220. Statz, A., et al., *Algal antifouling and fouling-release properties of metal surfaces coated with a polymer inspired by marine mussels.* Biofouling, 2006. **22**(6): p. 391-399.

221. Castner, D.G. and B.D. Ratner, *Biomedical surface science: Foundations to frontiers.* Surface Science, 2002. **500**(1-3): p. 28-60.

222. Ista, L.K. and G.P. Lopez, *Interfacial Tension Analysis of Oligo(ethylene glycol)-Terminated Self-Assembled Monolayers and Their Resistance to Bacterial Attachment.* Langmuir, 2012. **28**(35): p. 12844-12850.

223. Himmelhaus, M., et al., *Growth of a dense polymer brush layer from solution.* EPL (Europhysics Letters), 2003. **64**(3): p. 378-384.

224. Pale-Grosdemange, C., et al., *Formation of Self-assembled monolayers by chemisorption of derivates of oligo(ethylene glycol) of structure $HS(CH_2)_{11}(OCH_2CH_2)$meta-OH on gold.* Journal of the American Chemical Society, 1991. **113**(1): p. 12-20.

225. Bailey, F.E. and J.V. Koleske, *Poly(ethylene oxide)*1976, New York: Academic Press.

226. Miyazawa, T., Y. Ideguchi, and K. Fukushima, *Molecular vibrations and structure of high polymers. 3. Polarized infrared spectra, normal vibrations, and helical conformation of polyethylene glycol.* Journal of Chemical Physics, 1962. **37**(12): p. 2764-2777.

227. Nuzzo, R.G., L.H. Dubois, and D.L. Allara, *Fundamental studies of microscopic wetting on organic-surfaces. 1. Formation and structural characterization of a self-consistent series of polyfunctional organic monolayers.* Journal of the American Chemical Society, 1990. **112**(2): p. 558-569.

228. Dubois, L.H., B.R. Zegarski, and R.G. Nuzzo, *Fundamental studies of microscopic wetting on organic-surfaces. 2. Interaction of secondary adsorbates with chemically textured organic monolayers.* Journal of the American Chemical Society, 1990. **112**(2): p. 570-579.

229. Zolk, M., *In situ Untersuchen von funktionalisierten und unfunktionalisierten Alkanthiol-Monolagen auf Gold- und SIlberoberflächen mittels IR vis Summenfrequenzspektroskopie*, 2001, Heidelberg.

230. Cao, X., *Antifouling properties of smooth and structured polyelectrolyte thin films*, 2008, University of Heidelberg.

231. Heinke, L., H. Gliemann, and C. Wöll, *Systemchemie an Grenzflächen.* Nachrichten aus der Chemie, 2013. **61**(2): p. 116-120.

232. Patrick, R., *The effects of increasing light and temperature on the structure of diatom communities.* Limnology and Oceanography, 1971. **16**(2): p. 405-421.

233. Luk, Y.-Y., M. Kato, and M. Mrksich, *Self-Assembled Monolayers of Alkanethiolates Presenting Mannitol Groups Are Inert to Protein Adsorption and Cell Attachment.* Langmuir, 2000. **16**: p. 9604-9608.

234. Ma, H.W., et al., *"Non-fouling" oligo(ethylene glycol)-functionalized polymer brushes synthesized by surface-initiated atom transfer radical polymerization.* Advanced Materials, 2004. **16**(4): p. 338-341.

235. Hucknall, A., et al., *Simple Fabrication of Antibody Microarrays on Nonfouling Polymer Brushes with Femtomolar Sensitivity for Protein Analytes in Serum and Blood.* Advanced Materials, 2009. **21**(19): p. 1968-1971.

236. Hucknall, A., et al., *Versatile synthesis and micropatterning of nonfouling polymer brushes on the wafer scale.* Biointerphases, 2009. **4**(2): p. FA50-FA57.

237. Nagarkar, S. and G.A. Williams, *Comparative techniques to quantify cyanobacteria dominated epilithic biofilms on tropical rocky shores.* Marine Ecology-Progress Series, 1997. **154**: p. 281-291.

12.3. Abbreviations

AA: alginic acid

AFM: atomic force microscopy

APTMS: 3-aminopropyltrimethoxy silane

ASW: artificial seawater

AUDT: 11-amino-undecanethiol

C. marina: Cobetia marina

CA: water contact angle

CBD: 1,4-benzendicarboxylic acid

CS: chondroitin sulfate

DDT: dodecanethiol

DLVO: Derjaguin, Landau, Verwey, Overbeek

DSMZ: "deutsche Sammlung von Mikroorganismen und Zellkulturen", german collection of microorganisms and cell cultures

EDC: N-(3 dimethyl amino propyl)-3 ethyl carbodiimide hydrochloride

EG: ethylene glycol

EPS: extracellular polymeric substances

ESEM: environmental scanning electron microscopy

FCS: fluorescence correlation spectroscopy

FDPFS: freeze drying of plunge-frozen samples

FEG-ESEM: field emission gun environmental scanning electron microscopy

FUDT: 11-tridecafluorooctyloxy-undecanethiol

h: hour

HA: hyaluronic acid

HEPES: 4 (2 hydroxyethyl) piperazine-1 ethane sulfonic acid

HUDT: 11-hydroxy-undecanethiol

HV: high vacuum

ICM: ice cold methanol

IR: infrared

IRRAS: infrared reflection-absorption spectroscopy

LPE: liquid phase epitaxy

MA: marine agar

MB: marine broth

MHDA: mercaptohexadecanoic acid

min: minute

MOFs: metal-organic frameworks

NA: numerical aperture

NHS: N-hydroxysuccinimide

NSW: natural seawater

OD_{600}: optical density at a 600 nm wavelength

PA: peptic acid

PDMS: polydimethoxysiloxane

PEG: polyethylene glycol

PMMA: poly(methyl methacrilate) 18; Poly(methyl methacrylate)

PNIPAAM: poly(N-isoprophyacrylamide)

POEGMA: poly[oligo(ethylene glycol) methyl methacrylate

PS: polysaccharides

QS: bacterial quorum sensing

Re: Reynolds number

rpm: revolutions per minute

s: second

SAM: self-assembled monolayers

SEM: scanning electron microscopy

TFEA: 2,2,2-trifluoroethylamine

UHV: ultra-high vacuum

XPS: X-ray photoelectron spectroscopy

XRD: X-ray diffraction

12.4. List of publication related to this work

M. P. Arpa-Sancet, C. Christophis and A. Rosenhahn (2012): Microfluidic Assay to Quantify the Adhesion of Marine Bacteria. *Biointerphases*. 7(1): 1-9. Published.

S. Bauer, M. P. Arpa-Sancet, J. Finlay, M. Callow, J. Callow and A. Rosenhahn (2013): Adhesion of marine fouling organisms on hydrophilic and amphiphilic polysaccharides. *Langmuir*. Published.

M. P. Arpa-Sancet, M. Hanke, Z. Wang, S. Bauer , *et al.*: Surface anchored Metal-organic framework coatings as stimulus responsive antifouling coatings. In preparation.

M. P. Arpa-Sancet, I. Thome, S. Bauer, K. Zargiel, *et. al.*: Early colonization of self assembled monolayers, ethylene glycols and polysaccharides by biofouling organisms studied at the FIT test site (2012). In preparation.

12.5. Acknowledgments

I would like to express my gratitude to everyone, family, friends and colleagues, who helped me in any way. Since I do not have enough space to individually thank all of them, I feel obliged to summarize so I am sorry if I forgot anyone. I would like to express my gratitude to…

Prof. Michael Grunze, not only for accepting me in his group, for the suggestion of the field tests and his help during these experiments but also for his generosity and good taste of wine during the numerous group events.

Prof. Axel Rosenhahn for his supervision, suggestions, and discussions during my work and for the nice company during group excursions. Particularly I want to thank him for the numerous corrections of my thesis even if he was very busy and the time was tight.

Prof. Joachim Spatz for being the second referee of my thesis and offering the chance to use the installations of his group in Heidelberg.

Prof. Swain and his whole crew of the Florida Institute of Technology for the support during the field tests.

Prof. Gabriel López from Duke University and Dr. Linnea Ista for their hospitality during my time in Albuquerque and their help and the introduction to the bacterial culture.

Prof. Christoph Wöll and Zhengbang Wang for providing me with the samples of SURMOF 2.

Prof. Ursula Obst for allowing me to use the microbiology lab and its installations, and her group, especially Silke and Silke-Mareike, for the kind advice.

Prof. Ashutosh Chilkoti and Dr. Angus Hucknall for providing me with the POEGMA brushes.

Prof. Robert Lamb and Dr. Alex Wu from the University of Melbourne, Australia, for their hospitality and the interesting meeting.

Prof. Armin Gölzhäuser and PD Dr. André Beyer for the support by the HeIM measurements.

All colleagues from our group, former and present ones, for the nice time during these years, barbecues, Christmas parties and group excursions, particularly the one to Europa Park.

The people of the PCI institute in Heidelberg, administrative and technical staff and colleagues, for the kind work atmosphere. Especially I want to thank Niko, Bürgis guys, and of course my own group, with whom I could share fabulous times cooking pasta, testing schnaps and wine, watching films and having barbecues.

Dr. Christoph Christophis -Toffy- for the development of the microfluidic system and his support, especially during my first assays.

Dr. Niko Meyerbröcker, for his help with XPS measurements and the scientific discussions. I thank him especially for his patience and help with my thesis during the last weeks and his companionship during my whole stay in the institute.

Max Hanke, Dr. Carlos Azucena, Linlin Xiao, Stefan Heißler and Dr. Frank Friedrich for the scientific support and corrections of my work.

Stella Bauer for the preparation of the polysaccharides, the scientific support, and the great and helpful numerous corrections, not only for this thesis but also during the last year.

Kelly Zargiel for her help during the field tests, with the data analysis, and the nice time in Florida.

Isabel Thomé for the preparation of the SAMs which were needed for the field tests.

Stojan Maleschlijski for his help when struggling with my computer at the KIT and for his numerous corrections.

Everyone who also helped correcting my thesis: Julia Lochead, Irena Wallbaum, Hernán Sendra, Mercedes Dragovits, Maria Alles, Tawheed Mohamed, and Gonzalo G. Prado.

Svenja Stuppy, Isabel Thomé and Maria Alles for their help during the field tests and the incredible nice time spent in Florida which was one of the best periods of my PhD. Special thanks to the latter, with whom I had fun travelling around the world.

Everyone who was in any way involved in my Erasmus year for making that time one of the best of my life and convincing me to stay in Heidelberg.

My friends and former flat mates from the student house for the five delightful years.

My new flat mates: mis conejitos Lili y Limón.

Viola und Gert Senkbeil, da sie wie meine deutsche Familie sind.

All my friends, particularly Leti, Sara, Barbi, Irena and Zeltia for the friendship and making me smile when I most needed it.

Gonzalo García Prado y Lisa Glatz por ser unos amigos estupendos con quien compartir cenas, vinos, fiestas y videos de youtube. ¡Somos un gran equipo!

Julia Lochead for being my german-french-scottish sister, the person who was always there, no matter what, during my whole time in Heidelberg.

Tobias Senkbeil, mi rubio guapo y listo, thank you so much for taking care of me, your help with the thesis, your love and for the great time we spend together.

Por último, pero no menos importante, quiero expresar mi más profunda gratitud a mi famila al completo, especialmente a mi familia más íntima. Mis queridísimos papá, mamá, yaya, Nana, Carmen y Carolina. Gracias por lo bien que nos lo pasamos y por lo que me mimáis cuando voy de visita. Aunque principalmente os quiero agradecer vuestro constante apoyo, tanto moral como económico, especialmente durante estos últimos años en la distancia. Sin vosotros no habría podido conseguirlo.

Eidesstattliche Versicherung gemäß § 8 der Promotionsordnung der Naturwissenschaftlich-Mathematischen Gesamtfakultät der Universität Heidelberg

1. Bei der eingereichten Dissertation zu dem Thema

Influence of surface properties on adhesion of *Cobetia marina* and accumulation of marine microfoulers in the ocean

handelt es sich um meine eigenständig erbrachte Leistung.

2. Ich habe nur die angegebenen Quellen und Hilfsmittel benutzt und mich keiner unzulässigen Hilfe Dritter bedient. Insbesondere habe ich wörtlich oder sinngemäß aus anderen Werken übernommene Inhalte als solche kenntlich gemacht.

3. Die Arbeit oder Teile davon habe ich ~~wie folgt~~/bislang nicht[1)] an einer Hochschule des In- oder Auslands als Bestandteil einer Prüfungs- oder Qualifikationsleistung vorgelegt.

Titel der Arbeit: _____

_____

Hochschule und Jahr:_____

Art der Prüfungs- oder Qualifikationsleistung:_____

4. Die Richtigkeit der vorstehenden Erklärungen bestätige ich.

5. Die Bedeutung der eidesstattlichen Versicherung und die strafrechtlichen Folgen einer unrichtigen oder unvollständigen eidesstattlichen Versicherung sind mir bekannt.

Ich versichere an Eides statt, dass ich nach bestem Wissen die reine Wahrheit erklärt und nichts verschwiegen habe.

Heidelberg, 28.03.2013 _____

Ort und Datum Unterschrift

1) Nicht Zutreffendes streichen. Bei Bejahung sind anzugeben: der Titel der andernorts vorgelegten Arbeit, die Hochschule, das Jahr der Vorlage und die Art der Prüfungs- oder Qualifikationsleistung.